

# Seismic Performance of Steel Girder Bridge Superstructures with Conventional Cross Frames

by  
**Lyle P. Carden, Ahmad M. Itani and Ian G. Buckle**



Technical Report MCEER-08-0001

January 7, 2008

## NOTICE

This report was prepared by the University of Nevada, Reno as a result of research sponsored by MCEER through a contract from the Federal Highway Administration. Neither MCEER, associates of MCEER, its sponsors, the University of Nevada, Reno, nor any person acting on their behalf:

- a. makes any warranty, express or implied, with respect to the use of any information, apparatus, method, or process disclosed in this report or that such use may not infringe upon privately owned rights; or
- b. assumes any liabilities of whatsoever kind with respect to the use of, or the damage resulting from the use of, any information, apparatus, method, or process disclosed in this report.

Any opinions, findings, and conclusions or recommendations expressed in this publication are those of the author(s) and do not necessarily reflect the views of MCEER or the Federal Highway Administration.

## Seismic Performance of Steel Girder Bridge Superstructures with Conventional Cross Frames

by

Lyle P. Carden,<sup>1</sup> Ahmad M. Itani<sup>2</sup> and Ian G. Buckle<sup>3</sup>

Publication Date: January 7, 2008

Submittal Date: October 17, 2005

Technical Report MCEER-08-0001

Task Number 094-C-3.2

FHWA Contract Number DTFH61-98-C-00094

- 1 Design Engineer, Martin & Chock, Inc.; Former Graduate Assistant, Department of Civil and Environmental Engineering, University of Nevada, Reno
- 2 Associate Professor, Department of Civil and Environmental Engineering, University of Nevada, Reno
- 3 Professor, Department of Civil and Environmental Engineering, University of Nevada, Reno

MCEER

University at Buffalo, The State University of New York

Red Jacket Quadrangle, Buffalo, NY 14261

Phone: (716) 645-3391; Fax (716) 645-3399

E-mail: [mceer@buffalo.edu](mailto:mceer@buffalo.edu); WWW Site: <http://mceer.buffalo.edu>

---

## **NTIS DISCLAIMER**



This document has been reproduced from the best copy furnished by the sponsoring agency.

## Preface

The Multidisciplinary Center for Earthquake Engineering Research (MCEER) is a national center of excellence in advanced technology applications that is dedicated to the reduction of earthquake losses nationwide. Headquartered at the University at Buffalo, State University of New York, the Center was originally established by the National Science Foundation in 1986, as the National Center for Earthquake Engineering Research (NCEER).

Comprising a consortium of researchers from numerous disciplines and institutions throughout the United States, the Center's mission is to reduce earthquake losses through research and the application of advanced technologies that improve engineering, pre-earthquake planning and post-earthquake recovery strategies. Toward this end, the Center coordinates a nationwide program of multidisciplinary team research, education and outreach activities.

MCEER's research is conducted under the sponsorship of two major federal agencies, the National Science Foundation (NSF) and the Federal Highway Administration (FHWA), and the State of New York. Significant support is also derived from the Federal Emergency Management Agency (FEMA), other state governments, academic institutions, foreign governments and private industry.

The Center's Highway Project develops improved seismic design, evaluation, and retrofit methodologies and strategies for new and existing bridges and other highway structures, and for assessing the seismic performance of highway systems. The FHWA has sponsored three major contracts with MCEER under the Highway Project, two of which were initiated in 1992 and the third in 1998.

Of the two 1992 studies, one performed a series of tasks intended to improve seismic design practices for new highway bridges, tunnels, and retaining structures (MCEER Project 112). The other study focused on methodologies and approaches for assessing and improving the seismic performance of existing "typical" highway bridges and other highway system components including tunnels, retaining structures, slopes, culverts, and pavements (MCEER Project 106). These studies were conducted to:

- assess the seismic vulnerability of highway systems, structures, and components;
- develop concepts for retrofitting vulnerable highway structures and components;
- develop improved design and analysis methodologies for bridges, tunnels, and retaining structures, which include consideration of soil-structure interaction mechanisms and their influence on structural response; and
- develop, update, and recommend improved seismic design and performance criteria for new highway systems and structures.

The 1998 study, “Seismic Vulnerability of the Highway System” (FHWA Contract DTFH61-98-C-00094; known as MCEER Project 094), was initiated with the objective of performing studies to improve the seismic performance of bridge types not covered under Projects 106 or 112, and to provide extensions to system performance assessments for highway systems. Specific subjects covered under Project 094 include:

- development of formal loss estimation technologies and methodologies for highway systems;
- analysis, design, detailing, and retrofitting technologies for special bridges, including those with flexible superstructures (e.g., trusses), those supported by steel tower substructures, and cable-supported bridges (e.g., suspension and cable-stayed bridges);
- seismic response modification device technologies (e.g., hysteretic dampers, isolation bearings); and
- soil behavior, foundation behavior, and ground motion studies for large bridges.

In addition, Project 094 includes a series of special studies, addressing topics that range from non-destructive assessment of retrofitted bridge components to supporting studies intended to assist in educating the bridge engineering profession on the implementation of new seismic design and retrofitting strategies.

*Past earthquakes have shown that the considerable in-plane strength of most bridge superstructures is not always sufficient to prevent damage to superstructures with steel plate girders. This report describes a series of cyclic and shake table experiments on a 2/5th scale model of a simply supported steel girder bridge superstructure, with two steel plate I-girders, a reinforced concrete deck slab and single angles cross frames. The experiments were conducted to determine the effect of transverse seismic loading on this type of bridge superstructure in regions of high seismicity. From the experimental results, it is shown the superstructure deforms in a flexural-torsional mode with transverse seismic forces distributed along the span and resisted at the supports. At the supports, the loads are transferred from the deck slab into the girders through the shear studs located near the girder supports or through a top chord connecting the deck slab to the end cross frames. The transverse loads are then distributed to the base of the girders through the end cross frames and into the substructure through the bearings and transverse bearing restraints. Each of these critical components should be designed for transverse seismic loading.*

## ABSTRACT

Past earthquakes have shown that the considerable in-plane strength of most bridge superstructures is not always sufficient to prevent damage to components of steel plate girder superstructures during moderate to large earthquake excitation. Cyclic and shake table experiments on a  $2/5$ th scale model of a simply supported steel girder bridge superstructure, with two steel plate I-girders, a reinforced concrete deck slab and single angles cross frames are described in this report. These experiments were conducted to determine the effects of transverse seismic loading on this type of bridge superstructure in high seismic regions. From the experimental results it is shown the superstructure deforms in a flexural-torsional mode with transverse seismic forces distributed along the span and resisted at the supports. At the supports, the loads are transferred from the deck slab into the girders through the shear studs located near the girder supports or through a top chord connecting the deck slab to the end cross frames. The transverse loads are then distributed to the base of the girders through the end cross frames and into the substructure through the bearings and transverse bearing restraints. Each of these critical components should be designed for transverse seismic loading.





## **ACKNOWLEDGEMENTS**

This project was funded by the Federal Highway Administration through the Highway Project at the Multidisciplinary Center for Earthquake Engineering Research, University of Buffalo under contract DTFH61-98-C-00094. Additional funding was provided by the California Department of Transportation under contract 59Y564. Grateful acknowledgement is made of both agencies for their generous support.

The authors would also like to acknowledge the contribution of Francisco Garcia-Alvarez for an enormous effort in the construction of the bridge and early experimentation. Thanks is also extended to the laboratory manager, Patrick Laplace, and development technician, Paul Lucas for their efforts.

This report was prepared by the first author and as part of this authors' doctoral dissertation and supervised by the second and third authors. Opinions expressed in this report are those of the authors and do not necessarily reflect the views of the funding organisations.



## TABLE OF CONTENTS

SECTION	TITLE	PAGE
<b>1</b>	<b>INTRODUCTION</b>	<b>1</b>
1.1	Overview	1
1.2	Typical Steel Plate Girder Bridges	1
1.3	Seismic Performance of steel Plate Girder Bridges During Previous Earthquakes	1
1.4	Previous Research into Seismic Load Path	7
1.5	Seismic Design of Bridges	7
1.5.1	Specifications	7
1.5.2	Connection between the Deck Slab and the Girders	8
1.5.3	Design of Cross Frames and Diaphragms	9
1.5.4	Girders	11
1.5.5	Bearings	11
1.5.6	Shortcomings of Current Seismic Design Provisions	12
1.6	Objectives and Scope	12
<b>2</b>	<b>THE BRIDGE MODEL</b>	<b>13</b>
2.1	Introduction	13
2.2	Four Girder Simply Supported Bridge Prototype	13
2.3	Two Girder Simply Supported Bridge Prototype	13
2.4	Design of Bridge Model	14
2.4.1	Overview	14
2.4.2	Girders	15
2.4.3	Deck	16
2.4.4	Shear Studs	17
2.4.5	Intermediate Cross Frames	17
2.4.6	Bearings	18
2.4.7	Superstructure Weight	19
2.5	Design of Critical Components in the Transverse Response of the Bridge	20
2.5.1	Overview	20
2.5.2	“Heavy” X-Braces	20
2.5.3	“Light” Single Angle X-Braces	21
2.5.4	Ductile End Cross Frames using Unbonded Braces - Elastic Substructure	22
2.5.5	Seismic Isolation using Lead Rubber Bearings	24
2.6	Simulation of Earthquake Loading	26
2.6.1	Reversed Static Transverse Loading	26
2.6.2	Shake Table Earthquake Simulation	34
2.7	Instrumentation	37
2.7.1	Introduction	37
2.7.2	Load Cells	44
2.7.3	Displacement Transducers	46
2.7.4	Accelerometers	52
2.7.5	Strain Gages	52

## TABLE OF CONTENTS (CONT'D)

SECTION	TITLE	PAGE
<b>3</b>	<b>OVERVIEW OF DEFORMATIONS AND MODAL RESPONSE OF THE BRIDGE MODEL DURING REVERSED STATIC AND SHAKE TABLE EXPERIMENTS</b>	<b>57</b>
3.1	Introduction	57
3.2	Overview of Results from Reversed Static Experiments	57
3.3	Overview of Shake Table Experiments	62
3.4	Detailed Finite Element Analysis of Bridge Model	81
3.4.1	Model	81
3.4.2	Reversed Static Response Comparison	82
3.4.3	Dynamic Response Comparison	82
<b>4</b>	<b>DECK SLAB AND COMPOSITE ACTION</b>	<b>91</b>
4.1	Introduction	91
4.2	Deck Slab	91
4.2.1	Response and Modeling of Deck Slab During the First Experiment	91
4.2.2	Deck Slab Models using Transformed Sections	94
4.2.3	Response during Subsequent Experiments	99
4.2.4	End Shear in the Deck	100
4.3	Influence of Shear Studs in Response of Bridge	101
4.3.1	Stiffness of Shear Studs in the Partially Composite Bridge Model	101
4.3.2	Damage to Shear Studs at the North End of Bridge Model	105
4.3.3	Transverse Shear Stud Forces	105
4.3.4	Longitudinal Shear Forces	107
4.3.5	Axial Stud Forces	109
4.4	Overall Superstructure Response including Effective Deck Stiffness and Partial Composite Action	109
<b>5</b>	<b>ELASTIC RESPONSE OF THE CROSS FRAMES</b>	<b>113</b>
5.1	Introduction	113
5.2	Relative Forces in End and Intermediate Cross Frames	113
5.3	Effect of Top and Bottom Chords and Other Components on End Cross Frame Stiffness	115
<b>6</b>	<b>IMPACT OF GIRDERS ON TRANSVERSE RESPONSE OF THE END CROSS FRAMES</b>	<b>123</b>
6.1	Introduction	123
6.2	Transverse Stiffness of the End of the Girder	123
6.2.1	Elements in the Model	123
6.2.2	Torsional Properties of the Girder	124
6.2.3	Rotational Bearing Stiffness	128
6.2.4	Bearing and Web Stiffeners	128
6.2.5	Shear Stud Stiffness	129

## TABLE OF CONTENTS (CONT'D)

SECTION	TITLE	PAGE
6.2.6	Influence of Different Components	130
6.2.7	Comparison with Measured Bridge Model Stiffness	133
6.3	Strength Limits of Various Girder Components	134
6.3.1	Overview	134
6.3.2	Girders	134
6.3.3	Shear Studs and Top Flange	136
6.3.4	Rotational Capacity of the Bearings	138
6.3.5	Bearing Stiffeners	139
6.4	Continuous Girders	139
6.4.1	Girder Stiffness	139
6.4.2	Girder Flange Bending Moments	141
<b>7</b>	<b>DISTRIBUTION OF FORCES IN BEARINGS</b>	<b>145</b>
7.1	Introduction	145
7.2	Capacity of Elastomeric Bearings for Extreme Events	145
7.3	Rotational Actions in the Bearings	146
7.4	Axial Loads on the Bearings	148
7.5	Shear Forces in Transversely Restrained Bearings	157
7.6	Combined Actions in the Bearings	159
7.7	Distribution of Forces between Supports	162
<b>8</b>	<b>ANALYTICAL MODEL TO REPRESENT THE STEEL GIRDER BRIDGE SUPERSTRUCTURE</b>	<b>165</b>
8.1	Introduction	165
8.2	Description of the Model	165
8.3	Calibration of the Simplified Finite Element Model to the Experimental Model	167
8.4	Comparisons of Analytical Model with Detailed Finite Element Model	170
<b>9</b>	<b>SUMMARY, CONCLUSIONS AND RECOMMENDATIONS</b>	<b>173</b>
9.1	Summary	173
9.2	Conclusions	174
9.3	Recommendations	175
<b>10</b>	<b>REFERENCES</b>	<b>177</b>
	<b>APPENDIX A. PROPERTIES OF ELASTOMERIC BEARINGS IN BRIDGE MODEL</b>	<b>181</b>
	<b>APPENDIX B. PROPERTIES OF LEAD RUBBER BEARINGS FOR BRIDGE MODEL</b>	<b>185</b>
	<b>APPENDIX C. LIST OF SHAKE TABLE SIMULATIONS</b>	<b>191</b>

## TABLE OF CONTENTS (CONT'D)

SECTION	TITLE	PAGE
APPENDIX D.	LOAD CELL CALIBRATIONS	199
APPENDIX E.	VALIDATION OF SINE SWEEP FOR CALCULATING DYNAMIC PROPERTIES OF THE BRIDGE MODEL	211

## LIST OF FIGURES

FIGURE	TITLE	PAGE
1-1	Typical K-brace cross frame	2
1-2	Damage to bearing assembly of Santa-Clara River bridge during 1994 Northridge earthquake (Astaneh-Asl, 1994)	3
1-3	End cross frame gusset plate fracture in Pico-Lyons Overcrossing during 1994 Northridge earthquake (Astaneh-Asl, 1994)	3
1-4	Bearing stiffener damage in Pico-Lyons Overcrossing during 1994 Northridge earthquake (Astaneh-Asl, 1994)	4
1-5	Damage to girders of Hanshin Expressway during 1995 Hyogen-Nanbu earthquake (Public Works Research Institute of Japan, 1995)	5
1-6	Damage to girders and bracing of Hanshin Expressway during 1995 Hyogen-Nanbu earthquake (Public Works Research Institute of Japan, 1995)	5
1-7	Fractured lateral bracing and buckled cross frame in Capitol Arch bridge during 2001 Nisqually earthquake (WSDOT, 2001)	6
1-8	Damaged web stiffener in Capitol Arch bridge during 2001 Nisqually earthquake (WSDOT, 2001)	7
1-9	Typical X-brace cross frame shown at intermediate cross frame location	10
2-1	Four span (continuous), four girder prototype bridge	14
2-2	Four span (simply supported), two girder prototype bridge	14
2-3	Section through prototype bridge superstructure at end support	15
2-4	Section through prototype bridge at intermediate cross frame	15
2-5	Steel slab-on-girder bridge superstructure model.	16
2-6	Bridge model deck slab reinforcing	17
2-7	Steel plate girder bridge model - girder and deck slab dimensions	17
2-8	Typical intermediate cross frame in bridge model	18
2-9	Laminated elastomeric bearing	19
2-10	Lead rubber bearing with transverse restraints	19
2-11	“Heavy” end cross frames at the north end in the bridge model	21
2-12	“Heavy” end cross frames at the south end in the bridge model	22
2-13	“Heavy” end cross frames in the bridge model with welded connections	23
2-14	“Light” end cross frames in the bridge model	24
2-15	Unbonded brace in the bridge model	25
2-16	Lead rubber bearing	26
2-17	Actuator connected to bridge model at 1/3 points along length of bridge	27
2-18	Actuator displacements vs time for Experiment RSHXB	29
2-19	Actuator forces vs time for Experiment RSHXB	30
2-20	Actuator forces vs time for Experiment RSHXB2	30
2-21	Actuator forces vs time for Experiment RSNECF	31
2-22	Actuator forces vs time for Experiment RSNBC	31
2-23	Actuator forces vs time for Experiment RSFC	32
2-24	Actuator forces vs time for Experiment RSNCF	32
2-25	Actuator forces vs time for Experiment RSPC	33

## LIST OF FIGURES (CONT'D)

FIGURE	TITLE	PAGE
2-26	Actuator forces vs time for Experiment RSLXB	33
2-27	Bridge Model attached to three 50 ton shake tables	35
2-28	Acceleration time histories for a) 180 component and b) 270 component of El Centro	38
2-29	Acceleration time histories for a) 360 component and b) 90 component of Sylmar	39
2-30	Acceleration time histories for a) 00 component and b) 90 component of Kobe	40
2-31	Acceleration time histories for El Centro 180 component through soil layer	41
2-32	Theoretical earthquake response spectra (5% damping)	41
2-33	Earthquake response spectrum for 2.0 El Centro (5% damping)	42
2-34	STLRB - Response spectra for the target and achieved shake table accelerations at shake tables 1 and 3 in the longitudinal axis of the bridge model in response to 1.0 El Centro	42
2-35	STLRB - Response spectra for the target and achieved shake table accelerations at shake tables 1 and 3 in response to 1.0 Sylmar	43
2-36	STLRB - Response spectra for the target and achieved shake table accelerations at shake tables 1 and 3 in response to 1.0 Kobe	43
2-37	Multi-axial load cell during construction	45
2-38	Load cell axial calibration	45
2-39	Load cell calibration in shear	46
2-40	Instrumentation - load cells	47
2-41	Instrumentation - displacement transducers	48
2-42	Instrumentation - typical displacement transducers for end X-braces	49
2-43	Instrumentation - displacement transducers for unbonded braces	50
2-44	Instrumentation - accelerometers	51
2-45	Instrumentation - strain gages on end cross frames	52
2-46	Instrumentation - strain gages on typical intermediate cross frame	53
2-47	Instrumentation - additional strain gages on end stiffener	53
2-48	Instrumentation - strain gages on east girder	54
2-49	Instrumentation - strain gages on west girder	55
3-1	RSHXB - Deformed deck slab of bridge model during transverse loading	58
3-2	Transverse flexural cracking observed along the length of the bridge model propagating from the edges of the deck slab	58
3-3	Shear cracking observed in the end thirds of the deck slab at an angle of approximately 45 degrees to the longitudinal and transverse directions	59
3-4	RSHXB - Failure of shear stud at north end of bridge model	59
3-5	Removal of concrete for rehabilitation of shear studs at north end of bridge model	60
3-6	RSHXB2 - Onset of buckling in diagonal member of end X-brace	60
3-7	RSHXB2 - Deformation of bridge model at +133 kN	63
3-8	RSHXB2 - Deformation of bridge model at -133 kN	63
3-9	RSLXB - Deformation of single angle X-braces at the north end	63



## LIST OF FIGURES (CONT'D)

FIGURE	TITLE	PAGE
3-10	RSLXB - Deformation of bridge model at +133 kN	64
3-11	RSLXB - Deformation of bridge model at -133 kN	64
3-12	RSLXB - Deformation of bridge model at -320 kN	64
3-13	STLRB - Transfer function amplitude for transverse accelerometers at deck slab level	66
3-14	STLRB - Transfer function amplitude for transverse accelerometers above bearings	66
3-15	STLRB - Transfer function amplitude for vertical accelerometers at deck slab level	67
3-16	STLRB - Mode shape for first transverse mode from Fourier analysis	68
3-17	STLRB - Mode shape for second transverse mode from Fourier analysis	68
3-18	STLRB - Mode shape for third transverse mode from Fourier analysis	68
3-19	STLRB - Average shake table displacement time history	70
3-20	STLRB - Amplification factor for displacements at the deck slab of bridge model for sine sweep excitation	70
3-21	STLRB2S - Transfer function amplitude for transverse accelerometers at deck slab level	71
3-22	STLRB2S - Mode shape for first transverse mode from Fourier analysis	71
3-23	STLXB - Transfer function amplitude for transverse accelerometers at deck slab level	73
3-24	STLXB - Transfer function amplitude for transverse accelerometers above bearings	73
3-25	STLXB - Transfer function amplitude for vertical accelerometers at deck slab level	74
3-26	STLXB - Mode shape for first transverse mode from Fourier analysis	75
3-27	STLXB - Mode shape for second transverse mode from Fourier analysis	75
3-28	STLXB - Mode shape for third transverse mode from Fourier analysis	75
3-29	Effect of shear studs removed by through the deck slab around the studs	76
3-30	STPUB - Transfer function amplitude for transverse accelerometers at deck slab level	77
3-31	STPUB - Mode shape for first transverse mode from Fourier analysis	77
3-32	STFUB2S - Transfer function amplitude for transverse accelerometers at deck slab level	78
3-33	STFUB2S - Mode shape for first transverse mode from Fourier analysis	78
3-34	STNECF - Transfer function amplitude for transverse accelerometers at deck slab level	79
3-35	STNECF - Mode shape for first transverse mode from Fourier analysis	79
3-36	STHXB - Transfer function amplitude for transverse accelerometers at deck slab level	80
3-37	STHXB - Mode shape for first transverse mode from Fourier analysis	80
3-38	Finite element model of bridge model in SAP2000	81
3-39	FEPUB - Mode shape for first transverse mode from Fourier analysis	86

## LIST OF FIGURES (CONT'D)

FIGURE	TITLE	PAGE
3-40	FEPUB - Mode shape for first transverse mode from Ritz vector analysis	86
3-41	FEPUB - Mode shape for second transverse mode from Fourier analysis	86
3-42	FEPUB - Mode shape for second transverse mode from Ritz vector analysis	87
3-43	FEPUB - Mode shape for third transverse mode from Fourier analysis	87
3-44	FEPUB - Mode shape for third transverse mode from Ritz vector analysis	87
4-1	RSHXB - Hysteresis loop for north actuator (first amplitude cycles)	92
4-2	RSHXB - Hysteresis loop for south actuator (first amplitude cycles)	92
4-3	RSHXB - Hysteresis loop for north actuator	93
4-4	RSHXB - Hysteresis loop for south actuator	93
4-5	RSHXB - Elastic modulus and Shear modulus for deck slab of finite element models to correlate with experiment	95
4-6	RSHXB - Envelopes for transverse midspan deck slab displacement for experimental and finite element models	95
4-7	RSHXB - Envelopes for transverse midspan deck slab rotation for experimental and finite element models	96
4-8	RSHXB - Deck displacements along the length of the bridge model at different amplitudes for experimental and finite element models	96
4-9	Transformed equivalent steel section for bridge model with gross deck slab properties	98
4-10	Transformed equivalent steel section for I/Ig of the deck slab equal to 40% to allow for shrinkage cracking	98
4-11	Stress, strain and force distribution in deck slab of bridge model	98
4-12	Transformed equivalent steel section for bridge model assuming a fully cracked section in tension, I/Ig for the deck slab = 33%	99
4-13	RSHXB2 - Strain gages at midspan	100
4-14	Different stud models considered for bridge model	102
4-15	Cracks observed in haunch of bridge model around shear stud location	103
4-16	Elastic modulus vs shear stud stiffness for midspan displacement in finite element model correlated to measured displacement in bridge model	104
4-17	Displacements from finite element model normalized to measured displacements for different shear stud models	104
4-18	RSHXB - Actuator forces versus time	106
4-19	Transverse shear stud forces in bridge model from finite element model	106
4-20	Longitudinal shear stud forces in bridge model from finite element model	108
4-21	Axial shear stud forces in bridge model from finite element model	110
4-22	Analysis of shear flow in girders of bridge model	111
5-1	RSHXB2 - Estimated forces in end and intermediate cross frames for different total applied actuator forces	114
5-2	RSLXB - Estimated forces in end and intermediate cross frames for different total applied actuator forces	114

## LIST OF FIGURES (CONT'D)

FIGURE	TITLE	PAGE
5-3	STLXB - Estimated forces in end and intermediate cross frames for different earthquake levels	115
5-4	CNEXF - End shear force versus horizontal end displacement	117
5-5	RSNBC - End shear force versus horizontal end displacement	117
5-6	RSFC - End shear force versus horizontal end displacement	118
5-7	RSNCF - End shear force versus horizontal end displacement	118
5-8	RSPC - End shear force versus horizontal end displacement	119
5-9	RSPC, RSNECF - Comparative end hysteresis loops at north end	119
5-10	RSPC, RSNECF - Comparative end hysteresis loops at south end	120
6-1	Model of end of typical girder	123
6-2	Torsional girder deformations	125
6-3	Deformed finite element model of end girder segment for bridge model	127
6-4	Shear stud deformations	129
6-5	Effective section required to carry gravity loads and remaining flange width for seismic forces	138
6-6	Deformed end cross frame region of bridge model with gap opening between the deck slab and girders	138
6-7	Bearing stiffener bending moments	140
6-8	Continuous bridge girder	140
7-1	STNECF - Measured bending moments in base of bearing stiffener at north end in response to 0.25 - 1.0 El Centro compared with theoretical bearing bending moment	147
7-2	Deformation of elastomeric bearing with rotation applied to bearing in bridge model	148
7-3	RSLXB - Axial bearing forces at the north end for first five cycles	149
7-4	RSLXB - Axial bearing forces at the south end for first five cycles	149
7-5	Axial forces in bearings as a result of transverse force and overturning moment	150
7-6	RSNCF - Axial bearing forces at the north end	151
7-7	RSNCF - Axial bearing forces at the south end	151
7-8	Axial forces in restrained bearings as a result of transverse force and overturning moment from shake table experiments	152
7-9	STHXB - Axial bearing forces at the north end for 2.0 El Centro (NE load cell faulty)	153
7-10	STHXB - Axial bearing forces at the south end for 2.0 El Centro	153
7-11	STNECF - Axial bearing forces at the north end for 1.0 El Centro (NE load cell faulty)	154
7-12	STNECF - Axial bearing forces at the south end for 1.0 El Centro	154
7-13	Axial forces in isolator bearings as a result of transverse force and overturning moment from shake table experiments	155
7-14	STLRB - Axial bearing forces at the north end for 2.0 El Centro	155

## LIST OF FIGURES (CONT'D)

FIGURE	TITLE	PAGE
7-15	STLRB - Axial bearing forces at the south end for 2.0 El Centro	156
7-16	STLRB - Axial bearing forces at the north end for 2.0 El Centro in the longitudinal direction	158
7-17	STLRB - Axial bearing forces at the south end for 2.0 El Centro in longitudinal direction	158
7-18	RSHXB2 - Transverse shear forces in bearings	160
7-19	RSLXB - Transverse shear forces in bearings	160
7-20	STHXB - Transverse shear forces in bearings in response to 2.0 El Centro	161
7-21	STLXB - Transverse shear forces in bearings in response to 2.0 El Centro	161
7-22	RSHXB2 - End shear forces measured in the load cells	163
7-23	STLXB - End shear forces measured by the load cells in response to 2.0 El Centro	163
7-24	STUB2S - End shear forces measured by the load cells in response to 0.5 El Centro	164
8-1	Illustration of simplified non-linear analytical model of bridge	166
8-2	RSHXB1 - Backbone curve for displacement of deck slab at midspan	168
8-3	RSHXB1 - Backbone curve for rotation of superstructure at midspan	168
8-4	RSHXB1 - Degradation in the effective moment of inertia and torsion constant for the bridge model during the first experiment	169

## LIST OF TABLES

TABLE	TITLE	PAGE
2-1	Reversed Static Experiments	28
2-2	Shake Table Experiments	36
2-3	Earthquake Data for Shake Table Experiments	37
3-1	Relative End to Midspan Displacement for Different Reversed Static Experiments	62
3-2	Natural Periods and Flexibility Coefficient for Bridge Model Isolated with Lead Rubber Bearings	65
3-3	Natural Periods and Flexibility Coefficient for Bridge Model with Different End Cross Frames	72
3-4	RSHXB2 - Comparison of Finite Element and Experiment Results for Total Applied Actuator Force of approximately 133 kN	83
3-5	RSNECF - Comparison of Finite Element and Experiment Results for Total Applied Actuator Force of approximately 133 kN	84
3-6	RSLXB - Comparison of Finite Element and Experiment Results for Total Applied Actuator Force of approximately 133 kN	85
3-7	Natural Periods for Three Transverse Modes of Detailed Finite Element Model	88
3-8	Modal Mass Participation Factors for Three Transverse Modes of Detailed Finite Element Model	88
5-1	End Stiffnesses from Reversed Static Experiments	116
5-2	Effective Elastic Contribution of Different Components to Transverse Stiffness for Heavy X-Brace Cross Frames	120
5-3	Effective Elastic Contribution of Different Components to Transverse Stiffness for Light X-Brace Cross Frames	121
6-1	Parametric Study on Transverse Stiffness of Simply Supported Girder	128
6-2	Parametric Study of Transverse Stiffness and Bending Moments at the End of a Girder	132
6-3	Parametric Study of Transverse Stiffness and Bending Moments at an Intermediate Support of a Continuous Girder	142
7-1	Ratio of measured maximum axial load to calculated maximum axial load in bearings for selected experiments	157
8-1	Natural Periods for Three Transverse Modes of Simplified Analytical Model	171
8-2	Modal Mass Participation Factors for Three Transverse Modes of Simplified Analytical Model	171



## LIST OF SYMBOLS

$a$	Girder property constant
$A$	Acceleration coefficient
$A_b$	Bonded rubber area
$A_c$	Area of lead core
$A_f$	Area of flange
$A_g$	Cross sectional area of girder
$A_i$	Total bearing rubber area less area of core
$A_r$	Overlapping bonded rubber area at large displacements
$A_s$	Cross sectional area of shear stud connector
$A_t$	Total bearing rubber area
$A_w$	Area of web
$b$	Width of plate
$b_d$	Width of deck slab
$b_{efb}$	Remaining effective width at edge of flange after consideration of gravity loads
$b_{fb}$	Width of bottom flange
$b_{ws}$	Width of web stiffeners
$B$	Damping coefficient
$B_c$	Width (diameter) of lead core
$B_b$	Bonded bearing rubber width (diameter)
$B_t$	Total bearing width (diameter)
$d_{gf}$	Girder depth (between centroid of flanges)
$d_i$	Displacement of ductile end cross frame / isolation bearing
$e$	Eccentricity between centroid of deck and shear center
$E$	Elastic modulus
$E_b$	Effective elastic modulus for rubber layer
$f_b$	Factor for bending stiffness of bearing
$f_c'$	Concrete strength
$f_{unft}$	Normal stress in top flange
$f_{uvft}$	Shear stress in top flange
$F_{bg}$	Shear force and the base of the girder
$F_d$	Design force
$F_{tg}$	Shear force and the top of the girder

$F_y$	Nominal yield stress
$F_y$	Yield force
$F_{yb}$	Nominal yield strength of bottom flange
$g$	Acceleration due to gravity
$G$	Shear modulus
$G_l$	Shear modulus of lead
$h_{eff}$	Effective height between bearings and center of mass (or actuator load)
$H$	Bearing height
$I$	Moment of inertia
$I_b$	Effective moment of inertia of bearing
$I_{fb}$	Moment of inertia of bottom flange
$I_{gy}$	Moment of inertia for girder about vertical axis
$I_s$	Moment of inertia for shear stud
$I_y$	Effective moment of inertia about vertical axis
$I_{ws}$	Moment of inertia for web stiffener about its strong axis
$J$	Torsion constant
$J_f$	Flange torsion constant
$J_{ft}$	Top flange torsion constant
$J_g$	Girder torsion constant
$k_a$	Axial stiffness
$\bar{k}$ $k_{bar}$	Rubber constant
$k_b$	Effective flexural stiffness of shear stud
$k_{da}$	Design (post-yield) axial stiffness
$k_{di}$	Design (post-yield) stiffness of individual ductile end cross frame / isolation bearing
$k_{effi}$	Effective (secant) stiffness of ductile end cross frame / isolation bearing
$k_l$	Shear stiffness of lead core
$k_s$	Effective shear stiffness of shear stud
$k_s$	Shear stiffness of bearing
$k_{st}$	Total shear stud stiffness
$k_t$	Effective transverse stiffness of girder
$k_{tb}$	Effective transverse stiffness of girder due to flexure
$k_{tt}$	Effective transverse stiffness of girder due to torsion
$k_u$	Initial stiffness



$k_{\theta b}$	Rotational stiffness of bearing
$k_{\theta g}$	Torsional stiffness of girder between end and first intermediate cross frame
$k_{\theta s}$	Effective rotational stiffness of a collection of studs at each web stiffener
$K_g$	Equivalent transverse girder stiffness
$l$	Length of member
$l_s$	Distance along girder between bearing stiffener and first row of shear studs
$L$	Length of bridge span
$L_1$	Length of girder between end and first intermediate cross frame
$L_s$	Clear length of shear stud
$L_{seff}$	Effective length for bending of shear stud
$M_{efb}$	Maximum girder flange bending moment due to transverse displacement at top of girder resulting from earthquake loads
$M_f$	Maximum girder flange bending moments due to torsion
$M_{nfb}$	Nominal residual capacity of bottom flange for seismic loads after consideration of gravity loads
$n$	ratio of $E_{steel}$ to $E_{concrete}$
$n_g$	Number of girders
$n_r$	Number of rubber layers in bearing
$n_s$	Number of studs in a transverse row
$P_b$	Bearing axial load
$P_{cro}$	Critical buckling load for small displacements
$P_{cr}$	Critical buckling load for large displacements
$P_e$	Euler buckling load
$P_u$	Ultimate axial force
$Q$	Shear flow between deck slab and girders
$Q_{di}$	Characteristic strength of individual ductile end cross frame / isolation bearing
$r_i$	Distance from the center of rotation to the center of shear stud
$R$	Shear stiffness per unit height
$s_g$	Spacing between the girders
$S$	Site coefficient
$S$	Shape factor for rubber layers
$t$	Thickness of plate
$t_c$	Thickness of cover in bearing

$t_d$	Thickness of deck slab
$t_i$	Individual rubber layer thickness
$t_{fb}$	Thickness of bottom flange
$t_p$	Thickness of top and bottom plates
$t_s$	Thickness of shims
$t_w$	Thickness of web
$t_{ws}$	Thickness of web stiffener
$T_{eff}$	Effective period
$T_f$	Torque in the girder flange
$T_g$	Torque applied to girder
$T_r$	Total rubber thickness
$T_s$	Total shim thickness
$T_{usr}$	Ultimate torsional resistance of a row of studs
$V$	Shear force in cross section
$V_e$	Shear force at support of bridge
$W_i$	Weight per bearing
$x_g$	Horizontal distance from centroid of section to centroid of girder
$\bar{y}_g$	Horizontal distance from centroid of deck slab to girders
$\alpha$	Superstructure displacement to overall displacement ratio
$\beta_i$	Equivalent viscous damping of end cross frame / isolation bearing
$\delta$	Overlap factor
$\Delta_t$	Transverse displacement at the top of girder
$\gamma_c$	Shear strain due to axial loads
$\gamma_r$	Shear strain due to rotation from service loads
$\gamma_{r,eq}$	Shear strain due to rotation from seismic loads
$\gamma_{e,eq}$	Shear strain due to shear from seismic loads
$\theta_b$	Rotation at bottom of girder
$\theta_g$	Average rotation at end of girder
$\theta_s$	Rotation at top of girder
$\rho$	Girder stiffness parameter
$\tau_y$	Yield shear strength of lead

# SECTION 1 INTRODUCTION

## 1.1 Overview

Highway bridges with concrete superstructures generally have diaphragms at the abutments and bents or piers which are monolithic with the deck slab and girders. As a result, transverse earthquake forces can be distributed from the deck slab to the substructure through the support diaphragms. In contrast to the monolithic nature of concrete superstructures, steel plate girder bridge superstructures consist of a number of distinct components. The interaction and subsequent design of the various superstructure components is generally well understood for gravity loads, but not so well known for seismic loads. In the past it has been assumed that seismic forces transferred by the superstructure will be below levels that cause inelastic response of the critical superstructure components. However, recent moderate to large earthquakes have shown that this assumption is invalid and damage to superstructures has been observed in steel bridges (Astaneh-Asl, 1994; Shinozuka, 1995; Bruneau, 1996). Consequently, it is necessary to understand the load path through steel plate girder bridges and once the critical components have been identified then these components can be designed accordingly.

## 1.2 Typical Steel Plate Girder Bridges

The focus of this study is on straight steel plate girder bridges both as a series of simply supported spans or continuous spans. The effect of large skews and curvature on these bridges is outside the scope of this study, although many of the concepts will still apply. The typical properties of steel plate girder bridges of the type considered in this study are described below. The deck slab is typically constructed from insitu reinforced concrete and is connected to the steel plate girders through shear connectors. The shear connectors are typically stud type connectors using Nelson Headed Studs (TRW Nelson Division, 1988). The steel girders are usually built-up from stiffened steel plates. Vertically oriented cross frames or diaphragms are typically placed between the steel girders and can be designed using a number of configurations, such as the K-brace configuration shown in Figure 1-1. Lateral bracing, placed between the girders and connected to the bottom flanges in a horizontal plane, is not considered in this study. The connection between the superstructure and the substructure is considered to be made through some type of thermal expansion bearing (elastomeric bearings in this study). Integral bent caps and abutments are not considered.

## 1.3 Seismic Performance of Steel Plate Girder Bridges During Previous Earthquakes

Steel plate girder bridges have generally suffered minor to moderate damage in past earthquakes compared to the significant damage suffered by structural concrete bridges. Nevertheless these earthquakes have identified some design deficiencies in steel girder bridges. Damage due to movement of steel girder bridge superstructures in the longitudinal direction was generally confined to restrainer damage and localized spalling at joints during previous earthquakes. Complete collapse of a steel girder bridge superstructure span was rare, with the notable example of the collapsed deck span of the San-Francisco-Oakland Bay Bridge during the 1989 Loma Prieta earthquake. Damage to abutments, joints and restrainers, and the required seat width to prevent collapse of a bridge span is outside the bounds of this study. Instead, the focus of this study is on



**FIGURE 1-1 Typical K-brace cross frame**

the transverse response of steel plate girder bridges, which accounts for most of the damage observed in steel plate girder bridge superstructures during past earthquakes.

In 1992 a series of three earthquakes, of magnitudes 7.0, 6.0 and 6.5 respectively, were recorded in a 24 hour period near the town of Petrolia in Northern California (CALTRANS, 1992). During these earthquakes there was notable damage to two steel plate girder bridges. In the Southbound Van Duzen River bridge, a straight steel plate girder bridge, buckling was reported in the end cross frames and lateral bracing. In addition there was also spalling of concrete observed in the connection between the reinforced concrete deck slab and the steel girders indicating insufficient shear connectors in the region. The South Fork Eel River bridge was also damaged during these earthquakes. The curved steel plate girder bridge suffered considerable damage at the hinge locations and buckling and fracture of the end cross frames resulting in loss of service load capacity. These earthquakes highlighted the importance of composite action between the deck slab and the girders in the seismic load path. They also identified the end cross frames and connected components as critical in the transverse load path.

During the 1994 Northridge earthquake structural damage to several steel plate girder bridges was reported (Astaneh-Asl, 1994). Most of these bridges were located on Interstate 5 near the center of Newhall in Southern California. This is the region where the rupture of the hidden thrust fault would have projected to the surface. The nearest record at Newhall registered a peak ground acceleration of 0.63g and 0.62g in the horizontal and vertical components respectively. Typical damage included failure of bearing assembly at the abutments and bent caps, as shown in Figure 1-2. Observed bearing damage coupled with relatively small seat widths, based on modern standards, caused the potential for unseating of the superstructure in some of these bridges. Other damage in the superstructure included buckling of end cross frames or fracture of the connections between the end cross frames, gusset plates and web stiffeners as shown in Figure 1-3. In the case of the Pico-Lyons over-crossing there was no positive connection between web or bearing stiffeners and the bottom flange of the girders at the end cross frame locations. As a result, the



**FIGURE 1-2 Damage to bearing assembly of Santa-Clara River bridge during 1994 Northridge earthquake (Astaneh-Asl, 1994)**

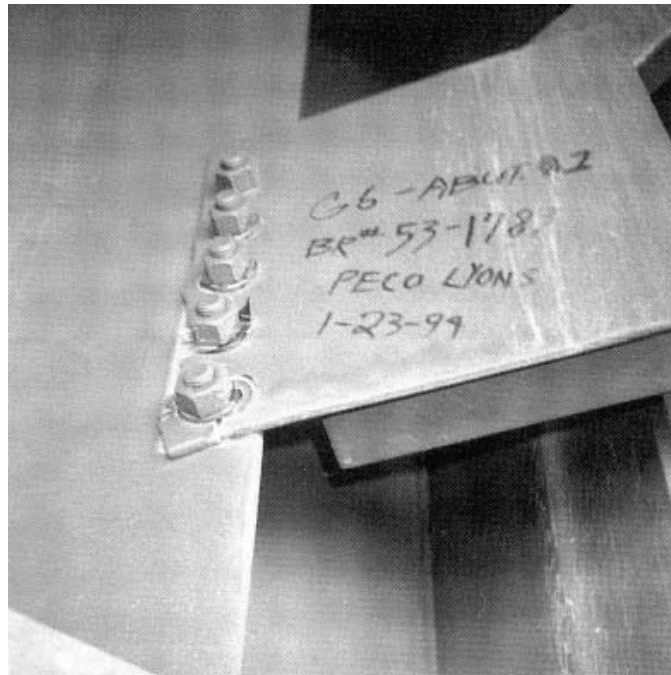


**FIGURE 1-3 End cross frame gusset plate fracture in Pico-Lyons Overcrossing during 1994 Northridge earthquake (Astaneh-Asl, 1994)**



**FIGURE 1-4 Bearing stiffener damage in Pico-Lyons Overcrossing during 1994 Northridge earthquake (Astaneh-Asl, 1994)**

web was damaged at the termination of the weld between the web and the stiffener as illustrated in Figure 1-4. For these bridges there was minimal observed damage to the columns and piles indicating that much of the displacement demand was accommodated in the superstructure of each of these bridges.

The 1995 Hyogoken-Nanbu earthquake in Kobe, Japan caused a large amount of damage to steel plate girder bridges. The concentration of steel bridges in the area was much larger than for any other previous earthquake and therefore the vulnerability of aspects of these bridges was highlighted. Damage was suffered to many steel columns, bearings, seismic restrainers, and superstructure components (Bruneau, 1996; Chung, 1996; Shinozuka, 1995). The assumption that steel girder bridges, much lighter than their concrete counterparts, would be immune to substructure failure was erased as there were numerous, sometimes non-ductile, substructure failures. These were similar to observed failures in past earthquakes (Priestley, 1996). Steel substructures were also damaged with buckling and sometimes fracture of the steel column bents. There was also severe damage observed in the superstructure of these bridges due to bearing failures and overload of end cross frames and diaphragms. Figure 1-5 shows localized torsional deformations of the girders as a result of bearing damage. This is further illustrated in Figure 1-6 where the bearings have failed causing the whole superstructure to translate laterally except at one exterior girder. The resistance of one girder caused twisting of the girder and buckling of the lateral bracing. It was also observed that the column bent at this location had no apparent damage, therefore, deformation in the superstructure appeared to protect the substructure.

The Kobe earthquake emphasized the importance of the end cross frames and girders in the transverse seismic load path. However, Figure 1-6 shows the ability for these girders to undergo



**FIGURE 1-5 Damage to girders of Hanshin Expressway during 1995 Hyogen-Nanbu earthquake (Public Works Research Institute of Japan, 1995)**



**FIGURE 1-6 Damage to girders and bracing of Hanshin Expressway during 1995 Hyogen-Nanbu earthquake (Public Works Research Institute of Japan, 1995)**

large deformations. If these deformations are limited to levels that prevent permanent damage with the use of special ductile end cross frames, it is apparently possible to protect the substructure of a steel bridge using these superstructure components.

Some damage to steel plate girder bridges was also observed during the 2001 Nisqually Earthquake in Washington. Similar damage was observed to that in Northridge and Kobe earthquakes with damage to the end cross frames and bearing stiffeners (EERI, 2001). Examples of damage to the Capitol Arch bridge are shown in Figures 1-7 and 1-8. Although damage was minor and confined to a few bridges, the level of ground shaking during this earthquake was relatively low, therefore much more damage might have been expected during a larger event.

From these past earthquakes, the critical elements in the seismic load path for a steel plate girder bridge superstructure identified are:

- Shear studs or connection between the deck slab and the girders;
- End cross frames or diaphragms;
- Girders and bearing stiffeners, and;
- Bearings.



**FIGURE 1-7 Fractured lateral bracing and buckled cross frame in Capitol Arch bridge during 2001 Nisqually earthquake (WSDOT, 2001)**





**FIGURE 1-8 Damaged web stiffener in Capitol Arch bridge during 2001 Nisqually earthquake (WSDOT, 2001)**

#### **1.4 Previous Research into Seismic Load Path**

Previous research has given further insight into the transverse seismic load path through analytical studies (Astaneh-Asl, 1996; Itani, 1996; Zahrai, 1998). This research highlighted the importance of end cross frames, particularly, in the transverse seismic response of the bridge while showing that intermediate cross frames have a limited role. This is consistent with the observed behavior during recent earthquakes.

#### **1.5 Seismic Design of Bridges**

##### **1.5.1 Specifications**

The seismic design of highway bridges is still a relatively immature field. The AASHTO LRFD Specifications for the Design of Highway Bridges (AASHTO, 1998) specify procedures for calculating the elastic seismic demand on a bridge then modifying the elastic demand using response modification factors. This is a force based design methodology. The substructure can then be detailed to allow for the necessary ductility capacity with some minimum requirements provided for these details. More thorough criteria for detailing the ductile components in a bridge in response to moderate to large magnitude earthquakes is given in the CALTRANS Seismic Design Criteria (CALTRANS, 2001). These criteria again assume that inelasticity will occur in the substructure.

While a ductile substructure is allowed for, the bridge design specifications provide little guidance for the seismic design of components in a steel plate girder bridge superstructure. AASHTO (1998) states that:

“The Engineer shall demonstrate that a clear, straightforward load path to the substructure exists and that all components and connections are capable of resisting the imposed load effects consistent with the chosen load path.”

It goes on to identify critical components including the girders, slab-to-girder interface, end cross frames and the bearing assembly, stating that they should be designed to remain elastic. ATC 32 (ATC, 1996) for the design of California bridges identifies the same components as critical in the seismic load path. It distinguishes between deck slabs which are able to carry diaphragm action and those that are not and therefore require intermediate cross frames and bottom flange lateral bracing to contribute in the transverse load path. The ATC/MCEER specifications (ATC/MCEER, 2003) also has similar provisions for the seismic load path, although, this document recognises that members in the superstructure can be designed to be ductile, which is a departure from the previous specifications.

The most recent specifications in Japan have provided additional detail for the design of steel girder bridge superstructures (PWRI/CRL, 2002), such as recommendations for the design of end cross frames or diaphragms. As with the AASHTO and ATC specifications, they are intended to promote elastic response of the superstructure. PWRI/CRL (2002) also provide considerable guidance for evaluating the forces on the bearings and to prevent excessive bearing displacements.

The components damaged during past earthquakes compares well to the components identified for seismic design in these standards. If the standards are applied appropriately damage to new bridges should be reduced, however, there is still much uncertainty in the design practice. This is perhaps because the specifications are typically vague in expressing the need to evaluate the load path. Consequently, typical design procedures for the critical components in the transverse load path do not often consider seismic loading. The typical design and current state of research for each of the critical components is discussed in the following sections.

### **1.5.2 Connection between the Deck Slab and the Girders**

The deck slab of a steel plate girder bridge is generally connected to the girders through shear connectors, which can be channel type connectors, but more commonly stud type connectors are used. Using AASHTO (1998) the shear connectors are designed for two limit states, fatigue during live loading, and strength based on the capacity of the deck slab. Generally the fatigue limit state, based on research by Slutter and Fisher (1967), governs the design. Therefore, the number of shear connectors required for full composite action based on the strength limit state is more than adequate. The strength of shear studs in composite beams has been studied by many researchers including Slutter and Driscoll (1965), Ollgaard et al. (1971), Oehlers and Johnson (1987), Lloyd and Wright (1990), Oehlers (1995), and others. Consequently, the strength of shear studs is well understood and the codes reflect much of this research. Procedures for design of Nelson Headed Anchor studs are also given by the manufacturers of the studs (TRW Nelson Division, 1977; 1988).

The reversed static behavior of shear studs has also been studied (Gattesco, 1996; Seracino, 2001), although loading was unidirectional, as for reversed static gravity loads, not fully reversed as in earthquake loading. These studies showed that the reversed static behavior tends to degrade the strength and stiffness of shear connectors reducing the composite behavior of beams over time. The seismic effects on shear studs were investigated by Hawkins and Mitchell (1984). They showed that the failure mode of a stud greatly affects its ductile performance. A concrete failure tends to be quite brittle while a failure of the steel section tends to be much more ductile. This paper also showed that the stiffness of the shear studs tended to degrade on application of repeated loading. The effect of placing a cone around shear studs in order to unconfine part of the studs and allow it to deform in a more ductile manner was investigated by McMullin and Astaneh-Asl (1994). This was shown to be quite successful at improving the ductile behavior of the shear studs.

As fatigue typically governs the design, the required number of shear studs for strength limit states in a fully composite beam are typically exceeded in new bridges. However, many older bridges have fewer shear connectors and are therefore only partially composite. For partially composite beams the force transferred between the concrete slab and the steel beam is dependent on the stiffness of the connection between the slab and girders. There have been many studies into the partial composite action in beams with details described in the following chapters.

### **1.5.3 Design of Cross Frames and Diaphragms**

Cross frames or diaphragms are placed transversely between the girders in a steel plate girder bridges. While the terms cross frames and diaphragms are often used interchangeably to describe these members, AASHTO (1998) defines cross frames as transverse truss components between the girders, and diaphragms are defined as a transverse flexural components between the girders. These definitions are used in this report, with members acting primarily with axial actions defined as cross frames, while members with flexural actions are defined as diaphragms. In general the term cross frame is used as most components described resist transverse loading with axial actions.

End cross frames are defined as those at the end of each span including those located at intermediate supports in a multi-span bridge. Intermediate cross frames are defined as those located along a span between the supports. Typical configurations for end cross frames include X-braces, as illustrated in Figure 1-9, and Chevron or K-braces, as illustrated at the intermediate cross frame locations in Figure 1-1. X-braces are generally designed with single angle diagonals, sometimes with and without single or double angle top and bottom chords. K-braces typically use double angle diagonal members connected to a top chord or bottom chord. These cross frames resist transverse loads with axial forces in the diagonal members. Typical diaphragms include relatively rigid diaphragms using sections with depths similar to that of the girders, as illustrated as part of the column bents in Figure 1-1. Channel sections are also used and connected to the web or bearing stiffeners of the girders. The lateral resistance of channel diaphragms is based on framing action with the bearing stiffeners and is therefore highly dependant on the connections and properties of the stiffeners.

A procedure for the design of cross frames in straight steel girder bridges is not well defined. In Section 6.7.4.1 of AASHTO, the requirements for the design of cross frames are summarized by:



**FIGURE 1-9 Typical X-brace cross frame shown at intermediate cross frame location**

- “The need for diaphragms and cross frames shall be investigated for all stages of assumed construction procedures and the final condition.”
- “This investigation should include, but not be limited to, the following:
  - Transfer of lateral wind loads from the bottom of the girder to the deck slab and from the deck slab to the bearings,
  - Stability of the bottom flange for all loads when in compression,
  - Stability of the top flange in compression prior to curing of the deck, and
  - Distribution of vertical dead and live loads applied to the structure.”
- “If the permanent cross-frames or diaphragms are included in the structural model used to determine force effects, they shall be designed for all applicable limit states for the calculated force effects.”

In considering the above requirements, investigation of wind loads typically requires relatively small cross frames, if any, to distribute loads from the bottom flange. Often the exterior girder can be efficiently designed so that they are not necessary. The stability of the flanges is one important consideration for cross frame design. For stability of the bottom flange, cross frames are only necessary in negative moment regions of continuous girders and usually require relatively small members. Stability of the top flange is generally only necessary during construction and for this purpose the cross frames can be designed as temporary members. Cross frames have also been shown to have minimal effect in the distribution of vertical dead and live load between the girders as the deck slab effectively plays this role. This resulted in the Guide Specifications for Distribution of Loads for Highway Bridges (1994), which neglect the presence of cross frames. Using AASHTO (1998) distribution factors are calculated neglecting the presence of cross frames, although, a check is performed assuming a rigid cross section. These can be considered lower and upper bounds without the size of the cross frame members being considered. The mandatory requirement of cross frames spaced at 7.6 m in the Standard Specifications (AASHTO, 1996) has been removed from the LRFD Specifications (AASHTO, 1998).

A further role in which cross frames are important, although not included in Section 6.7.4.1 of AASHTO, is during the event of an impact due to an over height vehicle under a bridge. Cross frames are able to distribute the impact loads from the bottom flange of the exterior girder to some or all of the other girders. The benefits of this are questionable due the trade-off between potentially considerable damage to a single girder without cross frames or lesser damage to a larger number of girders with cross frames. Moreover collisions between cross frames have been shown to result in plastic deformations while damage near cross frames has shown more brittle fractures (Mertz, 2001).

The number of potential design requirements for cross frames, with no clearly quantified requirement has generated much uncertainty in their design. To clarify some issues, Mertz (2001) provides a good discussion of the need for intermediate cross frames and subsequent design recommendations for these. However, there was no consideration of cross frame design for seismic loads. During past earthquakes the end cross frames of many bridges sustained some damage indicating their importance in the transverse seismic load path. Itani and Rimal (1996) showed analytically that the end cross frames transferred the majority of the transverse seismic loading from the deck level into the substructure. The intermediate cross frames were shown to have minimal effect on the transverse seismic response. These observations were confirmed by Zahrai and Bruneau (1999). Therefore seismic loading should be considered to be one of the major design considerations for end cross frames of steel plate girder bridges in high seismic zones.

#### **1.5.4 Girders**

Seismic actions are not considered in the design of the girders in a steel plate girder bridge. In past earthquakes such as Kobe, which resulted in damage to the girders, the damage can be attributed to failure of other components particularly the bearings. Therefore assuming these components are appropriately designed for earthquake loading, the girders are likely to remain undamaged. The observed girder damage was shown to be concentrated at the ends of the girders. Bearing stiffeners at the ends of girders are generally designed for the gravity loads in order provide sufficient shear and bearing capacity in the web. However these are also necessary for connection of the end cross frames and therefore play a role in the transverse seismic load path. The Japanese specifications have recognised this and provide

#### **1.5.5 Bearings**

Although integral connections between the superstructure and substructure are becoming more common to avoid the use of bearings and maintenance issues associated with bridge joints, bearings are often required to allow for thermal effects. These are generally placed between the superstructure and the substructure at the column bents and abutments. There are a range of bearings used in steel plate girder bridges designed principally for thermal expansion. The different types of bearings include unreinforced and reinforced elastomeric bearings, flat and curved polytetrafluorethylene (PTFE) sliders, pot bearings; pin and rocker bearings, roller bearings and a few others (AISI, 1996). All of the different types of bearings have different force and displacement capacities associated with the different translational and rotational degrees of freedom.

### **1.5.6 Shortcomings of Current Seismic Design Provisions**

While AASHTO (1998) recognizes the importance of understanding the seismic load path through a bridge superstructure, and various critical components have been identified, seismic design procedures for these components is limited. The previous section showed that past design of superstructure elements is generally based on non-seismic criteria. These components should be designed based on capacity design principles so that the strength of each component is greater than the forces at the ultimate capacity of the ductile substructure, or maximum elastic seismic demand in the bridge.

### **1.6 Objectives and Scope**

The primary objective of this report is to study the transverse seismic load path through straight steel plate girder bridges experimentally using a single span scale model of a two girder bridge superstructure and corresponding analytical models. By studying the load path, the critical components are identified and seismic forces on these components quantified in order to establish more prescriptive design procedures for each component.

The study is limited to straight unskewed steel plate girder bridges and therefore the effect of skew and curvature on the seismic response is not considered. The girders are built-up I-girders. The response of the bridge is generally limited to excitation in the transverse direction with limited investigation of longitudinal excitation. No consideration of vertical excitation is made. The response of the bridge model with ductile components in the superstructure is described in another report (Carden, 2005).

## **SECTION 2 THE BRIDGE MODEL**

### **2.1 Introduction**

This chapter describes the preliminary analysis, design and construction of a twin girder, simply supported model of a slab-on-girder bridge superstructure, used in order to study the effects of earthquake loads on a typical straight steel plate girder bridge. The bridge model was based on a prototype bridge, scaled by a factor of  $2/5$ , as described below.

### **2.2 Four Girder Simply Supported Bridge Prototype**

The overall geometry of the bridge model was initially derived from a prototype bridge which, while not modeled on any particular real bridge, was designed to represent a typical straight, unskewed, multi-span bridge of this type. The prototype bridge was a four span, four girder bridge, as illustrated in Figure 2-1. The configuration and approximate section sizes for the main girders and the deck slab were provided by the California Department of Transportation (CALTRANS) (Duan, L., Private Communication), based on CALTRANS Bridge Design Specifications (CALTRANS, 1993), which are similar to the Load Factor Design procedure described in the AASHTO Standard Specifications (1996). The prototype bridge consisted of two 40.4 m end spans and two 48.8 m intermediate spans. The intermediate spans were supported by single column drop bent caps. The sizes of the main components in the composite superstructure were checked using an analysis based on the AASHTO LRFD (1998) specifications. Some thickening of the girder flanges was required near the column bents to accommodate the negative bending moments in the continuous girders. The structure was analyzed for typical gravity and wind loading.

Transverse earthquake loads were also considered using the CALTRANS analysis procedure (CALTRANS, 2001), whereby the displacement demand of the structure is determined based on an elastic analysis, which is compared to the displacement capacity of a proposed column from a cross sectional and pushover analysis. This resulted in 1.82 m diameter columns being proposed for each of the single column bents.

### **2.3 Two Girder Simply Supported Bridge Prototype**

For both economic reasons and benefits of simplicity, it was decided that the bridge model was to be a two girder, simply supported bridge superstructure. The transverse response of a two girder bridge was expected to be quite different to that of the four girder bridge as the transverse stiffness was considerably less. Consequently, a two girder bridge prototype was developed, as illustrated in Figure 2-2. The prototype was assumed to be a multispan bridge consisting of a series of simply supported 46 m spans. Two types of substructure were assumed. The first consisted of 1.52 m diameter single column bents, 7.92 m long with 1.82 m high bent caps, with properties calculated based on the same CALTRANS analysis procedure as for the columns of the 4 girder bridge. Alternatively a rigid substructure was also assumed, which could be in the form of abutments or relatively short piers founded on stiff soil.

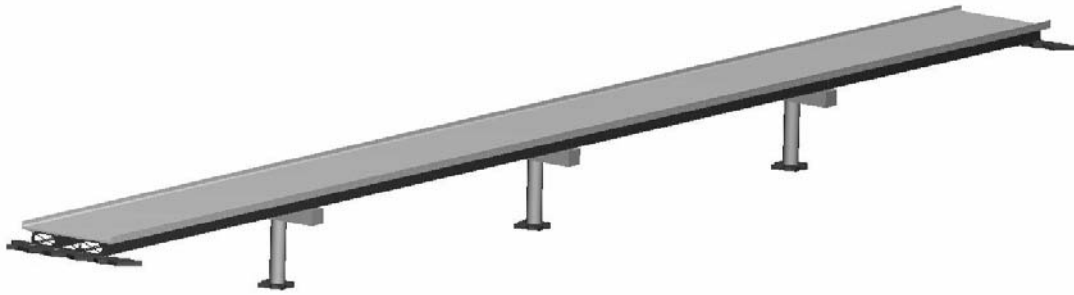


**FIGURE 2-1 Four span (continuous), four girder prototype bridge**



**FIGURE 2-2 Four span (simply supported), two girder prototype bridge**

The superstructure was assumed to consist of two steel plate girders, spaced of 3.35 m apart, with a 219 mm thick reinforced concrete deck slab, as shown in Figure 2-3. It was assumed that cross frames were placed every 7.62 m along the length of the bridge, which is the specified spacing in the AASHTO Standard Specifications (1996) and considered typical in most current bridges, although the AASHTO LRFD (1998) specifications do not specify a minimum spacing.

## **2.4 Design of Bridge Model**

### **2.4.1 Overview**

The steel plate girder bridge superstructure model used for experiments in this study is shown in Figure 2-5. The overall dimensions of the model were scaled down directly by a factor of  $\frac{2}{5}$  from the two girder bridge prototype described in the previous section. Other aspects such as the deck



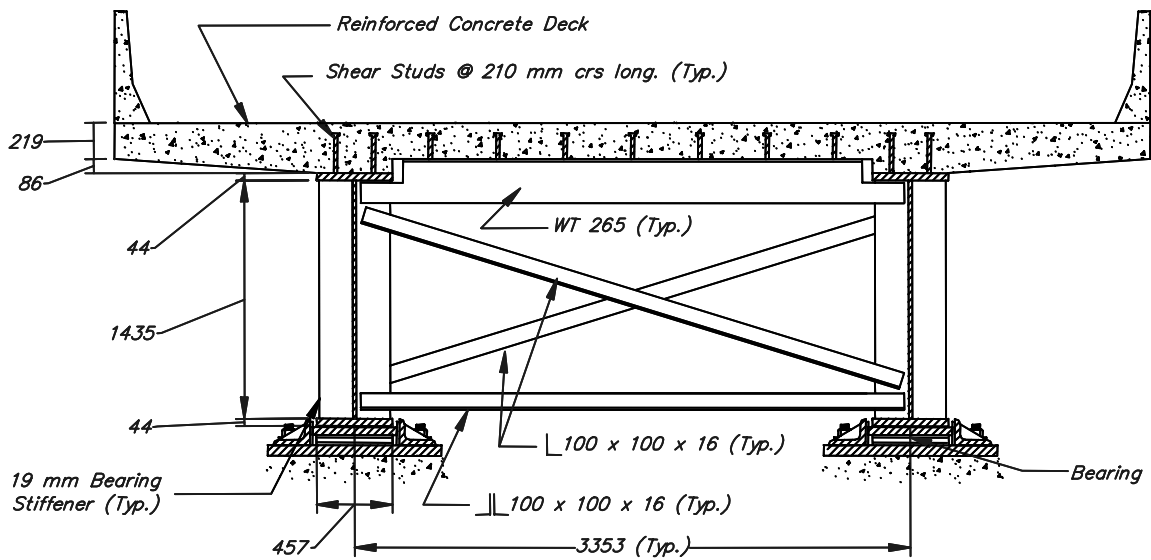


**FIGURE 2-3 Section through prototype bridge superstructure at end support**

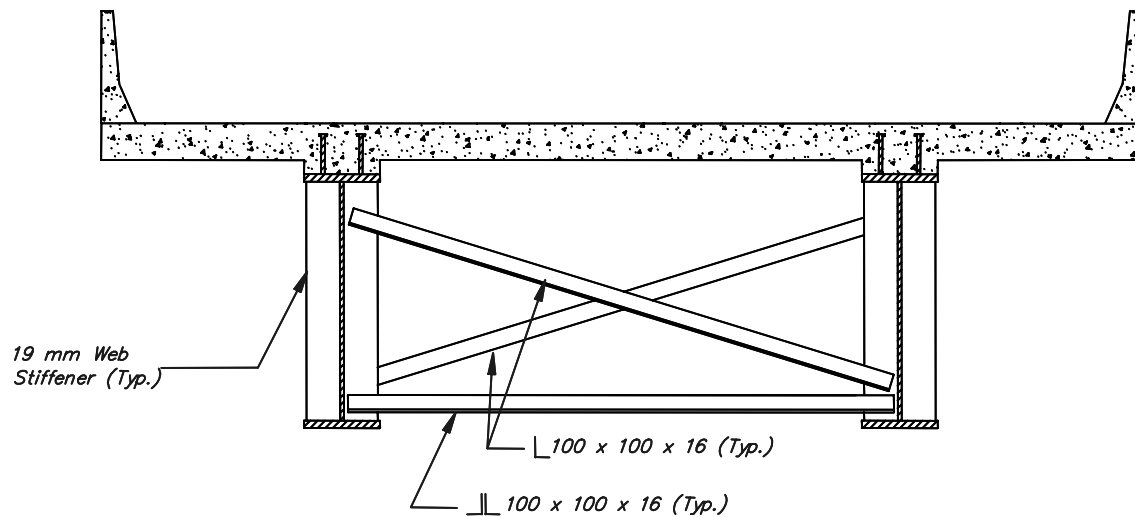


**FIGURE 2-4 Section through prototype bridge at intermediate cross frame**

slab reinforcing, cross frames, shear studs and bearings were designed specifically for the bridge model, based on forces scaled from the prototype bridge. The design of each component is discussed in the following sections. Further details for the design of the bridge model are described by Garcia-Alvarez (2001).

## 2.4.2 Girders

The overall girder dimensions for the bridge model were scaled down from the two girder prototype. This resulted in 18.2 m long girders with cross sectional properties as shown in Figure 2-6. The webs and flanges were built-up from plates which were welded with 10 mm fillet welds



**FIGURE 2-5 Steel slab-on-girder bridge superstructure model.**

along the length of the girders. Transverse stiffeners, 10 mm thick, were placed at 3.05 m centers on the exterior face of the girders and 1.52 m centers on the interior face. The web and flanges were constructed from ASTM A709 Gr50 steel, all other components were ASTM A36. The girders were generally simply supported, except during a few experiments where an intermediate support was added to the bridge resulting in two continuous spans. The girders and other steelwork were constructed by the local steel fabricator, Reno Iron Works.

### **2.4.3 Deck**

The thickness of deck slab and haunch, spacing of the girders, and length of overhang were scaled down from the prototype bridge resulting in cross sectional deck slab dimensions as shown in Figure 2-6. Four layers of reinforcing were placed in the deck slab consisted of #3 bars at 203 mm centers in each of two layers in the longitudinal direction and 178 mm spacing in two transverse layers (Fig. 2-7). This corresponded to reinforcement ratios of 0.40% and 0.45% in each layer of the longitudinal and transverse reinforcement respectively. The reinforcement was split equally between the top and bottom layers and distributed evenly throughout the deck slab. In the transverse direction reinforcement was scaled from the CALTRANS design charts (CALTRANS, 1993). In the longitudinal direction the most heavily reinforced section was in the bottom layer between the girders. The required area of reinforcement in this region was calculated using the design charts. This amount of reinforcement was extended to the edges of the deck slab and also used in the top layer. This resulted in reinforcement ratios greater than the minimum specified based on the AASHTO (1998) empirical procedure of 0.2% in the top layers and 0.3% in the bottom layer. The deck slab was formed, poured and a curing compound added by Lucky Concrete

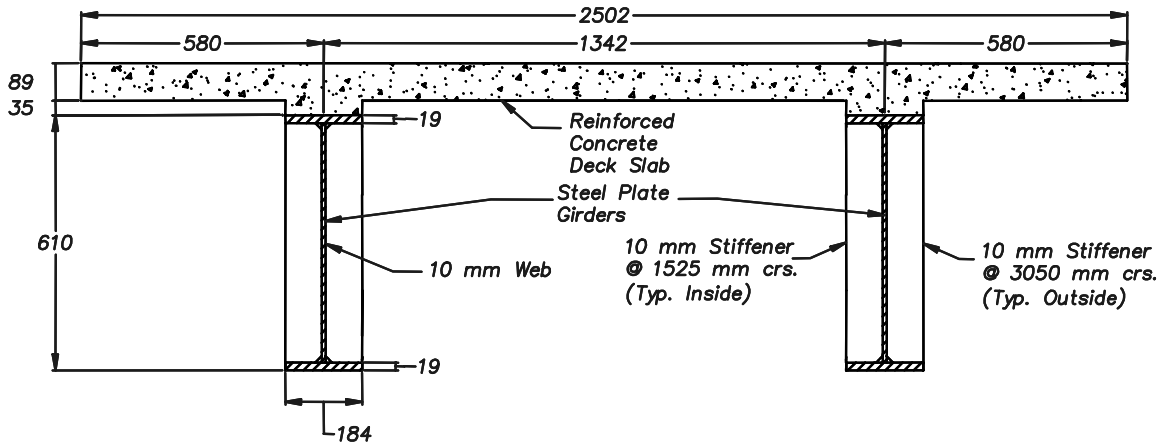


**FIGURE 2-6 Steel plate girder bridge model - girder and deck slab dimensions**

Inc. The specified strength of concrete for the deck slab was 28 MPa, while the average 28 day strength calculated from cylinder tests was 29.8 MPa (Garcia-Alvarez, 2001).

#### 2.4.4 Shear Studs

Two rows of 10 mm diameter Nelson Headed Anchor studs (TRW Nelson Division, 1977; 1988) were placed on each of the girders, as shown in Figure 2-7, spaced at 457 mm centers. These studs were not sufficient to provide full composite action to the bridge model for gravity loads and therefore provided a partial composite section. According to AASHTO (1998), in order to provide full composite action using strength requirements an equivalent spacing of 127 mm, and in order to satisfy fatigue specifications an equivalent spacing of 101 mm, would be required. The stud spacing was therefore representative of older bridges with partial composite sections. The implications of this are discussed in subsequent chapters.

#### 2.4.5 Intermediate Cross Frames

The intermediate cross frames in the prototype bridge were spaced at 7.62 m based on the AASHTO LRFD Specifications (1998). After scaling the intermediate cross frames in the bridge model were spaced 3.05 m apart.

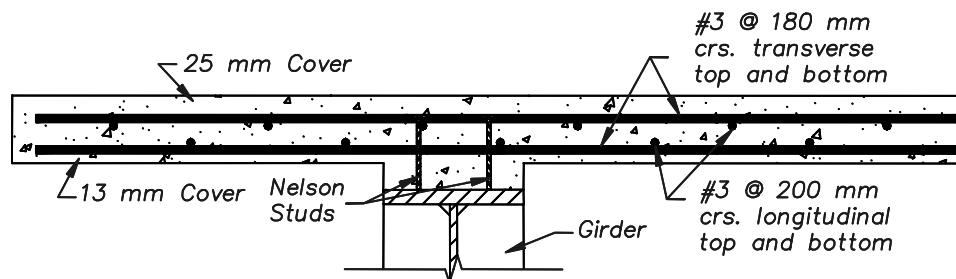


**FIGURE 2-7 Bridge model deck slab reinforcing**

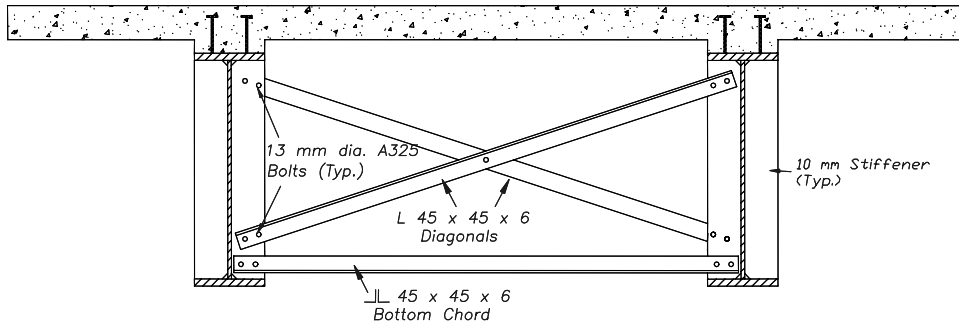


**FIGURE 2-8 Typical intermediate cross frame in bridge model**

Typical intermediate cross frames for the bridge model are shown in Figure 2-8. These were constructed using the same angle sections as those used in the heavy end cross frames described in Section 2.5.2. Compared with the end cross frames, the connection details for the intermediate cross frames were simplified, with connections directly to the stiffeners without the use of gusset plates, as strong connections to promote potential inelastic behavior were not necessary. There was a double angle bottom chord, but no top chord, as in the prototype.

#### **2.4.6 Bearings**

For the reversed static experiments, which focused on the transverse load path and end cross frames, the bridge model was placed on four reinforced elastomeric bearings. These are typical of those used to accommodate temperature fluctuations in the longitudinal direction of a bridge superstructure. They are shown to require relatively little maintenance and are a low cost option for bridge bearings, with good resilience for extreme loading conditions (AISI, 1996).

The elastomeric bearings consisted of three layers of elastomer sandwiched between steel shims as shown in Figure 2-9. The bearings were constructed from a neoprene polymer with a shear modulus of 0.86 MPa. They were restrained in the transverse direction with stiffened angles as shown. Typically in this type of bridge there is some gap between the bearing and transverse restraint, however for the bridge model this gap was minimized using custom fitted shims in an attempt to simplify the transverse response. The bearings were able to allow rotation of the girder about a longitudinal axis, seen as advantageous with the use of ductile end cross frames which are described in the following section. Rotation about the vertical axis was partially restrained by the custom fitted shims, but was generally considered unrestrained. The properties of the elastomeric pads are summarized in Appendix 1. Appendix 1 summarizes the calculated axial, translational and rotational stiffness of the bearings as well as the capacity of these bearings for axial, shear and flexural actions.

Lead rubber seismic isolation bearings were used in the shake table experiments. The properties of these bearings are discussed in Section 2.5.5. They were used as isolation bearings, but were also restrained in order to study forces in the various end cross frame configurations. The transversely restrained lead rubber bearings are illustrated in Figure 2-10. These restraints were similar to those used for the elastomeric pads, with the angles orientated in the opposite direction for convenience of connection to the load cells. The restraints allowed rotation about the longitudinal axis of the bridge. As the tight-fitted shims were cut to a relatively short length of 76 mm, and

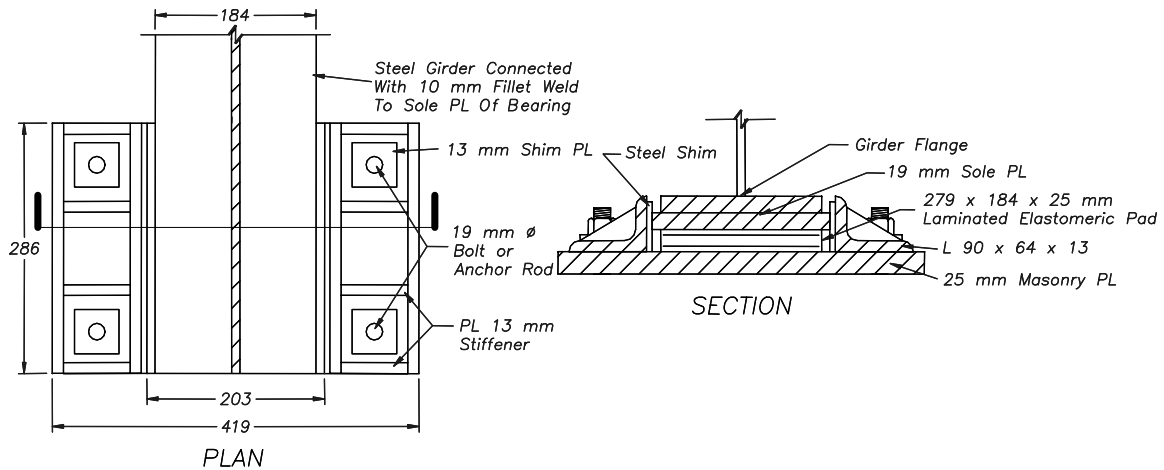


**FIGURE 2-9 Laminated elastomeric bearing**

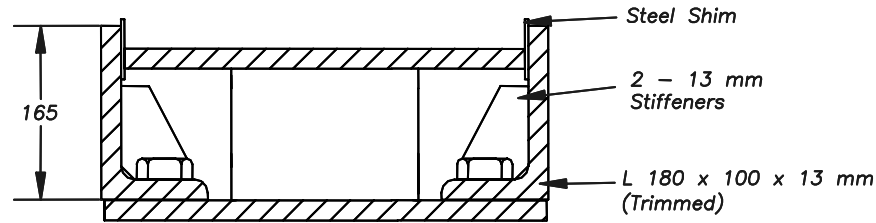


**FIGURE 2-10 Lead rubber bearing with transverse restraints**

placed at the center of the bearing, they were able to allow effectively free rotations about the vertical axis of the bridge. The properties of the isolation bearings are given in Appendix 2.

### 2.4.7 Superstructure Weight

The weight of the superstructure is critical for determining the dynamic response of the bridge. Assuming a density of reinforced concrete of  $25 \text{ kN/m}^3$  and steel of  $77 \text{ kN/m}^3$  the weight of the superstructure was calculated at 140 kN. The calculated weight of additional lead required for similitude was equal to 210 kN, 1.5 times the bridge weight. The resulting total calculated weight of the bridge was equal to 350 kN.

The measured weight of lead added to the bridge model was equal to 207 kN, equally distributed in six steel frames on the deck slab of the bridge model. The total weight of the bridge including lead, as measured from the load cells and checked using a crane scale at one end of the bridge, was 170 kN at the north end and 171 kN at the south end, summing to 341 kN. Therefore the weight of the bridge model alone was equal to 134 kN. The measured weight of the bridge model was within 6% of the expected weight. Dividing the weight equally between each of the bearings resulted in forces of 33.5 kN per bearing for the reversed static experiments, with no added lead. Similarly, the force during shake table experiments, with added lead, was equal to 85.4 kN per bearing. The load cells confirmed that the forces were evenly distributed between all the bearings as required for equilibrium.

## **2.5 Design of Critical Components in the Transverse Response of the Bridge**

### **2.5.1 Overview**

Three approaches were considered to allow a ductile response of the steel girder bridge model subjected to transverse earthquake excitation. Along with an assumed ductile substructure response, the ductile response was promoted using ductile end cross frames and seismic isolation bearings. The ductile response of these components is discussed in a subsequent report (Carden, 2005). For the purposes of studying the transverse load path the essentially elastic response of the components is considered in this report. The properties of the different configurations of the bridge are described below, with more details given in the second report (Carden, 2005).

### **2.5.2 “Heavy” X-Braces**

The end shear was resisted by the diagonals of a single angle X-brace at the end of the bridge. These diagonals were first designed as relatively large members, with the implication that they would perform essentially elastically during design levels of seismic loading. Subsequently, 45 x 45 x 6 mm. single angles were selected. These satisfied the b/t ratio in accordance with AISC (2002) to ensure that, if any inelastic action occurred, local buckling would be prevented. They also satisfied the slenderness ( $Kl/r$ ) ratio in accordance with AASHTO (1998) for secondary members, which was more limiting than the AISC provisions. Top and bottom chords were designed to distribute earthquake forces evenly between the girders and bearings in the event that buckling of the diagonal members occurred and uneven forces resulted in the tension and compression diagonals. For this 45 x 45 x 6 mm double angles were used, as illustrated in Figure 2-11. In addition the top chord was connected to the deck slab using a built-up T-section, as illustrated in Figure 2-12, initially at the south end and then also at the north end after the first experiment demonstrated its influence in the transverse seismic load path. This type of composite connection, using WT or channel members, is typically used at abutments to minimize the effect of wheel loading where traffic travels onto a bridge. The T-section was connected to the deck slab using bolts grouted into holes cored in the deck slab to facilitate removal of the member when necessary in changing end cross frame configurations in the bridge model. It is recognized that in practice shear studs would be more effective than bolts in this type of connection, however additional bolts were used to ensure failure was prevented.

Two types of connection configurations were used at different stages of experiments on the bridge model. The first configuration, for which the above calculations apply, had bolted connections. The diagonal, top and bottom chords of the end cross frames were connected to gusset plates which in turn were connected to the web stiffeners as shown in Figures 2-11 and 2-12. Gusset plates were used instead of connecting directly to the stiffeners in order to provide adequate connection strength and ensure any inelasticity would occur in the members and not result in failure of the connections. The second configuration used welded connections. For this configuration, as illustrated in Figure 2-13, no gusset plates were required as the angles were welded directly to the bearing stiffeners. In this configuration, used for shake table experiments, isolation bearings were used with transverse restraints in order to provide an effectively pinned connection between the girders and substructure for studying the response of the cross frames. These restraints were later removed for experiments investigating an isolated configuration.

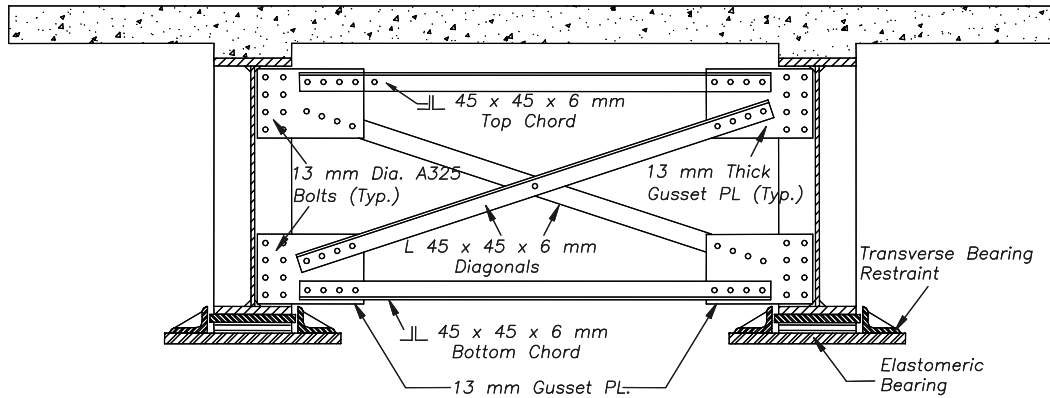
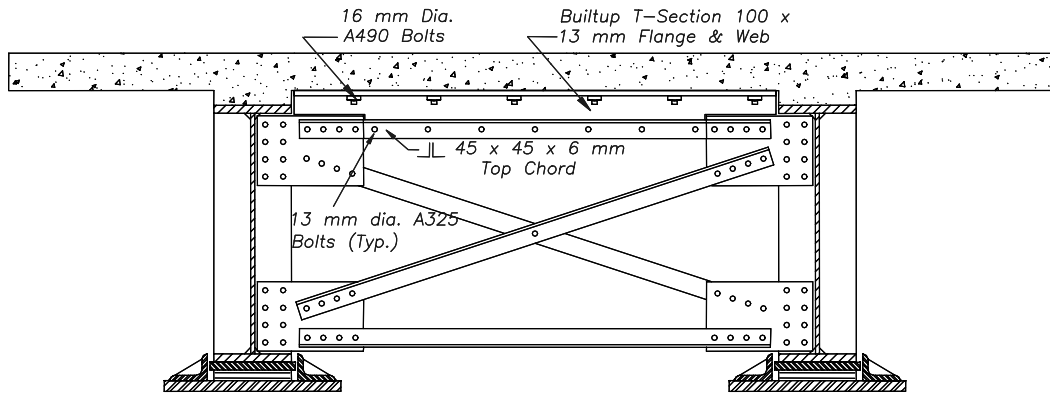


FIGURE 2-11 “Heavy” end cross frames at the north end in the bridge model

### 2.5.3 “Light” Single Angle X-Braces

In order to reduce the elastic seismic demand in the bridge model, the end cross frames were also designed to respond inelastically using “lighter” angle members. As single angle X-braces are commonly used in bridges due to their cost effective and simple design and construction, it was considered valuable to study the potential for using these members as ductile elements. These act as concentric braced frames similar to those used in buildings, with more details on the inelastic behavior of these members provided in the subsequent report (Carden, 2005).

Single angles (25 x 25 x 5 mm) were selected for the cross frames designed to yield with a strength below the strength of the substructure, termed the “light” X-braces. These members had sufficient



**FIGURE 2-12 “Heavy” end cross frames at the south end in the bridge model**

capacity to elastically resist wind loads and also satisfied the  $b/t$  and  $Kl/r$  ratios for special concentrically braced frames (AISC, 2002) and bracing members (AASHTO, 1998). The bridge model configuration with these X-braces is shown in Figure 2-14. They were welded directly to the bearing stiffeners, as shown, with welded connections designed to be stronger than the tensile capacity of the members to prevent premature failure and promote the best possible inelastic behavior.

#### **2.5.4 Ductile End Cross Frames using Unbonded Braces - Elastic Substructure**

Buckling restrained braces have been shown to provide very reliable strength, good energy dissipation and reduce lateral storey drift in building applications compared to concentric braced



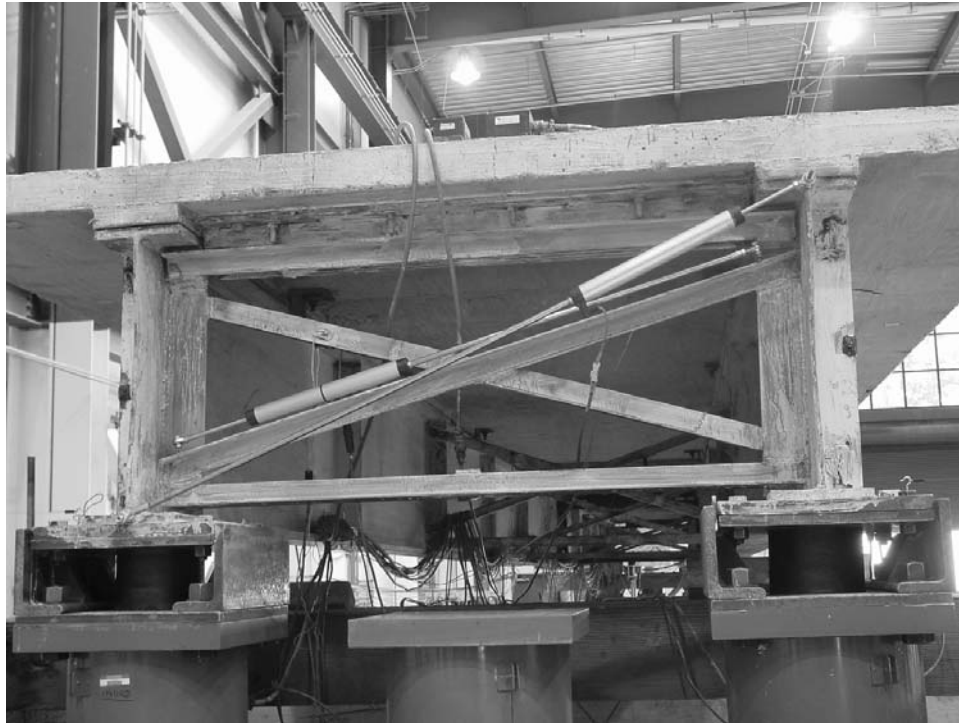
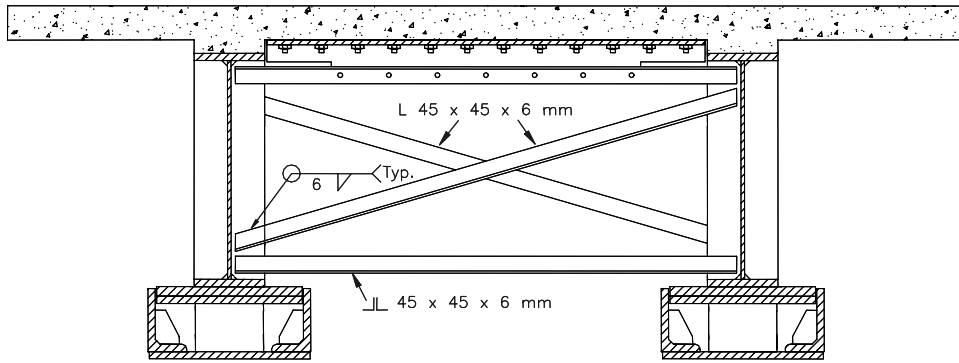


**FIGURE 2-13 “Heavy” end cross frames in the bridge model with welded connections**

framing systems (Black, 2002; Clark, 1999; Yamaguchi, 1998). These were considered to provide potential improvement in the response of steel plate girder bridges when used as ductile end cross frames, compared to special X-braces, and hence were investigated. As the braces have similar properties in tension and compression a single brace was necessary. Buckling restrained braces constructed by Nippon Steel Corporation, called an unbonded braces, were installed in the bridge model, as illustrated in Figure 2-15.

Nippon Steel typically design unbonded braces with fixed end connections that are capable of carrying any moment generated in the brace. These connections are designed to be slip critical using the serviceability requirements of AISC (1998) for buildings. As the braces designed for the bridge model were relatively short, there was a concern that the bending generated in the braces due to the deformed geometry would be large with fixed end connections, which could have an impact on the seismic performance of the brace. The alternative was to use pinned connections to

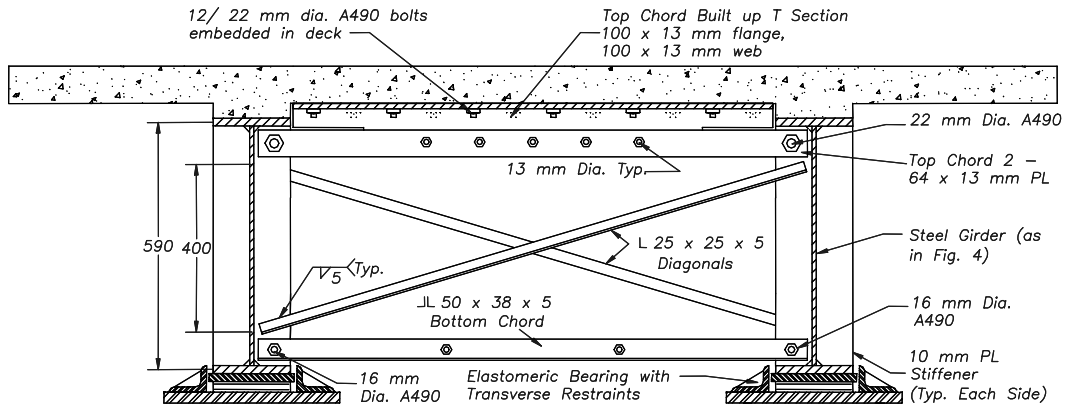


**FIGURE 2-14 “Light” end cross frames in the bridge model**

prevent bending moments being induced in the brace, however the impact of this is a connection that is not slip critical and a higher chance of buckling in the braces as the effective length was increased. Therefore, in order to allow testing of both configurations, the braces were designed with pinned end connections which were later welded in order to create fixed end connections. The top and bottom chords used for the unbonded braces were the same as those used for the ductile X-braces.

### **2.5.5 Seismic Isolation using Lead Rubber Bearings**

The third approach for protecting the bridge model during earthquakes was to seismically isolate the superstructure using lead rubber bearings. The resulting dimensions for the lead rubber

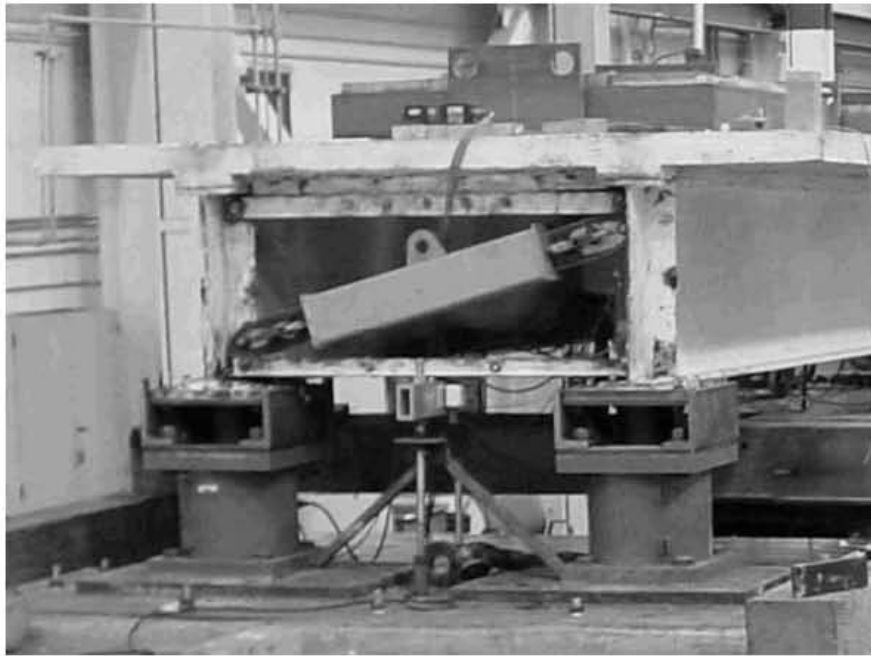


**FIGURE 2-15 Unbonded brace in the bridge model**

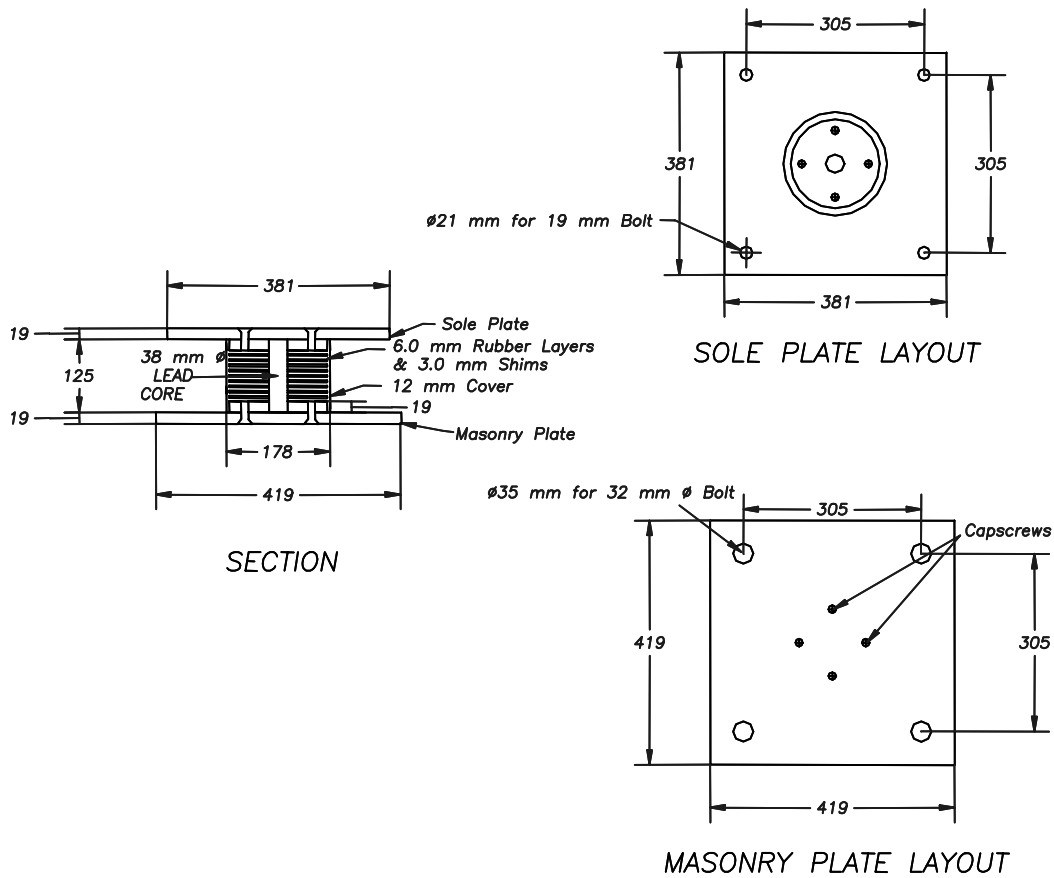


**FIGURE 2-16 Lead rubber bearing**

bearings are illustrated in Figure 2-16. The calculated properties of the bearings and design response are given in Appendix 2. The bearings were constructed with 10 layers of rubber with a shear modulus of 0.43 MPa. More details for the design and inelastic response of the isolated bridge are provided by Carden et al. (2005).

As the combined shear force in the bearings at each end of the bridge was much lower than the yield strength of the end cross frames, with both light X-braces or unbonded braces, experiments were first performed on the lead rubber bearings with the light X-braces. Bearing restraints were later added in order to increase the transverse shear capacity of the bridge, allowing the X-braces and unbonded braces respectively to become the weakest links in the system.

## 2.6 Simulation of Earthquake Loading

### 2.6.1 Reversed Static Transverse Loading

The first series of experiments on the bridge model simulated transverse earthquake loading of the model using actuators at the one thirds points along the bridge as shown in the Figure 2-5. The center of mass of the bridge model was slightly below the centerline of the deck slab with 75% of

the weight of the bridge model concentrated in the deck slab. If barrier rails, wearing surface and some live load is included the proportion of weight at and above deck slab level would have increased further. Consequently, the actuator supports were designed to apply loads just (41 mm) below the centreline of the deck slab. A cross section of the bridge model at one support is illustrated in Figure 2-17. A hydraulic actuator support was used after the second experiment to minimize the effect of the actuator weight on the connected side of the bridge. The support was designed to move vertically with the bridge but apply a constant force equal and opposite to the weight of the actuator at the support point. A section of the deck slab around the actuator supports was removed to ensure that loads were transferred into the bridge without localized damage to the deck slab. A double angle strut was also added to resist forces induced by twisting of the bridge during transverse loading.

The reversed static experiments investigated the effect of different end and intermediate cross frame configurations in the bridge model. Different configurations investigated included the influence of heavy diagonal X-braces, light X-braces, top chords, both with and without a direct connection to the deck slab, bottom chords and intermediate cross frames. Table 2-1 lists the 8 different reversed static experiments and the differences between them. The first part of the acronym in this table “C” stands for “reversed static” while the remainder refers to the configuration of the end cross frames. The first experiment (RSHXB1) had the relatively “heavy” 45 x 45 x 6 mm single angle end X-braces in the bridge model (Figs. 2-11 and 2-12). The configuration in the second experiment (RSHXB2) was similar to the first except that the composite top chord, shown to be effective at the south end of the first experiment, was added to the north end cross frame in the second experiment. Some additional instrumentation such as the load cells was also added. In the third experiment (RSNECF) all the end cross frame components were removed. In the fourth experiment the top chords (RSNBC) were replaced but there was no bottom chord. In the fifth experiment (RSFC) the both the top and bottom chord were added but there was no diagonal members. These chords are considered to have fixed moment resisting connections as there are four bolts at each end. In the sixth experiment (RSNCF) all the intermediate and end cross frame components were removed. In the seventh experiment (RSPC) the intermediate cross frames were replaced and pinned top and bottom chords were added to the ends of the bridge model as illustrated in Figure 2-14. In the final experiment (RSLXB) the “light” single angle X-brace diagonals were welded into the ends, attached to the bearing stiffeners of the bridge model.

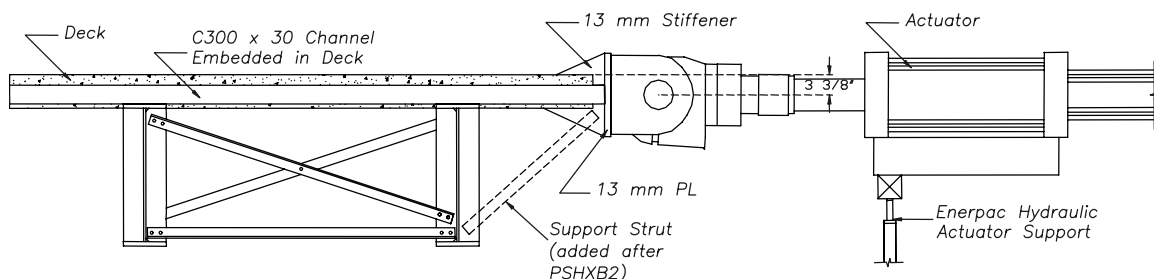


**FIGURE 2-17 Actuator connected to bridge model at 1/3 points along length of bridge**

**TABLE 2-1 Reversed Static Experiments**

No.	Abbrev. Name	Full Name	End Cross Frames					Intermediate Cross Frames
			Diagonals	Top Chord		Bottom Chord	Connections (Diag. / Chords)	
				Type	Composite			
1	RSHXB	Reversed Static "Heavy" X-Brace	Heavy Single L	Double L / T Section	South End Only	Double L	Bolted to Gusset Plates	Yes
2	RSHXB2	Reversed Static "Heavy" X-Brace 2	Heavy Single L	Double L / T Section	Both Ends	Double L	Bolted to Gusset Plates	Yes
3	RSNECF	Reversed Static No End Cross Frames	None	None	None	None	None	Yes
4	RSNBC	Reversed Static No Bottom Chord	None	Double L / T Section	Both Ends	None	Bolted to Gusset Plates	Yes
5	RSFC	Reversed Static Fixed Chords	None	Double L / T Section	Both Ends	Double L	Bolted to Gusset Plates	Yes
6	RSNCF	Reversed Static No Cross Frames	None	None	None	None	None	None
7	RSPC	Reversed Static Pinned Chords	None	Double PL / T Section	Both Ends	Double L	Weided / Single Bolt to Stiff.	Yes
8	RSLXB	Reversed Static "Light" X-Brace	Light Single L	Double PL / T Section	Both Ends	Double L	Weided / Single Bolt to Stiff.	Yes

The loading history for the first experiment followed the Applied Technology Council (ATC) 24 (1992) recommendation for testing components of steel structures. The loading history is illustrated in Figure 2-18. This loading history was displacement controlled with equal displacements in each actuator. A problem with this type of control was that a small phase lag between the actuators resulted in them opposing each other for short periods of time. Different conditions in the two ends of the bridge also resulting in very different forces in the two actuators, as shown in Figure 2-19. Therefore, in the second and subsequent experiments one actuator was in displacement control while the second actuator maintained a force equal to that in the first actuator. In order to reduce the effects of cumulative cycles on the cracked deck slab of the bridge model, the three cycles at each amplitude, as recommended by ATC 24, was reduced to two cycles. Loading histories for the reversed static experiments are given in Figures 2-19 to 2-26. These show equal forces in the two actuators at all times for all but the first experiment.

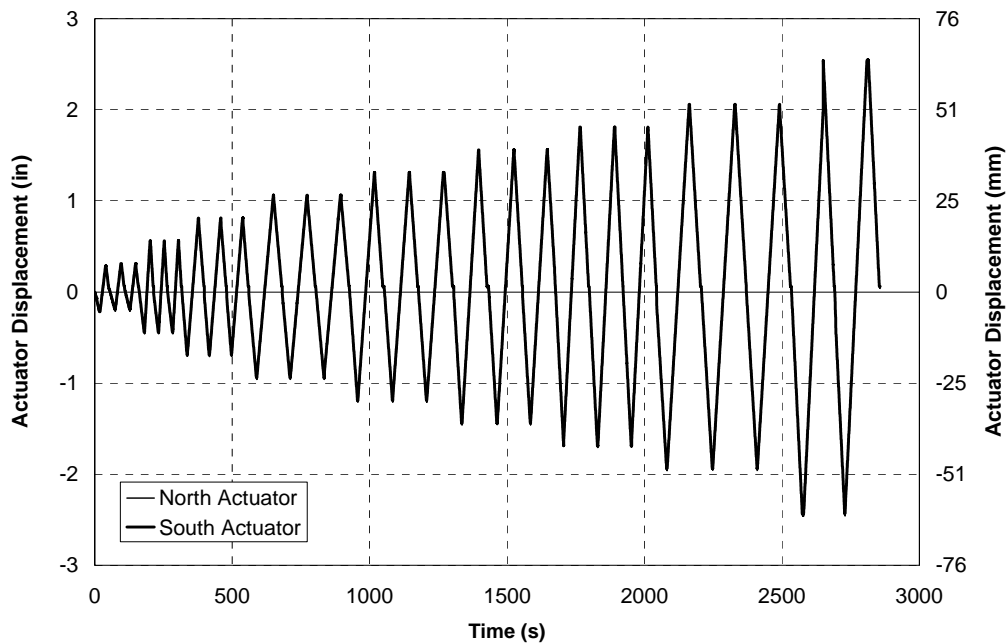


**FIGURE 2-18 Actuator displacements vs time for Experiment RSHXB**

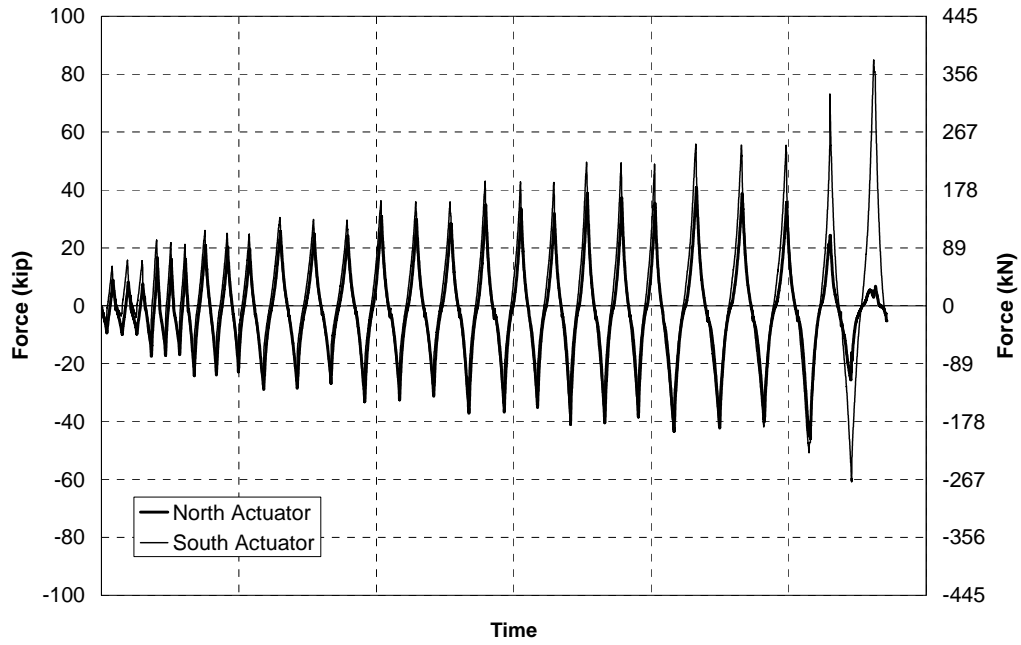


**FIGURE 2-19 Actuator forces vs time for Experiment RSHXB**

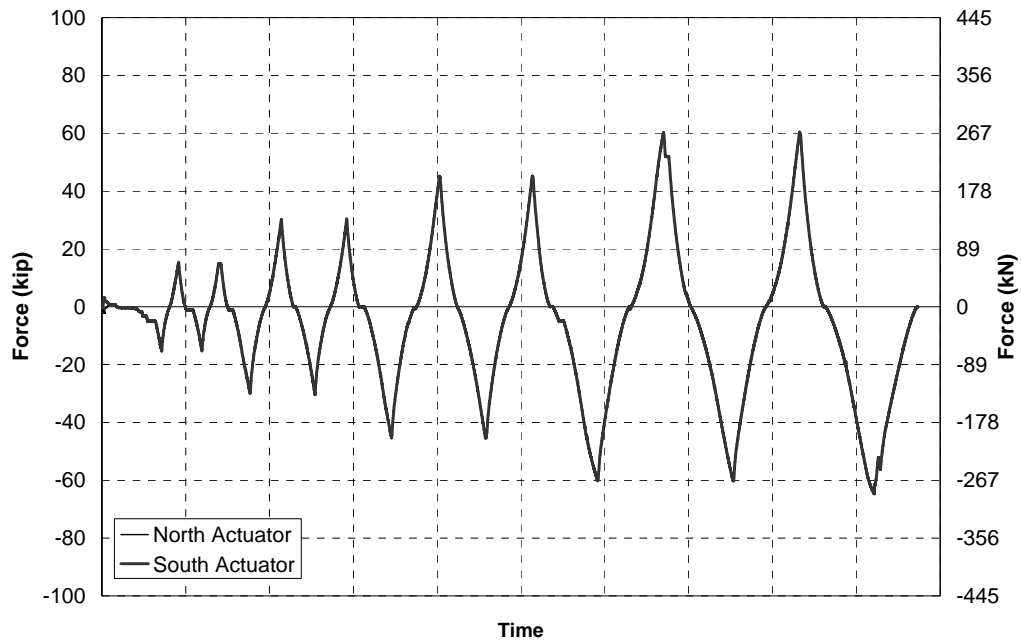


**FIGURE 2-20 Actuator forces vs time for Experiment RSHXB2**



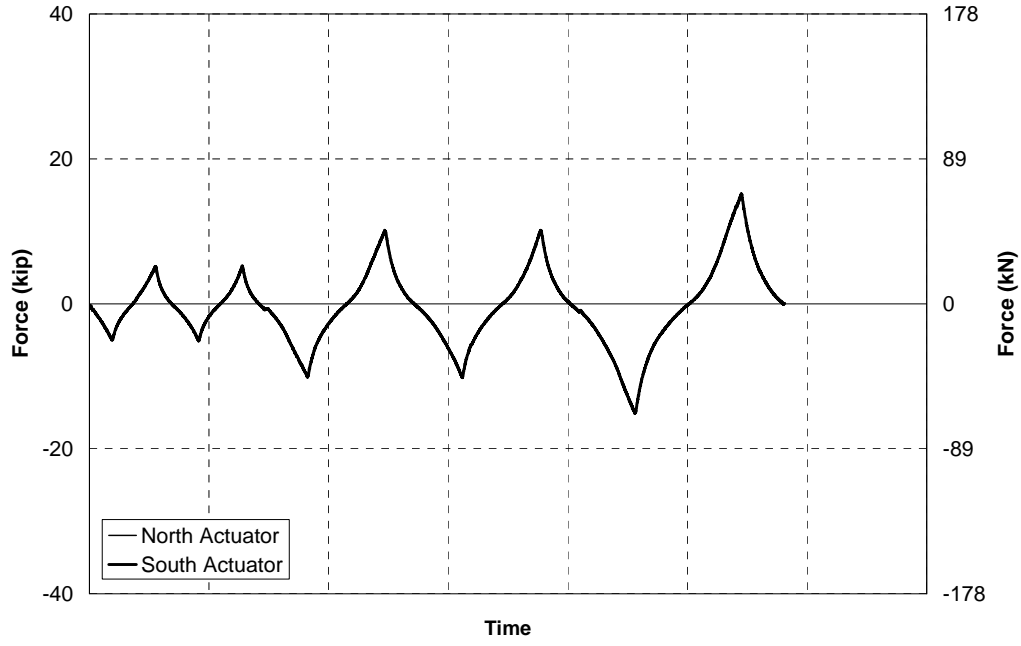


**FIGURE 2-21 Actuator forces vs time for Experiment RSNECF**

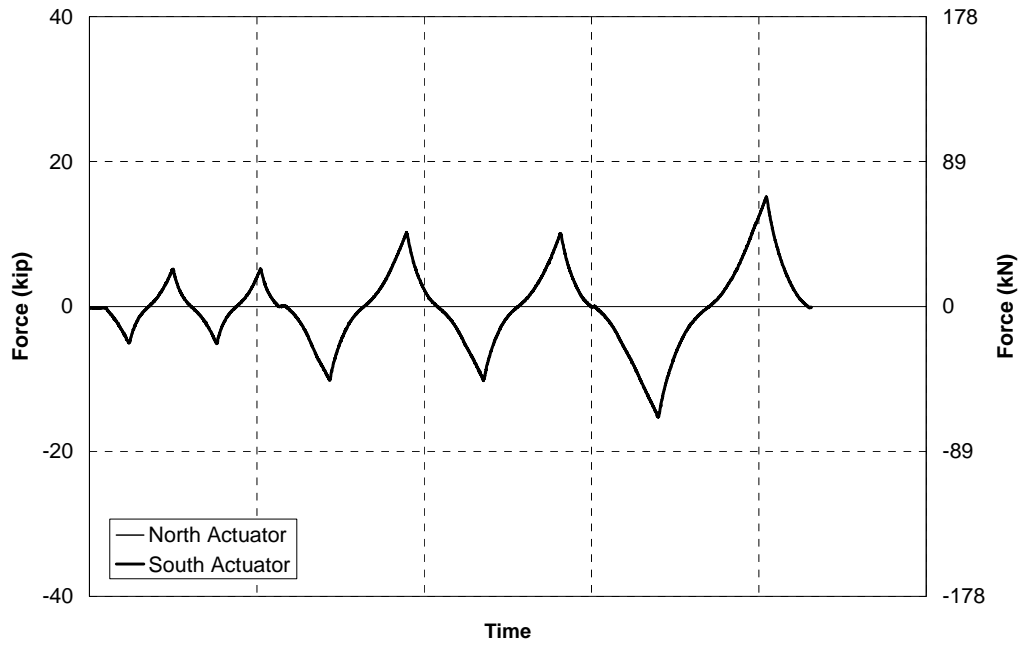


**FIGURE 2-22 Actuator forces vs time for Experiment RSNBC**

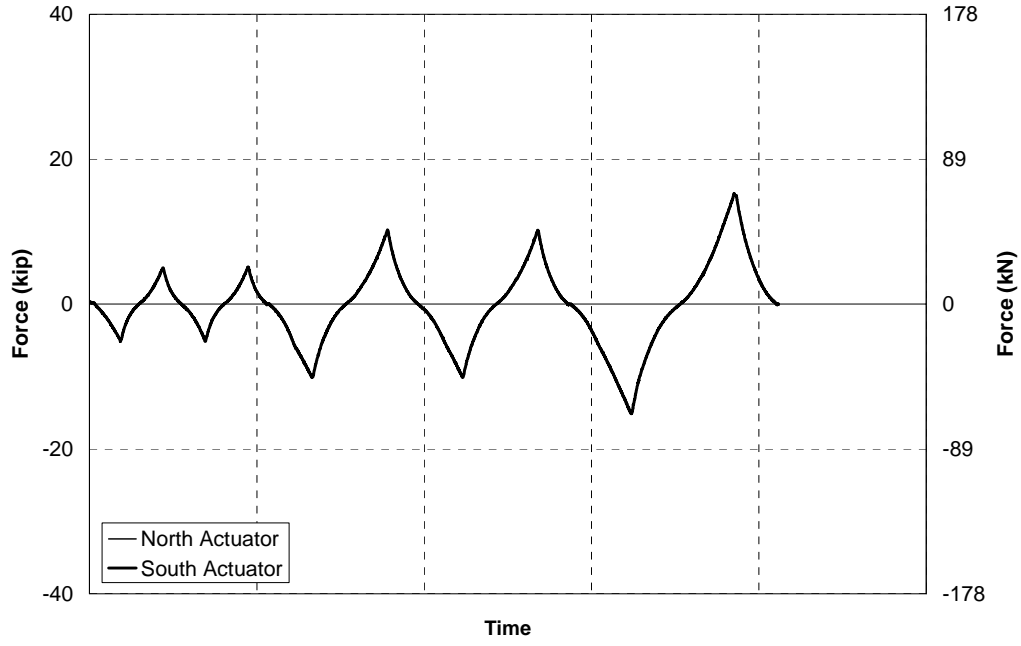


**FIGURE 2-23 Actuator forces vs time for Experiment RSFC**

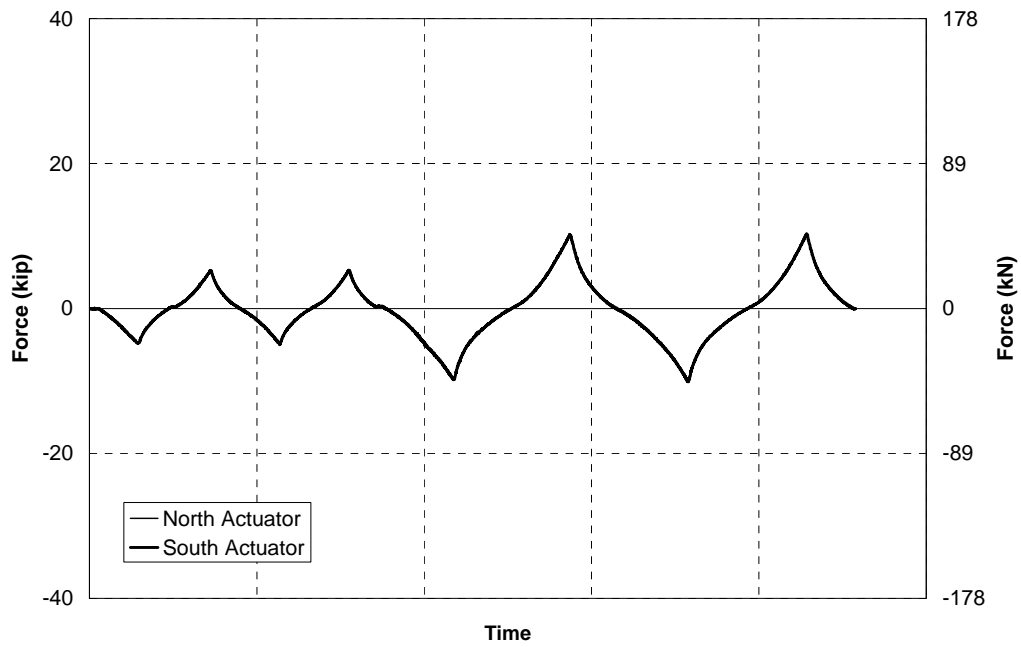


**FIGURE 2-24 Actuator forces vs time for Experiment RSNCF**

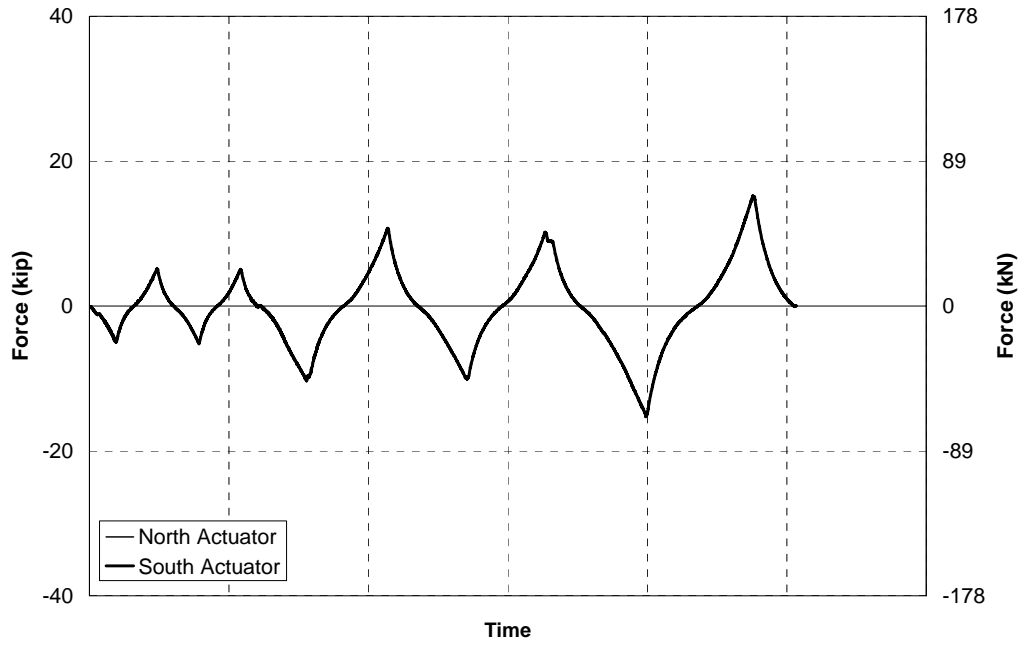


**FIGURE 2-25 Actuator forces vs time for Experiment RSPC**

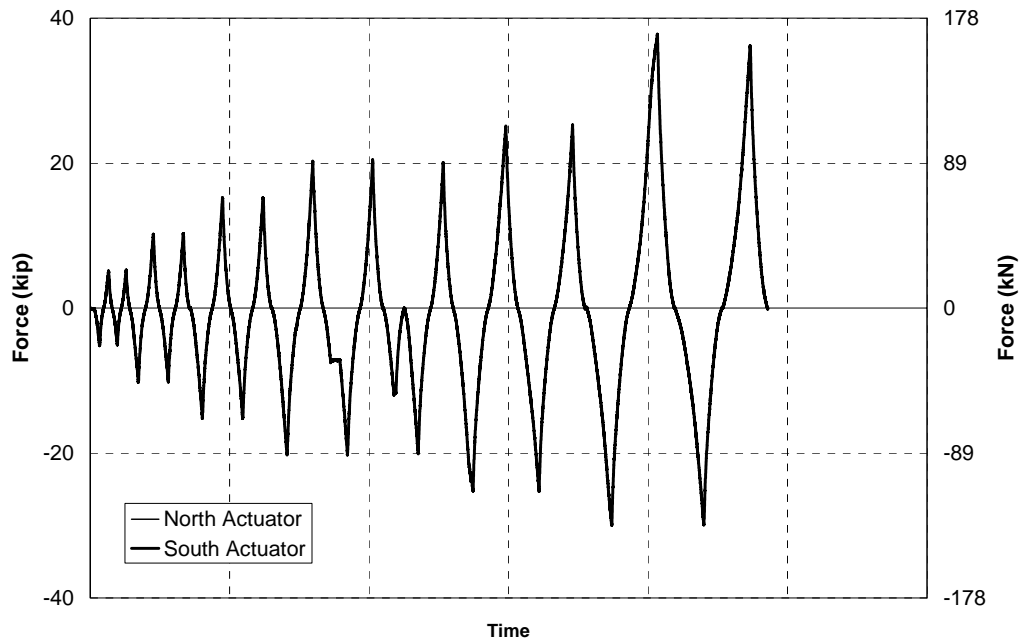


**FIGURE 2-26 Actuator forces vs time for Experiment RSLXB**

## 2.6.2 Shake Table Earthquake Simulation

Following the series of reversed static experiments on the bridge model, a series of shake table experiments were performed. There were several advantages of shake table experiments over the reversed static experiments. One was a more realistic loading as the bridge was loaded directly by its own inertia, as in an earthquake. Another advantage was that the actual response of the bridge to a given level of excitation was found and not just the properties up to a specified displacement or force. This allowed the elastic response to be compared to the inelastic response and also the design response for a given seismic demand. The trade-off was a more complex system to be analyzed. Shake table experiments utilized three 50 ton capacity shake tables. The bridge was attached as a simply supported span to Shake Tables 1 (north end) and 3 (south end), and also as a two span bridge to Shake Table 2 at the midspan (Fig. 2-27). The different series of experiments are listed in Table 2-2. The bridge was first investigated as an isolated bridge with lead rubber bearings at the ends of the bridge (STLRB), with properties as described in Section 2.5.5. In the second experiment lead rubber bearings were added to the midspan of the bridge in order to achieve a two span bridge configuration (STLRB2S). Roller isolation bearings (STRB) were then placed in the bridge model in a simply supported configuration. For the next series of experiments (STLXB) the lead rubber isolation bearings in the simply supported bridge model were restrained in the transverse direction and a series of experiments were performed in order to determine the inelastic behavior of the “light” diagonal X-braces. After considerable inelastic deformation in these braces they were replaced by unbonded braces at the ends of the bridge (STUB). An unbonded brace was also installed at the midspan of the bridge, although this had little effect on the response while the bridge was simply supported. However for the next series of experiments (STUB2S) transversely restrained bearings were placed at the midspan of the bridge in order to determine its response with ductile unbonded braces in a two span configuration. The unbonded braces were then removed and earthquakes were simulated on the bridge model with no end cross frames (STNXF) in a simply supported configuration. “Heavy” single angle cross frames were then installed in the bridge in order to calculate the elastic response of the bridge to compare with the inelastic response of the ductile end cross frames. Following on, simulations on the isolated bridge model with the unrestrained lead rubber bearings were repeated to see if there was any change in response with the heavier cross frames (STLRB2), and to investigate potential degradation in the bearings. Finally, experiments were performed on the bridge model in a single span configuration with a ball bearing isolation system.

For each series of experiments, a number of earthquakes were simulated in the bridge model. A complete list of earthquake simulations is given in Appendix 3. Three earthquakes were used for shake table experiments. The first was from the 1940 Imperial Valley earthquake recorded at the El Centro station. This was selected because of its extensive use in the past for analytical and shake table experiments. The second record was from the 1994 Northridge earthquake recorded at the Sylmar hospital station. This was one of the largest recorded motions in the United States and has been used for past shake table experimentation. The third earthquake was from the 1995 Kobe earthquake in Japan recorded at the KJMA station. This has a particularly high peak ground acceleration and velocity, comparable to the Sylmar record. The details of each earthquake are listed in Table 2-3.

The earthquakes were obtained from the PEER strong motion database (PEER, 2002). Time histories for each earthquake are shown in Figures 2-28 to 2-30. Coincidentally, the dominant component for each earthquake, ie. the component with largest peak acceleration, were the north-



**FIGURE 2-27 Bridge Model attached to three 50 ton shake tables**

south (0 or 180 degree) components. Therefore when considering only one component, unless specifically stated otherwise, the north-south component was used. The response spectrum for 2.0 x El Centro, as shown in Figure 2-33, compares reasonable well to the design spectra. This level of excitation is used for much of the analysis of the bridge model.

In addition the north-south component of El Centro was passed through a simulated soil layer using EduShake (EduPro, 1999). This motion assumed a 22.9 m layer of sand with a shear wave velocity of 275 m/s and density of 19 kN/m<sup>3</sup> corresponding to medium-stiff material for soil type III in AASHTO (1998). Average Seed and Idriss models (EduPro, 1999) were used for the modulus and damping curves. The resulting output time history at the top of the soil layer is shown in Figure 2-31. This motion was used to investigate the effect of differential ground motion at the different supports of the bridge.

The earthquakes were scaled in the time domain to account for scaling of the bridge model. The scale factor for time was equal to  $\sqrt{0.4} = 0.632$ . Response spectra for each of the time scaled earthquakes at 5% damping are shown in Figure 2-32. The El Centro spectra are below both the AASHTO LRFD (1998) and AASHTO Isolation (1999) design spectra at all periods. In contrast, the dominant components of the Sylmar and Kobe records exceed the design spectra up to periods in excess of 1.0 s. The soft soil El Centro record exhibits an amplified response of up to 3 times at around 0.55 s compared to the original El Centro record.

There is always some discrepancy between the achieved shake table accelerations and the originally recorded accelerations known as the target accelerations. Figure 2-34 shows the El

**TABLE 2-2 Shake Table Experiments**

No.	Abbrev. Name	Full Name	Cross Frames		Top & Bottom Chords	Bearings		Spans
			Type	Connection		Type	Restrictions	
1	STLRB	Shake Table Lead Rubber Bearings	Light X-Brace	Welded	Double PL & Double L - Pinned	LRBs	No	1
2	STLRB2S	Shake Table Lead Rubber Bearings 2 Span	Light X-Brace	Welded	Double PL & Double L - Pinned	LRBs	No	2
3 <sup>1</sup>	STRB	Shake Table Roller Bearings	Light X-Brace	Welded	Double PL & Double L - Pinned	Roller	No	1
4	STLXB	Shake Table "Light" X-Braces	Light X-Brace	Welded	Double PL & Double L - Pinned	LRBs	Yes	1
5	STPUB	Shake Table Pinned Unbonded Braces	Unbonded brace	Bolted / Pin	Double PL & Double L - Pinned	LRBs	Yes	1
6	STFUB	Shake Table Fixed Unbonded Braces	Unbonded brace	Welded	Double PL & Double L - Pinned	LRBs	Yes	1
7	STFUB2S	Shake Table Fixed Unbonded Braces 2 Span	Unbonded brace	Welded	Double PL & Double L - Pinned	LRBs	Yes	2
8	STNECF	Shake Table No End Cross Frames	None	-	None	LRBs	Yes	1
9	STHXB	Shake Table "Heavy" X-Braces	Heavy X-Brace	Welded	Double PL & Double L - Pinned	LRBs	Yes	1
10	STLRB2	Shake Table Lead Rubbers Bearing series 2	Heavy X-Brace	Welded	Double PL & Double L - Pinned	LRBs	No	1
11 <sup>1</sup>	STSBB	Shake Table Seismic Ball Bearings	Heavy X-Brace	Welded	Double PL & Double L - Pinned	Ball Bearings / LRBs	No	1

Notes: 1. These experiments are not discussed in this dissertation.

**TABLE 2-3 Earthquake Data for Shake Table Experiments**

Name	Comp.	Year	Earthquake	Station	Direction	PGA (g)	PGV (in/s)
El Centro	NS	1940	Imperial Valley	El Centro Array #9	180	0.313	11.7
	EW				270	0.215	11.9
Sylmar	NS	1994	Northridge	Sylmar Hospital	360	0.843	51.0
	EW				090	0.604	30.8
Kobe	NS	1995	Kobe	KJMA	000	0.821	32.0
	EW				090	0.599	29.3

Centro response spectra for the target and achieved accelerations at Shake Tables 1 and 3 for a typical earthquake simulation. It shows there is very good correlation between the two shake tables with almost identical response spectral ordinates. There was larger error between the target spectrum and achieved spectrum with up to a 15% difference for periods between 0.1 and 0.6 s. Figure 2-35 shows similar comparisons for the 360 component of the Sylmar record. Again the spectra for the two tables are very similar, however there is a larger difference (28%) between the target and achieved spectra and an apparent frequency shift for periods between 0 and 0.5 s. This may be related to the particularly high peak velocity in the record. The target north-south component of the Kobe spectrum compares very closely to the achieved spectra as shown in Figure 2-36.

There were also two white noise acceleration time histories generated by the shake table controller used for system identification. The first white noise time history was generated to achieve a constant Fourier spectral amplitude for frequencies between 1.0 and 30 Hz with a shake table peak acceleration of 0.25g. The second history had frequencies of 0.3 and 50 Hz in order to better capture low frequency response.

Several sine sweeps were also run in another attempt at system identification. These were generated with a constant table acceleration amplitude between frequencies of 0.3 to 30 Hz.

## **2.7 Instrumentation**

### **2.7.1 Introduction**

A number of instruments were placed on the bridge model in order to measure the deformations, forces, strains and accelerations in the bridge during reversed static and shake table experiments. A complete inventory of instruments shown graphically, with names for reference purposes, is given in the following sections. A convention for naming the instruments was used in order to describe the type of instrument, location of instrument and direction of measurement. For example, label DK15AccVE refers to an instrument on the deck of the bridge model, 4.6 m (15 ft) from the north end, measuring accelerations in the vertical direction on the eastern side of the bridge model. Not all the instruments shown were on the bridge model for every experiment, however reference is made to them as appropriate during analysis throughout the following chapters.

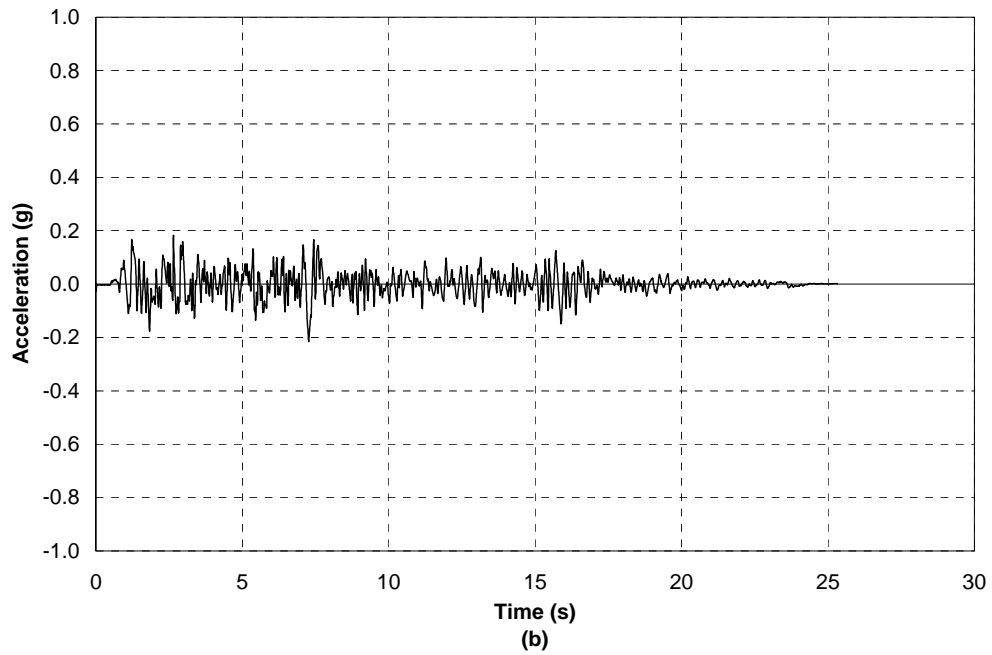
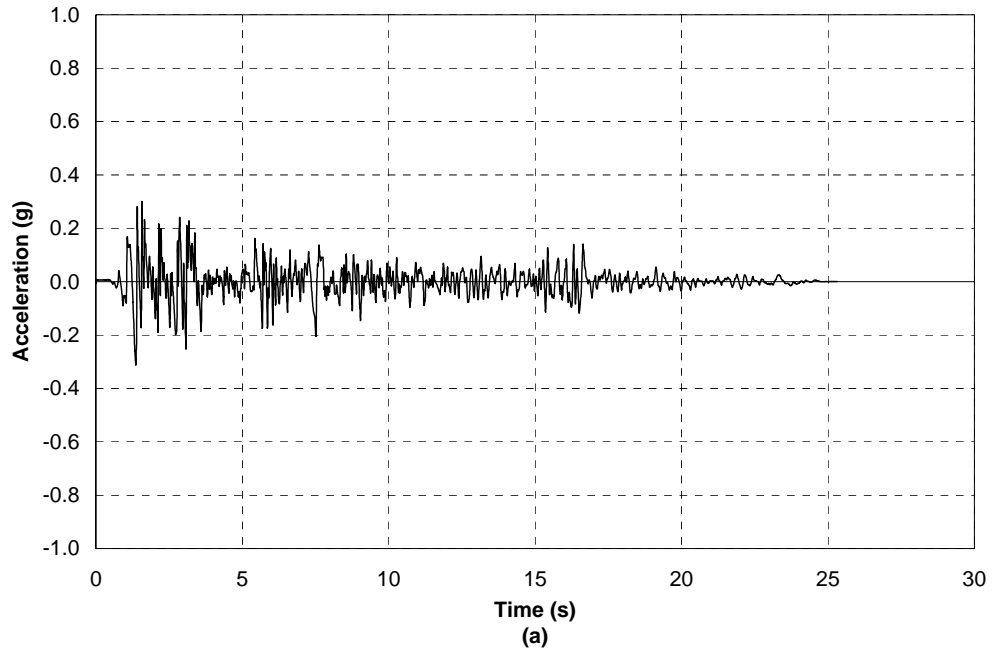


**FIGURE 2-28 Acceleration time histories for a) 180 component and b) 270 component of El Centro**



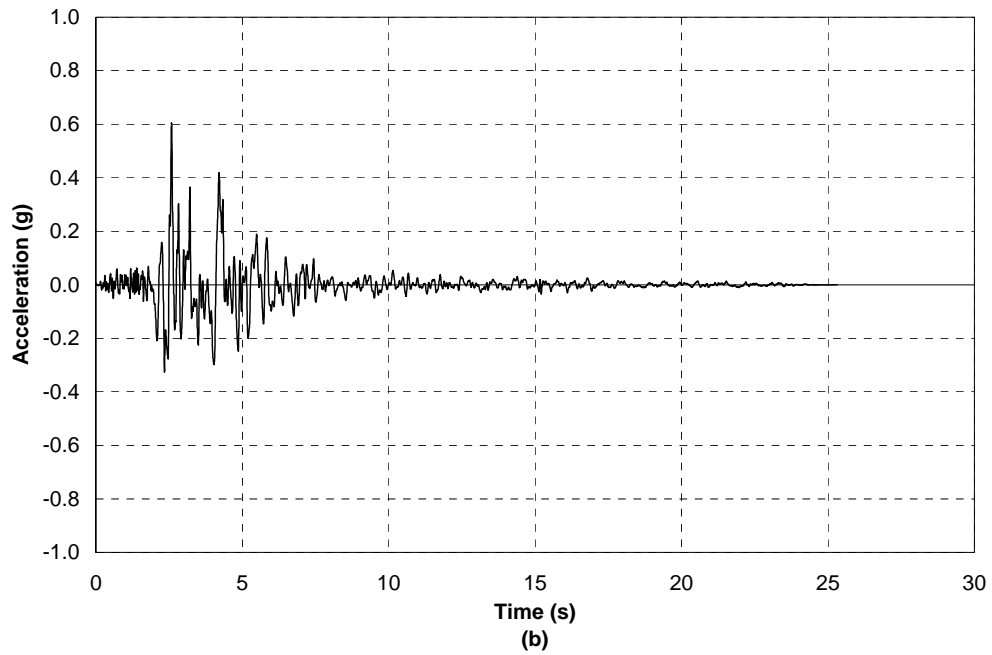
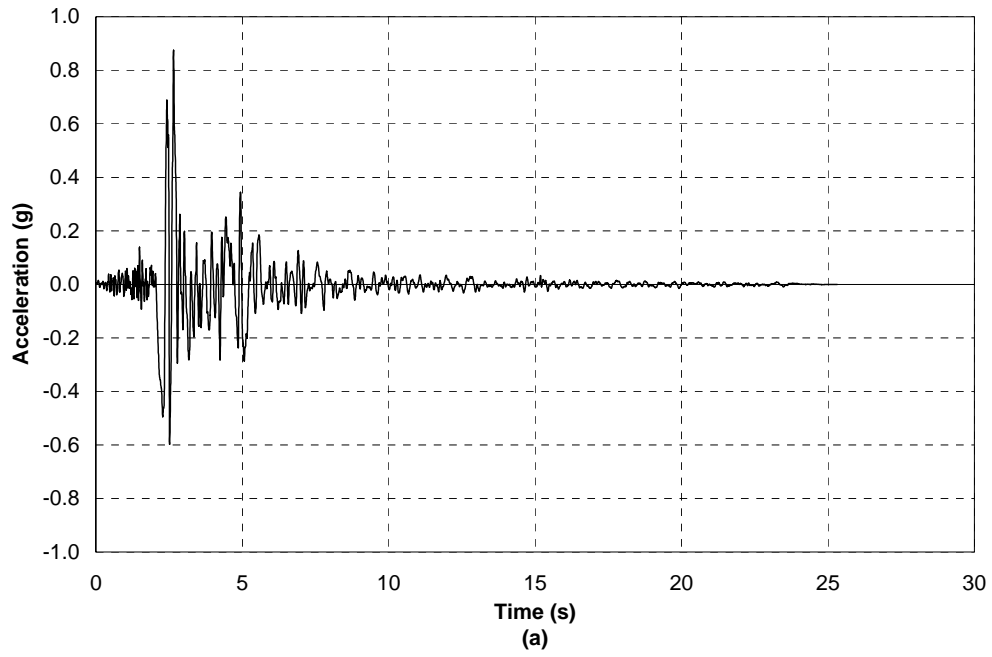


**FIGURE 2-29 Acceleration time histories for a) 360 component and b) 90 component of Sylmar**

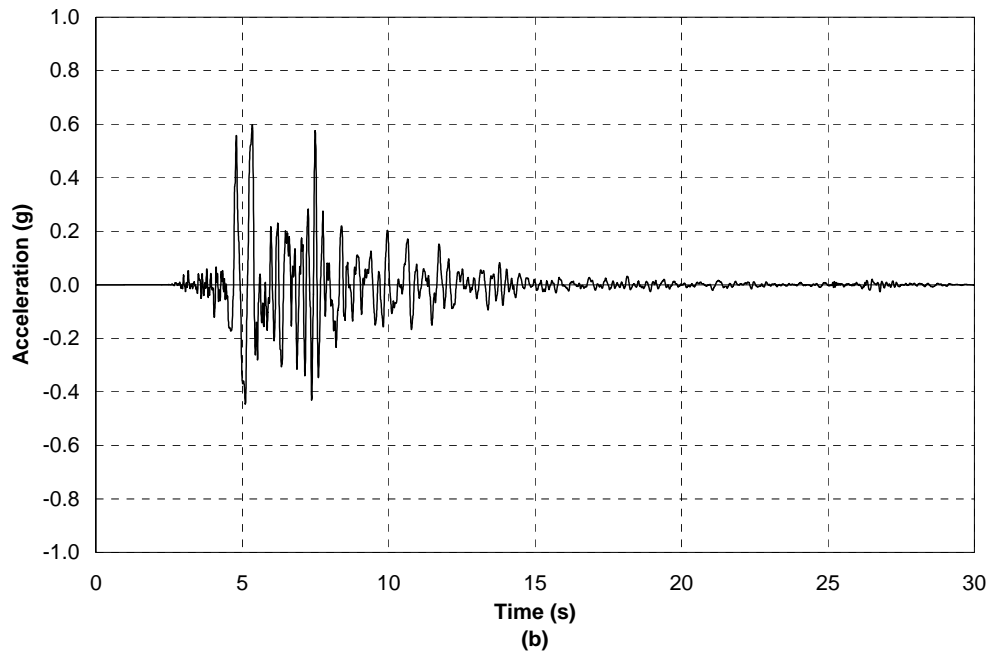
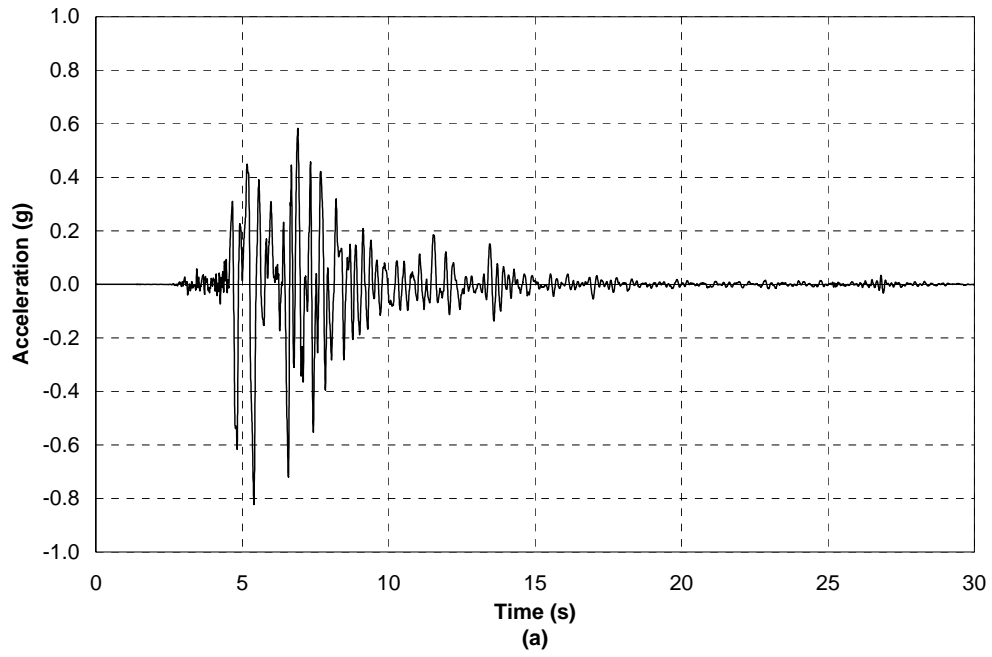


**FIGURE 2-30 Acceleration time histories for a) 00 component and b) 90 component of Kobe**

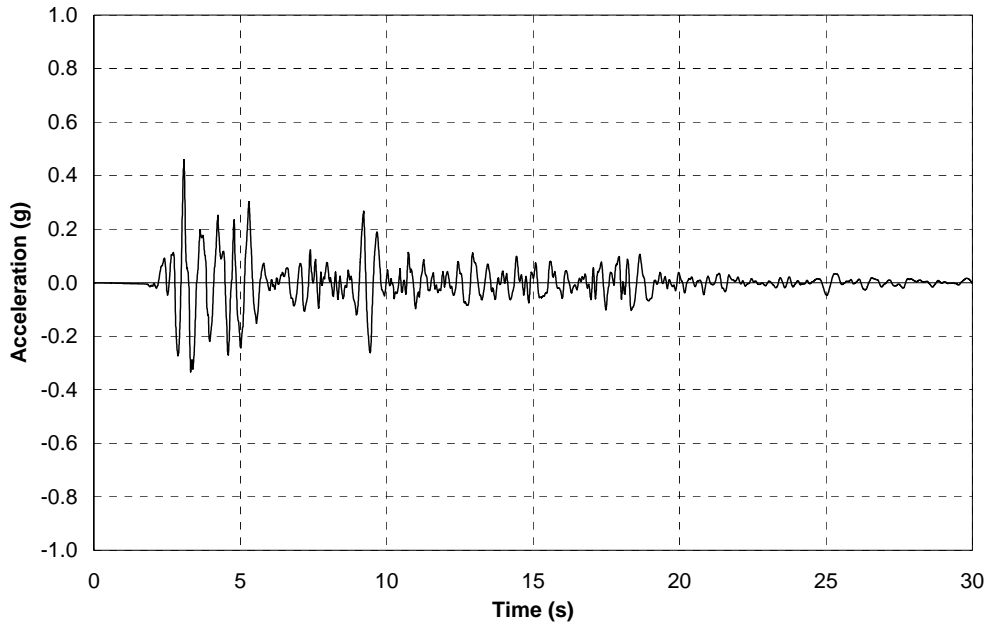


**FIGURE 2-31 Acceleration time histories for El Centro 180 component through soil layer**

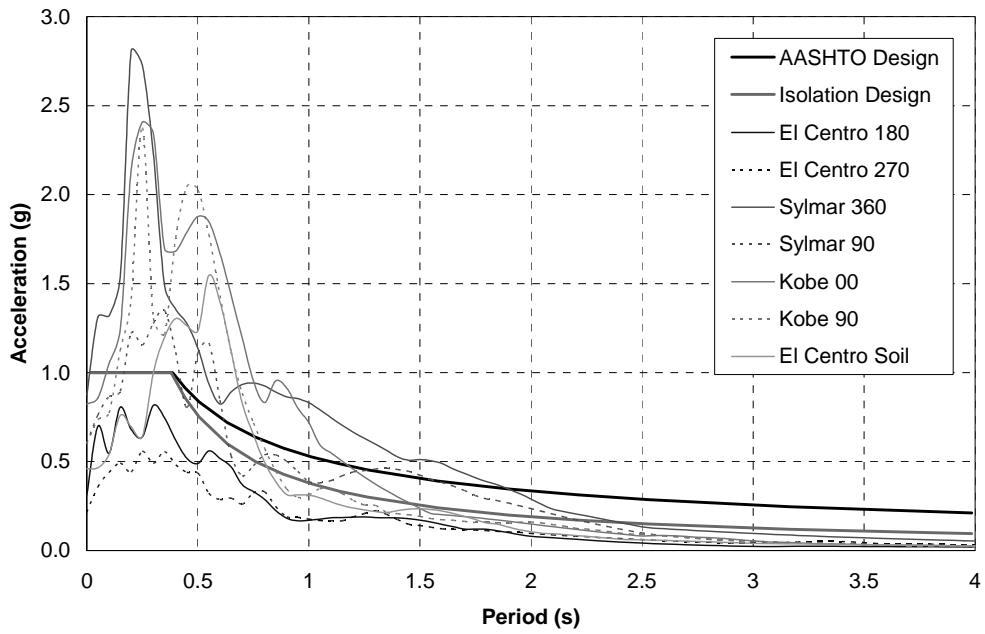


**FIGURE 2-32 Theoretical earthquake response spectra (5% damping)**

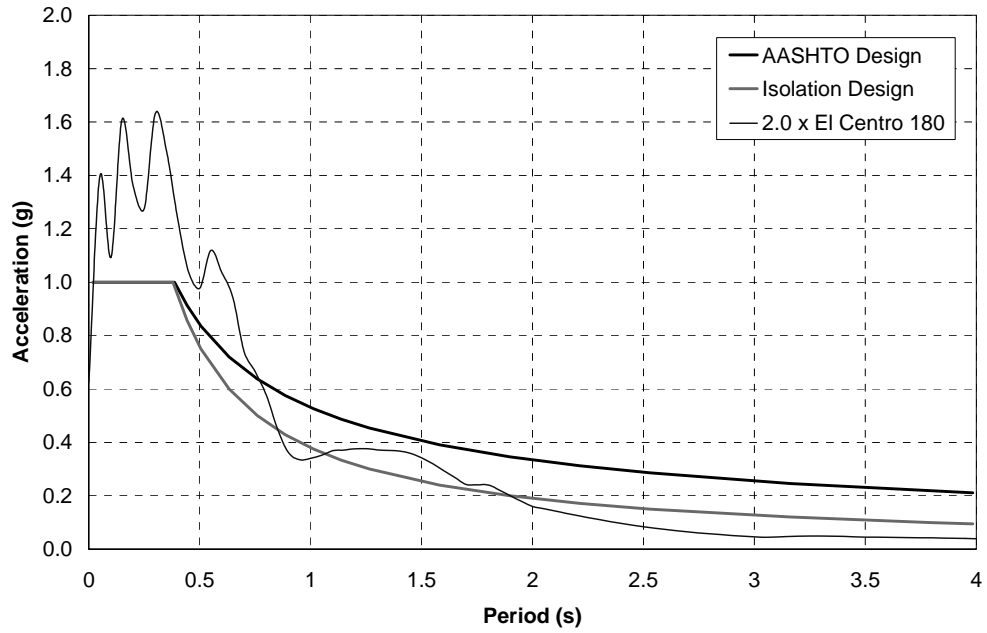


**FIGURE 2-33 Earthquake response spectrum for 2.0 El Centro (5% damping)**

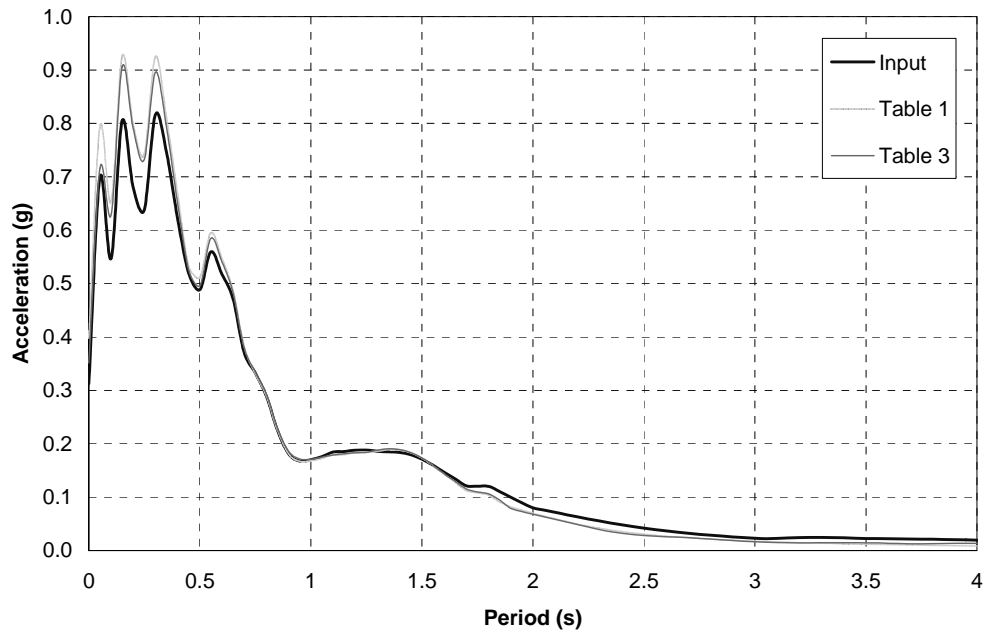


**FIGURE 2-34 STLRB - Response spectra for the target and achieved shake table accelerations at shake tables 1 and 3 in the longitudinal axis of the bridge model in response to 1.0 El Centro**

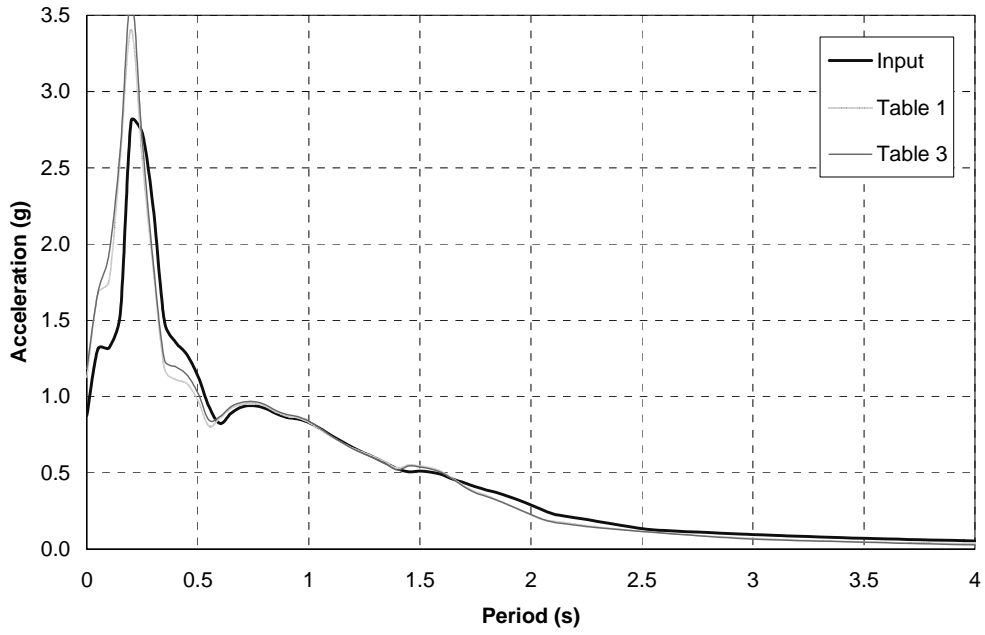


**FIGURE 2-35 STLRB - Response spectra for the target and achieved shake table accelerations at shake tables 1 and 3 in response to 1.0 Sylmar**

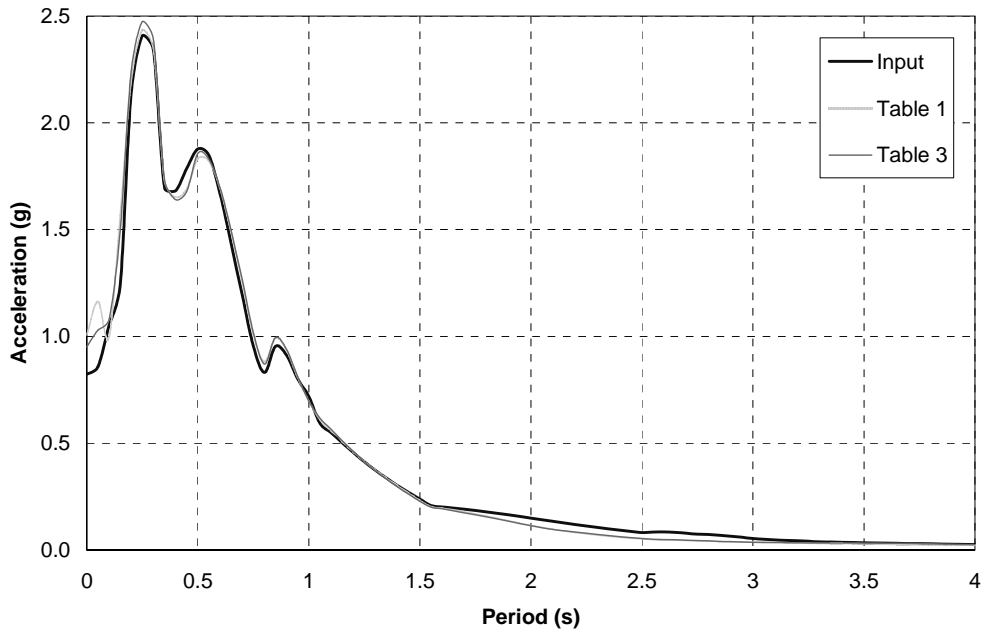


**FIGURE 2-36 STLRB - Response spectra for the target and achieved shake table accelerations at shake tables 1 and 3 in response to 1.0 Kobe**

## 2.7.2 Load Cells

Six multi-axial load cells were designed and constructed in order to measure the forces beneath the bearings in the bridge model. The load cells were designed using a series of strain gage circuits (Fig. 2-37) which were able to measure all six components of force, based on a design by Reinhorn, Bracci and Pekhan (2001).

The load cells were calibrated in the axial and two components of shear in order to convert the strain gage circuit output to forces. The apparatus for the axial and shear calibrations are illustrated in Figures 2-38 and 2-39 respectively. For the axial calibration a 980 kN MTS actuator was attached to a slider, designed to promote pure axial loads which in turn was attached to the load cell in series. Behind the load cell was a reaction frame. The shear calibrations were performed in a similar setup with two load cells calibrated in one direction at a time, as shown in Figure 2-39.

Plots of applied actuator force versus axial and shear output respectively, as a voltage differential, resulted in essentially straight lines. Hence a linear conversion from a voltage differential to a force for the three degrees of freedom of each load cell was calculated. Plots of applied actuator force versus calculated load cell force are shown in Appendix 4 for each calibrated load cell circuit. These plots show that there was good correlation between the measured and estimated forces. Although there is some hysteresis resulting in some error, this error was typically less than 5% at any given time. As the shear forces in the lead rubber bearings were much smaller than the maximum forces calibrated in the load cells, small amplitude cycles were applied in the shear calibration of load cells 5 and 6 for verification at low amplitude. Using the same calibration factors as calculated for the large amplitude calibration, the applied load versus calculated load cell shear forces for load cell six are shown in Figures A4.19 and A4.20. These figures show ideal elastic behavior in the load cells and forces which correlate to within 5%. Therefore the load cells were effective at measuring low amplitude forces as well as larger forces close to the maximum calibrated forces.

On each figure in Appendix 4 the forces for the degrees of freedom, other than that being calibrated are also shown. For the axial calibrations it can be seen that the shear forces were small, although not zero. The small shears were considered to be real shears due to small eccentricities in the loading. The shear calibrations show small orthogonal shear forces, which again were considered real forces. The shear calibrations also show relatively large axial loads, which were again considered to be real axial loads due to the test setup in shear not being able to completely eliminate secondary axial loads. As the orthogonal forces were generally small compared to the forces in the loaded direction, the interaction between applied forces and measured forces was considered negligible.

Loading was typically applied statically at a very slow loading rate and dynamically at a frequency of around 1 Hz during calibration of the load cells. Although 1 Hz is not a particularly high frequency loading, the amplitudes were relatively high, therefore the strain rates were as high as typically seen during shake table experiments. The difference between static and dynamic slopes was typically found to be around 2% or less, therefore dynamic effects were considered negligible.

The load cells were placed under the bearings at the ends of the bridge model and at midspan as illustrated, for example, in Figure 2-14. The load cells were numbered as shown in Figure 2-40. The axes with positive orientations are shown.



**FIGURE 2-37 Multi-axial load cell during construction**

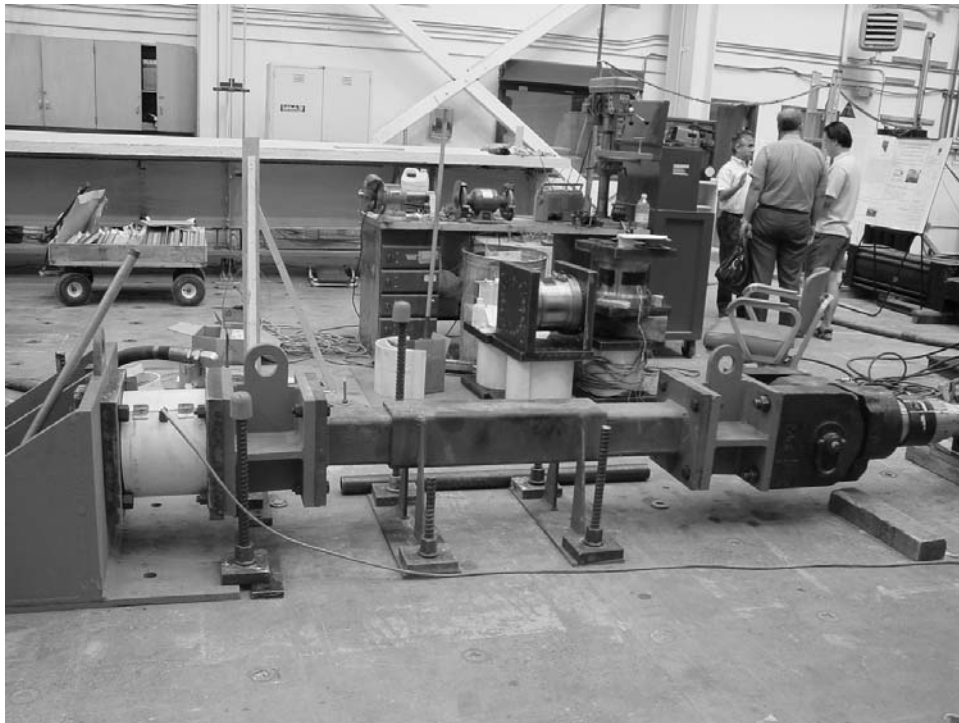


**FIGURE 2-38 Load cell axial calibration**

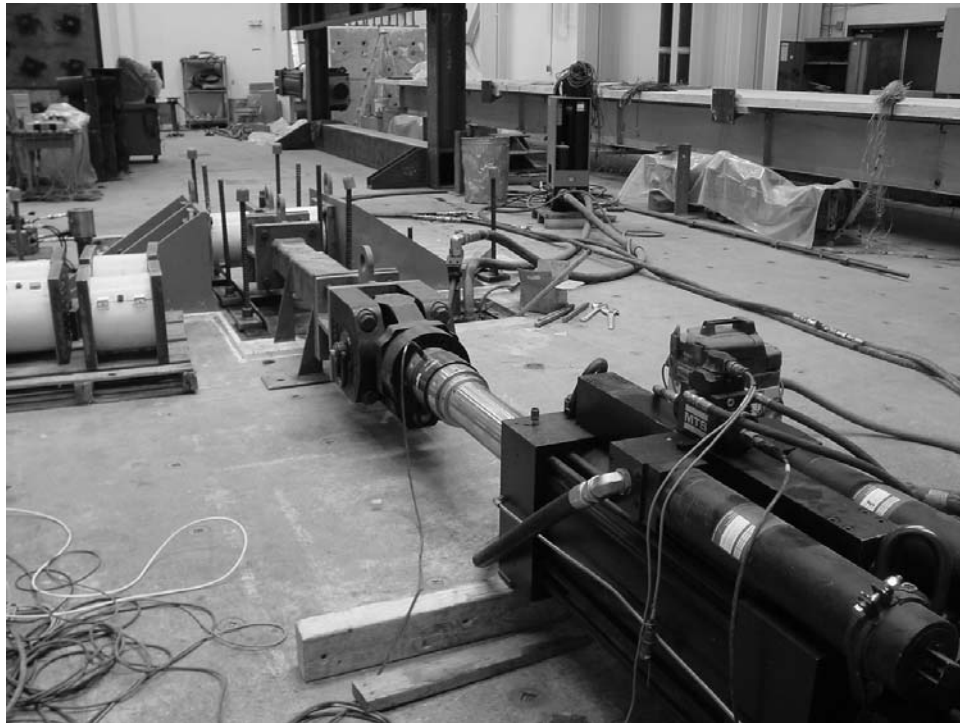


**FIGURE 2-39 Load cell calibration in shear**

### **2.7.3 Displacement Transducers**

Deformations in the bridge model were measured using displacement transducers attached to the bridge at different locations. Some transducers were attached to the bridge model and some fixed point in the laboratory, such as those attached to the deck slab, therefore measured absolute displacements. Others were attached to the bridge model and fixed points relative to the shake tables therefore measured relative displacements. The majority of displacement transducers used were Celesco PT100 series cable-extension transducers including the displacement transducers along the length of the superstructure, as shown in Figure 2-41. Celescocs were also used for the displacement transducers at the bearings, the length of the cables connecting the transducers to the bridge model were relatively short, therefore for bi-directional motion the longitudinal and transverse components were coupled, and corrections were made where necessary to the raw data to allow for this coupling.

At the end cross frames Novotechnik linear potentiometers were used to measure displacements in the end regions. The positions of these transducers are shown in Figures 2-42 and 2-43 respectively. Diagonally placed transducers were used to measure the lateral deformation between the top and bottom flanges of the girders as shown in these figures. Additional transducers were used to measure displacements across the yielding portions of the X-braces and unbonded braces respectively. At the north end transducers were also used to measure slippage in the top chord and unbonded brace connections.



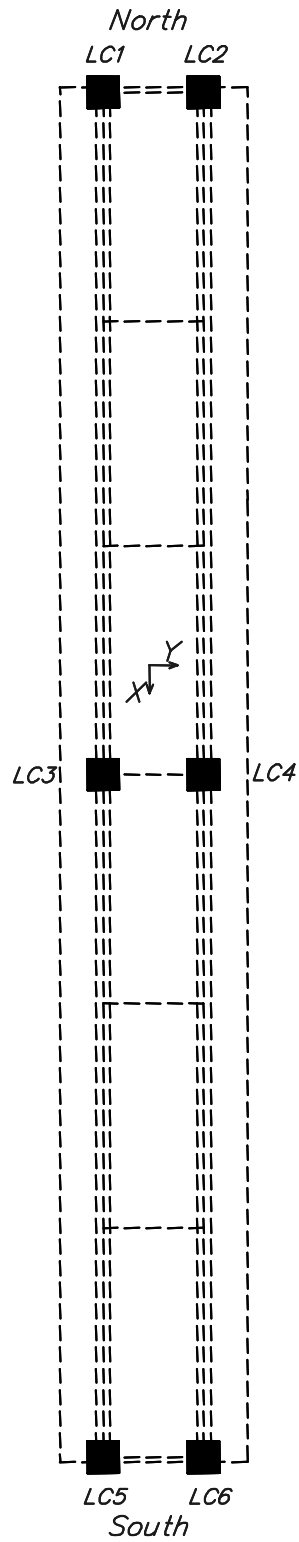


**FIGURE 2-40 Instrumentation - load cells**

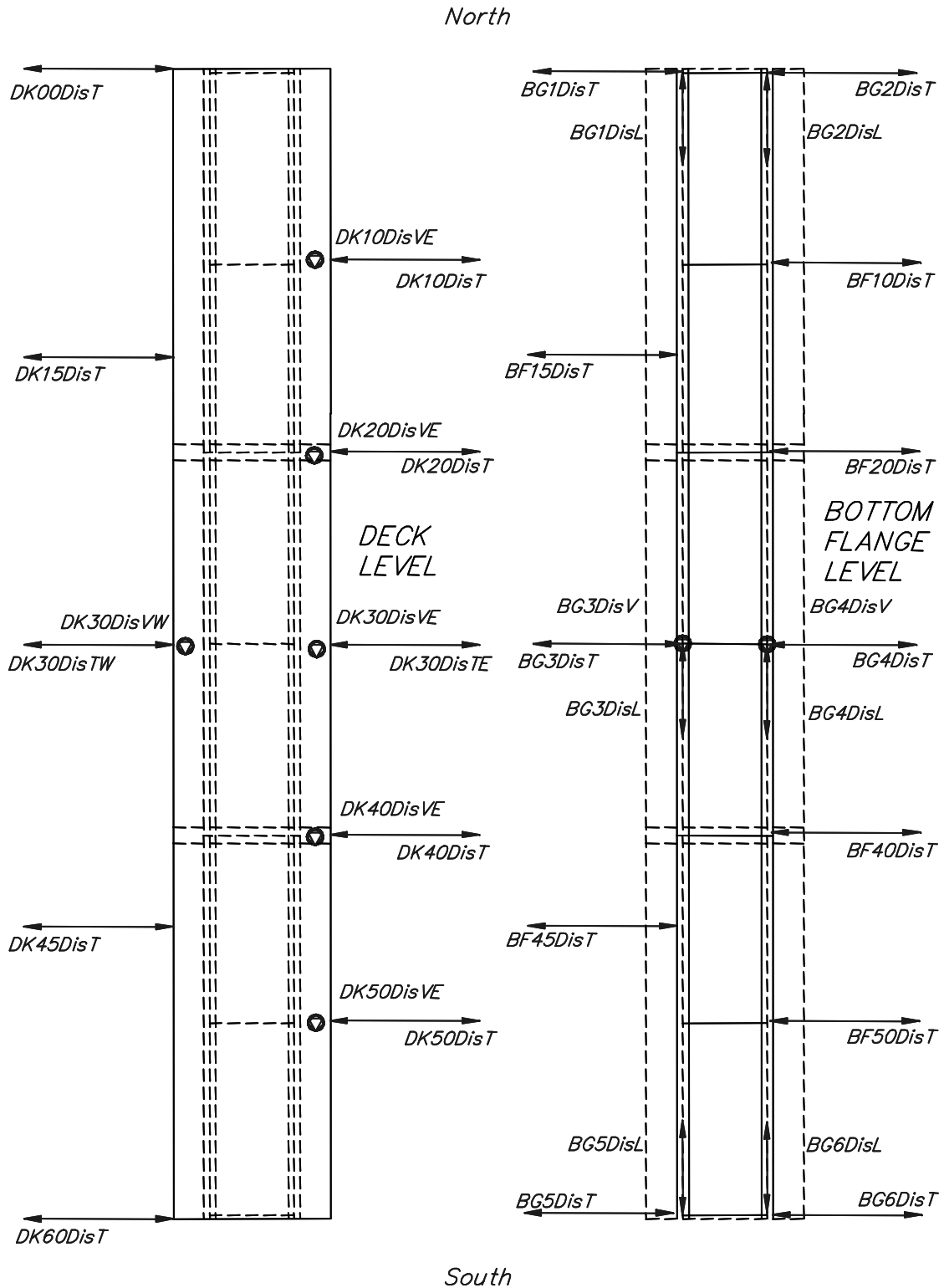


**FIGURE 2-41 Instrumentation - displacement transducers**

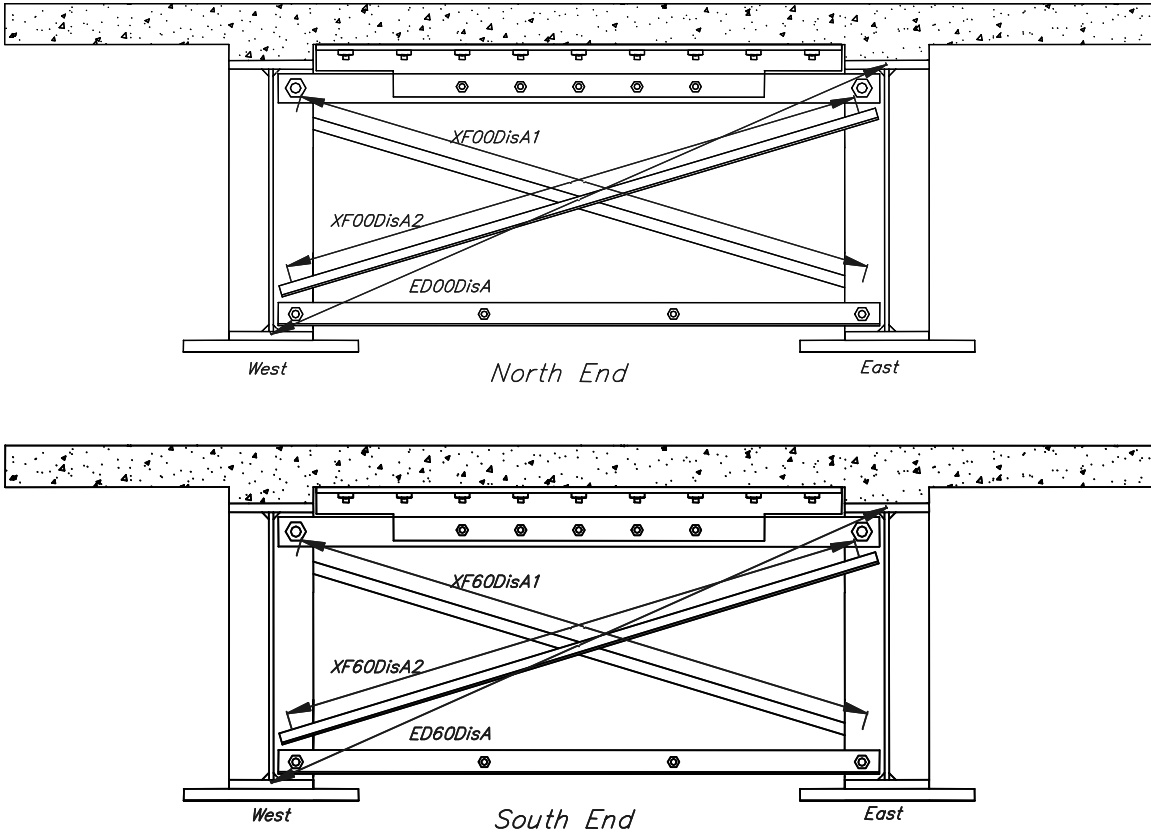


**FIGURE 2-42 Instrumentation - typical displacement transducers for end X-braces**

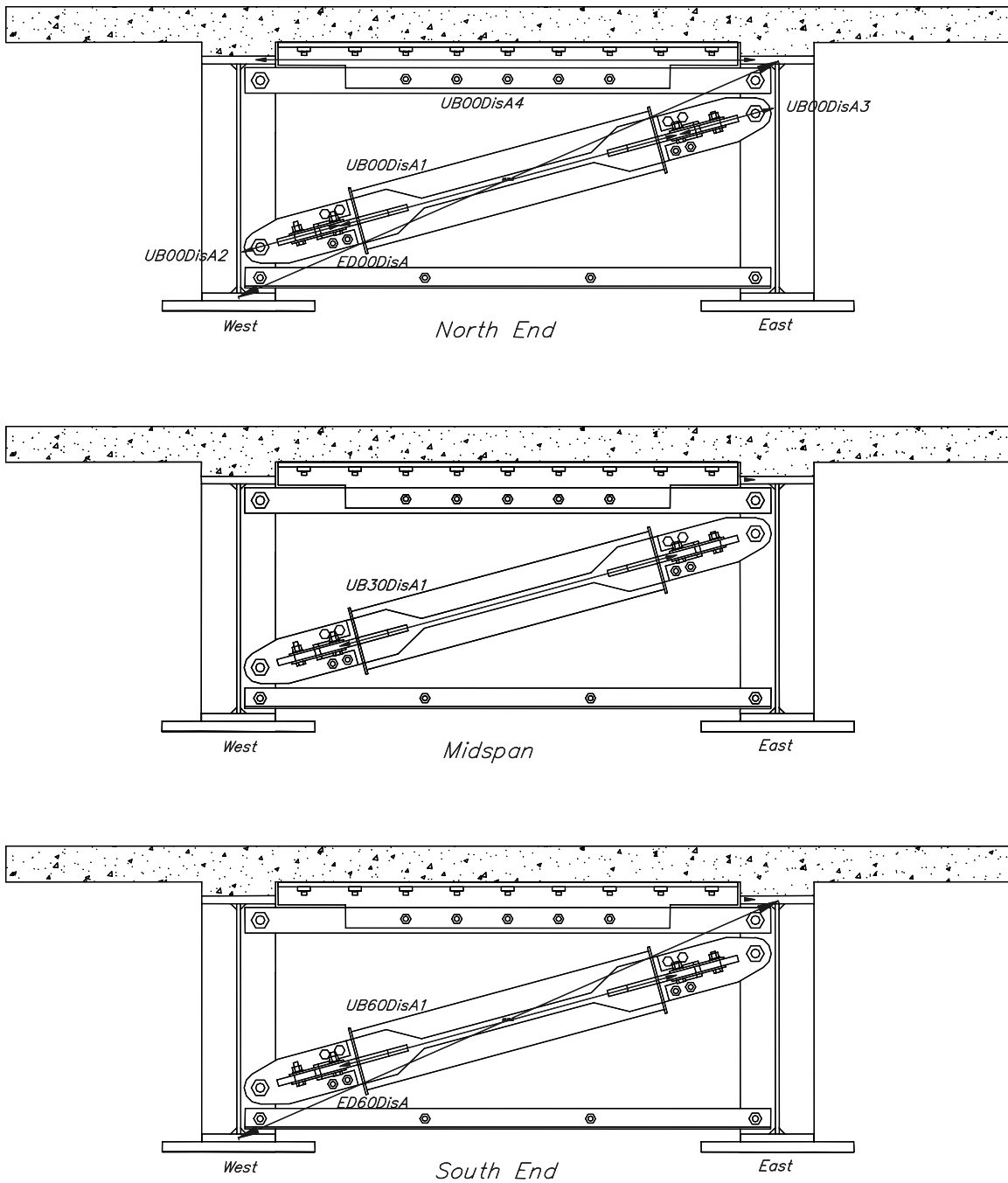


**FIGURE 2-43 Instrumentation - displacement transducers for unbonded braces**

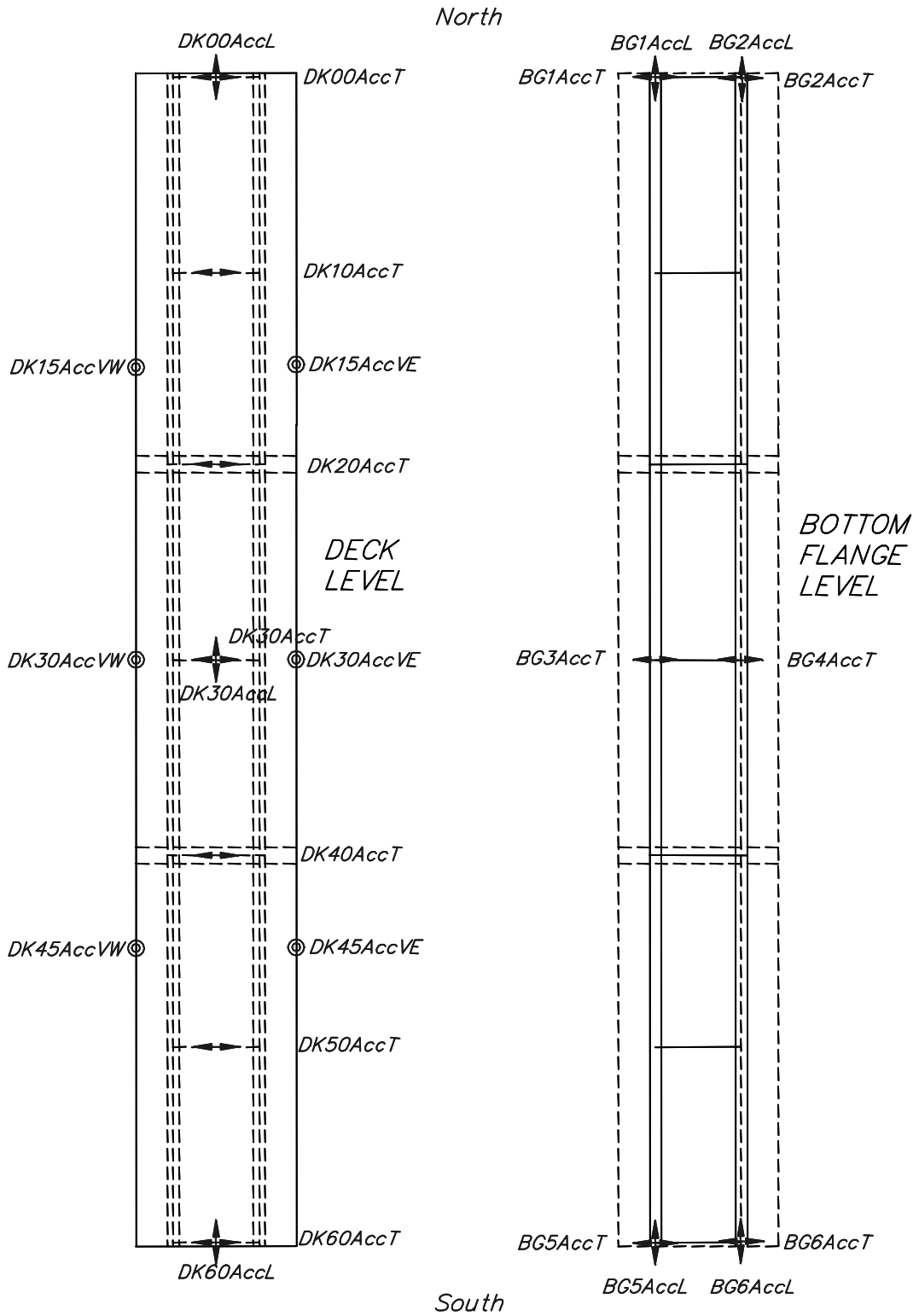


**FIGURE 2-44 Instrumentation - accelerometers**

## 2.7.4 Accelerometers

Accelerometers were situated throughout the bridge model for system identification, measurement of modeshapes and natural frequencies, and for comparison between shake table and bridge response. Accelerometers were placed on the deck slab, bottom flange and on top of bearings as shown in Figure 2-44. Horizontal accelerometers on the deck slab were Kinematic  $\pm 2g$  accelerometers. Horizontal accelerometers on the bottom flange and bearings were  $\pm 4g$  accelerometers. Vertical accelerometers were also  $\pm 4g$  accelerometers and were attached to the edges of the deck slab in order to measure vertical and rotational modes of deformation.

## 2.7.5 Strain Gages

Strain gages were placed throughout the bridge model in order to measure localized strains at critical locations on the plate girders and in the deck slab. They were also situated on the cross frames in an attempt to correlate strains to forces in the cross frames. To avoid clutter, dimensions for every strain gage are not shown however where necessary their locations can be scaled off the drawings.

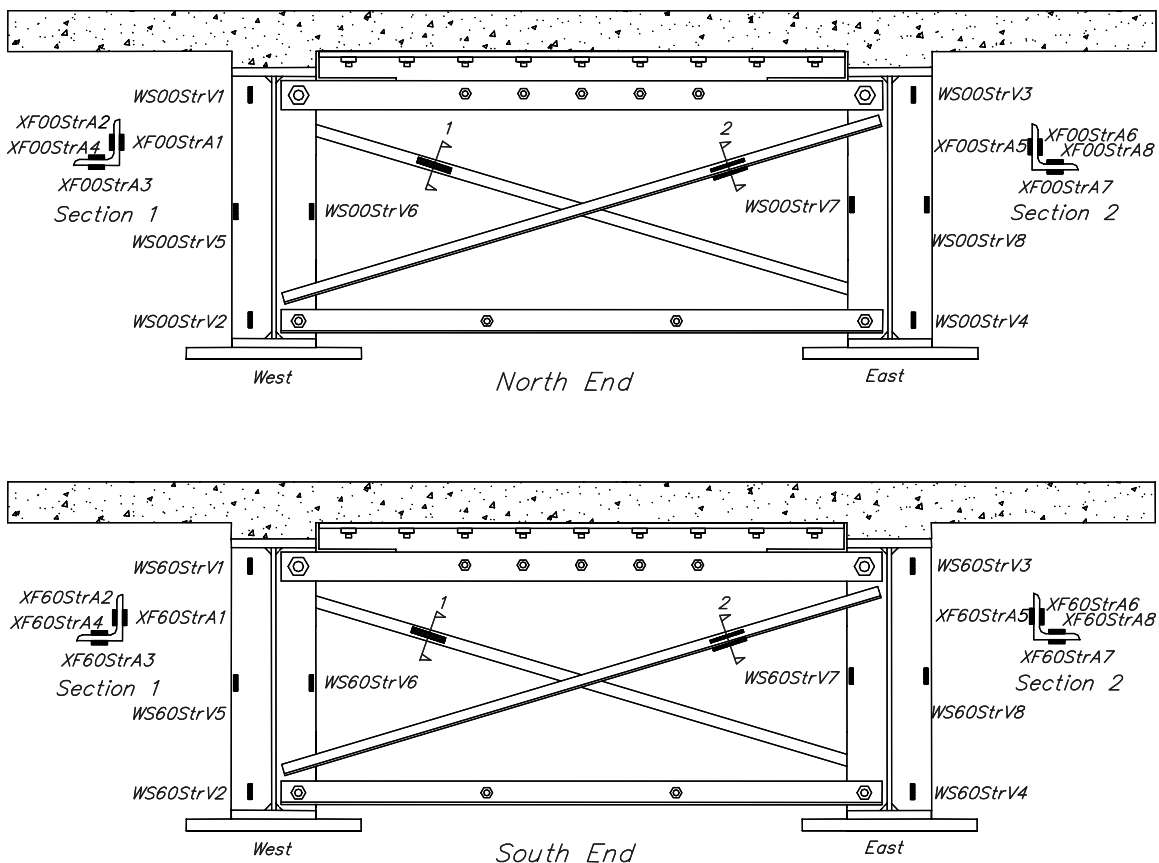
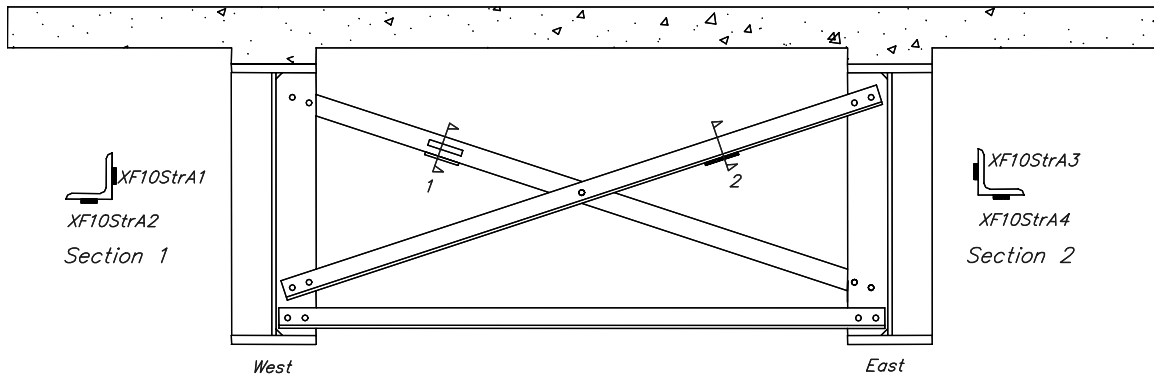


FIGURE 2-45 Instrumentation - strain gages on end cross frames

Eight strain gages were typically placed on the end cross frames as shown on Figure 2-45. It was shown from the end cross frames that the measured strains on the inside and outside of the angle members were similar. Therefore, the intermediate cross frames typically have four strain gages on each set as shown in Figure 2-46.

There were a number of strain gages placed on the stiffeners at the ends of the bridge model. Eight strain gages at each end are shown in Figure 2-45. In addition for another set of strain gages was placed on the bearing stiffener of the west girder, at the north end of the bridge at the edges of the stiffeners, in order to get a better understanding of the distribution of bending strains in the stiffener (Fig. 2-47).

A series of strain gages were also placed on the girders in order to measure the distribution of strains along the length of the girders. The strain gages on the east girder were distributed as shown in Figure 2-48. On the west girder strain gages were placed on the outside edges of the top and bottom flanges concentrated at the north end of the bridge model (Fig. 2-49) in order to get more detailed measurements of strain distributions at the end of a girder when there were large transverse deformations in the girders.



**FIGURE 2-46 Instrumentation - strain gages on typical intermediate cross frame**

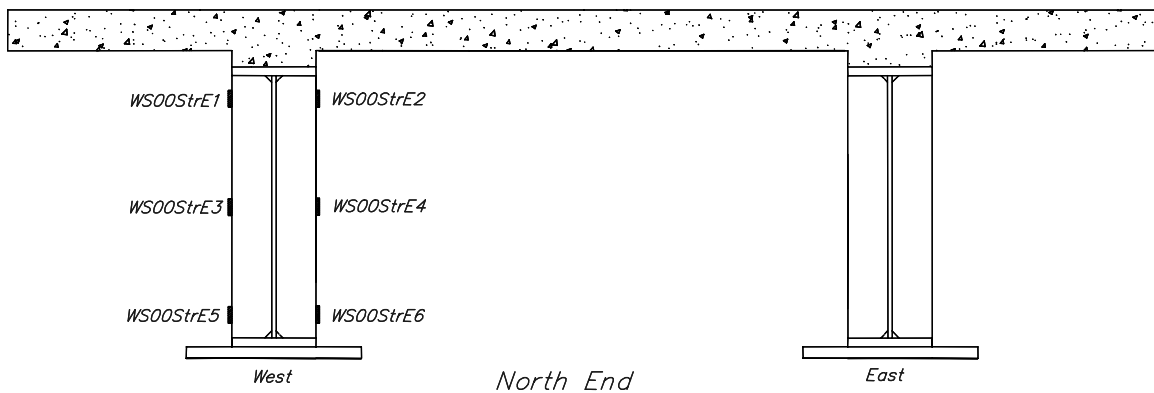


**FIGURE 2-47 Instrumentation - additional strain gages on end stiffener**

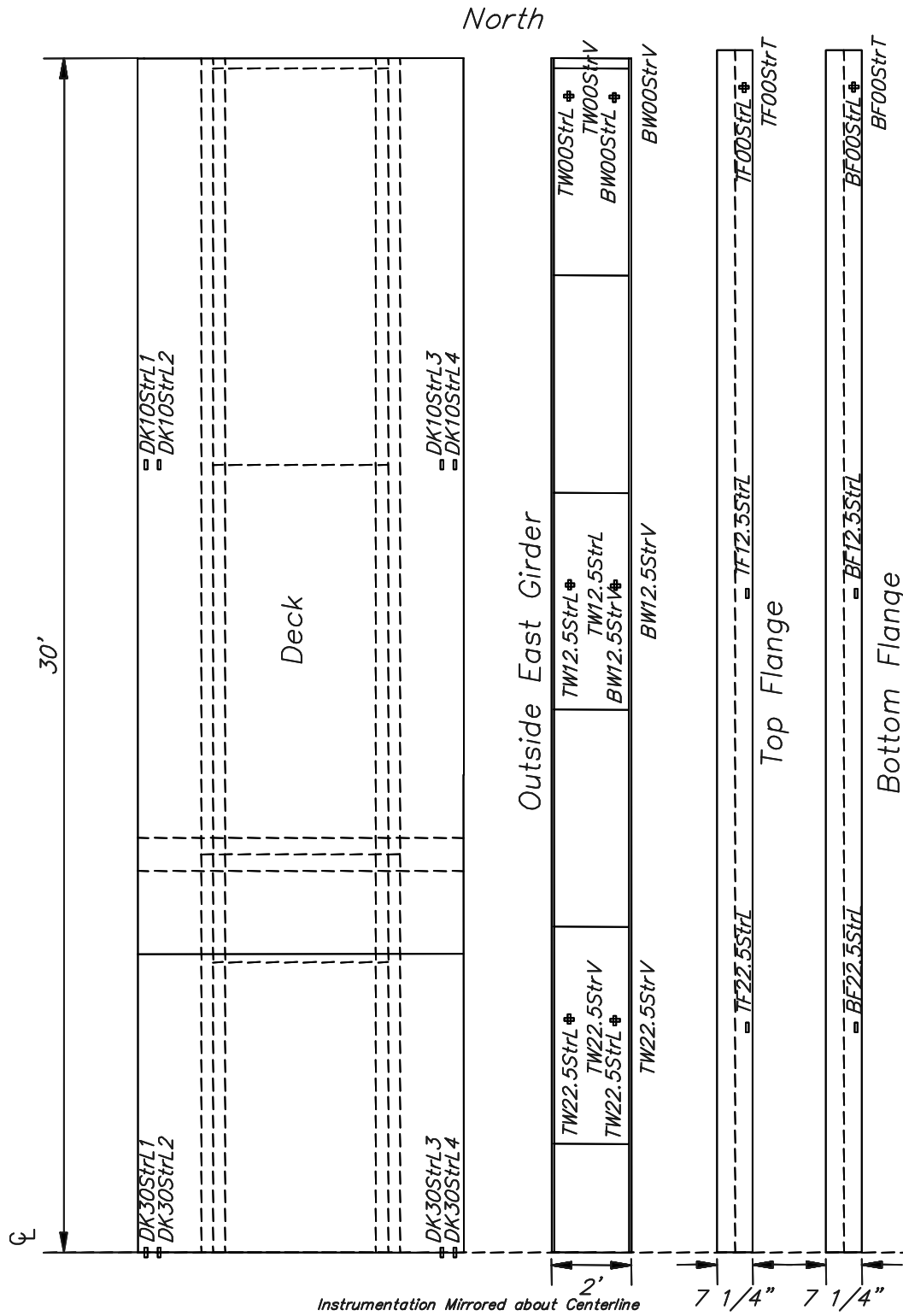


**FIGURE 2-48 Instrumentation - strain gages on east girder**



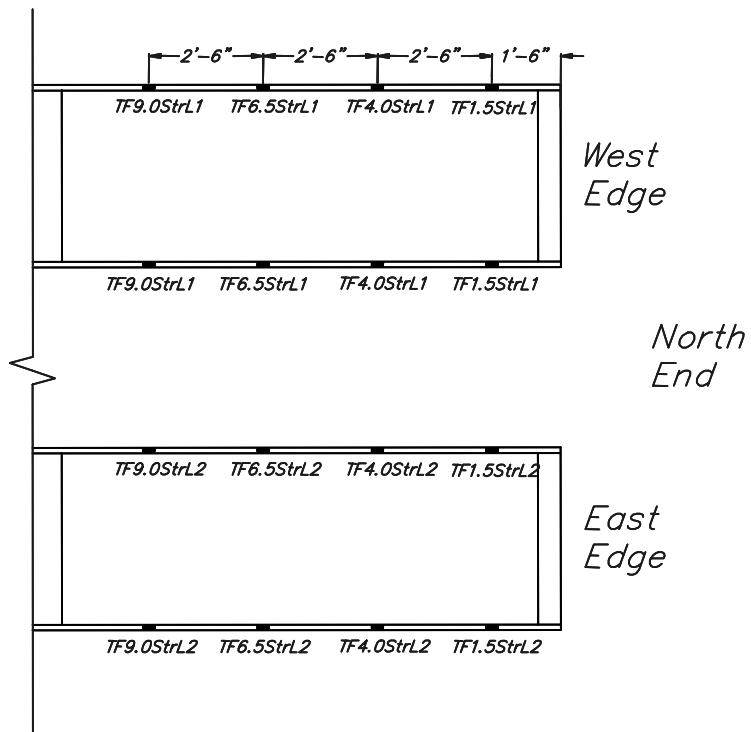


**FIGURE 2-49 Instrumentation - strain gages on west girder**



## SECTION 3

### OVERVIEW OF DEFORMATIONS AND MODAL RESPONSE OF THE BRIDGE MODEL DURING REVERSED STATIC AND SHAKE TABLE EXPERIMENTS

#### 3.1 Introduction

Before discussing details of the performance of the various bridge model components it is first necessary to examine the overall seismic response of the structure. The superstructure was shown to be relatively flexible due to only two girders and its relatively narrow width. This had a significant impact on the response of the bridge model. The responses during reversed static and shake table experiments are summarized in this chapter. A detailed elastic finite element analysis is introduced which is compared to the experimental results and later used to help determine the properties of the bridge model.

#### 3.2 Overview of Results from Reversed Static Experiments

A summary of the reversed static experiments performed is given in Table 2-1. The experiments were performed with different cross frames and with and without intermediate cross frames. The first experiment (RSHXB1) consisted of “heavy” 45 x 45 x 6 mm single angle diagonal X-braces at the ends of the bridge bolted along with double angle top and bottom chords to gusset plates. The gusset plates were bolted to the bearing stiffeners (Fig. 2-11). As reversed static transverse earthquake loads were applied to the bridge model, the bridge deformed laterally and rotated about its longitudinal axis, as shown in Figure 3-1. The rotation was attributed to an eccentricity between the shear center of the bridge. Cracking of the deck slab occurred almost immediately in the first cycles of loading with transverse flexural cracking observed along the length of the bridge propagating from the edges of the deck slab as shown in Figure 3-2. Shear cracking was also observed in the two end thirds of the deck slab at an angle of approximately 45° to the longitudinal and transverse directions (Fig. 3-3). At a total applied actuator load of around 270 kN cracks were observed in the haunch at the north end of bridge around where the shear studs were located. The test was terminated when it was apparent that several rows of shear studs had failed at the north end of the bridge (Fig. 3-4). There was no significant damage at the south end which is attributed to the transfer of forces between the deck slab and the end cross frames by the composite top chord at this end (Fig. 2-12). The end cross frames performed essentially elastically in this experiment with the onset of buckling observed.

For the second reversed static experiment (RSHXB2) the top chord detail for the end cross frame at the south end was replicated at the north end. An area of deck slab around the damaged studs was removed (Fig. 3-5), the damaged studs were replaced and grouted into the deck slab. As loads were applied during the second reversed static experiment, some cracking was observed in the grout around the repaired studs, which did not perform as well as anticipated. Despite this cracking the experiment was continued up to a base shear of 574 kN. Further onset of buckling was observed in the end cross frames as shown in Figure 3-6. The experiment was terminated before significant yield of the end cross frames was observed due to failure of one of the actuator supports. Large rotations of the bridge superstructure had resulted in bending moments due to P-delta effects for which the supports were not designed. This experiment gave valuable information on the transverse load path through the bridge model. The deformed shape of the bridge model measured using deck slab displacements at the ends and midspan at a base shear of 133 kN, is summarized in Table 3-1. The end displacement was averaged between the two ends. The



**FIGURE 3-1 RSHXB - Deformed deck slab of bridge model during transverse loading**



**FIGURE 3-2 Transverse flexural cracking observed along the length of the bridge model propagating from the edges of the deck slab**



**FIGURE 3-3 Shear cracking observed in the end thirds of the deck slab at an angle of approximately 45 degrees to the longitudinal and transverse directions**



**FIGURE 3-4 RSHXB - Failure of shear stud at north end of bridge model**



**FIGURE 3-5 Removal of concrete for rehabilitation of shear studs at north end of bridge model**



**FIGURE 3-6 RSHXB2 - Onset of buckling in diagonal member of end X-brace**

flexibility coefficient,  $\alpha$ , is defined as the ratio of the midspan superstructure displacement minus the end displacement divided by the midspan displacement, as illustrated in the figure associated with Table 3-1.

A more detailed representation of the deformed shape of bridge model with the “heavy” single angle cross frames, as measured by the displacement transducers in RSHXB2, is illustrated in Figures 3-7 and 3-8 for applied shears of negative and positive 133 kN corresponding to “pushing” and “pulling” reversals respectively. Each arrow on these figures have associated displacements in inches with negative values indicating displacements in the opposite direction to the arrow. The rotation of the bridge shows that the shear center was at some point above the bridge deck slab with the applied lateral force below the mid height of the deck slab. The magnitude of relative deformations at each end of the bridge model was quite variable due to slippage in the end cross frames. The slippage resulted in a variation in displacement amplitudes at the ends between 0.5 mm and 2.3 mm with an average of 1.8 mm. When compared to the displacements of the deck slab at midspan, the end displacements were small. The transverse deck slab displacement at midspan, averaged between the positive and negative cycles, was 21 mm. Therefore, the flexibility coefficient was 0.91. This shows that while the cross frames were elastic the deformation of the bridge model was dominated by the flexural-torsional deformation of the superstructure.

The following four reversed static experiments investigated the deformation of the bridge model with no end cross frame diagonals, no top and bottom chords and no intermediate cross frames. The absence of some or all of these components lowered the transverse stiffness of the bridge and increased the end displacement relative to the overall displacement (Table 3-1). Experiment RSFC shows that with no diagonals but moment resisting top and bottom chords still in place, and bolted to gusset plates and the bearing stiffeners with moment resisting connections, the end displacement remains small as bending action in the chords limits movement in the ends. When the bottom chord was removed (RSNBC) there was little difference in the relative deformations. With no diagonals or chords (RSNECF) then end displacement increased to 50% of the overall displacement. There was a further reduction in end stiffness when the intermediate cross frames were removed (RSNCF), although this was relatively minor.

The next experiment (RSPC) investigated the use of pinned top and bottom chords. Table 3-1 showed that in the overall deformation of the bridge model using these chords at the ends was much larger than with the fixed chord connections. This was expected to be beneficial in increasing the proportion of load carried by the diagonal members, making them more effective as ductile fuses in the system while minimizing the post yield increase in strength.

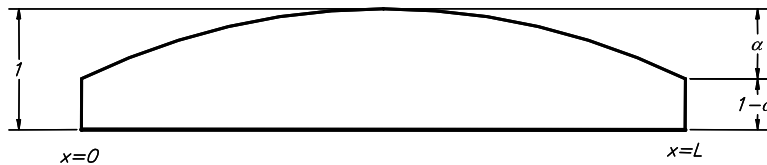
The last reversed static experiment (RSLXB) used the pinned top and bottom chords in the end cross frames along with “light” single angle diagonal members. The elastic deformation of the bridge model was similar to that for the “heavy” cross frames as indicated by Table 3-1. Once the elastic capacity of the braces was exceeded the diagonal members buckled and yielded, exhibiting significant inelastic deformations (Fig. 3-9).

The deformation of the bridge at applied shears of positive and negative 133 kN is shown in more detail in Figures 3-10 and 3-11 respectively. The ends have a similar average displacement, with the lower stiffness of the smaller diagonal members offset by the prevention of slippage using bolted connections. By this stage further cracking was observed in the grouted repairs around the

**TABLE 3-1 Relative End to Midspan Displacement for Different Reversed Static Experiments**

Expt	Average Displacements (mm) <sup>1</sup>		Alpha
	Midspan	End <sup>2</sup>	
RSHXB <sup>3</sup>	12	-	-
RSHXB2	21	2	0.92
RSLXB	30	3	0.91
RSFC	32	5	0.83
RSNBC	33	7	0.79
RSPC	40	15	0.63
RSNECF	47	24	0.50
RSNCF <sup>4</sup>	38	20	0.48

- Notes:
1. Displacements are averaged between positive and negative cycles
  2. Displacements are averaged between north and south ends
  3. No end displacements recorded
  4. Values taken at base shear of 89 kN rather than 133 kN



shear studs resulting in a lower transverse stiffness at the north end compared to the south end. As a result there was a relatively large displacement measured at the north end compared to the south end. The average deflection at midspan increased to 30 mm. This was likely to have been due to further cracking in the deck slab and some localized yielding of the reinforcing. The  $\alpha$  value, averaged between the two ends, is calculated at 0.91.

The displacements in the bridge model with the largest measured end cross frame displacements are shown in Figure 3-12. Comparison with Figure 3-11 shows that while the midspan displacements had increased the end displacements were much larger and the average flexibility coefficient was 0.63. The reduction in  $\alpha$  illustrates how the displacements were redistributed into the ends of the bridge once the cross frames yielded. Again there were larger displacements measured at the north end compared to the south end due to some damage to the shear studs and therefore lower effective stiffness at the south end. The effect of the shear studs and composite action is discussed further in Chapter 4, while the inelastic behavior of the cross frames is discussed in more detail in another report (Carden, 2005).

### 3.3 Overview of Shake Table Experiments

The experiments performed on the bridge model using the three shake tables were used to dynamically evaluate the performance of isolation systems and ductile end cross frames. Each earthquake simulation on the bridge model is listed in Appendix 3.



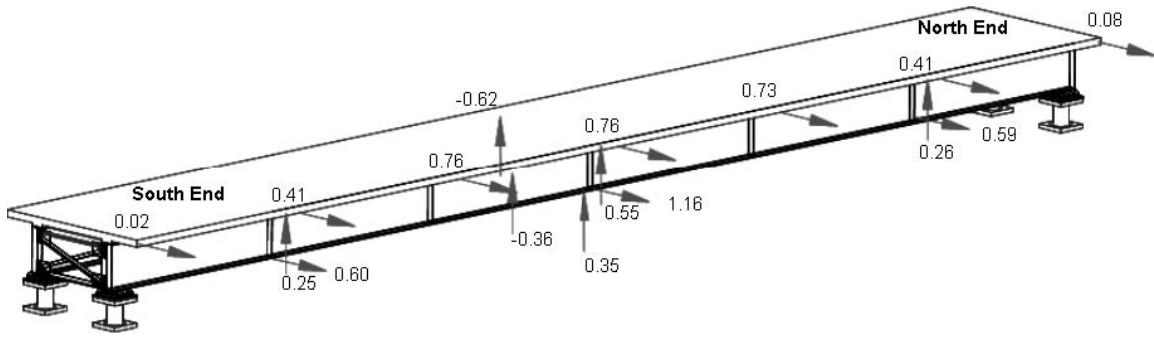


**FIGURE 3-7 RSHXB2 - Deformation of bridge model at +133 kN**

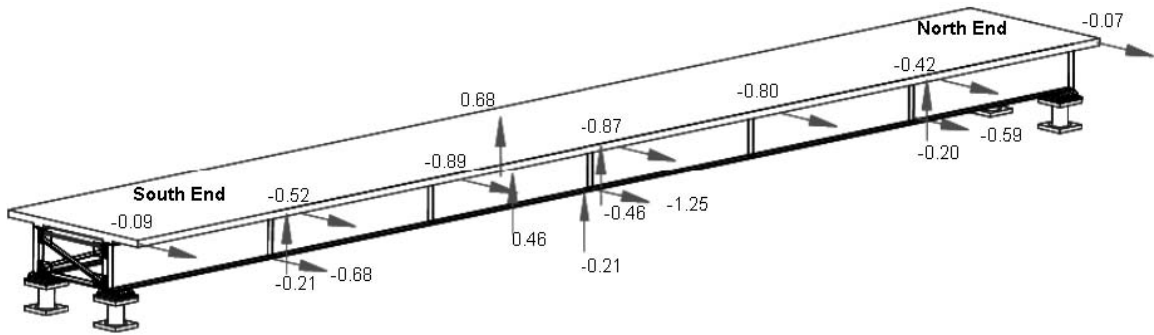


**FIGURE 3-8 RSHXB2 - Deformation of bridge model at -133 kN**

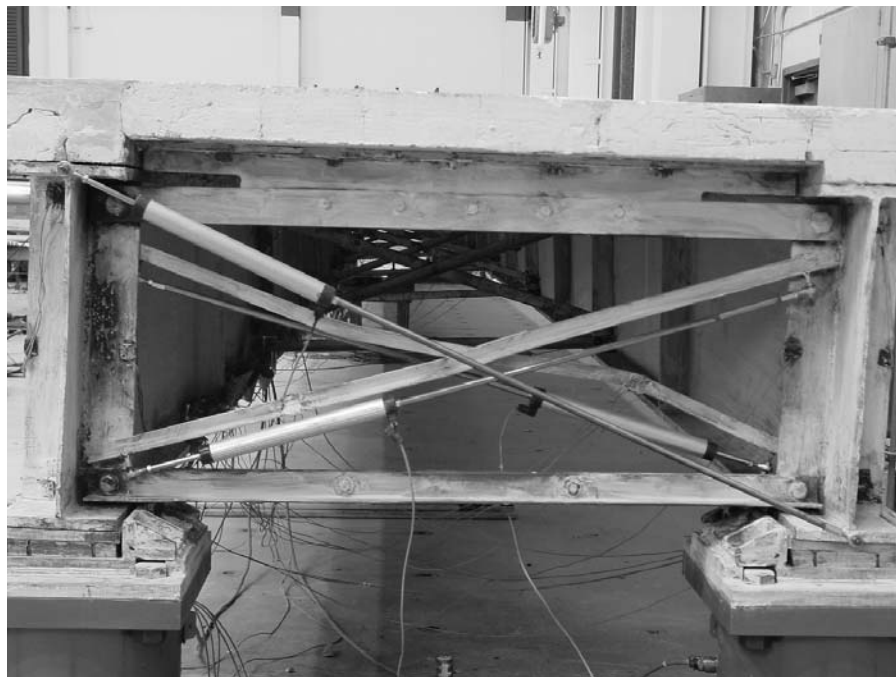


**FIGURE 3-9 RSLXB - Deformation of single angle X-braces at the north end**

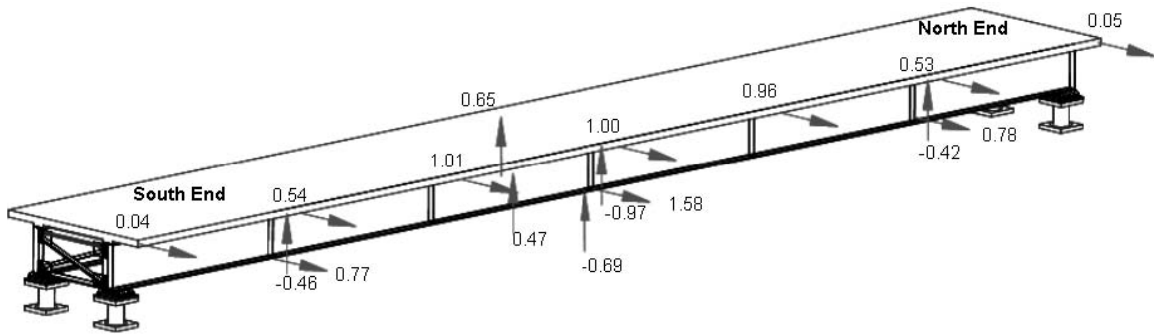


**FIGURE 3-10 RSLXB - Deformation of bridge model at +133 kN**

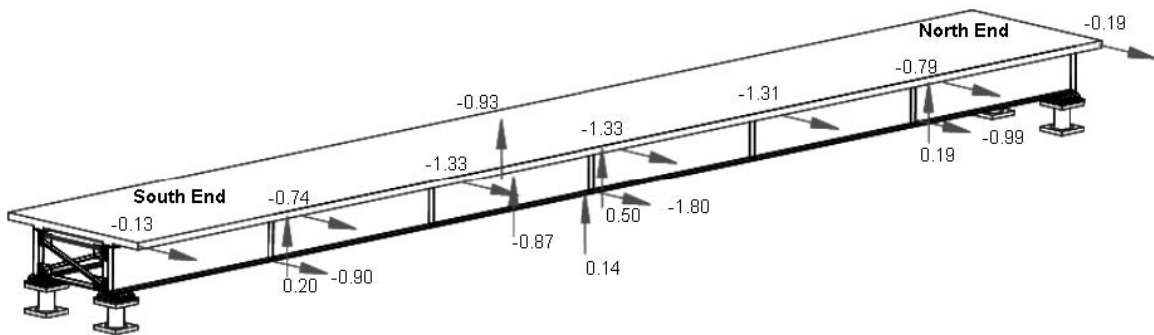


**FIGURE 3-11 RSLXB - Deformation of bridge model at -133 kN**

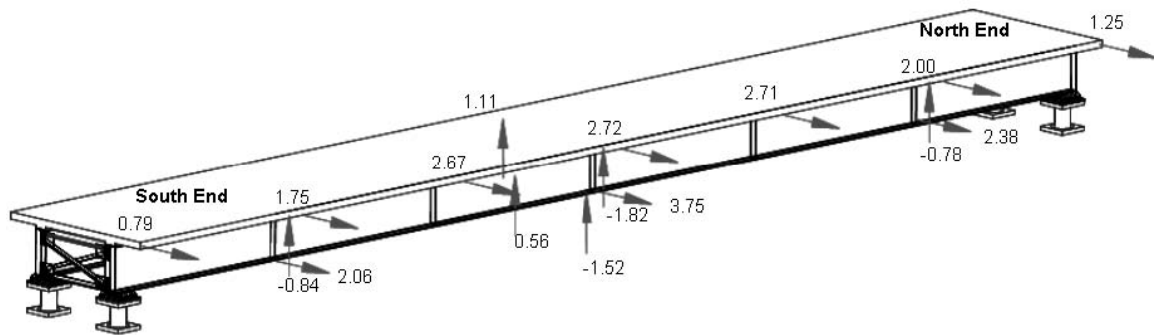


**FIGURE 3-12 RSLXB - Deformation of bridge model at -320 kN**

The bridge model was first excited dynamically in a simply supported seismically isolated configuration. Appendix 3 details the different earthquakes and different amplitudes. The bearings performed as expected up to their design displacement. As the bearings were relatively slender, they were susceptible to buckling at displacements in excess of their design displacements. Consequently, once the design displacements were exceeded, dynamic buckling of the bearings was observed, which is discussed further in another report (Carden, 2005).

The deformation of the bridge model during shake table experiments was measured using both displacement transducers and accelerometers. The bridge model was subjected to white noise excitations during each series of experiments. Using a Fourier analysis to compare the shake table input acceleration with those recorded at various locations in the bridge model it was possible to calculate the natural frequencies and modeshapes for both longitudinal and transverse excitation. In the Fourier analysis the acceleration records were broken up into equal length segments incorporating 2048 points, with each segment overlapping the previous segment by half of the length of the segment, resulting in 12 segments. The fast Fourier transforms and transfer functions were then calculated for each segment of each acceleration record. The segments were combined using Hamming windowing to give an average transfer function for each accelerometer on the bridge over the length of the white noise record. The transfer function gives the amplification of the response of the bridge model at different periods, indicating the effective resonant periods of the bridge model at the level of excitation defined by the white noise.

A summary of the dynamic natural periods for the seismically isolated bridge model are shown in Table 3-2. The modal properties were calculated using a white noise motion at the beginning of the series of experiments on the simply supported isolated bridge model, although there was little change in the properties after many earthquake simulations. The amplitude of the transfer function for the accelerometers on the deck slab of the bridge plotted against period is given in Figure 3-13. Figures 3-14 and 3-15 show similar transfer functions for the transverse accelerometers on top of the bearings and vertical accelerometers at the deck slab level. Because the amplitude of the motion was relatively low, with an average maximum transverse bearing displacement of 4 mm (only 7% of the design displacement), these periods represent the properties of the bridge model as the bearings performed essentially elastically. Despite being essentially elastic at this low

**TABLE 3-2 Natural Periods and Flexibility Coefficient for Bridge Model Isolated with Lead Rubber Bearings**

Expt. Series	No.	Natural Period (s)			Modeshape Alpha <sup>1</sup>	Comments
		Mode 1	Mode 2	Mode 3		
Single Span (Series 1)	1	0.49	0.27	0.10	0.55	From white noise at beginning of experiment series. Average max. bearing displ. of 0.15 in
	2	0.74	-	-	0.21	Estimated from sine sweep with average bearing displacement of 0.84 in
Two Span	1	0.40	-	-	-	From white noise at beginning of experiment series
Single Span (Series 2)	1	0.49	0.28	0.10	0.55	From white noise at beginning of experiment series

Notes: 1. Alpha given for mode 1

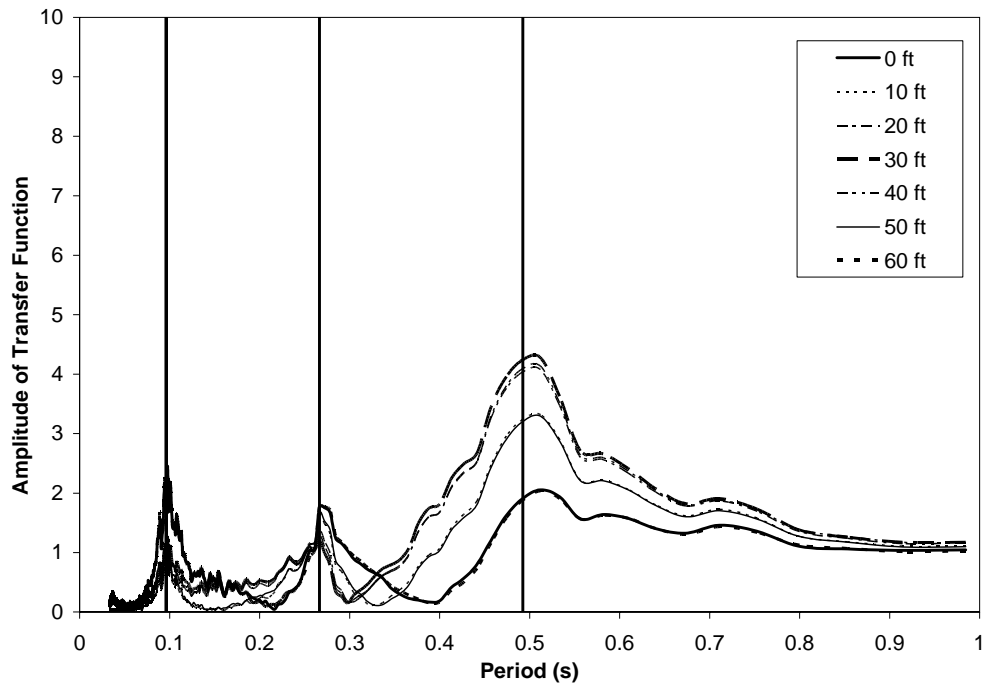


**FIGURE 3-13 STLRB - Transfer function amplitude for transverse accelerometers at deck slab level**

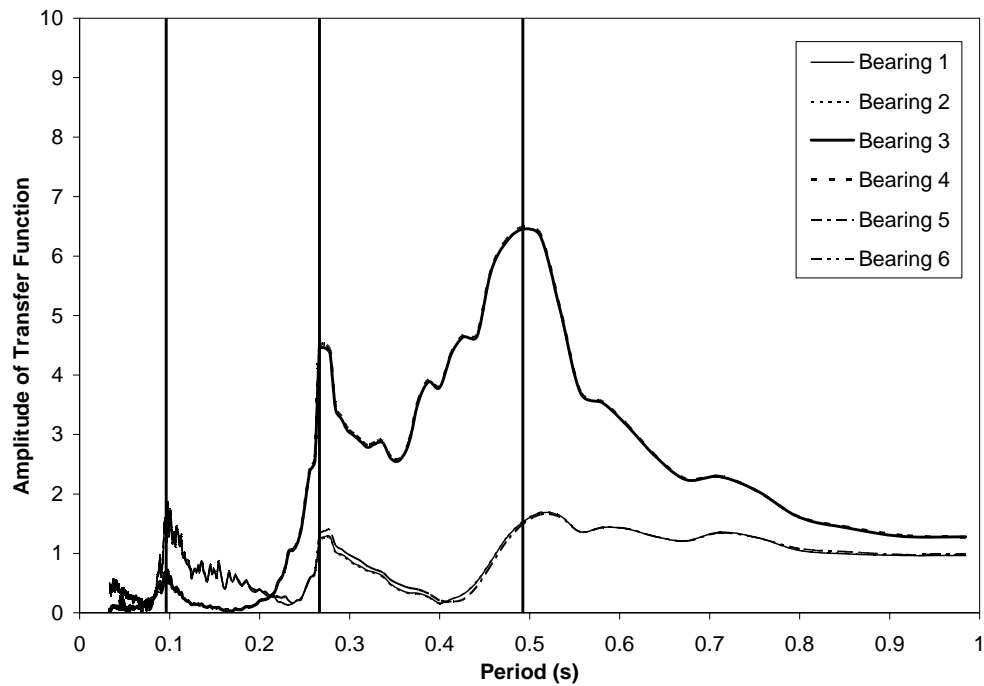


**FIGURE 3-14 STLRB - Transfer function amplitude for transverse accelerometers above bearings**

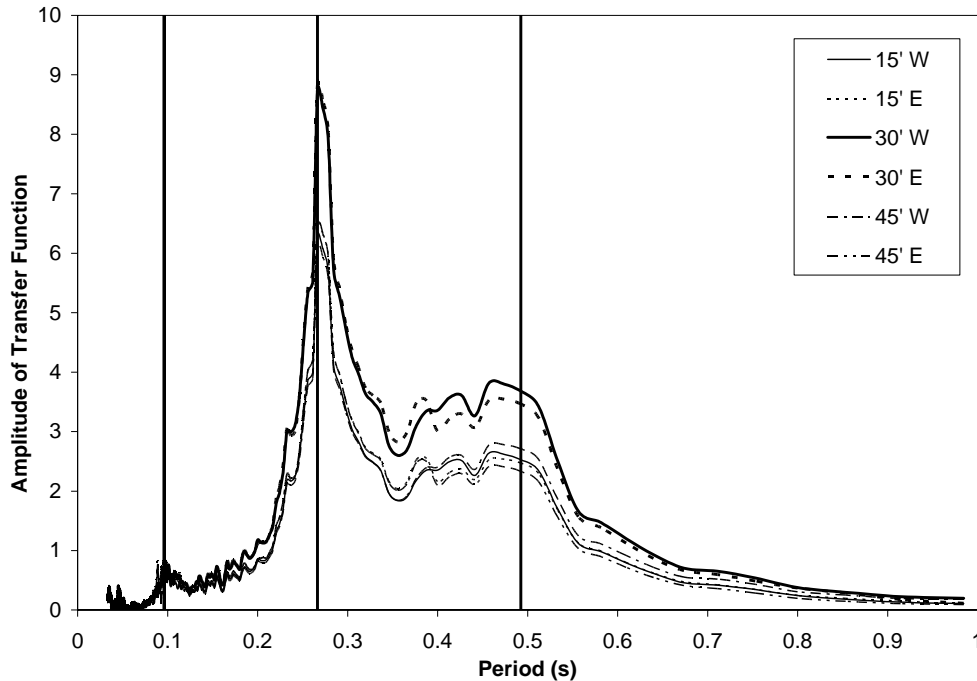


**FIGURE 3-15 STLRB - Transfer function amplitude for vertical accelerometers at deck slab level**

amplitude, there was some hysteresis observed in the bearings resulting in considerable damping. Figure 3-16 shows the mode shape for the first mode based on the relative transfer function

amplitude normalized to an ordinate equal to 1.0 at the midspan of the deck slab. This shows the flexural torsional mode, similar to the deformed shape of the bridge model during reversed static experiments. It was observed that the midspan deformation was relatively high compared to the end and bearing deformations despite the bridge being isolated. This is due to the relatively low levels of excitation during the Fourier analysis. Figures 3-17 and 3-18 show the second and third modes excited in the bridge. The second mode was a torsional mode with the bridge rotating due to axial deformation in the bearings and the third mode was a higher flexural torsional mode.

As the response of the bridge model was highly non-linear with the lead rubber bearings, a sine sweep was also used to help identify the properties of the isolated bridge model at larger bearing displacements. A sine sweep is a cyclic input motion which slowly changes frequency with time. The frequency change was gradual so that at any one frequency it could be assumed that steady state response of the bridge was achieved. In order to test the validity of the maximum sine sweep a series of finite element studies were performed on a single degree of freedom system subjected to the sine sweep displacement time history, averaged between the two end shake tables (Appendix 5). The maximum difference between the theoretical steady state response amplitude (Chopra, 1995) and the sine sweep analysis was around 10%.

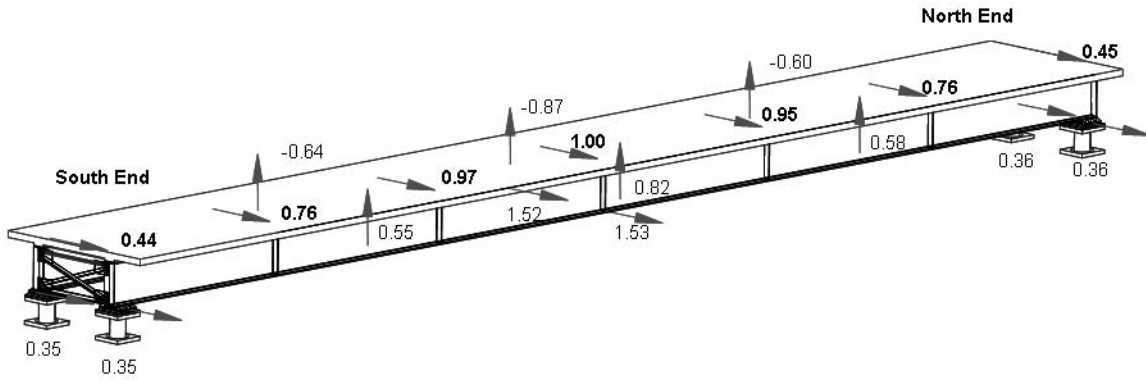


**FIGURE 3-16 STLRB - Mode shape for first transverse mode from Fourier analysis**

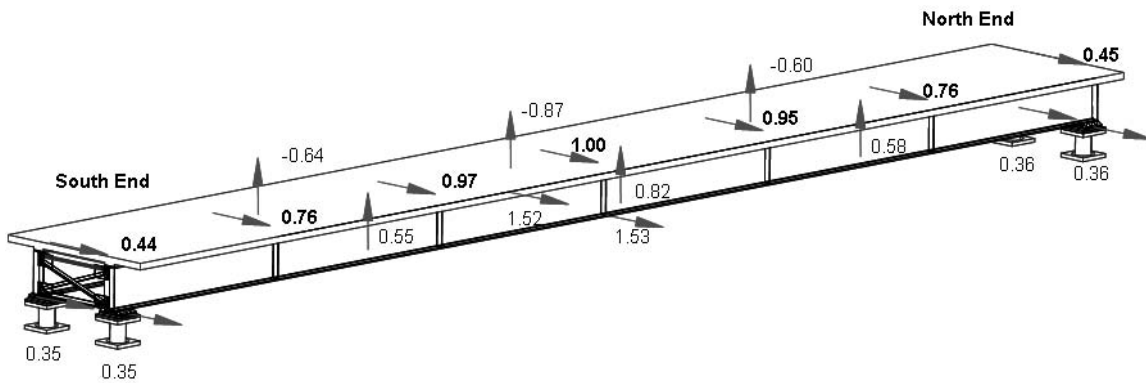


**FIGURE 3-17 STLRB - Mode shape for second transverse mode from Fourier analysis**

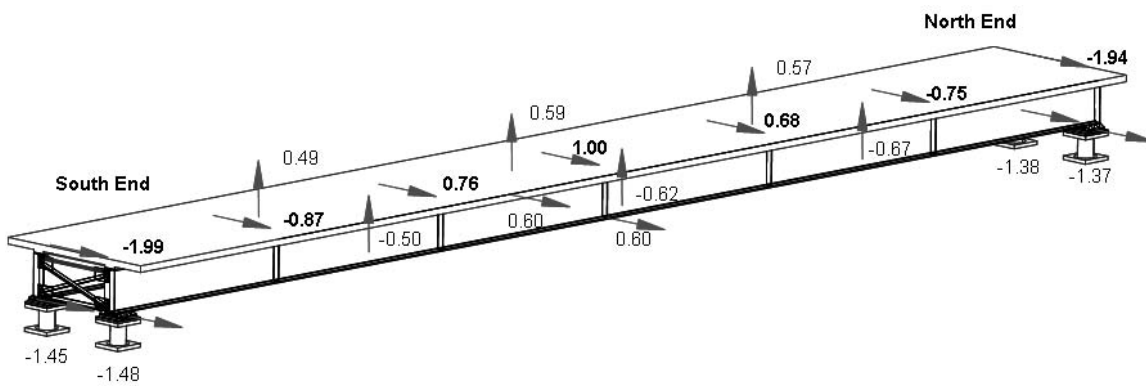


**FIGURE 3-18 STLRB - Mode shape for third transverse mode from Fourier analysis**

While several sine sweep motions were applied to the bridge model, focus was on the excitation with the maximum amplitude of accelerations and displacements. This was applied to the bridge model in the transverse direction. The sine sweep ramped up to a theoretically constant acceleration of 0.15 g. The resulting displacement time history, averaged between the two shake tables at each end of the bridge, is shown in Figure 3-19. The excitation was almost identical between the two tables. The displacement amplification factor for the ends and midspan of the bridge model is plotted against period from the sine sweep excitation in Figure 3-20. This figure shows that the first mode exhibited resonance at a period at around 0.74 s, although, the structure was heavily damped, hence the peak was not clearly defined. The displacement amplification factor at the natural period for the first mode, averaged between the ends and midspan, is equal to 1.9. Based on conventional theory (Chopra, 1995) the modal damping for an oscillator at resonance is given by:

$$\xi\sqrt{1-\xi^2} = \frac{1}{2\frac{d}{d_{st}}} \quad \dots 3.1$$

where:  $\xi$  is the modal damping coefficient;  $d$  is the relative displacement response of the oscillator, and;  $d_{st}$  is the static displacement response equivalent to the shake table input displacement excitation. Therefore the effective damping in the first mode was equal to 28%. The value of  $\alpha$  was 0.21 and therefore smaller than that calculated from the Fourier analysis. This indicates a larger relative bearing displacement compared to the superstructure flexural displacement and highlights that the mode shape and natural period of the bridge model, with the non-linear lead rubber bearings, was highly dependent on the magnitude of excitation. The average transverse displacement in the four lead rubber bearings at the peak excitation of the bridge was 21 mm, approximately one third of the design displacement. At this displacement the expected effective period of the bridge model was 0.76 s based on the design bearing properties (Appendix 2) and the measured weight of the structure. The equivalent damping was calculated at 45%. Therefore the calculated effective period was close to the measured value but the calculated damping was overestimated. This can be attributed to superstructure flexibility which resulted in lower damping than that estimated. A possible second mode is observable from the sine sweep at a natural period of 0.3 s, however due to the heavy damping the higher modes were unclear.

For the next series of experiments on the bridge model, bearings were placed at the midspan of the bridge to create a two span seismically isolated bridge model. It was again subjected to a series of increasing amplitude motions as listed in Appendix 3. In order to calculate the overall properties of the bridge a Fourier analysis was performed on a white noise motion at the beginning of the earthquake series. The transfer functions from the Fourier analysis, shown for the transverse accelerometers at deck slab level in Figure 3-21, show one heavily damped mode. For this mode the accelerations at the deck slab were almost identical. The mode shape is plotted in Figure 3-22 where it was shown that the bridge superstructure was relatively rigid with differential displacements resulting largely from differential isolator displacements. Slightly larger displacements were measured at the north end compared to the south end, which were attributed to slightly different bearing properties.

During the next series of experiments the bridge model was studied in a simply supported configuration with the same “light” single angle X-braces as those studied during the reversed

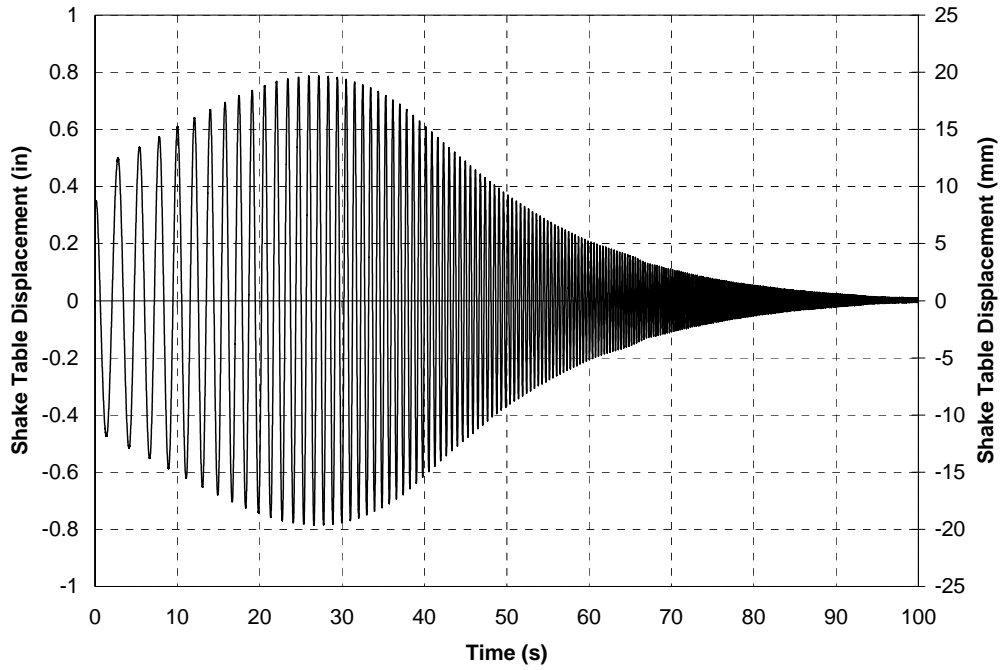


**FIGURE 3-19 STLRB - Average shake table displacement time history**

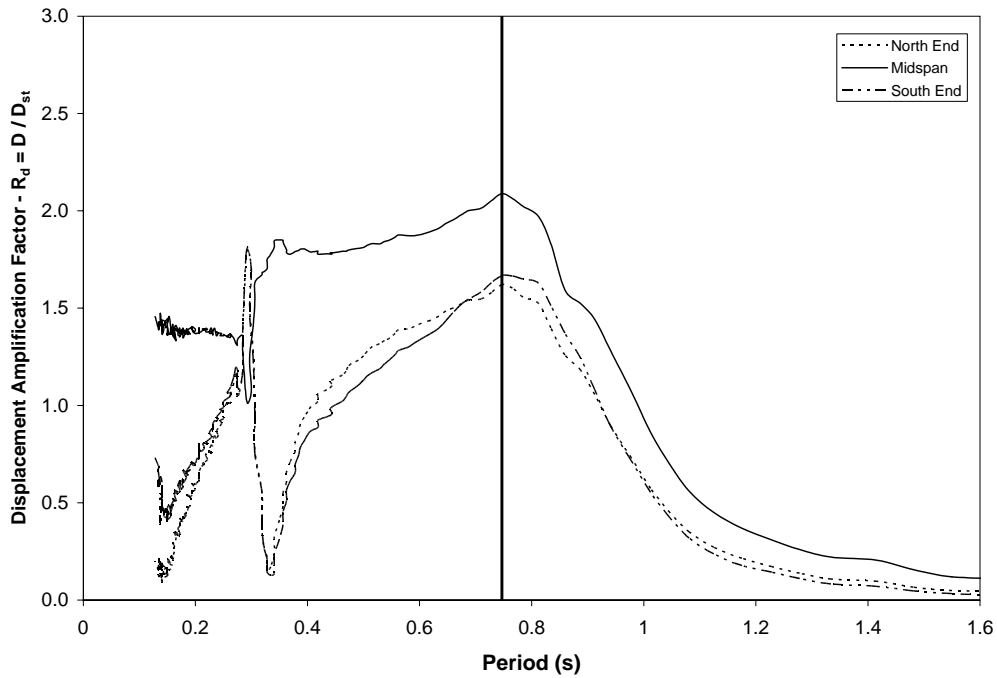


**FIGURE 3-20 STLRB - Amplification factor for displacements at the deck slab of bridge model for sine sweep excitation**



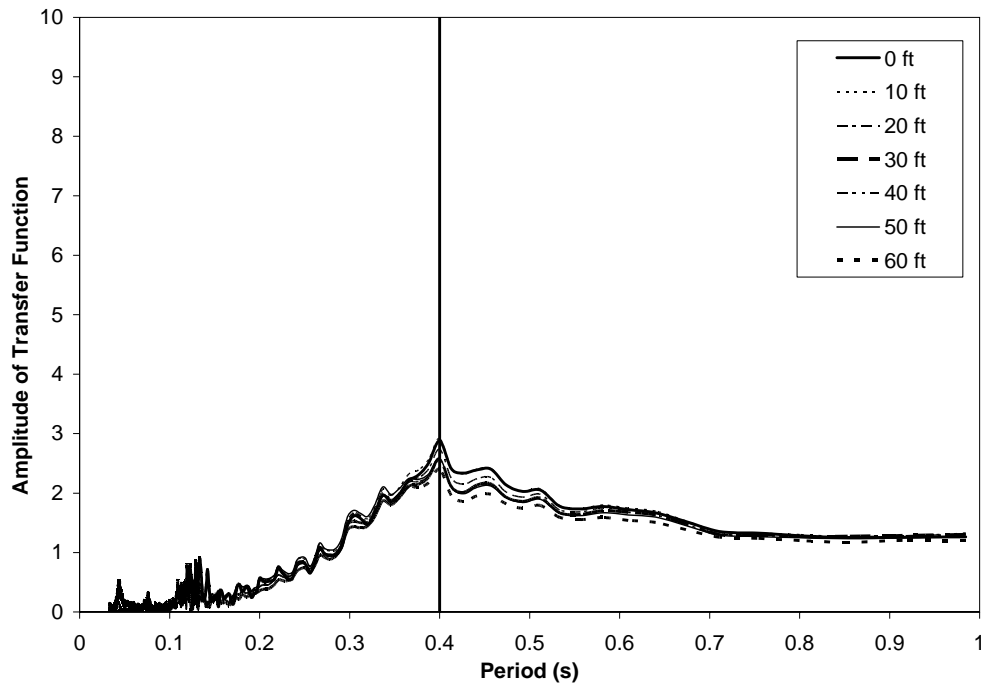


**FIGURE 3-21 STLRB2S - Transfer function amplitude for transverse accelerometers at deck slab level**

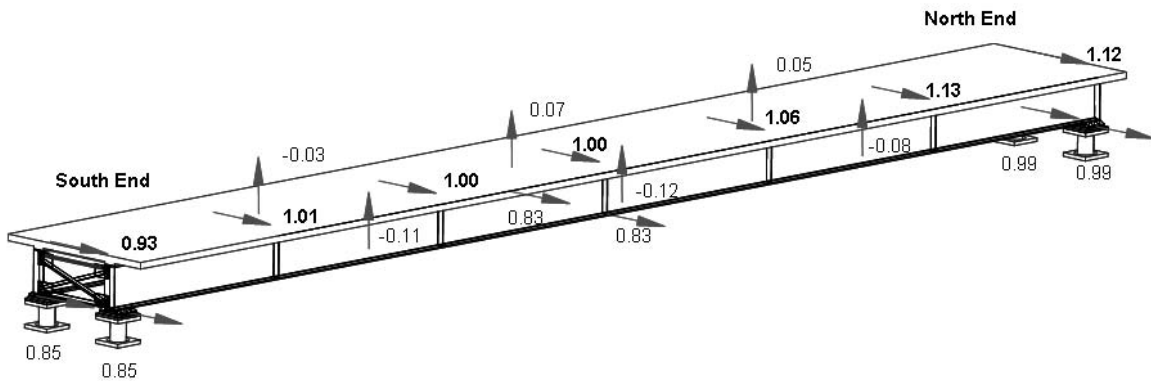


**FIGURE 3-22 STLRB2S - Mode shape for first transverse mode from Fourier analysis**

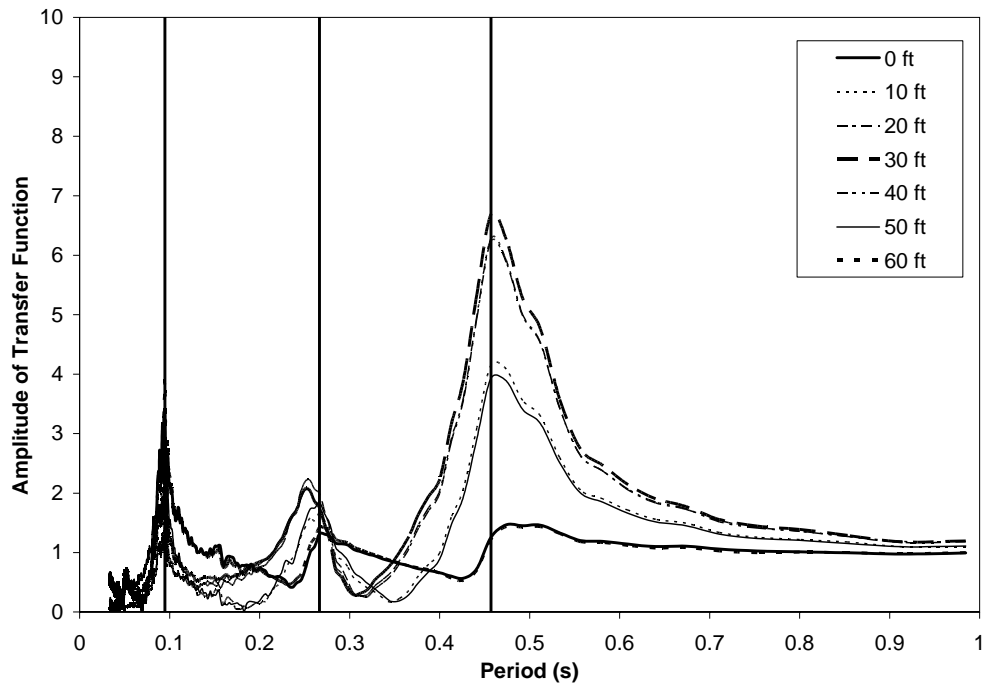
static experiments. The lead rubber bearings were restrained in the transverse direction. The restrained bearings were able to transmit much larger transverse shear forces into the end cross frames which subsequently buckled and yielded at higher levels of ground motion. A summary of the dynamic natural periods for the bridge model with the “light” end X-braces and other end cross frames configuration is shown in Table 3-3. These modal properties were determined from the Fourier analysis of the bridge model. No white noise was simulated at the beginning of the experiment series with the “light” X-braces, however a Fourier analysis was performed on white noise records after 1.5 El Centro when the onset of buckling was observed in the braces, and after 2.0 El Centro after considerable buckling and yielding in the braces. The transfer functions at the

**TABLE 3-3 Natural Periods and Flexibility Coefficient for Bridge Model with Different End Cross Frames**

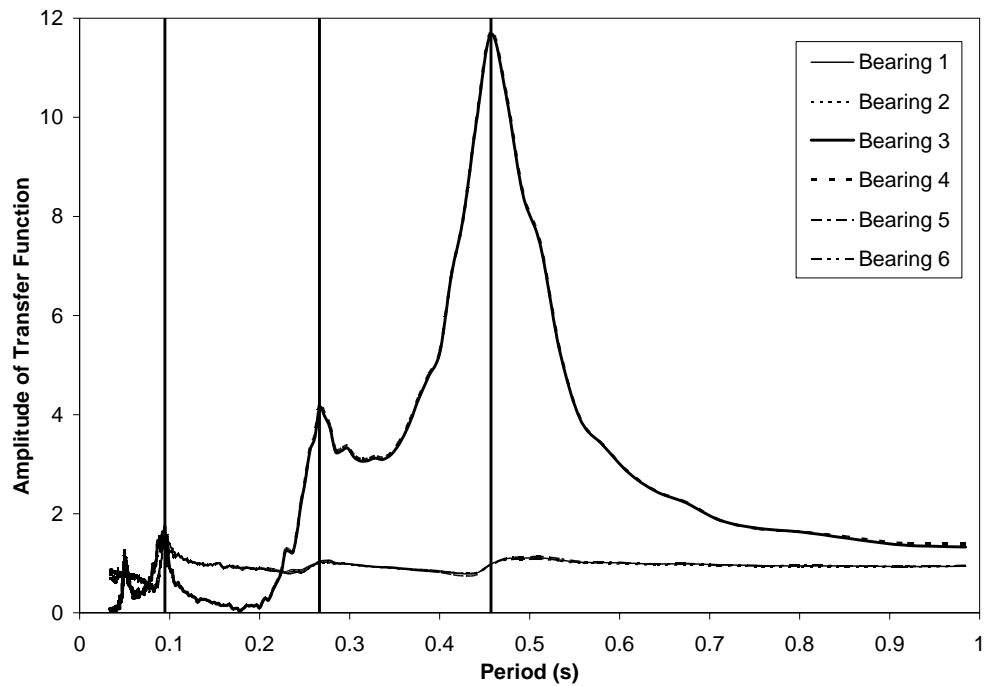
Expt. Series	No.	Natural Period (s)			Modeshape Alpha <sup>1</sup>	Comments
		Mode 1	Mode 2	Mode 3		
"Light" X-Braces	1	-	-	-	-	White noise at beginning of experiment series not available
	2	0.46	0.27	0.09	0.82	After 1.5 El Centro, onset of buckling previously observed
	3	0.51	0.28	0.11	0.70	At end of experiment series after large deformations in end X-braces
Unbonded Braces (Pinned)	1	0.46	0.27	0.09	0.83	From white noise at beginning of experiment series. Before studs removed
	2	0.46	0.26	0.09	0.81	After studs removed at ends and midspan of bridge model
	3	0.46	0.27	0.09	0.82	After 1.0 El Centro
	4	0.46	0.27	0.09	0.83	After 1.5 El Centro
	5	0.49	0.27	0.09	0.75	After 2.0 El Centro
Unbonded Braces (Fixed)	6	0.47	0.27	0.09	0.81	After connections welded to form moment resisting connections for unbonded braces
	7	0.53	0.30	0.09	0.67	After 1.0 Sylmar and Kobe
Unbonded Braces (2 Span)	1	0.22	0.18	0.09	-	From white noise at beginning of experiment series
	2	0.22	0.18	0.09	-	After 1.0 El Centro
	3	0.22	0.19	0.09	-	After 2.0 El Centro
	4	0.26	0.20	0.10	-	After 1.0 Sylmar and Kobe
No End Cross Frames	1	0.85	0.27	0.08	0.05	From white noise at beginning of experiment series
	2	0.93	0.28	0.08	0.05	From white noise at end of experiment series
"Heavy" X-Braces	1	0.35	0.22	0.07	0.69	From white noise at beginning of experiment series
	2	0.39	0.25	0.08	0.71	After 1.0 El Centro
	3	0.45	0.26	0.09	0.70	After 2.0 El Centro

Notes: 1. Alpha given for mode 1

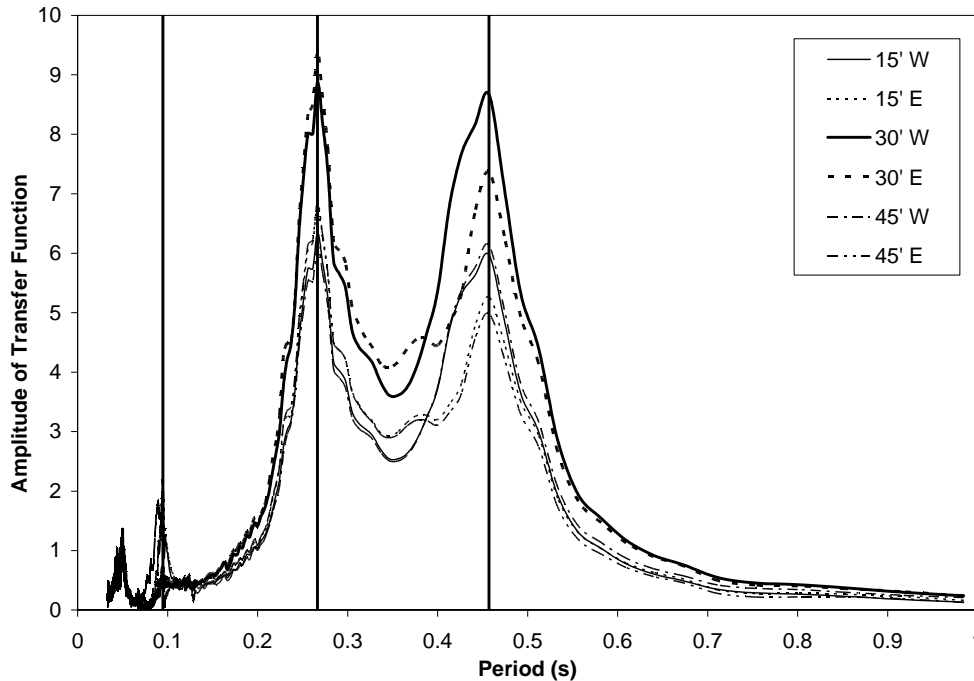
deck slab and bearing levels for the first Fourier analysis are shown in Figures 3-23 to 3-25. The modeshapes for the first three modes are shown in Figures 3-26 to 3-28. The first mode was flexural-torsional similar to the first deformation of the bridge model during reversed static experiments. The second mode was torsional (“rocking”) with axial deformations in the bearings, similar to that observed for the isolated bridge model. The third mode was a higher flexural torsional mode.



**FIGURE 3-23 STLXB - Transfer function amplitude for transverse accelerometers at deck slab level**



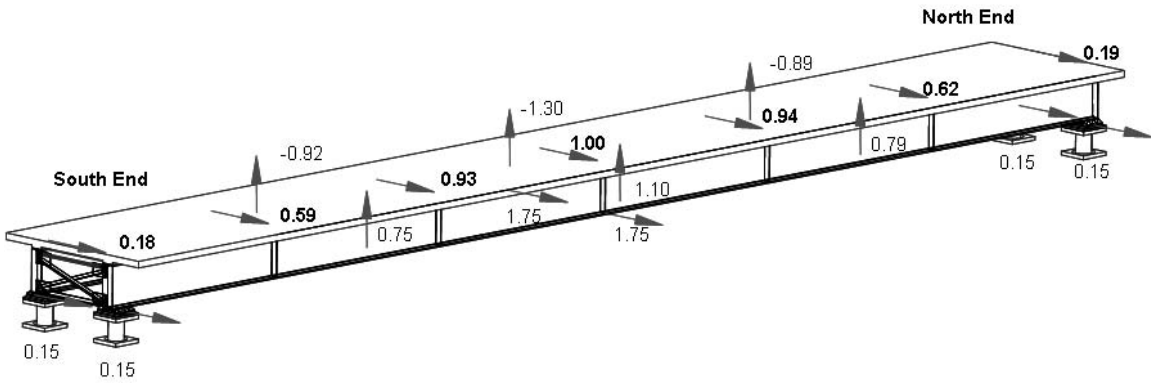
**FIGURE 3-24 STLXB - Transfer function amplitude for transverse accelerometers above bearings**



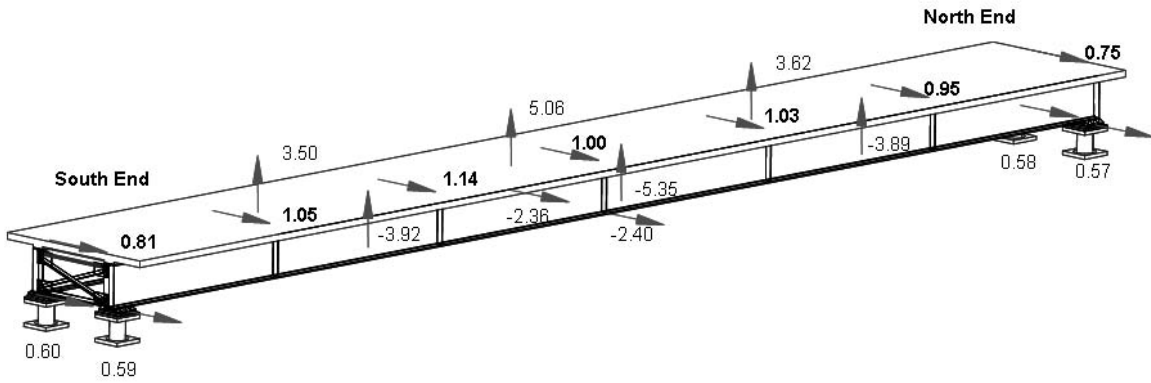
**FIGURE 3-25 STLXB - Transfer function amplitude for vertical accelerometers at deck slab level**

Table 3-3 shows that between the Fourier analysis after the 1.5 El Centro and 2.0 El Centro simulations, the natural period for each mode increased by around 10% which was attributed to stiffness degradation from buckling of the X-braces. Compared to a motion at the beginning of the experiments a larger change in stiffness would have been expected. The value of  $\alpha$  decreased indicating that the relative stiffness of the ends of the bridge model had decreased compared to the flexural stiffness of the superstructure. Other than damage in the end cross frames and additional cracking of concrete in the haunch around the repaired shear studs at the north end, there was no additional observed damage in the bridge model. Compared to the response at the end of the series of excitations on the bridge model with heavy X-braces the period was not largely different. Therefore the degradation in stiffness of the cross frames was not expected to greatly inhibit the serviceability of the bridge in the short term.

For the next experiment series, the “light” X-braces were replaced with unbonded braces. The bridge model was subjected to several small motions before the studs on top of the girders at the ends and midspan of the bridge were removed by coring around the studs as shown in Figure 3-29. Table 3-3 demonstrates no detectable change in the response of the bridge after coring in the elastic range. As the level of ground motion was increased the unbonded braces yielded. This apparently lengthened the elastic natural period of the bridge by less than 10% in the first mode while there was no detectable change in the other modes indicating minimal change in the serviceability of the bridge after at large magnitude earthquake.



**FIGURE 3-26 STLXB - Mode shape for first transverse mode from Fourier analysis**



**FIGURE 3-27 STLXB - Mode shape for second transverse mode from Fourier analysis**

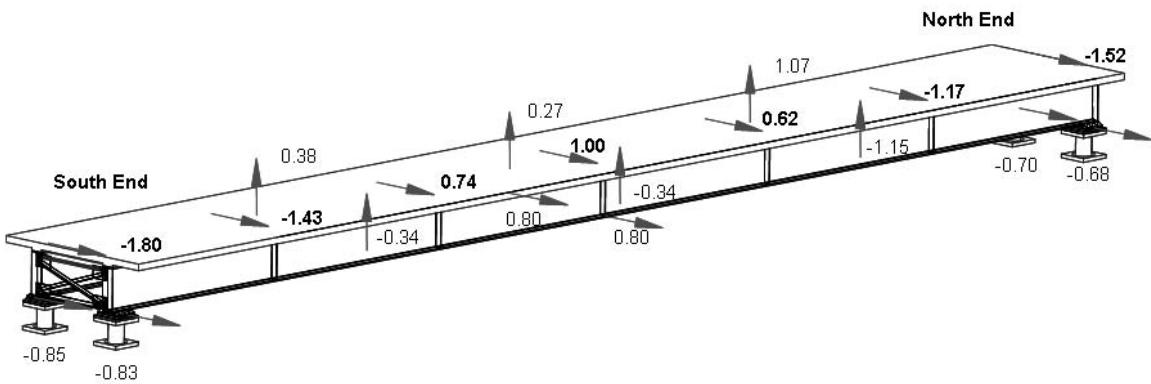


**FIGURE 3-28 STLXB - Mode shape for third transverse mode from Fourier analysis**



**FIGURE 3-29 Effect of shear studs removed by through the deck slab around the studs**

The amplitude of the transfer function at the beginning of the unbonded brace experiments for accelerometers on the deck slab of the bridge model is shown in Figure 3-30. The first mode shape from the same excitation is shown in Figure 3-31. Comparing these with the light single angle X-braces shows that there was very little difference in the essentially elastic response of the bridge.

After simulating earthquakes on the bridge model with pinned unbonded braces the connections of the braces were welded to provide moment resisting connections which were not able to slip. The change in response was barely noticeable for low amplitude white noise excitation as shown by comparing the periods in Table 3-3. After large magnitude Sylmar and Kobe ground motion there was a slight increase in the first mode period.

The next series of experiments on the bridge model investigated a two span bridge with an unbonded brace at the midspan cross frame location and the same braces at the ends as for the previous series of experiments. Transversely restrained lead rubber bearings were inserted at midspan. The magnitude of ground motion was increased as given in Appendix 3. At the end of experiments the unbonded braces had still not fractured and there was no additional observed damage in the bridge model. The Fourier analysis of white noise at different stages during this series of experiments showed that the bridge formed an S-shaped lateral torsional first mode. The amplitude of the transfer functions for deck slab accelerometers (Fig. 3-32) and the mode shape (Fig. 3-33) show that the south end was excited more than the north end. This may be attributed to a difference in the cross frame stiffness or perhaps bearing restraints developed at the two ends creating some torsion in the bridge. As the superstructure was more rigid in the two span configuration it was more sensitive to these end conditions, particularly at the low amplitude of the

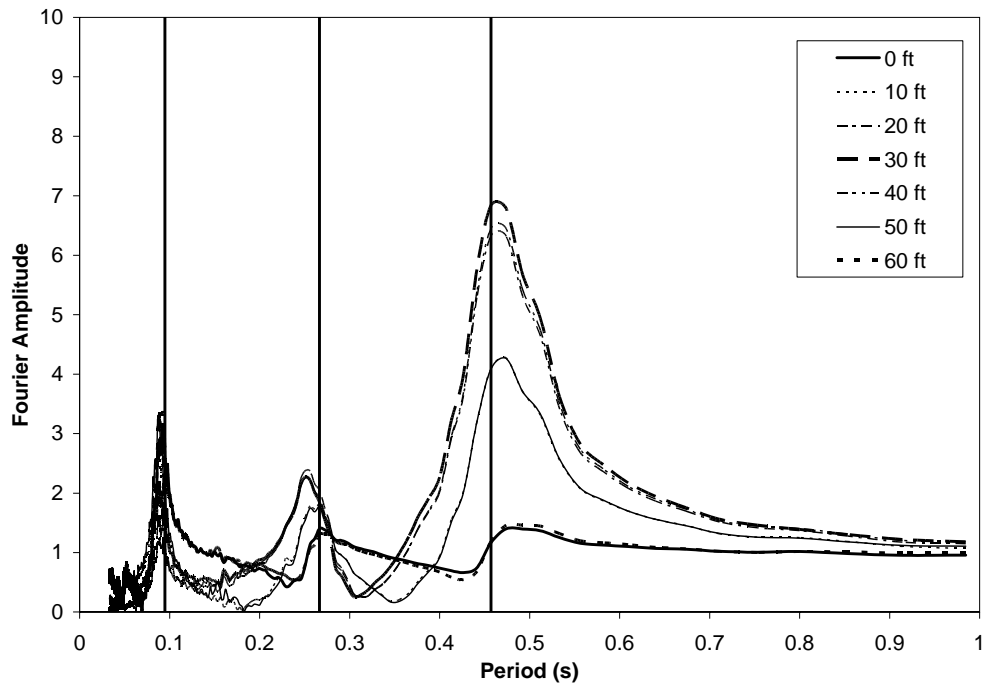


**FIGURE 3-30 STPUB - Transfer function amplitude for transverse accelerometers at deck slab level**

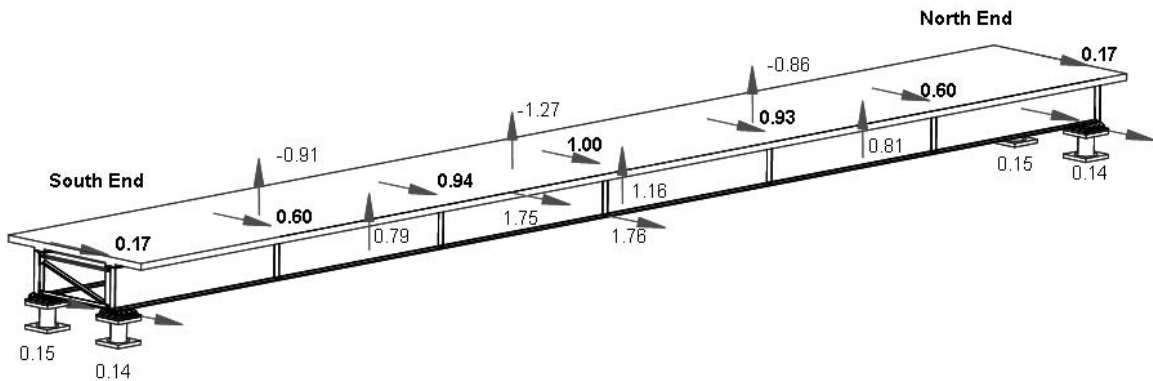


**FIGURE 3-31 STPUB - Mode shape for first transverse mode from Fourier analysis**

white noise excitation. As the level of ground motion increased the natural periods stayed relatively constant, although there was some lengthening after Sylmar and Kobe records.

The bridge model was then subjected to excitation in a simply supported configuration with transversely restrained bearings and no end cross frames. The bridge performed like an isolated model with a first mode natural period of 0.85 s at the beginning and 0.93 s at the end of the series of earthquake simulations. With no end cross frames the girders were effectively free to “rock” on top of the bearings and under the deck slab. From the acceleration transfer functions of the initial

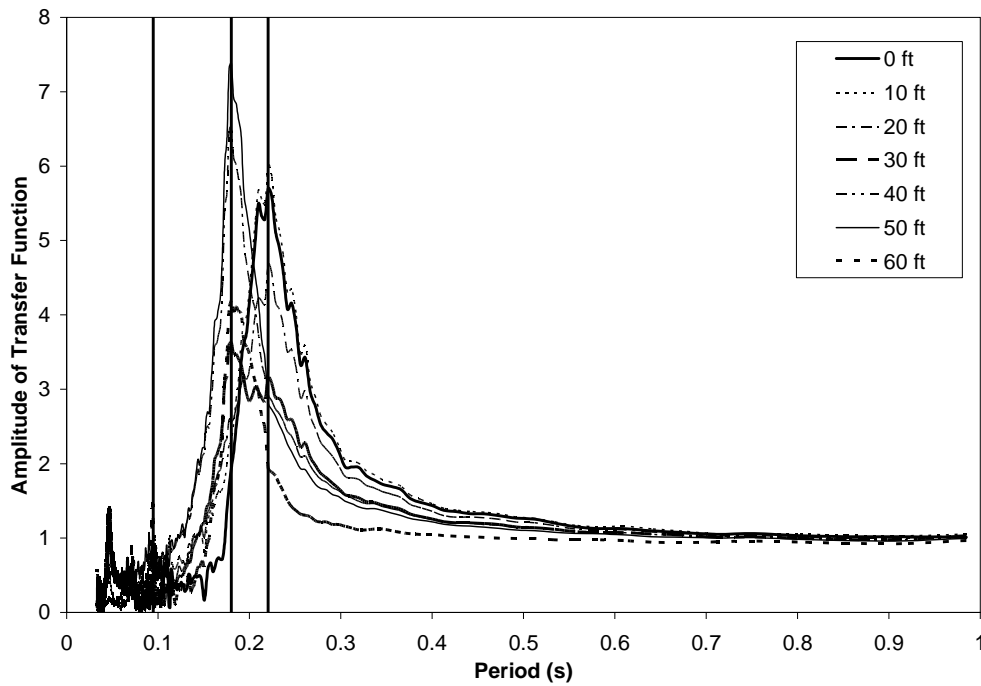


**FIGURE 3-32 STFUB2S - Transfer function amplitude for transverse accelerometers at deck slab level**

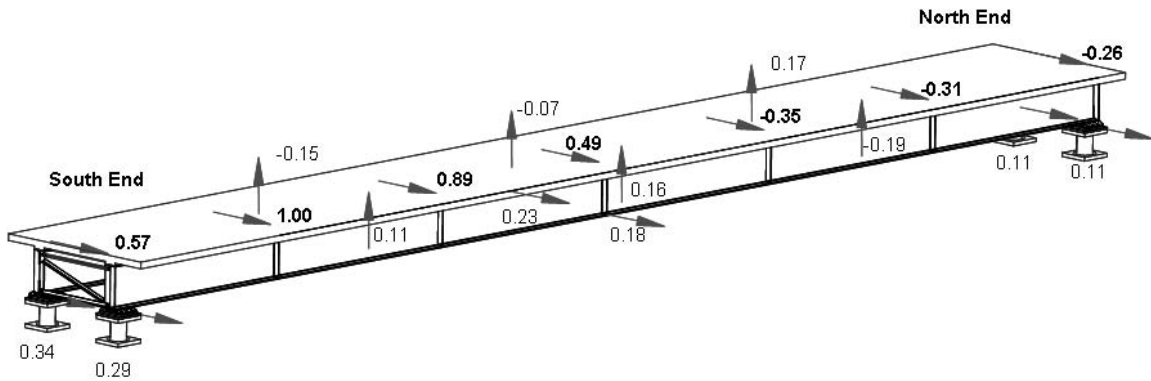


**FIGURE 3-33 STFUB2S - Mode shape for first transverse mode from Fourier analysis**

white noise excitation (Fig. 3-34), the mode shape for the first mode is illustrated in Figure 3-35. This mode shape shows that the deck slab of the bridge model was almost rigid with deformations concentrated in the ends of the bridge. The north end exhibited notably larger displacements than the south end. Although some of the shear studs were removed at both ends, damage to some of the remaining studs was considered to result in the difference in response at the two ends. This series of experiments showed the potential for using flexible end cross frames to “isolate” the bridge model in the transverse direction, whereby allowing larger deformations lowers the seismic demand in the bridge. During the next series of experiments “heavy” single angle cross frames



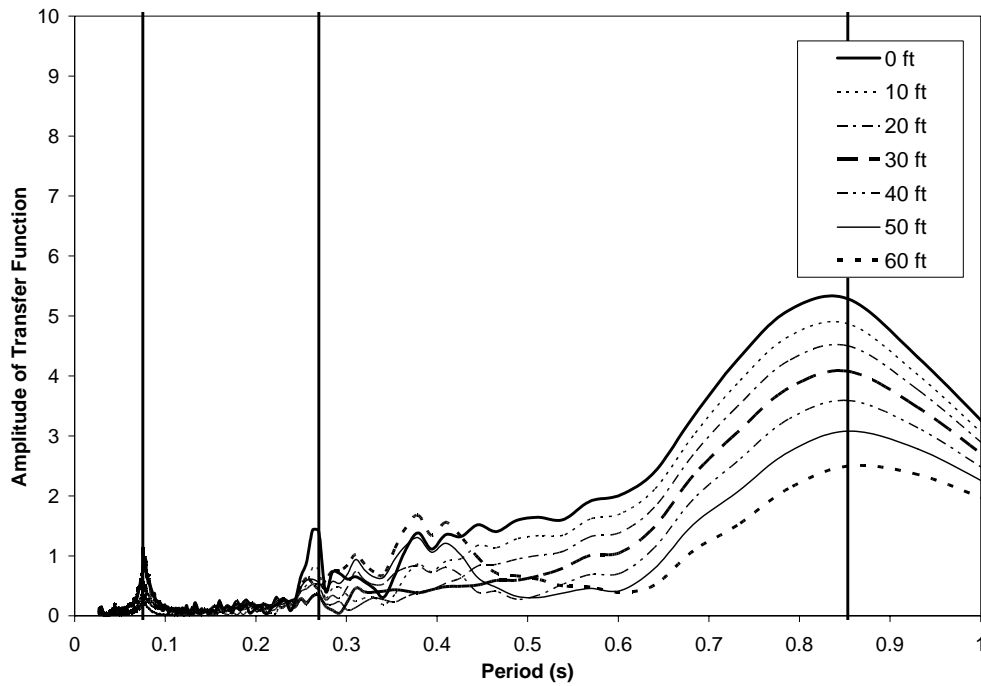


**FIGURE 3-34 STNECF - Transfer function amplitude for transverse accelerometers at deck slab level**

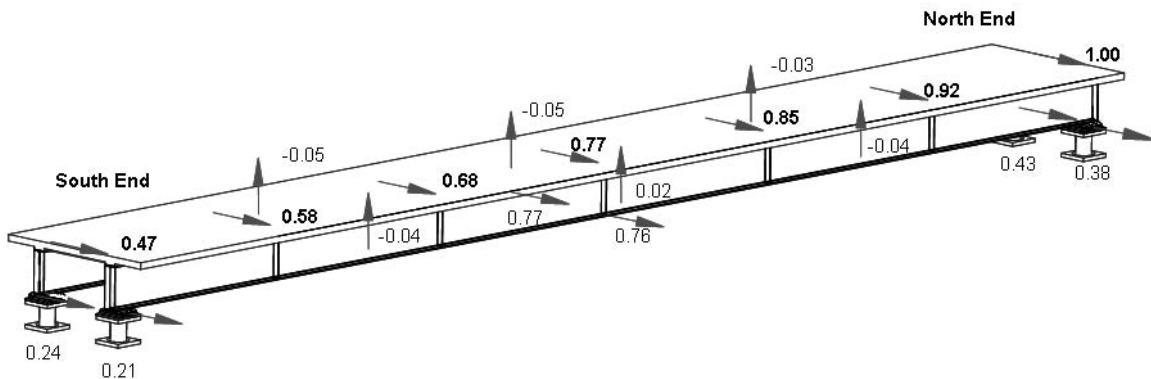


**FIGURE 3-35 STNECF - Mode shape for first transverse mode from Fourier analysis**

were placed in the bridge model. The model was subjected to increasing amplitude ground motions as outlined in Appendix 3 without any inelastic behavior observed in the end cross frames. The amplitudes of the transfer functions from white noise excitation at the beginning of the series plotted at deck slab level are shown in Figure 3-36. The mode shape for the first mode (Fig. 3-37) was similar to that for the “light” X-braces. Table 3-3 shows that the natural periods were also similar. Comparing the modal properties of the bridge model at the beginning of the experiment series with those at the end of the series demonstrates that the period of the bridge increased, particularly for the first mode. This increase cannot be attributed to cross frame

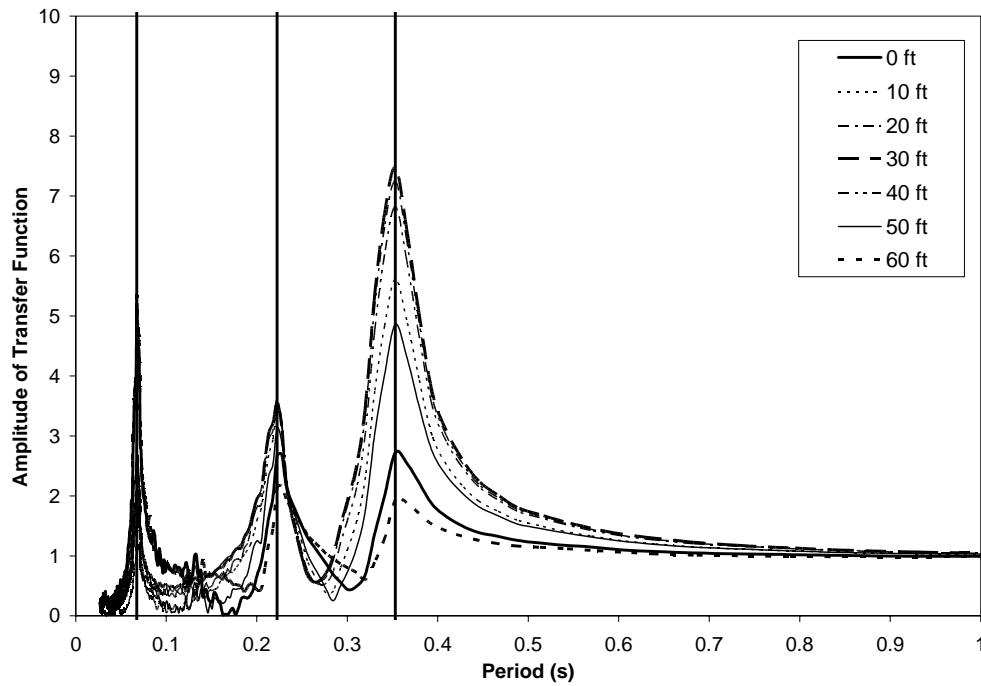


**FIGURE 3-36 STHXB - Transfer function amplitude for transverse accelerometers at deck slab level**

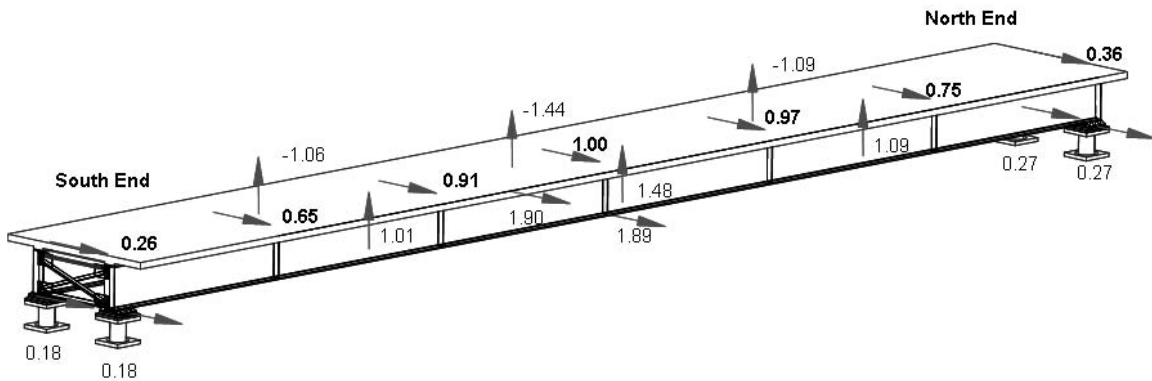


**FIGURE 3-37 STHXB - Mode shape for first transverse mode from Fourier analysis**

yielding as with the “light” X-braces and unbonded braces. Instead it is likely to be due to loosening of the bearing restraints, which had tight fitted shims prior to the beginning of the series of ground motions, but during the series were subjected to much higher forces than in previous experiments. There was a visible gap between the bearings and their restraints at the end of the series of earthquake simulations.

The last series of experiments performed on the bridge model was a repeat of some of the simulations on the simply supported isolated configuration. The differences between the second

series of lead rubber bearing experiments and the first series were that the bearings were heavily worked after the first series and the “heavy” end X-braces in the second series were more rigid than the “light” X-braces in the first series. Despite these changes comparisons of the modal properties in Table 3-2 show almost identical properties in the bridge model. The modeshapes were also very similar. Therefore the bridge superstructure properties appeared to have maintained consistent overall properties throughout the many series of experiments, at least as measured by low amplitude white noise excitation.

### **3.4 Detailed Finite Element Analysis of Bridge Model**

#### **3.4.1 Model**

A detailed finite element model of the bridge was constructed in order to study the elastic response of the bridge and provide information about the response that could not be obtained directly from experiments. The model was constructed in SAP2000 (Computers and Structures, 2003), and is shown in Figure 3-38. It was constructed from a series of shell elements to model the deck slab and girders and frame elements to model the cross frames and shear studs. Although, the bearings were modeled using NLinks (non-linear links), they were assumed to remain elastic during the elastic analyses. The deck slab was modeled with an effective elastic and shear moduli in order to reduce the gross stiffness of the deck slab to a more realistic value that allows for cracking. The main variables in the finite element model were the effective properties of the deck slab and the stiffness of the shear studs. The effective stiffness of the shear studs was varied using the bending stiffness of the studs based on a varied effective unrestrained length of the studs. Some rows of studs were removed at the ends of the bridge to allow for damage to these ends.

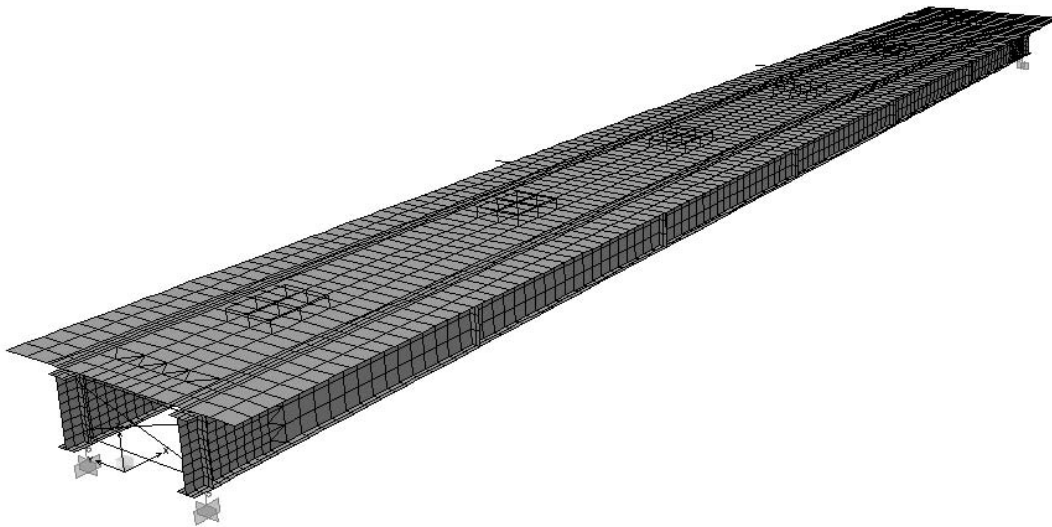


**FIGURE 3-38 Finite element model of bridge model in SAP2000**

### **3.4.2 Reversed Static Response Comparison**

The overall properties of the finite element model were compared and calibrated to the physical bridge model using the reversed static experiments. The displacements for the second reversed static experiment, with heavy X-braces at the ends, are shown in Table 3-4. The same forces as those measured in the actuators of the bridge model were applied to the finite element model. These forces were approximately equal at the north and south actuator, although there was some variation resulting in slightly asymmetric deformation in the finite element model. The effective elastic and shear moduli used for the deck slab were reduced to match the measured deformations in the bridge model. The flexural stiffness of the shear studs was also modeled as finite with the calculated stiffness discussed in the following chapter. One row of studs was removed from the north end to allow for damage at that end. Table 3-4 shows that the finite element model displacements compare well with those measured from the experiment for the transverse displacements at deck slab level. There was slightly more variation between the finite element and experimental values for the vertical displacements and transverse displacements at the bottom flange. This indicates that the finite element model tended to overestimate the rotation in the bridge superstructure.

Table 3-5 shows similar comparisons between the finite element and experimental deformations of the bridge model with no end cross frames. For this experiment the finite element model had displacements similar to the experimental displacements, although there was a tendency for the finite element model to overestimate the measured displacements by up to around 20%. Table 3-6 compares the finite element model with the experimental deformation of the bridge model with the “light” end cross frames. For this case the deformations were again comparable, but in this case the measured displacements, particularly in the transverse direction, typically exceeded those from the finite element model. This increase in relative measured displacement reflects an increased amount of cracking and some localized yielding of the reinforcing in the deck slab.

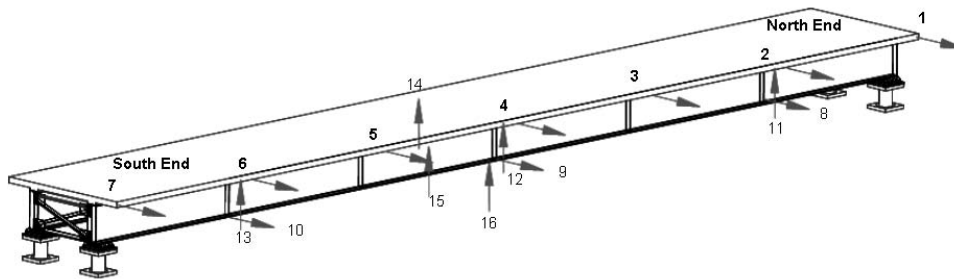
### **3.4.3 Dynamic Response Comparison**

The dynamic response of the finite element model was compared with the response of the bridge model during shake table testing. The dynamic properties of the finite element model was calculated in two ways; the first was using a Ritz vector analysis in SAP2000 and the second was using a Fourier analysis of a white noise during an elastic time history analysis. The white noise was defined using the acceleration output from the shake tables for the bridge model in a particular configuration. The acceleration was calculated based on the average from the output of the two or three shake tables used excite the bridge model. As an example, the mode shape and natural period of the simply supported bridge model with unbonded braces at the ends are compared between the Ritz analysis and the Fourier analyses. The responses can be compared for the first mode by comparing Figures 3-39 and 3-40. The comparison shows that the modeshapes were similar with slightly smaller ordinates at the ends of the bridge for the Ritz vector analysis compared to the Fourier analysis. The next two transverse modes were compared in Figures 3-41 to 3-44. The higher modes were also very similar for the two methods of analysis, as were the natural periods calculated using the two methods.

The natural periods calculated from the finite element model for the three transverse modes, corresponding to the same modes observed during experiments on the bridge model, are shown in Table 3-7. These were based on a Ritz vector analysis of the bridge model with different

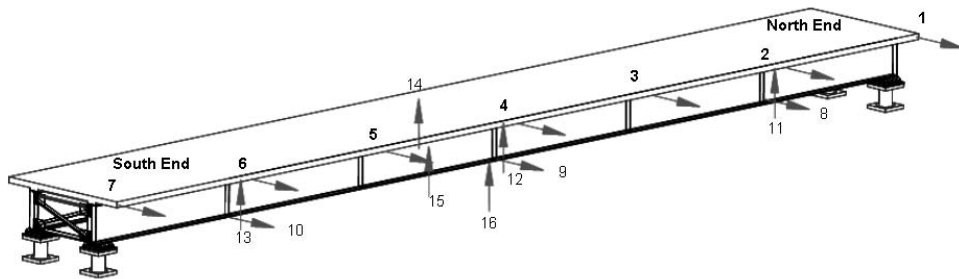
**TABLE 3-4 RSHXB2 - Comparison of Finite Element and Experiment Results for Total Applied Actuator Force of approximately 133 kN**

No.	Experiment			SAP2000		
	Positive Cycle	Negative Cycle	Total	Positive Cycle	Negative Cycle	Total
<b>Transverse Displacements (mm)</b>						
1	2	-2	4	2	-2	3
2	11	-10	21	13	-13	26
3	20	-18	39	23	-23	46
4	22	-19	41	24	-24	48
5	23	-19	42	22	-23	45
6	13	-11	24	13	-13	26
7	2	-1	3	2	-2	3
8	15	-15	30	20	-21	41
9	32	-29	61	39	-40	79
10	17	-15	32	20	-20	41
<b>Vertical Displacements (mm)</b>						
11	-5	7	-12	-11	11	-22
12	-12	14	-26	-23	24	-47
13	-5	6	-12	-11	11	-22
14	17	-16	33	23	-23	46
15	5	-9	14	17	-18	35
16	-12	9	-21	-20	20	-40



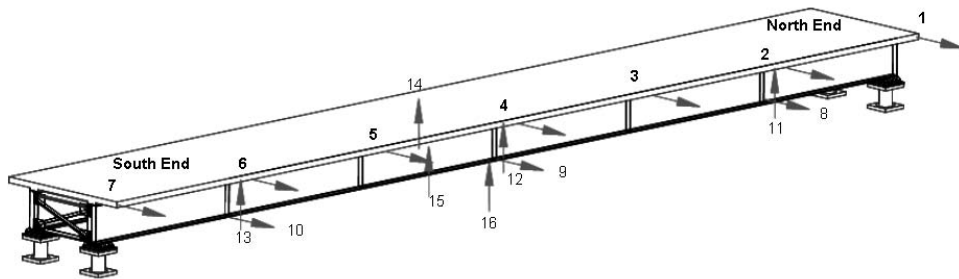
**TABLE 3-5 RSNECF - Comparison of Finite Element and Experiment Results for Total Applied Actuator Force of approximately 133 kN**

No.	Experiment			SAP2000		
	Positive Cycle	Negative Cycle	Total	Positive Cycle	Negative Cycle	Total
<b>Transverse Displacements (mm)</b>						
1	31	-25	56	34	-34	68
2	41	-35	75	43	-43	87
3	49	-47	95	51	-51	102
4	50	-45	94	51	-51	102
5	47	-45	92	48	-48	96
6	36	-30	66	37	-37	74
7	23	-16	39	25	-25	51
8	44	-38	82	49	-49	98
9	60	-55	115	64	-64	128
10	38	-28	66	43	-43	86
<b>Vertical Displacements (mm)</b>						
11	-1	7	-8	-8	8	-16
12	-10	17	-27	-20	20	-40
13	-3	7	-10	-8	8	-16
14	20	-13	33	19	-19	39
15	1	-13	14	15	-15	29
16	-17	6	-23	-17	17	-34



**TABLE 3-6 RSLXB - Comparison of Finite Element and Experiment Results for Total Applied Actuator Force of approximately 133 kN**

No.	Experiment			SAP2000		
	Positive Cycle	Negative Cycle	Total	Positive Cycle	Negative Cycle	Total
<b>Transverse Displacements (mm)</b>						
1	5	-1	6	4	-4	8
2	20	-13	34	15	-15	31
3	34	-25	58	25	-25	50
4	34	-25	59	26	-26	52
5	34	-26	60	25	-25	49
6	19	-14	33	15	-15	30
7	3	-1	4	4	-4	8
8	25	-20	45	23	-23	45
9	46	-40	86	41	-42	83
10	23	-20	43	22	-22	44
<b>Vertical Displacements (mm)</b>						
11	-5	11	-15	-11	11	-21
12	-13	25	-38	-23	23	-46
13	-5	12	-17	-11	11	-22
14	24	-16	40	22	-23	45
15	4	-18	21	17	-17	34
16	-22	12	-34	-20	20	-39



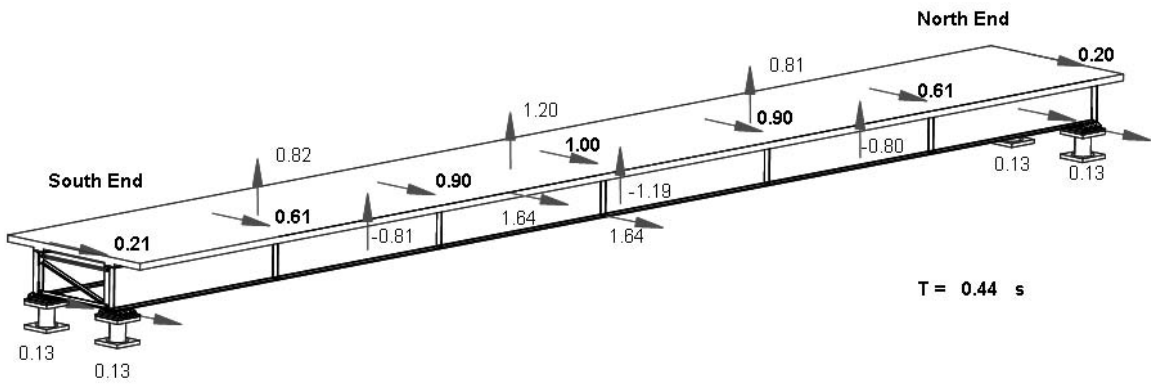


FIGURE 3-39 FEPUB - Mode shape for first transverse mode from Fourier analysis

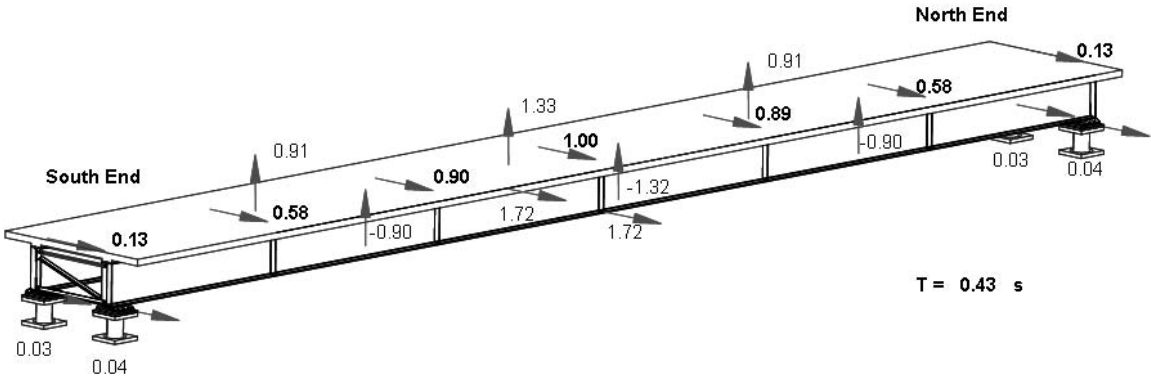


FIGURE 3-40 FEPUB - Mode shape for first transverse mode from Ritz vector analysis

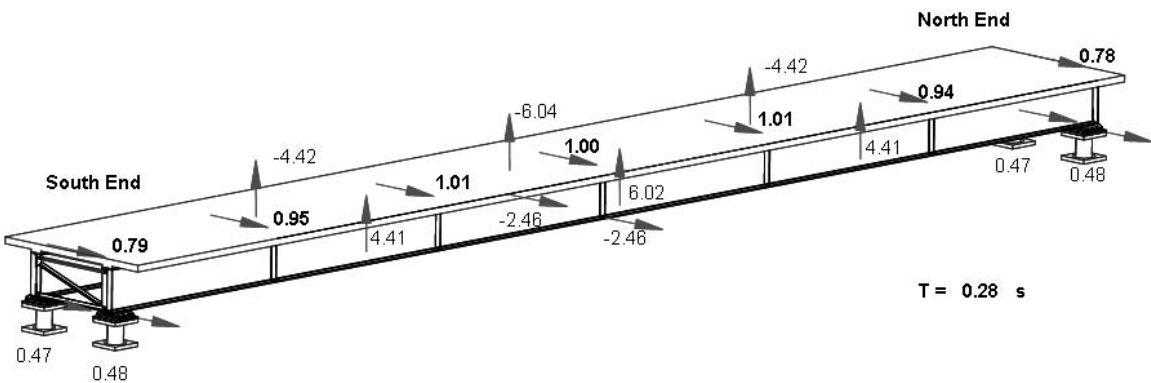


FIGURE 3-41 FEPUB - Mode shape for second transverse mode from Fourier analysis



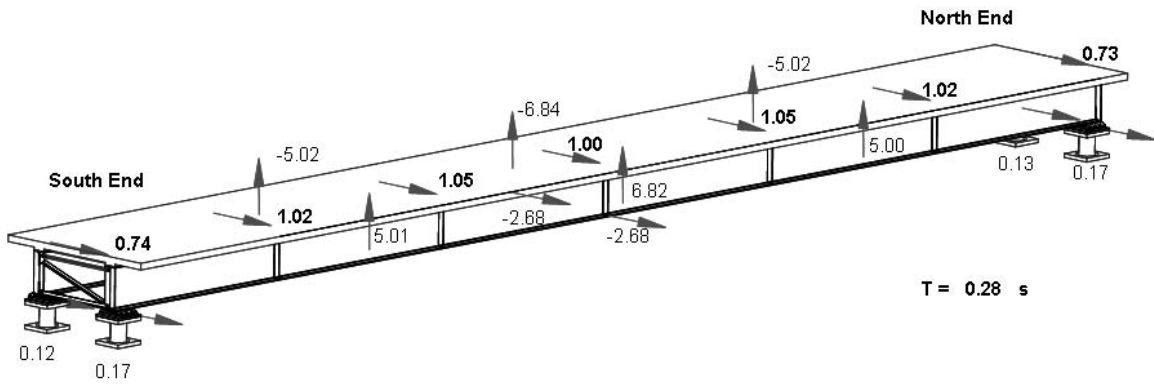


FIGURE 3-42 FEPUB - Mode shape for second transverse mode from Ritz vector analysis

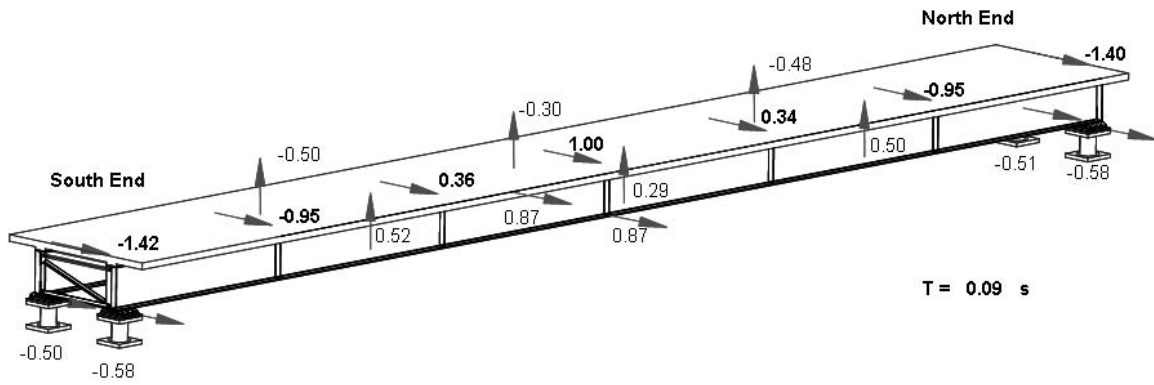


FIGURE 3-43 FEPUB - Mode shape for third transverse mode from Fourier analysis

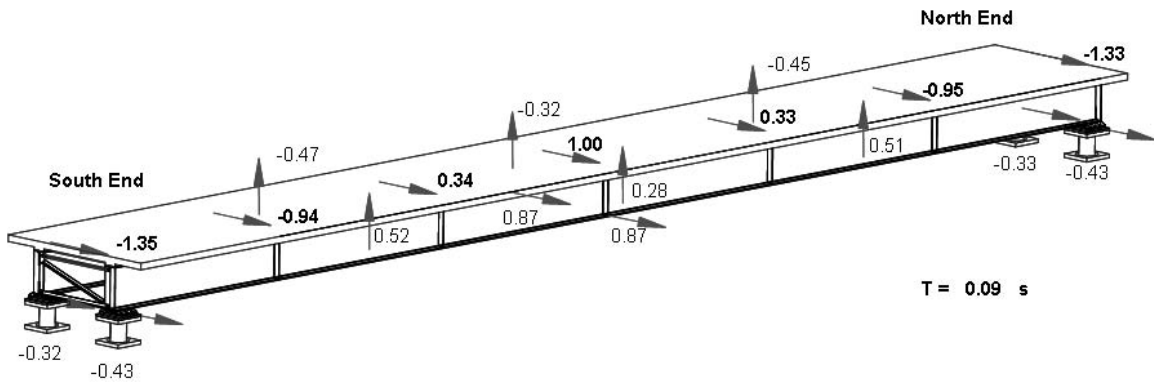


FIGURE 3-44 FEPUB - Mode shape for third transverse mode from Ritz vector analysis

**TABLE 3-7 Natural Periods for Three Transverse Modes of Detailed Finite Element Model**

Experiment Series	Natural Period (s)			Modeshape Alpha <sup>1</sup>
	Mode 1	Mode 2	Mode 3	
LRBs	0.59	0.32	0.12	0.46
LRBs (2 Span)	0.41	0.12	-	-
"Light" X-Braces	0.44	0.29	0.09	0.86
Unbonded Braces	0.43	0.28	0.09	0.87
Unbonded Braces (2 Span)	0.20	0.17	0.09	-
No End Cross Frames	0.75	0.32	0.12	0.25
"Heavy" X-Braces	0.43	0.28	0.09	0.90

Notes: 1. Alpha given for mode 1

**TABLE 3-8 Modal Mass Participation Factors for Three Transverse Modes of Detailed Finite Element Model**

Experiment Series	Mass Participation Factor (%)			
	Mode 1	Mode 2	Mode 3	Sum
LRBs	94	4	2	100
LRBs (2 Span)	99	1	-	100
"Light" X-Braces	69	21	8	98
Unbonded Braces	68	22	8	98
Unbonded Braces (2 Span)	92	0	2	94
No End Cross Frames	98	1	1	99
"Heavy" X-Braces	66	24	8	98

configurations of cross frames and bearings. Comparing the natural periods of the finite element model with those calculated from experiments on the bridge model (Tables 3-2 and 3-3) gave good correlations between the observed and modeled behavior. The modal mass participation factors for each of the modes are given in Table 3-8. These show that at least 94%, but typically 98% to 100%, of the effective modal mass in the transverse direction was captured in the first three modes. For the isolated configurations and without end cross frames the first mode captured over 90% of the effective modal mass. However for the configurations with restrained bearings and end cross frames both of the first two modes were necessary, with the first mode capturing only 65 to 70% of the effective modal mass.

For the bridge in a simply supported seismically isolated configuration the first mode period of the finite element model was 20% more than the observed period from the Fourier analysis of the bridge model. This indicates that the design stiffness of the bearings. This was of little concern as the response of the isolated bridge was not highly dependent on the initial stiffness of the bearings were designed for large ductilities. The mode shape for the first mode, as simply defined by the value of  $\alpha$ , indicates a slightly larger end displacement relative to the midspan displacement in the finite element model compared to the experimental model. This was consistent with a slightly underestimated bearing stiffness at small bearing displacements. The natural periods for the other two modes from the finite element analysis were closer to the observed natural periods at the small displacements. For the two span isolated model the first mode properties compare very closely. The modal participation factor shows that 99% of the mass is associated with this first mode, which can explain why no other transverse modes could be clearly identified from the sine sweep analysis of the bridge model.

The finite element models of the bridge model with “light” X-braces and unbonded braces in simply supported configurations compare closely to the observed modal properties for the three modes. This indicates a good calibration of the finite element model with the physical model. The two span configuration with an unbonded brace at midspan also compared well. Similarly to the two span isolated case, the second and third modes were shown to have very little modal mass participation.

With no end cross frames the finite element model had a first mode period of 0.98 s. This was 15% larger than the measured value in the bridge model during the first white noise simulation and 5% larger than the second measured value. Therefore it matched the second simulation well. Comparison of the other modes showed similar differences. The difference between the results is likely to be due to an underestimation of the end stiffness in the finite element model. This could be due to a number of factors including bearing restraints or the way that the connection between the deck slab and the girders was modeled.

The finite element modal response with the “heavy” X-braces compares best with the bridge response calculated after the bridge was subjected to 2.0 x El Centro. Before this level of excitation it is likely that the transverse bearing restraints, tightly fitted before the experiment, were providing some rotational restraint to prevent the ends of the girders rotating about the vertical axis. After the bearings were subjected to larger shears due to the elastically responding X-braces, these restraints loosened allowing rotation of the girders, as modeled in the finite element model.

In general the finite element model was able to accurately capture the static and dynamic properties of the bridge model. Further discussion of the response for the various superstructure components follows in subsequent chapters.



## SECTION 4 DECK SLAB AND COMPOSITE ACTION

### 4.1 Introduction

The deck slab is expected to provide a large portion of the lateral stiffness of a steel plate girder bridge superstructure by acting as a beam to resist transverse earthquake loads in the superstructure and distribute these loads towards the end of each span. Therefore, the condition and subsequent response of the deck slab in the bridge model was expected to have a significant effect on the overall response. As the bridge model was partially composite, the modeling of composite action between the deck slab and the girders also had a large effect on the overall transverse response. The level of composite action in the bridge model influenced the stiffness of the bridge with relative slip between the deck slab and the girders reducing the effective transverse stiffness. Furthermore, the strength of the shear studs was critical for transferring the transverse loads from the deck slab into the steel girders and end cross frames.

The transverse stiffness was shown to be reduced during successive bridge experiments. It was difficult to determine whether this reduction was due to deck slab cracking, or degradation in the composite connection between the deck slab and the girders, or a combination of them both.

### 4.2 Deck Slab

#### 4.2.1 Response and Modeling of Deck Slab During the First Experiment

After construction of the bridge model some fine cracks were observed in the deck slab due to shrinkage. The cracks were generally oriented in the transverse direction of the bridge and extended from the edges of the deck slab towards the girders with a length of typically around 150 to 300 mm. They were found every 600 to 1200 mm along the length of the bridge model. These cracks were likely to reduce the gross section stiffness of the deck slab even before transverse loads were applied.

The first experiment on the bridge model, RSHXB, was unique in that there was no deck slab cracking, apart from some localized shrinkage cracking at the beginning of the experiment. Figures 4-1 and 4-2 show the force-displacement relationship for each of the actuators after three cycles of loading at the initial loading amplitude. It can be seen that at the north actuator the behavior is essentially elastic but at the south actuator, even at low levels of force, there is evidence of some hysteretic behavior. This is attributed to cracking of the deck slab which occurred almost immediately on application of transverse earthquake loading. As the amplitude of loading was increased the hysteretic behavior in the bridge model became more evident (Figs. 4-3 and 4-4).

As the deck slab cracked the stiffness was reduced and it was apparent that it would be inaccurate to model the deck slab using the gross stiffness properties of the concrete. In order to determine the effective stiffness of the deck slab a detailed finite element model was used, similar to that shown in Figure 3-38, based on the configuration of the bridge in the experiment RSHXB. The model was analyzed at a number of different loading amplitudes based on maximum forces observed in the bridge model for the first of three cycles at each different amplitude during this experiment. This resulted in different forces at the two actuator locations being simulated.

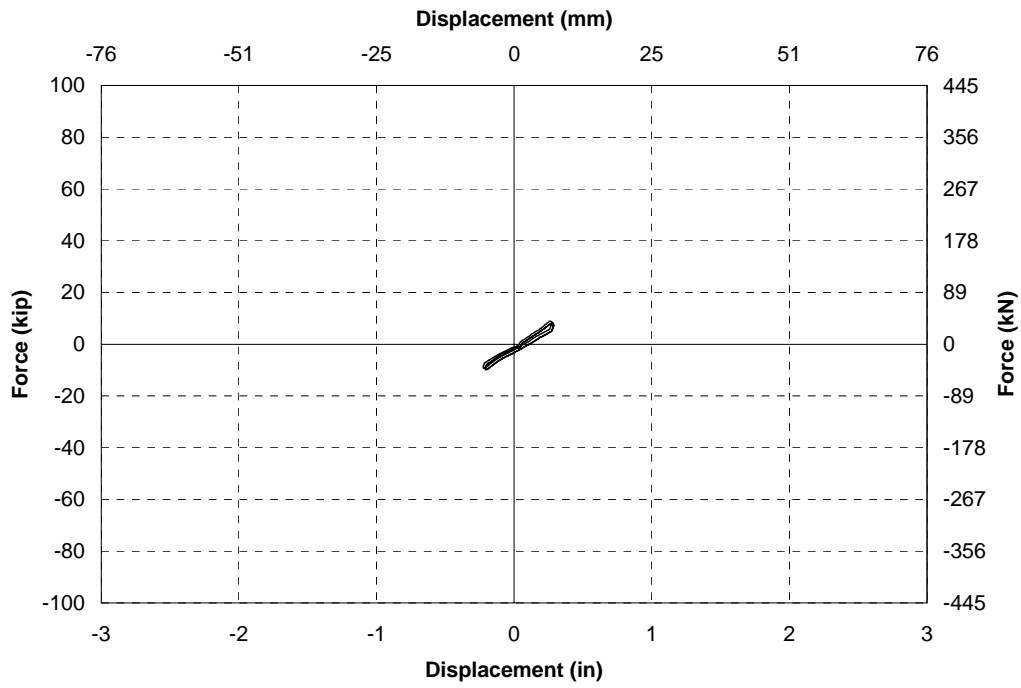


**FIGURE 4-1 RSHXB - Hysteresis loop for north actuator (first amplitude cycles)**

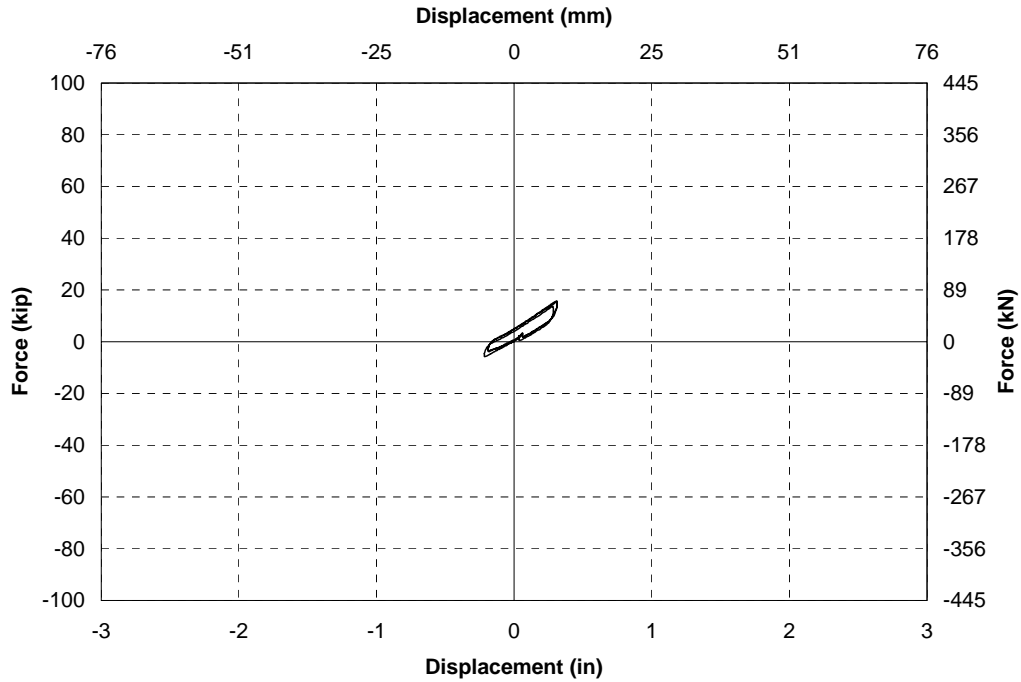


**FIGURE 4-2 RSHXB - Hysteresis loop for south actuator (first amplitude cycles)**

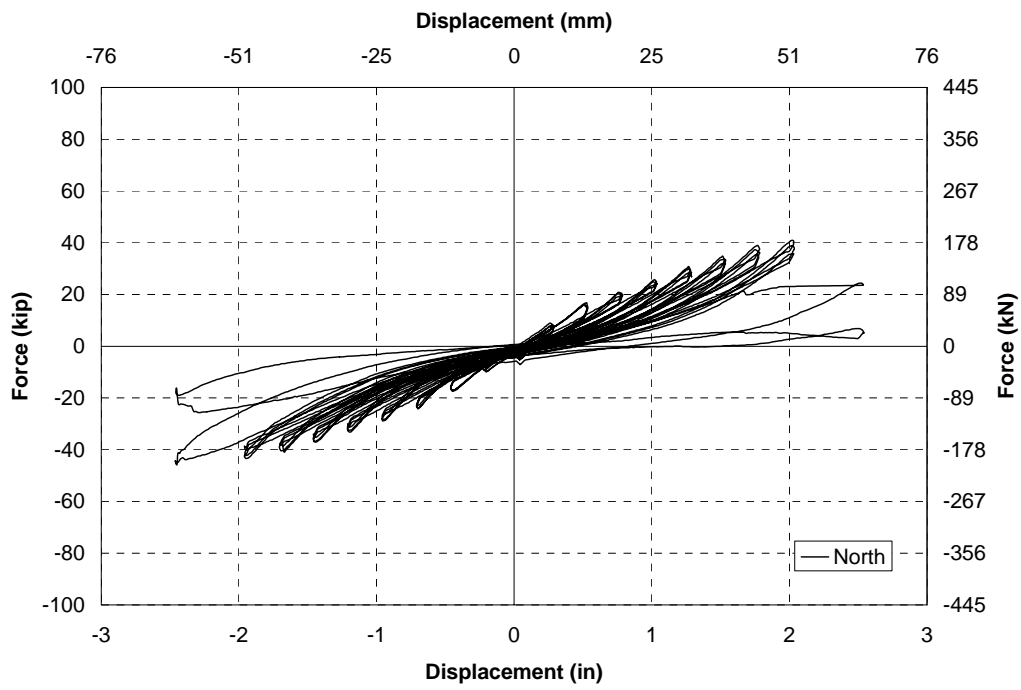


**FIGURE 4-3 RSHXB - Hysteresis loop for north actuator**

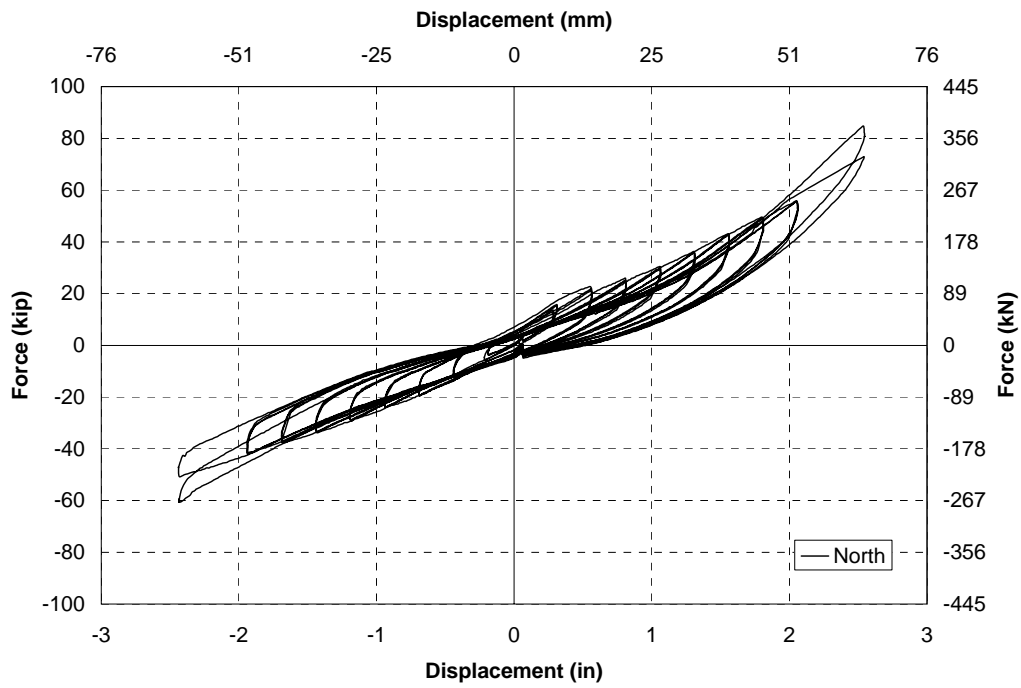


**FIGURE 4-4 RSHXB - Hysteresis loop for south actuator**

In order to correlate the finite element response with the measured bridge response there were three main variables which could be modified. The first was the level of composite action in the bridge model which was dependent on the stiffness of the shear studs. For the analysis of the deck slab an assumption was made about the stiffness of the shear studs based on the shear stud model B, discussed in Section 4.3. The studs were assumed to have a constant stiffness throughout except at the ends where studs were removed to simulate damage which occurred to them making them ineffective during the experiments. The other variables were the elastic properties of the concrete, which were modeled using an effective elastic modulus and shear modulus. The effective deck slab stiffness was modeled at each different amplitude cycle by varying the elastic and shear moduli. The resulting effective moduli, as a ratio of their theoretical gross values, are plotted against total applied actuator force in Figure 4-5. This figure shows that the elastic and shear moduli ratios were considerably lower than unity even at low applied forces. They decreased further as the amplitude of the forces and displacements in the bridge model increased due to increased cracking in the deck slab. As the deformation was dominated by flexure of the deck slab, the response was relatively insensitive to the shear modulus therefore the effective shear modulus as a function of the gross shear modulus was equated to the effective elastic modulus. The gross shear modulus was calculated based on an assumed Poisson's ratio of 0.2.

The envelope for the transverse displacement of the deck slab at midspan is plotted against the total force in Figure 4-6. The envelope shows very good correlation between the finite element and experimental model. The rotation at the midspan for the experimental and finite element model caused by transverse loading is shown in Figure 4-7. The correlation between the measured rotation in the bridge model and computed rotation in the finite element model is not as good as for the transverse displacements. This is due to second order forces caused by the angle of the actuator and angle of the bridge after some first order rotations resulting in a vertical actuator force component which increases or reduces the rotations depending on the direction of actuator forces. For negative transverse forces, the second order forces increase the rotations, while for positive transverse forces the second order forces decrease the rotations. This effect was not modeled in the finite element model. The deformation of the deck slab along the length of the bridge at different positive and negative displacement amplitudes is shown in Figure 4-8. Generally good correlation between the displacements along the length of the bridge was observed. Displacements were not measured at the ends during this experiment and therefore the plots extend to the first intermediate cross frames 3.05 m from each end. The model loses some accuracy in the last cycle at the north ends after the shear studs failed.

#### 4.2.2 Deck Slab Models using Transformed Sections

The transverse stiffness of a steel girder bridge superstructure can be basically described by the gross moment of inertia about the vertical axis of an equivalent cross section transformed into steel (or concrete) and the effective torsional moment of inertia for the same cross section. Based on conventional theory, the gross moment of inertia,  $I_y$ , can be calculated using:

$$I_y = \frac{t_d b_d^3}{12n} + \sum_1^{n_g} A_g x_g^2 \quad \dots 4.1$$



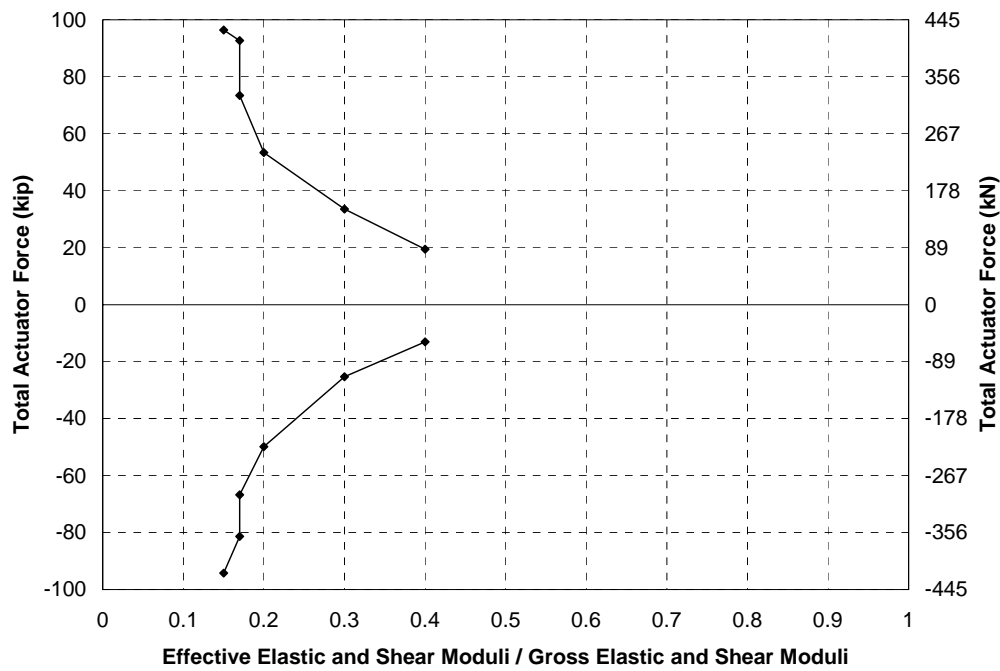


**FIGURE 4-5 RSHXB - Elastic modulus and Shear modulus for deck slab of finite element models to correlate with experiment**

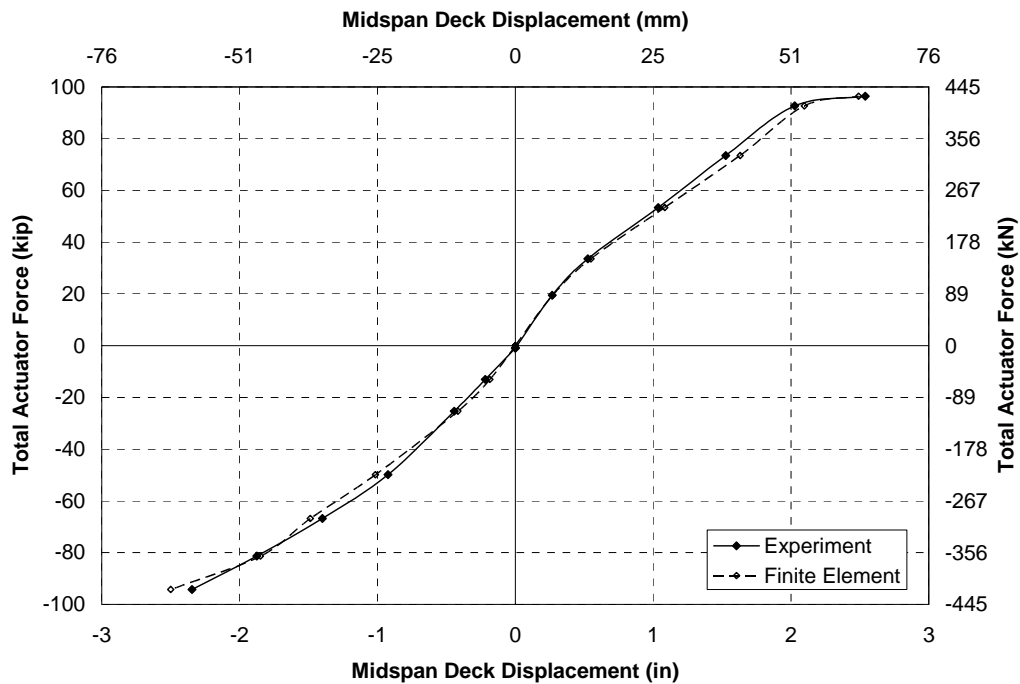


**FIGURE 4-6 RSHXB - Envelopes for transverse midspan deck slab displacement for experimental and finite element models**

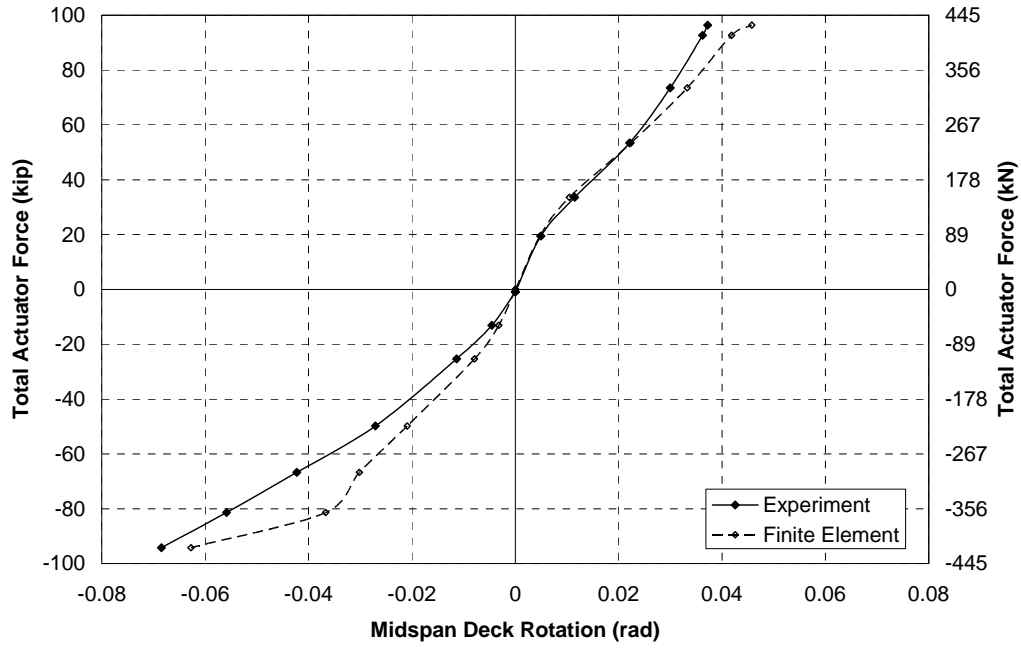


**FIGURE 4-7 RSHXB - Envelopes for transverse midspan deck slab rotation for experimental and finite element models**

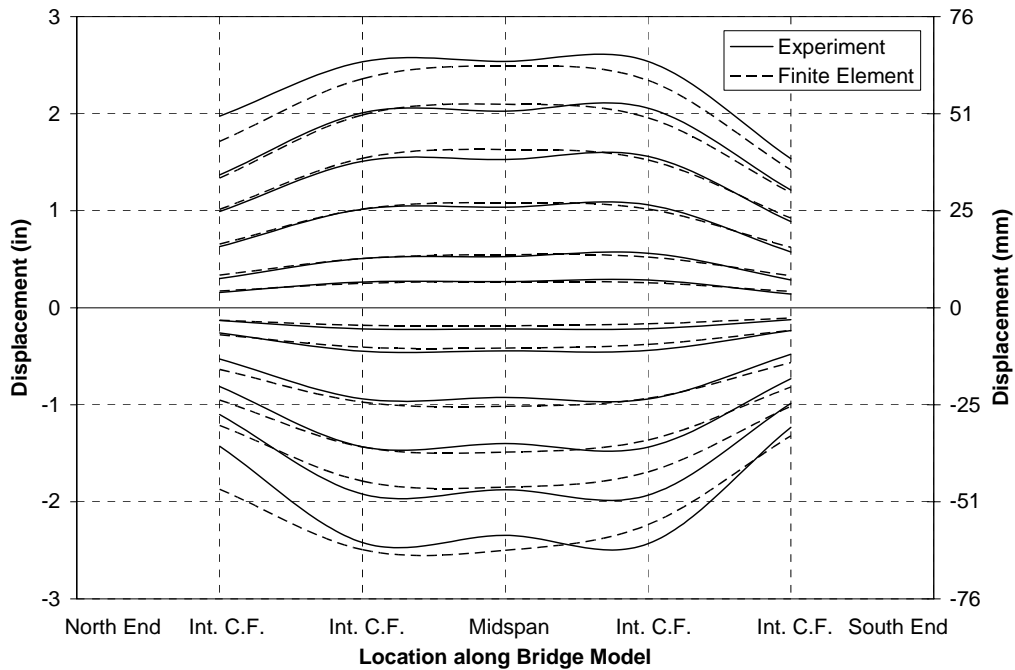


**FIGURE 4-8 RSHXB - Deck displacements along the length of the bridge model at different amplitudes for experimental and finite element models**

where:  $t_d$  is the thickness of the deck slab;  $b_d$  is the width of the deck slab;  $n$  is the ratio of elastic moduli,  $E_s/E_c$ ;  $n_g$  is the number of girders;  $A_g$  is the area of the girders, and;  $x_g$  is the distance from the centroid of the section to each girder. The gross torsional moment of inertia,  $J$ , can be calculated assuming an open cross section by:

$$J = \frac{t_d b_d^3}{3n} + \sum_1^{n_g} (d_{gf} t_w^3 + b_{fb} t_{fb}^3) \quad \dots 4.2$$

where:  $d_{gf}$  is the depth of the girder between the centroid of the flanges;  $t_w$  is the thickness for the web;  $b_{fb}$  is the width of the bottom flange, and;  $t_{fb}$  is the thickness of the bottom flange. In reality partial composite action between the deck slab and the girder as well as deck cracking results in effective moments of inertia that are less than the gross values. The above equations are used as a basis for comparison between the calculated stiffness of the bridge model and the measured stiffness.

Equivalent sections were considered to account for the reduced effective stiffness of the deck slab calculated using the calibrated finite element model. Figure 4-9 shows a section of the bridge model transformed to an equivalent steel section using gross section properties for the deck slab. Assuming full composite action between the deck slab and the girders the deck slab would provide 57% of the total transverse stiffness,  $EI$ , of the bridge model. The remainder could be attributed to the stiffness of the girders. However, as the girders in the bridge model are not fully composite, in reality the deck slab accounts for a larger proportion of transverse stiffness.

As the deck slab stiffness is proportional to the cube of the width of the deck slab, a small reduction in the effective width had a significant effect on the effective stiffness of deck slab. For a section with low initial transverse loads, where the cracked section properties resulted in an effective moment of inertia for the deck slab equal to 40% of the gross deck slab moment of inertia, the effective deck slab width was approximately 75% of the actual width of the section. This resulted in a width of 1870 mm compared to the original width of 2500 mm. This was equivalent to removing 315 mm from each side of the deck slab, which is approximately equal to the length of the shrinkage cracks observed in the edges of the deck slab. Therefore, the reduced deck slab stiffness at the beginning of the experiment can be accounted for by this shrinkage cracking. The transformed section for this case is shown in Figure 4-10.

After several cycles of transverse loading the transverse stiffness of the bridge was seen to have dropped due to increased cracking of the deck slab. A transformed section was considered after the deck slab was considered to be fully cracked and no strength was assumed in the concrete subjected to tension. If the compression strains in the concrete deck slab due to gravity loads were considered negligible compared to the strains due to transverse loading, and the concrete strains were below the ultimate concrete strain, then the stress and strain profiles in the section could be considered to be linear and constant until first yielding of the reinforcing steel. This profile is illustrated in Figure 4-11. The forces in the concrete,  $C_c$ , reinforcing,  $C_s$  and  $T_s$ , and girders,  $C_g$  and  $T_g$  can be calculated from the stresses and cross sectional area of each component. The the resulting section transformed into steel is shown in Figure 4-12. The equivalent  $EI$  for the deck slab for this transformed section was 33% of the gross deck slab  $EI$ . The finite element model

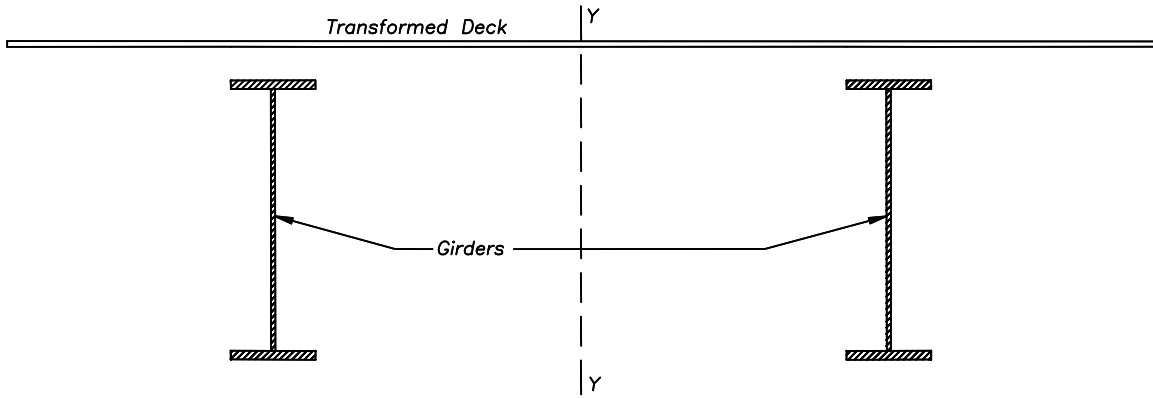


**FIGURE 4-9** Transformed equivalent steel section for bridge model with gross deck slab properties

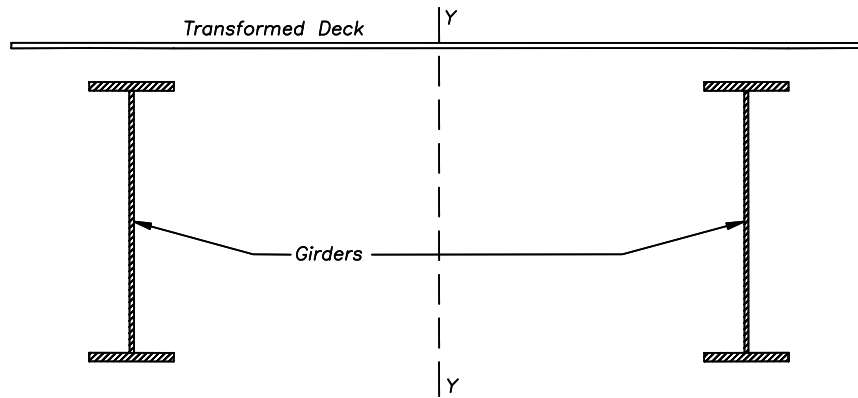


**FIGURE 4-10** Transformed equivalent steel section for  $I/I_g$  of the deck slab equal to 40% to allow for shrinkage cracking

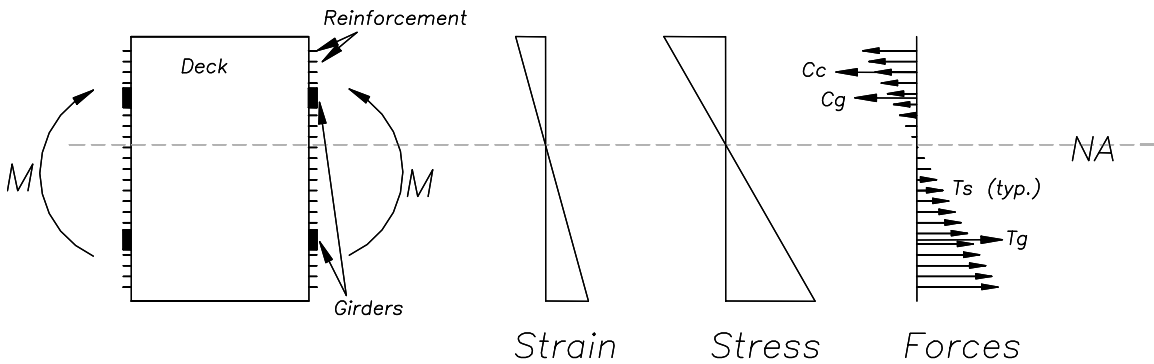


**FIGURE 4-11** Stress, strain and force distribution in deck slab of bridge model

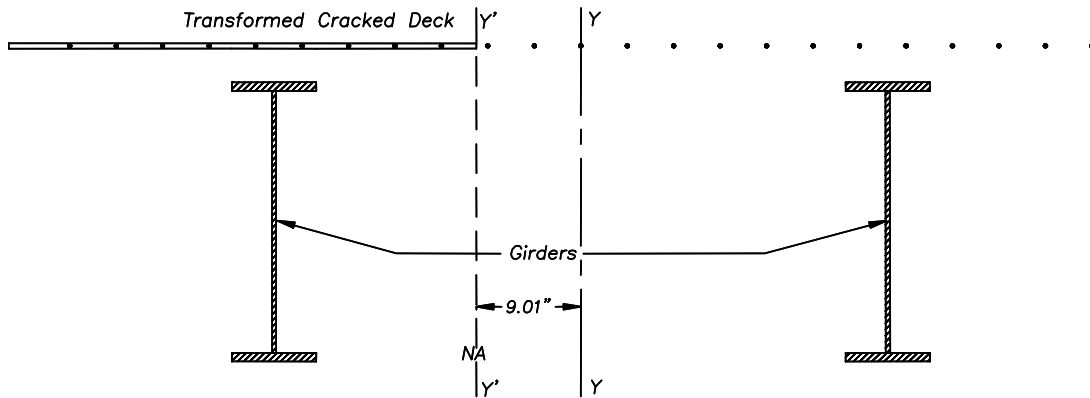


**FIGURE 4-12 Transformed equivalent steel section for bridge model assuming a fully cracked section in tension,  $I/I_g$  for the deck slab = 33%**

shows that the effective EI for the deck slab drops even further to as low as 15% for this experiment. This indicates that further lowering of the deck slab stiffness occurred, potentially due to yielding of the reinforcement in the deck slab. Hence it was necessary to investigate the bending moment in the deck slab at which yielding would be expected.

Strain gages in the deck slab showed a maximum measured strain of 0.17% which is below the expected yield strain at around 0.21%. However, as the measured strain was close to the yield strain it was possible that localized strains exceeded the yield value in other locations along the length of the reinforcing bars, at locations not instrumented with strain gages. Once yielding occurred in the reinforcement at one location, probably around a crack, then the strains in the other parts of the bar did not increase as the force in the bar was limited by the yield force. Hence it was reasonable to assume that localized yielding had occurred to lower the effective deck slab stiffness.

### 4.2.3 Response during Subsequent Experiments

During the second reversed static experiment, RSHXB2, yielding of the deck slab reinforcement was clearly observed in one of the outer longitudinal bars, as shown in Figure 4-13. The outer bar on the east side of the bridge model was shown to yield at an average actuator force of around 270 kN. Although this bar clearly yielded, there was no evidence of yielding in the bar located right next to it and the outer bars on the other side of the bridge deck slab. This suggests that the yielding was localized over a short length of the reinforcement and it is probable that the other bars also yielded but over lengths that were not instrumented with strain gages.

Localized yielding of the reinforcement had no visible impact on the condition of the deck slab as cracking had already occurred before yielding was observed. Furthermore, it may require significantly more reinforcement concentrated at the edges of the deck slab to design against localized yielding. Therefore it is not recommended that the deck slab be designed to prevent some yielding during an extreme seismic event. The width of the deck slab, even for the bridge model which was a relatively narrow bridge, assured that there was sufficient flexural strength in the bridge even under extreme seismic loading. Therefore designing the longitudinal

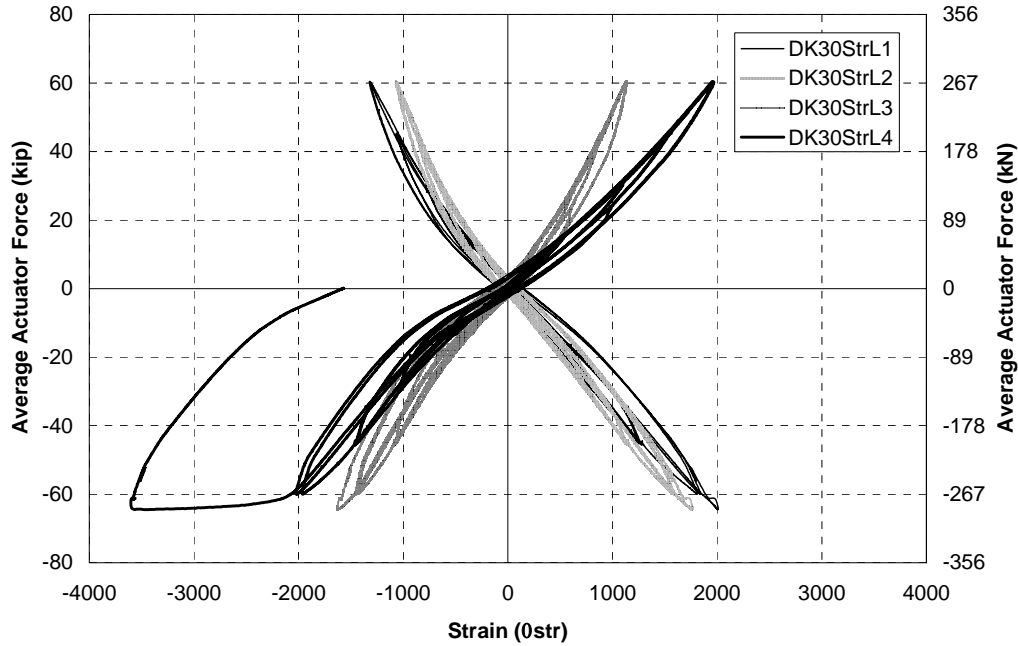


**FIGURE 4-13 RSHXB2 - Strain gages at midspan**

reinforcement for flexural actions resulting from transverse seismic loading is not considered necessary.

As the finite element model was calibrated to the remaining reversed static experiments it was observed that the superstructure stiffness had reduced further. Once the effective deck slab stiffness had been reduced to 15% of the gross deck slab stiffness the analysis became relatively insensitive to a further reduction because at this point the deck slab contributed relatively little to the overall stiffness of the bridge model. The stiffness of the superstructure became more sensitive to the stiffness of the connection between the deck slab and the girders. Therefore degradation of composite action after each experiment could explain the reduction in superstructure stiffness. This was incorporated into the finite element model and is discussed further in Section 4.3.

#### **4.2.4 End Shear in the Deck**

Considerable shear cracking, at an orientation of 45 degrees to the transverse and longitudinal axes of the bridge, was observed between the ends and the actuators located 6.10 m from the ends in the model. Furthermore, as the distribution of the transverse shear stud forces showed, whether the transverse shear forces were transferred down from the deck slab to the girders through additional shear studs on the ends of the girders, or through shear studs on the top chords of the end cross frames, it was necessary for the deck slab to transfer the shear to the ends of the bridge. Thus, it was prudent to check the deck slab reinforcing for the required shear capacity.

For the bridge model the maximum applied end shear was likely to be in the first experiment. Although there were no load cells measuring end shear for this experiment, from the actuator

forces, the end shear was estimated at around 310 kN. Based on AASHTO (1998) for a reinforced concrete beam analyzed using a sectional design model (Section 5.8.3), the shear strength of the concrete in the deck slab was 150 kN, and was thus exceeded by the demand in the bridge model. The maximum shear strength of the deck slab including reinforcing was equal to 710 kN and was therefore easily adequate.

Given that the demand in the bridge model was high and the shear capacity was easily adequate, it is not considered necessary to check the deck slab reinforcing for shear at the ends of typical bridges. Furthermore, no shear failures through the deck slab have been known to occur in steel plate girder bridges or reinforced concrete bridges due to transverse earthquake loading.

### **4.3 Influence of Shear Studs in Response of Bridge**

#### **4.3.1 Stiffness of Shear Studs in the Partially Composite Bridge Model**

As discussed in Chapter 2 the number of shear studs connecting the deck slab of the bridge to the steel girders was less than that required for either strength or fatigue based on recent AASHTO (1998) requirements. As the AASHTO strength requirements were not satisfied the bridge model can be considered a partially composite bridge. For a partially composite section the relative stresses in the slab and the girders are dependent on the stiffness of the connection between the two interfaces. Therefore in order to model the bridge effectively, a reasonable estimate of the shear connector stiffness is necessary.

There has been considerable research into the strength of partially composite sections, for example: Johnson and May (1975), Oehlers and Coughlan (1986), Wright (1990), Wang (1998), Seracino et al. (2001). Despite the relative beam and deck slab stresses being based on the stiffness of the shear connection, most design equations resulting from research are based on the flexural strength of the shear connection, such as in AISC (1997). Wang (1998) proposed a procedure which was based on the stiffness of the shear connectors but acknowledged that calculating this stiffness was difficult and there was much variation between different experiments. An empirical relationship for the stiffness of shear studs was proposed that was, like other studies, based on the strength of the studs. Seracino (2001) developed a model for evaluating the partial-interaction flexural stresses in composite bridge beams where the stiffness of the shear connection was used but no guidance given as to how to determine this stiffness except to state that it should be based on rational analysis.

Four different models to calculate the shear stud stiffness were considered, as illustrated in Figure 4-14. The bending stiffness,  $k_b$ , of each stud is defined by:

$$k_b = \frac{12EI_s}{L_{seff}^3} \quad \dots 4.3$$

where:  $E$  is the elastic modulus of the steel stud (200 GPa);  $I_s$  is the moment of inertia of the stud, and;  $L_{seff}$  is the effective length that is unrestrained for bending in stud. The shear stiffness,  $k_s$ , of the stud is defined by:

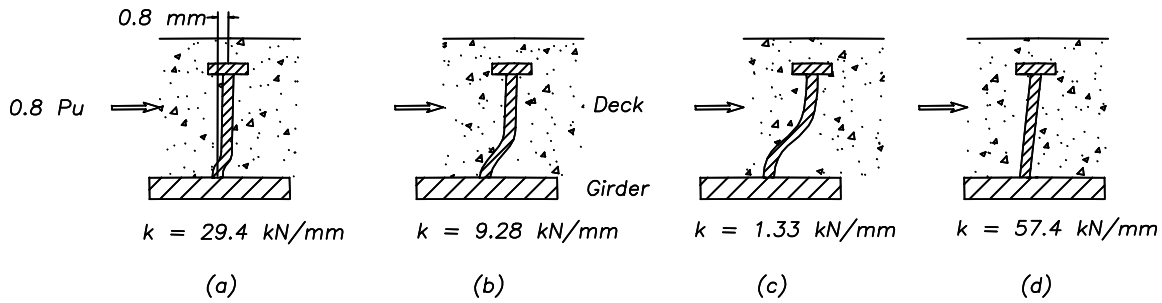


**FIGURE 4-14 Different stud models considered for bridge model**

$$k_s = \frac{GA_s}{L_s} \quad \dots 4.4$$

where:  $G_s$  is the shear modulus (77 GPa);  $A_s$  is the cross sectional area of the shear stud and;  $L_s$  is the clear length of the shear studs (89 mm). The combined stiffness,  $k_{st}$ , is equal to:

$$k_{st} = \frac{1}{\frac{1}{k_b} + \frac{1}{k_s}} \quad \dots 4.5$$

The first model (Figure 4-14a) was based on the empirical relationship from Wang (1998) who stated that; based on a large number of pushout tests from different researchers with studs of different sizes and types, the stiffness of shear studs can be defined by a constant displacement of 0.8 mm at 80% of the ultimate shear capacity of the studs. Variation ranged from 50% to 200% of this value. Consideration was given to reducing the displacement for this model based on the scale factor of the bridge, however the test data showed that even for smaller studs the displacement was relatively constant, therefore no reduction was made. This assumed model resulted in a stiffness equal to 29.4 kN/mm for the studs in the bridge model. If flexibility in each stud was assumed to be due to shear over the length of the stud and bending along some length of the stud, the equivalent length for bending resulting in this corresponding stiffness was 25 mm.

Studs were generally tested using pushout tests with studs embedded in concrete slabs or slabs with corrugated metal formwork providing good confinement around the shear studs. However in the haunch of the bridge model, as in typical steel plate girder bridges, the concrete is unreinforced and as a result has little confinement. Small cracks were observed corresponding to the stud locations in the haunch as observed in Figure 4-15. Consequently, a second model (Fig. 4-14b) was considered in which half the length of the studs (44 mm), approximately corresponding to the length of each stud in the haunch, was considered free to bend due to lack of confinement caused by cracking around the stud. The stud was also free to deform in shear. The resulting stiffness was calculated to be 9.3 kN/mm, this being approximately one third of the stiffness calculated from the first model.

A third model was considered (Fig. 4-14c) in which the studs were free to bend over their entire length. This resulted in an equivalent length of 89 mm and a stiffness of 1.4 kN/mm. The model



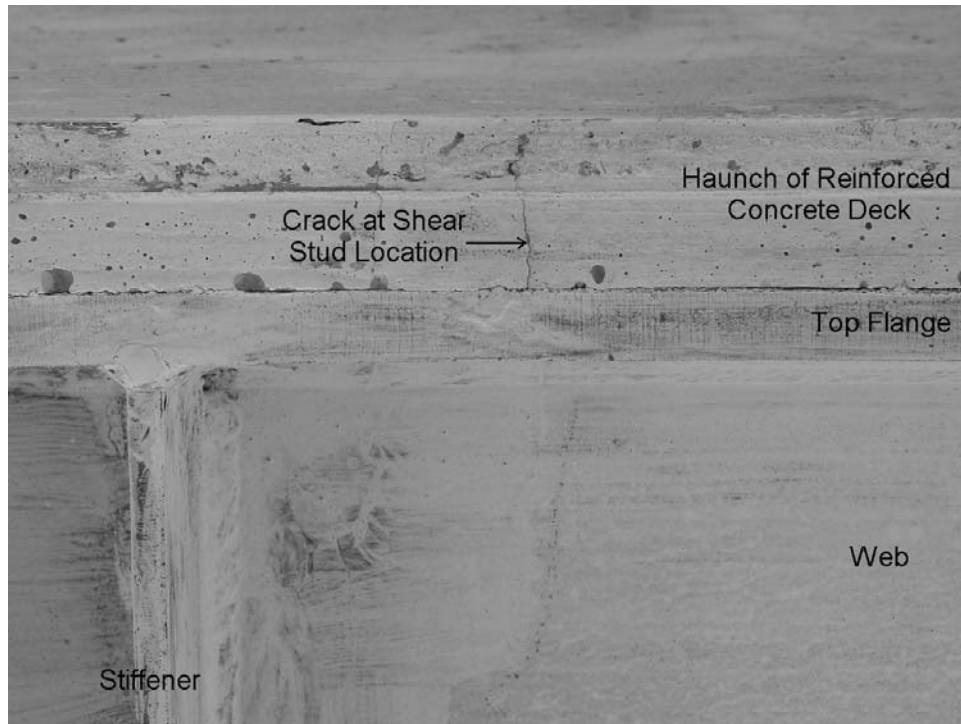


**FIGURE 4-15 Cracks observed in haunch of bridge model around shear stud location**

assumed cracking around the full height of the stud and is considered a lower bound for the stiffness. A fourth model considered the studs to be restrained from bending and free only to deform in shear as shown in Figure 4-14d. This resulted in a high stiffness and an upper bound stiffness with a value equal to 57.4 kN/mm. Besides the four stud models, an arbitrary fifth model E with a stiffness of 155 kN/mm was also used in order to give a smoother relationship in the following analyses.

The four different shear stud models were assumed in finite element analyses. The elastic modulus of the deck slab was varied depending on the stud model in order to correlate the transverse midspan displacement in the finite element with the measured midspan displacement in the RSHXB experiment. The loads corresponded to the maximum applied positive and negative actuator loads for the first cycle of loading in the bridge model, when the bridge was in its least damaged state. The effective shear modulus as a ratio of the gross shear modulus was assumed to be equal to that for the elastic modulus. The resulting effective elastic modulus as a ratio of the gross modulus for the concrete is plotted against shear stud stiffness in Figure 4-16. This figure shows that as the stiffness of the shear studs reduced the effective deck slab modulus increased as the model was modified from a fully composite section to one with minimal composite action. Although the midspan displacements for the finite element model correlated with the measured displacements for each of the different shear stud models, the rotations at the midspan and the displacements near the ends of the bridge did not correlate. Figure 4-17 shows the displacements and rotations in the finite element model normalized to the measured displacements in the bridge model and averaged between the positive and negative reversal. The midspan displacement was relatively constant and close to unity as this was used for calibration of the finite element model. The midspan rotation was seen to be overestimated for high shear stud stiffnesses and

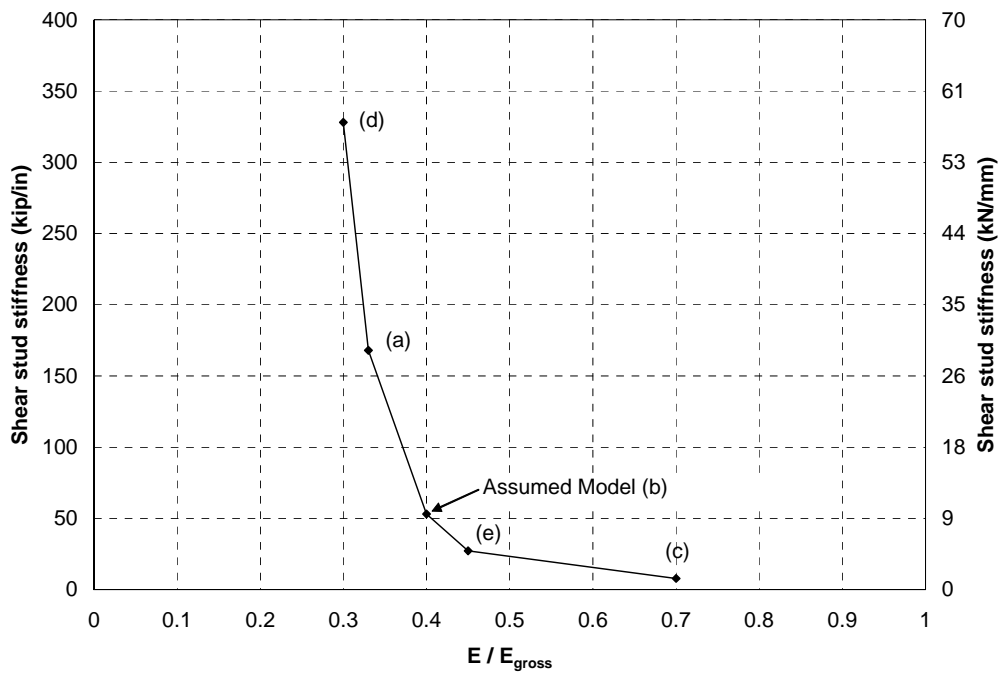


**FIGURE 4-16 Elastic modulus vs shear stud stiffness for midspan displacement in finite element model correlated to measured displacement in bridge model**

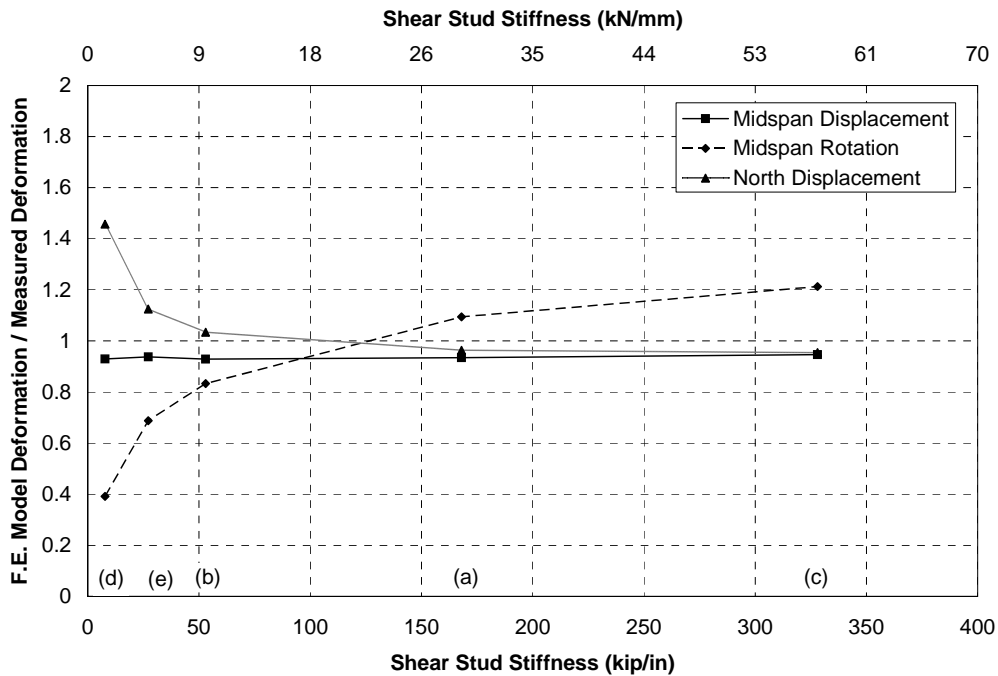


**FIGURE 4-17 Displacements from finite element model normalized to measured displacements for different shear stud models**

underestimated for low shear stud stiffnesses. The displacement of the model at the first intermediate cross frame at the north end was shown to be overestimated with a low shear stud stiffness. Based on these observations, a shear stud stiffness somewhere between models A and B was most appropriate.

Oehlers and Coughlan (1986) and Gattesco and Giuriani (1996) demonstrated that when subjected to cyclic loads permanent slips are generated that are largely irrecoverable due to the accumulation of damage in concrete around the studs. Experiments in these publications did not apply fully reversed cyclic loading only unidirectional cyclic loading, as typical due to gravity loads in composite beams. This accumulated damage was also seen in tests which have fully reversed loading (McMullin, 1994; Hawkins, 1984). Such accumulated damage could help to explain the degradation in stiffness of the bridge model after a number of cycles of transverse loading. Therefore using model B for the shear studs, which predicts a more conservative stiffness than model A, is likely to become more realistic after the bridge model was subjected to a number of cycles of loading.

### **4.3.2 Damage to Shear Studs at the North End of Bridge Model**

The first reversed static experiment was displacement controlled and therefore the forces in each actuator were not necessarily equal, unlike the subsequent experiments which were controlled with equal forces in both actuators. Figure 4-18 shows that the actuator forces were similar for each cycle as the amplitude of the cycles increased, with exception of the last few cycles, where the north actuator force decreased almost to zero while the south actuator force increased to 380 kN. This redistribution of forces was as a result of failure of the shear connectors at the north end of the bridge, which were shown to be critical in the transverse load path.

The strength of shear studs is calculated using both the strength of the surrounding concrete cones and the strength of the studs themselves. For the shear studs in the bridge model these two criteria from AASHTO (1998) resulted in very similar calculated ultimate forces in the studs at 30 kN and 29 kN respectively. During Experiment RSHXB cracks were observed in the haunch of the deck slab where there was no reinforcement providing confinement for the concrete around the studs, however, the studs ultimately failed through shearing of the studs just above where they were welded to the girder flanges.

### **4.3.3 Transverse Shear Stud Forces**

The finite element model was used to evaluate forces in the shear connectors. The shear studs in the finite element model were based on the stiffness of the shear connectors using model B, and applied force of 210 kN in each actuator was based on the average maximum actuator force in the bridge model just before observed failure of the shear studs. The deck slab stiffness was assumed to have an EI of 15% of the gross EI as calculated for the bridge model at the end of RSHXB experiment. The transverse shear in each row of shear connectors along the length of the girders is shown in Figure 4-19. This figure shows a large concentration of transverse shear forces in the studs located at the north end. The maximum forces at the end of the bridge were in excess of the calculated ultimate shear of 29.4 kN and can therefore explain the failure of the studs. As the studs in the end row failed, the forces were transferred in the next row of studs causing progressive failure of three rows and severe damage to the fourth row before completion of the experiment. At the south end the forces in the shear studs were much smaller. This was because the forces were

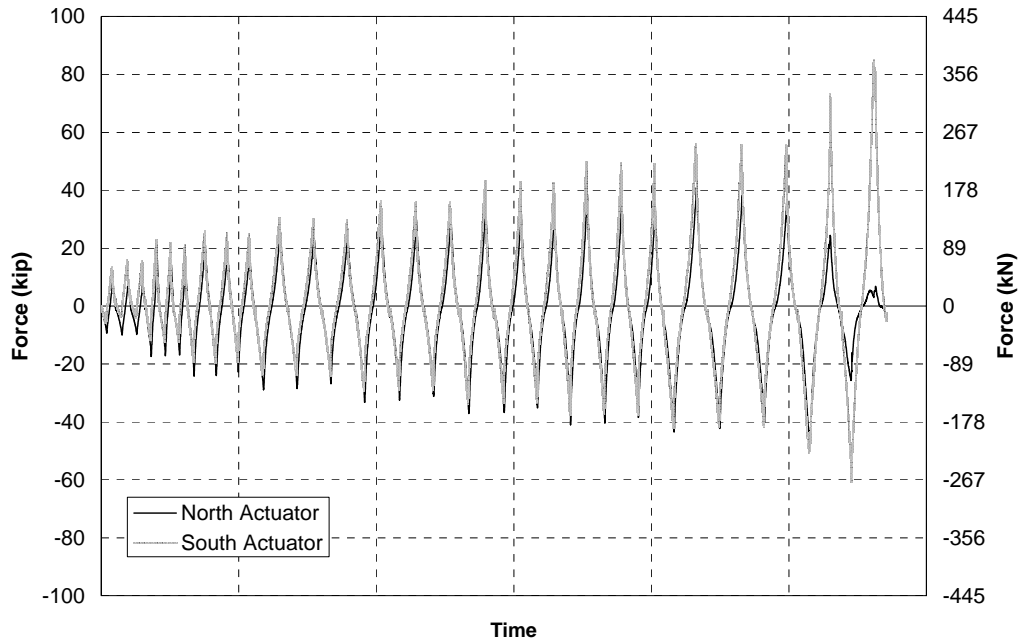


**FIGURE 4-18 RSHXB - Actuator forces versus time**

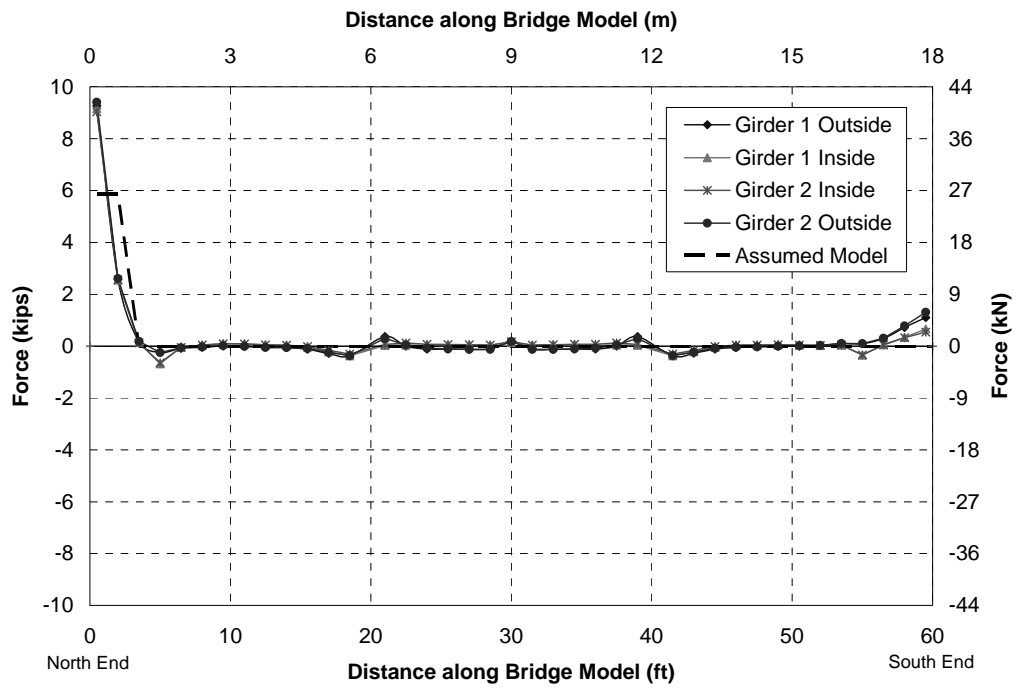


**FIGURE 4-19 Transverse shear stud forces in bridge model from finite element model**

transferred from the deck slab into the end cross frames through the composite top chord as shown in Figure 2-12.

If all the transverse shear forces in the shear studs at the north end are added together the sum of the shear forces is equal to 196 kN, that is close to the total shear at each end, equal to the applied actuator force, of 209 kN. The difference can be attributed to a small proportion of transverse forces transmitted to the end by transverse bending and torsion of the girder flanges. As the proportion of transverse shear force carried by the flanges was small, it is reasonable that shear studs should be designed for the full end shear. A model is considered in which forces are carried by studs located within a length along the girder from the end equal to the depth of the girder. As the girders were 610 mm deep, then two rows of shear studs at the end of the bridge model would be effective in carrying transverse shear forces. As there are two rows of studs along each girder and two girders, a total of eight shear studs can be considered to transfer the transverse shear from the deck slab into the ends of the bridge. Therefore based on a total end shear of 210 kN, the force in each stud was 26 kN, slightly less than the calculated capacity of 29 kN. This subsequent distribution of forces is shown by the assumed model in Figure 4-19. The distribution compares well with the calculated distribution of forces from the finite element model. It assumes some forces are redistributed for the studs at the very end of the bridge model but there should be enough ductility in the studs to allow this redistribution. Generally when there is a connection between the deck slab and the girders, like that at the south end of the bridge model, the top chord can be designed to carry the full end shear.

If the bridge model was designed to be fully composite, in accordance with AASHTO, the studs in a length equal to the depth of the girder would be adequate to transfer the shear forces in the end cross frames. This should also be the case for other typical bridges. However it is common practice in many states not to provide composite action in negative moment regions of continuous girders. In this case a top chord of the end cross frame located above the column bent or pier should be designed to carry the seismic shear from the deck slab into the end cross frames (Carden, 2002). As it is also proposed with the used of ductile end cross frames that shear connectors be removed from the top of the girders to allow the girders to rotate, a composite top chord should also be used in this situation to provide adequate transverse seismic load path. In general, it is recommended that some form of composite connection be provided to transfer the transverse earthquakes loads from the deck slab into the cross frames located above the supports, either utilizing connectors on top of the girders, within a length equal to the depth of the girders, or a composite top chord.

#### **4.3.4 Longitudinal Shear Forces**

The finite element model showed that there were also some longitudinal shear forces in the shear studs due to transverse loading. The distribution of forces for the same applied actuator force of 209 kN per actuator is shown in Figure 4-20. This figure shows that the magnitude of the longitudinal forces was significant, with a maximum force close to the shear capacity of the studs. Therefore these forces undoubtedly contributed to failure of the shear studs at the ends of the bridge when combined with the transverse shears.

In order to explain and quantify the longitudinal shear forces a transformed section, similar to that shown in Figure 4-9 is considered with an effective EI equal to 15% of the gross EI for the deck slab. For 210 kN forces applied to the bridge model through each of the two actuators, the shear

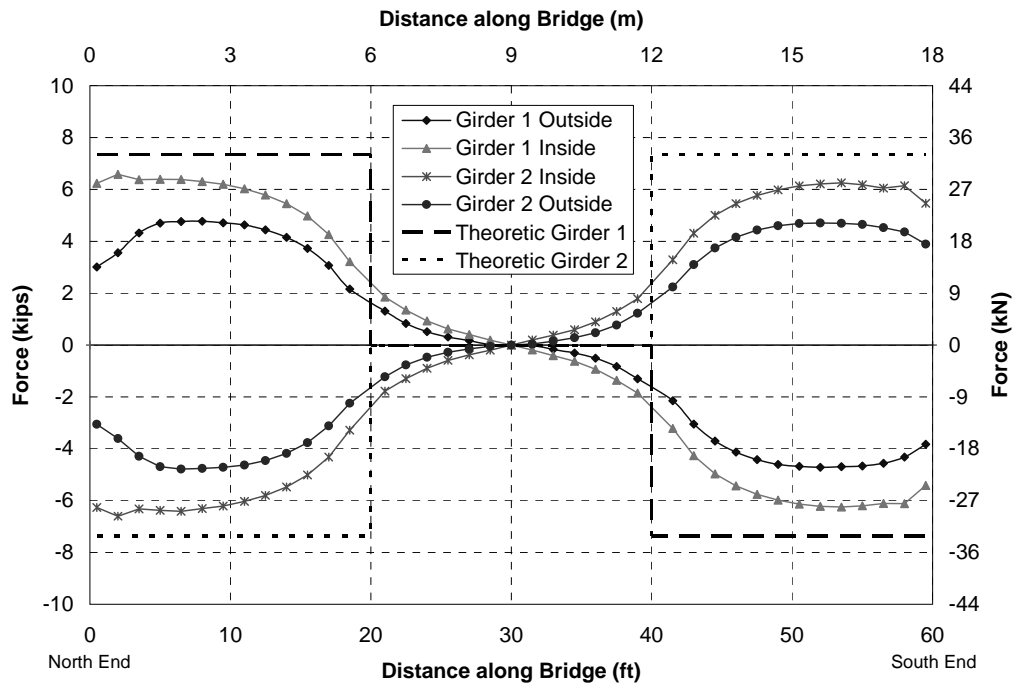


**FIGURE 4-20 Longitudinal shear stud forces in bridge model from finite element model**

force was constant and equal to 210 kN for the first third of the length of the bridge superstructure, zero for the next third, and equal to -210 kN for the final third. The shear flow is considered between the girders and the deck slab. Ignoring torsional effects the shear flow,  $Q$ , is given by:

$$Q = \frac{VA_g\bar{y}_g}{I_y} \quad \dots 4.6$$

where:  $A_g$  is the cross sectional area of a girder;  $\bar{y}_g$  is the horizontal distance between the centroid of the transformed section and center of the girder, and;  $I_y$  is the effective transformed moment of inertia for the section about the vertical axis. Therefore for the first third length of bridge model the shear flow is calculated to be 0.142 kN/mm and -0.142 kN/mm respectively for the two girders. Note that the shear flows for each girder were equal and opposite as the neutral axis was assumed to be in the center of the section. For two rows of the studs on each girder, and studs spaced at 460 mm centers, the shear force in each stud was equal to 32.6 kN and -32.6 kN respectively. For the middle third the shear forces are equal to zero and for the last third the shear forces are equal and opposite to the first third. The theoretical forces are shown on Figure 4-20. The theoretical longitudinal shear forces in the studs were therefore larger than the design strength of the studs and failure could have been expected at these loads due to longitudinal forces alone. The pattern of theoretical forces was similar to the pattern calculated in the finite element model, although there was some transition between the levels of force at the one third points along the length of the bridge. The theoretical forces were also larger than the calculated finite element forces because they were calculated based on full composite action, while in reality the shear studs

have finite stiffness resulting in some slippage between the deck slab and the girders and a reduction in the stud forces.

The analysis presented above was based on a symmetric cross section with an equivalent moment of inertia for the deck slab. A cracked transformed section was considered, with the neutral axis located as in Figure 4-12, but the same moment of inertia as the previous model. The resulting longitudinal shear forces in the studs on the two girders are 21.4 kN and -43.7 kN respectively along the first third of the bridge length. These may be more realistic for relative forces in the two girders of the bridge model, although they will be still conservatively high for the partially composite section.

For fully composite sections, with the number of studs recommended by AASHTO, it was demonstrated that the longitudinal shear forces were likely to be lower than the capacity of the studs. However when combined with transverse forces, the force in the studs is increased compared to studs subjected to unidirectional actions. This analysis supports the use of a composite top chord to transfer the transverse seismic shear from the deck slab into the end cross frames above each support, removing the transverse shear from the studs on top of the girders allowing these studs to carry the longitudinal loads alone.

#### **4.3.5 Axial Stud Forces**

Axial forces were also observed in the shear studs at the ends of the bridge model where the studs resisted the rotation of the end of the girders about their longitudinal axes. The rotation was resisted by the shear studs as well as contact between the haunch and the girders on the compression edge. The contact was modeled using pinned links along the compression edge which were rigid in compression but unable to transmit shear and bending moments. The resulting axial forces in each row of shear studs is shown in Figure 4-21. This figure shows relatively large axial loads at both ends adding to the longitudinal and transverse shear forces already observed. Further analysis shows that the axial forces would be negligible if the bridge model had been fully composite and the cross frames remained relatively rigid limiting rotation of the girders. However with relatively flexible end cross frames, when designed to be ductile, the axial forces in the studs increased. Moreover, the axial stiffness in the studs had a significant effect on the stiffness of the end region which affects the response of ductile end cross frames, as discussed in a subsequent report (Carden, 2005).

#### **4.4 Overall Superstructure Response including Effective Deck Stiffness and Partial Composite Action**

The transverse effective stiffness of the superstructure was found to be affected by cracking in the deck slab, as described earlier, but also due to slippage in the connection between the deck slab and the girders. From analysis of a simplified analytical model, which is described at the end of the chapter, it was found that an effective stiffness of the superstructure required to match the experimental data was as little as 12% of the gross stiffness of the fully composite section.

Calculating a theoretical torsional stiffness for the bridge model was not trivial as the geometry was complex and the properties were affected by partial composite action, warping and distortion in the section. The torsional moment of inertia,  $J$ , of open cross sections is often calculated using Equation 4.2. Applying this equation to the equivalent transformed section for the superstructure

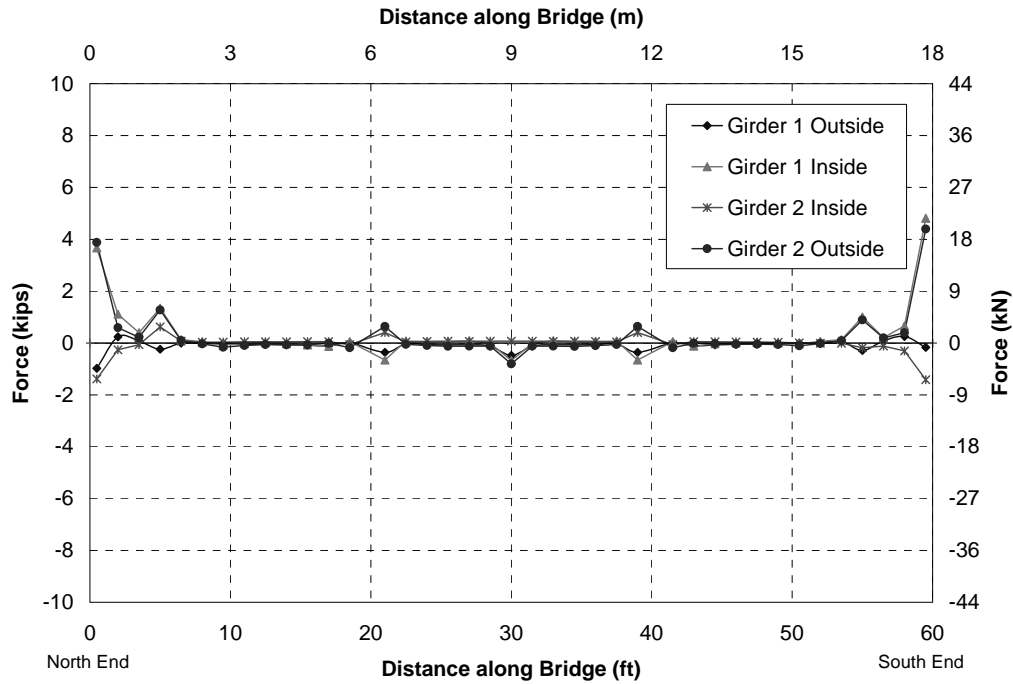


**FIGURE 4-21 Axial shear stud forces in bridge model from finite element model**

of the bridge model, assuming gross section properties, gave a torsional moment of inertia of  $79 \times 10^6 \text{ mm}^4$ . From the analytical model a torsional moment of inertia of  $100 \times 10^6 \text{ mm}^4$  was found to be appropriate for modeling the rotation in the girders after the first two experiments in which the properties of the deck slab and shear studs stabilized. Therefore the calculated torsional moment of inertia was underestimated compared to the measured value. This is attributed to warping not being included in the analytical model, which is being compensated for by the effective torsional moment of inertia. This is demonstrated when studying torsion in the girders in Chapter 6. This is discussed further in the development of the analytical model described in Chapter 8.

In order to estimate the transverse displacement due to torsion of the superstructure, at a given height such as deck slab level, it was necessary to locate the height of the shear center of the bridge superstructure. The shear center was known to be located at some point above the deck slab from the observed torsion in the superstructure. The shear center can be calculated based on an analysis of the shear flow as a transverse load is applied to a cross section of the bridge, as shown in Figure 4-22. The resulting eccentricity between the centroid of the deck slab and the shear center,  $e$ , for a two girder bridge is given by:

$$e = \frac{(2A_f + A_w)s_g^2 d_{gf}}{4I_y} \quad \dots 4.7$$

where:  $A_f$  is the area of each bottom flange,  $A_w$  is the area of each web  $s_g$  is the spacing of the girders,  $d_{gf}$  is the depth of the girders between the centroid of the flanges, and;  $I_y$  is the effective



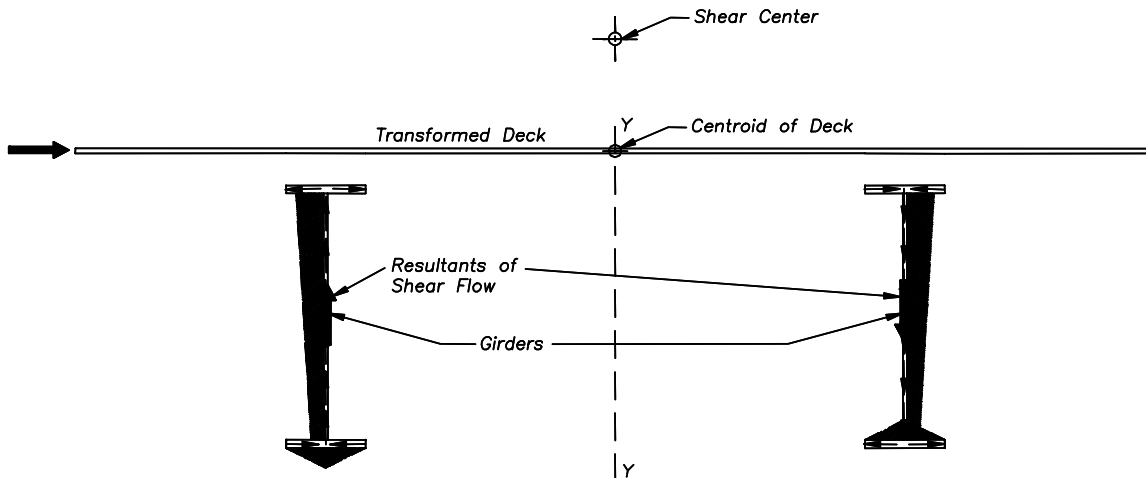


**FIGURE 4-22 Analysis of shear flow in girders of bridge model**

moment of inertia for the section. Based on analysis of the shear flow in the transformed bridge section, assuming an effective deck slab stiffness of 15% of the gross deck slab stiffness, the shear center was calculated at 242 mm above the deck slab of the bridge model. This analysis assumed full composite action between the deck slab and the girders, but was relatively insensitive to this assumption, as a reduction in the effective transverse  $I_y$  due to partial composite action reduces the shear flow in the girders, resulting little change in the shear center eccentricity. Applying lateral loads to the detailed finite element model at different heights showed that no rotation was achieved when the loads were applied at a height of 280 mm above the deck slab. Therefore the estimated shear center height was within 13% of the calculated height from the finite element model. The comparison would be better if compared at the height of the center of mass.

This section showed that there was a large uncertainty in the calculation of the torsional properties, particularly the torsional moment of inertia, for the bridge model. Finite element analyses showed that torsional properties did not greatly affect the overall dynamic properties of the structure as they increased the transverse displacement of the center of mass of the superstructure by less than 20%. For most practical cases the torsional properties can be neglected.



## SECTION 5 ELASTIC RESPONSE OF THE CROSS FRAMES

### 5.1 Introduction

The relative forces in the end and intermediate cross frames of the bridge model as they respond essentially elastically are considered in this chapter. The top and bottom chords girders are each shown to have an effect on the elastic transverse response of the cross frames. The inelastic response of the end cross frames is investigated in a separate report (Carden, 2005).

### 5.2 Relative Forces in End and Intermediate Cross Frames

Analytical studies have shown that a large percentage of the transverse seismic forces in a bridge are transferred from the deck slab into the substructure through the end cross frames, at the end of each span, meanwhile the intermediate cross frames were shown to have small forces from seismic loading (Itani, 1995; Zahrai, 1998). This was also observed experimentally in the bridge model.

In each experiment on the bridge model the relative forces in the cross frames, while the cross frames remained elastic, were estimated using a series of strain gages on sections of the single angle diagonal X-brace members. Component experiments on the diagonal members showed that the strain gages were not accurate in estimating the true forces in the cross frames therefore only relative values could be considered.

From RSHXB2 the estimated relative shear forces in the end and intermediate cross frame diagonals are shown in Figure 5-1 for different levels of applied actuator force. This figure shows that the end cross frame forces were typically four to five times larger than the largest intermediate cross frame force at any given level of applied actuator load. The strain gages on the midspan cross frame were faulty and therefore the estimated relative shear at midspan was not shown in the figure.

Once the end cross frames of the bridge model started to yield the forces in the intermediate cross frames closest to the ends of the bridge were shown to increase a small amount, however the measured strains remained well below yield levels. The estimated relative cross frame shear forces during Experiment RSLXB are shown in Figure 5-2. At the intermediate cross frames corresponding to the actuator locations the relative forces were different to those seen in Figure 5-1 due to the additional double angle used to support the vertical component of actuator loads. Focus of the discussion will therefore center on the first intermediate cross frames, 3.05 m from each end of the bridge, and the end cross frames. As with the large X-braces the majority of the relative shear estimated in the cross frames was concentrated in the end cross frames.

A similar distribution of shear forces in the various cross frames can be seen during the dynamic experiments. Figure 5-3 shows the estimated relative forces in each of the end and intermediate cross frames for the bridge model with heavy X-braces at the ends in response to increasing amplitude scaled El Centro ground motion. The end cross frames carried over 90% of the total shear in the cross frames.

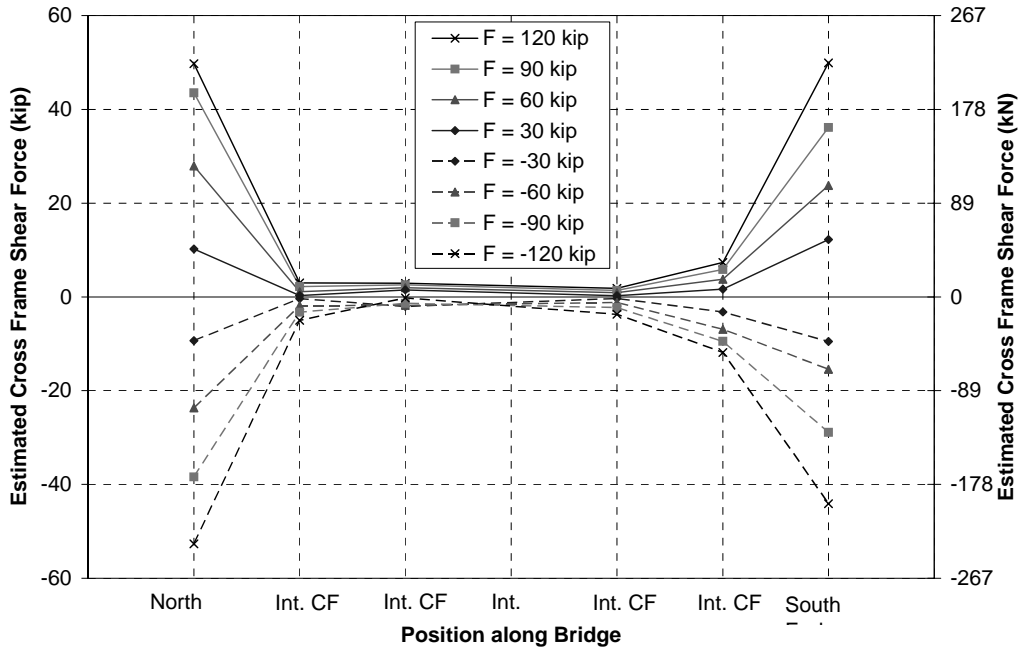


**FIGURE 5-1 RSHXB2 - Estimated forces in end and intermediate cross frames for different total applied actuator forces**

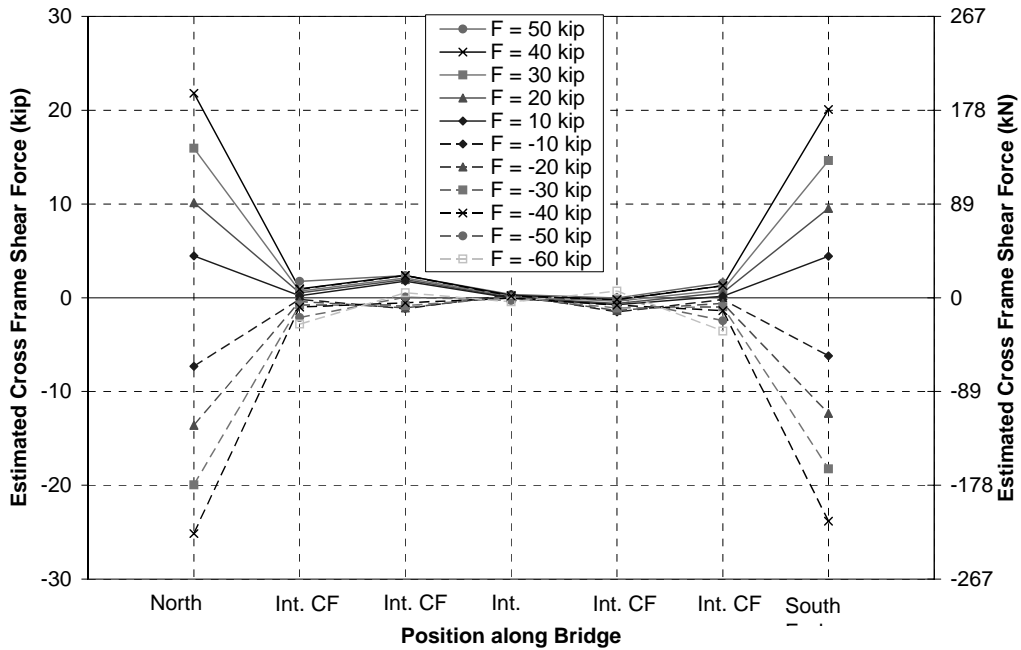


**FIGURE 5-2 RSLXB - Estimated forces in end and intermediate cross frames for different total applied actuator forces**

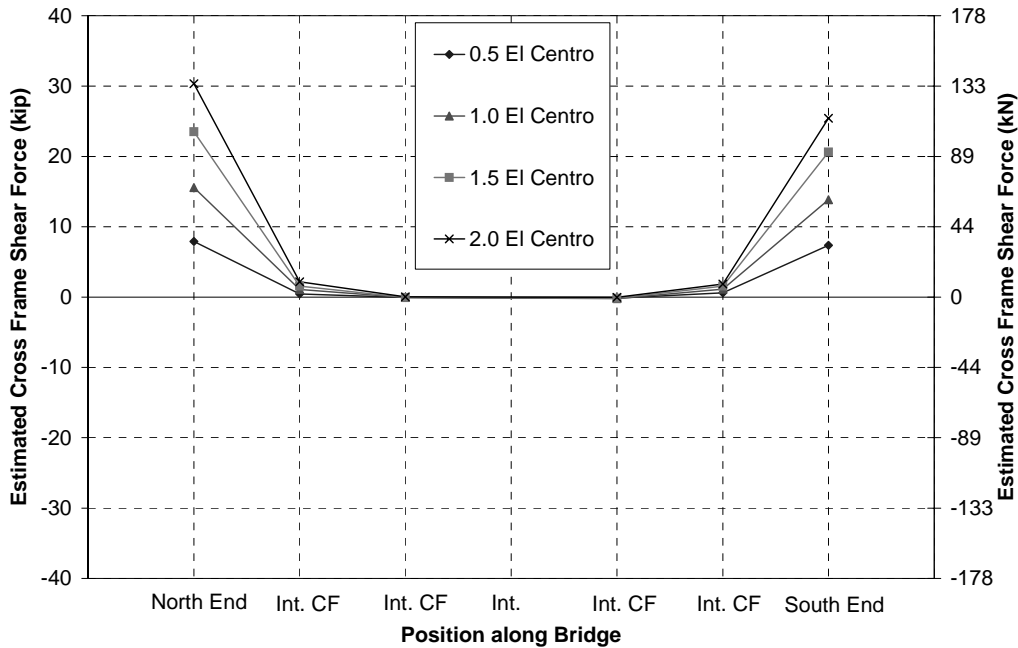


**FIGURE 5-3 STLXB - Estimated forces in end and intermediate cross frames for different earthquake levels**

### 5.3 Effect of Top and Bottom Chords and Other Components on End Cross Frame Stiffness

Reversed static Experiments 3 to 7 were conducted in order to characterize the effect of the top and bottom chords of the end cross frames, the intermediate cross frames and the lateral girder stiffness in the transverse end stiffness of the bridge model. The different reversed static experiments with different bridge model configurations are listed in Table 2-1.

The hysteresis loops for the ends of the bridge model during Experiments RSHXB2 and RSLXB with the “heavy” and “light” end cross frames are described in a subsequent report (Carden, 2005). In order to calculate the influence of the different cross frame components on the transverse stiffness of the end regions, it was first necessary to estimate the essentially elastic stiffness of the ends with the end cross frames. With the bolted cross frames slippage resulted in non-linearities in the hysteresis loops even though the cross frame diagonals remained essentially elastic. The initial stiffness of these cross frames at each end was defined as the average slope of the backbone curve from the hysteresis loop of each end region. The average slope was calculated by fitting a linear regression through the essentially elastic portion of the backbone curves. For the “light” welded X-braces the stiffness was estimated by the average slope of the backbone curves up to yielding of the diagonal members of the cross frames. The resulting stiffness at each end of the bridge model during Experiments RSHXB2 and RSLXB is given in Table 5-1.

In the other reversed static experiments various components were removed from the bridge as described in Table 2-1. Resulting plots of end shear force versus relative horizontal end

**TABLE 5-1 End Stiffnesses from Reversed Static Experiments**

Expt	North End Stiffness (kN/mm)	South End Stiffness (kN/mm)
RSHXB2	39.5	45.0
RSNECF	2.5	3.4
RSNBC	8.2	8.7
RSFC	9.3	11.4
RSNCF	2.0	2.7
RSPC	2.9	4.7
RSLXB	24.4	37.8

displacement between the top and bottom flanges of the girder are illustrated in Figures 5-4 to 5-8. In Figures 5-4 and 5-7, for which the bridge model had no end cross frame components, the ends exhibit relatively linear behavior with minimal hysteresis. However, in the other experiments when a top or bottom chord was added to the system there was appreciable hysteresis at the ends that was attributed to slippage in the connections. It was particularly noticeable in Experiment 7 which had the pinned top and bottom chords. Table 5-1 indicates that in this experiment the effective stiffness had increased compared to the model with no end cross frames. However, Figures 5-9 and 5-10 show that the tangential stiffnesses of the end regions were approximately the same, with the effect of the top and bottom chords better explained by a hysteretic elasto-plastic model than additional elastic stiffness. The hysteretic behavior in the south end was slightly larger than that at the north end attributed to different slip coefficients in the connections. However an approximate elasto-plastic model with a yield force of 9.0 kN was considered to model the hysteretic behavior at both ends. This is nominally approximately 10% of the yield strength for the light X-braces and buckling restrained braces, discussed in a subsequent report (Carden, 2005).

Comparing each experiment allowed the contribution of the diagonals, top and bottom chords, intermediate cross frames and other components in the transverse load path to be determined based on their relative effective stiffness. Table 5-2 shows the effective stiffness for the “heavy” X-braces at both ends of the bridge model. The two ends showed similar relative contributions to the stiffness with the difference being attributed to a slightly lower stiffness in the girders, bearings and shear studs at the north end, as a result of damage. The table shows that only 75% of the of the relative stiffness was attributed to the diagonal members while the top and bottom chords contributed around 17%. This was as a result of bending moments in the chord members allowing frame action between the chords and the web stiffeners.

Table 5-3 shows the relative elastic contributions for the “light” X-braces. Again there was good comparison between the relative distribution of stiffness in the different components at each end, although, overall the north end was more flexible than the south end. This indicates that damage to the shear studs reduced the stiffness of the top and bottom chords, girders and even the diagonals due to interaction of the components. Overall the stiffness of the diagonals accounts for 88% of the end stiffness. Even though the angles have a much smaller cross sectional area than those used in the elastic X-braces, their effective elastic stiffness was similar. This is due to the welded connections which eliminated slippage in the connections. During the shake table experiments the initial effective stiffness of the heavy X-braces was larger as no slippage was allowed in the

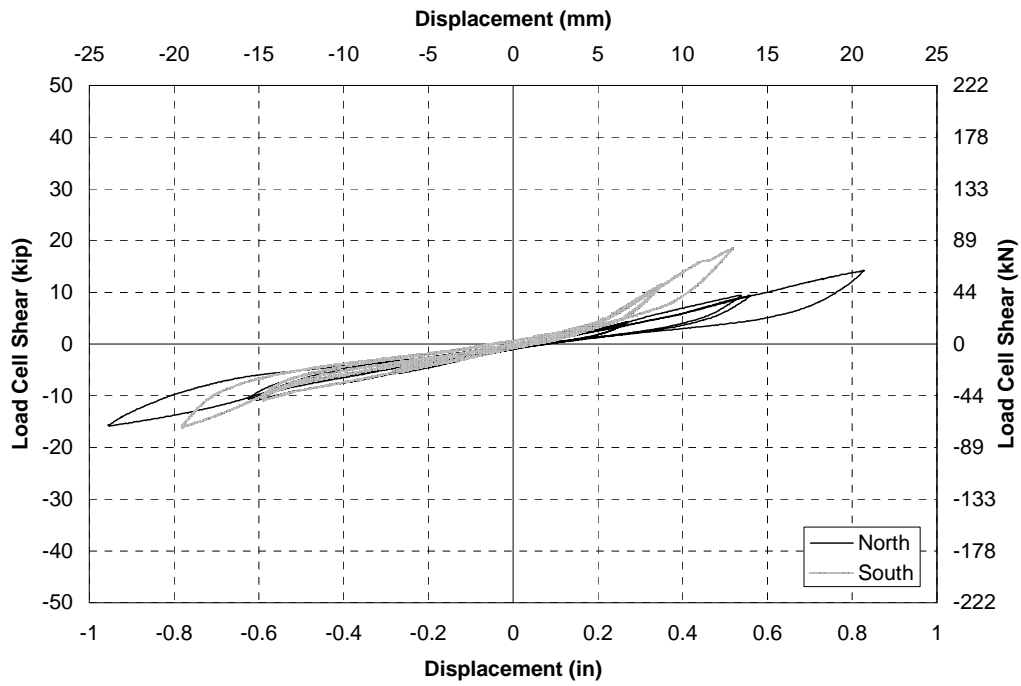


**FIGURE 5-4 CNEXF - End shear force versus horizontal end displacement**

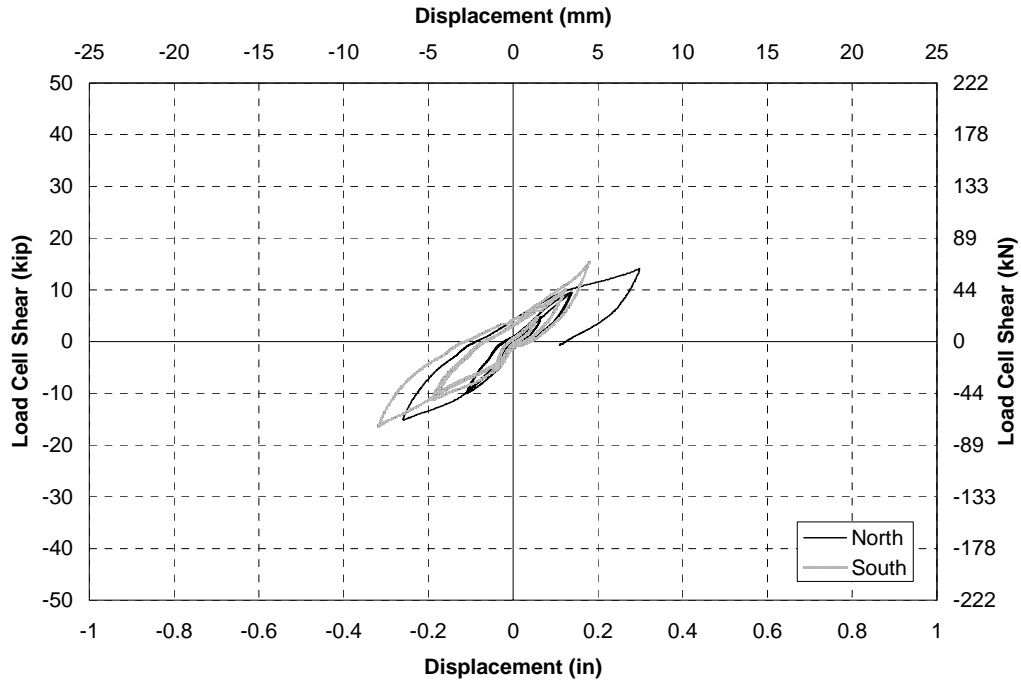


**FIGURE 5-5 RSNBC - End shear force versus horizontal end displacement**

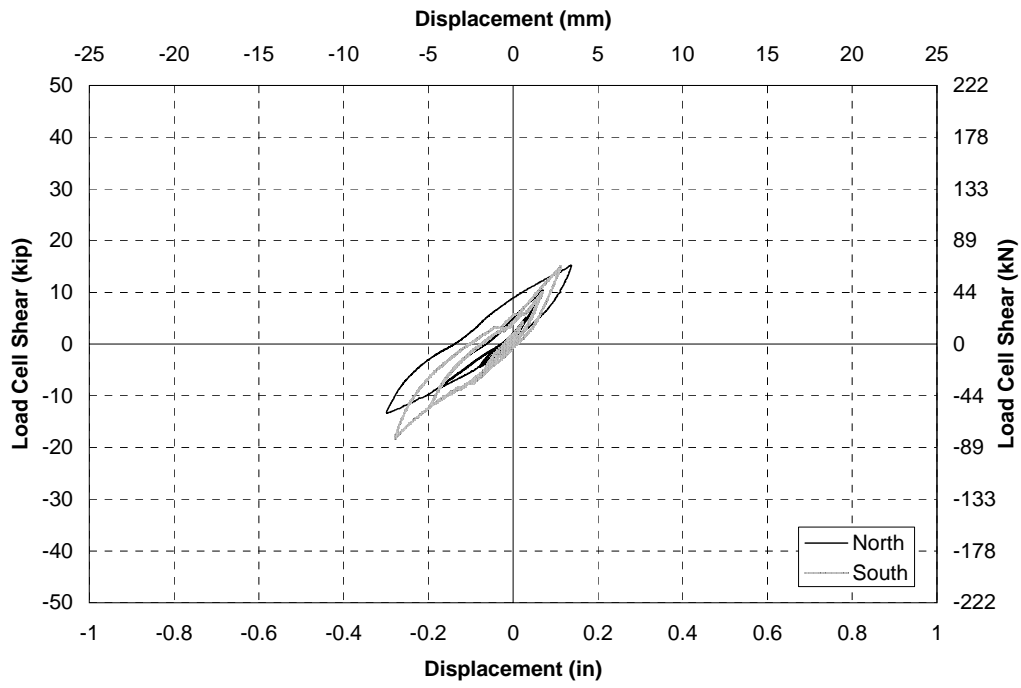


**FIGURE 5-6 RSFC - End shear force versus horizontal end displacement**

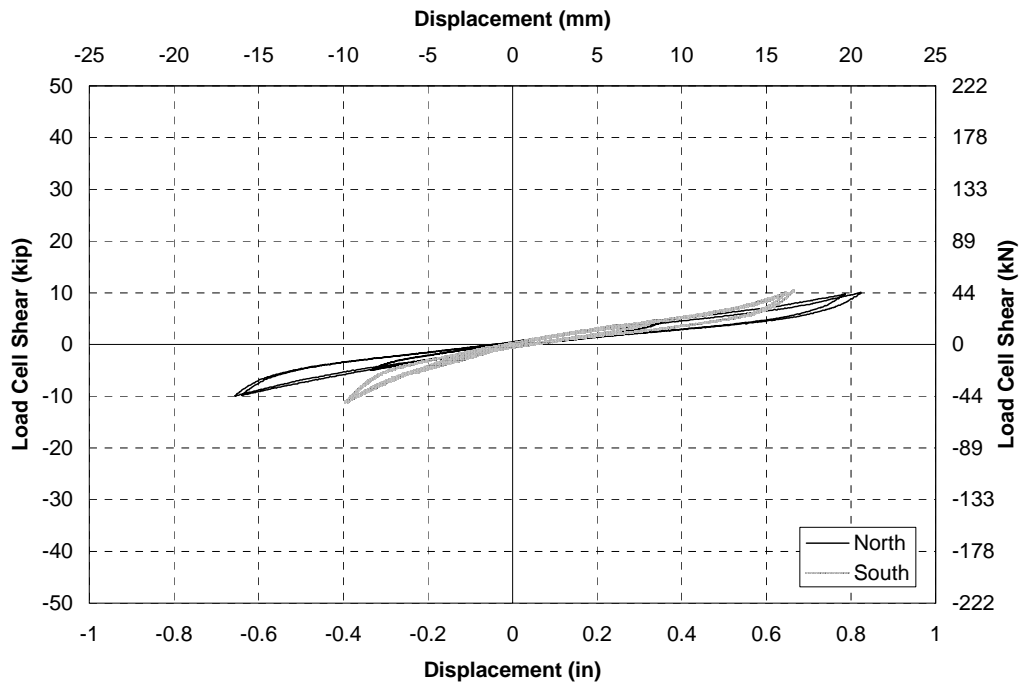


**FIGURE 5-7 RSNCF - End shear force versus horizontal end displacement**



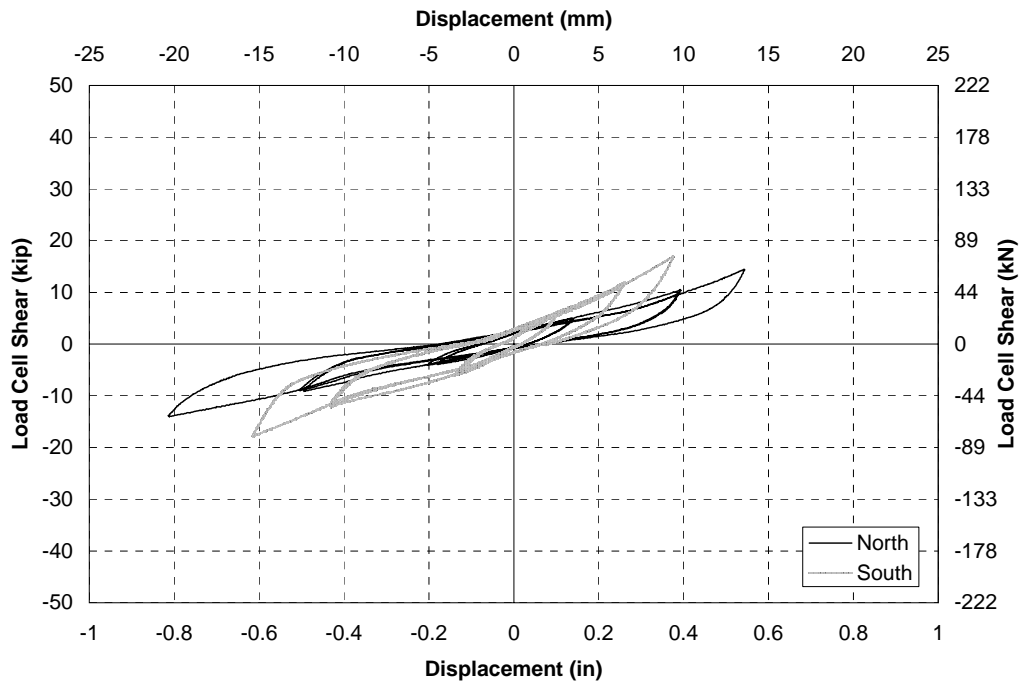


**FIGURE 5-8 RSPC - End shear force versus horizontal end displacement**

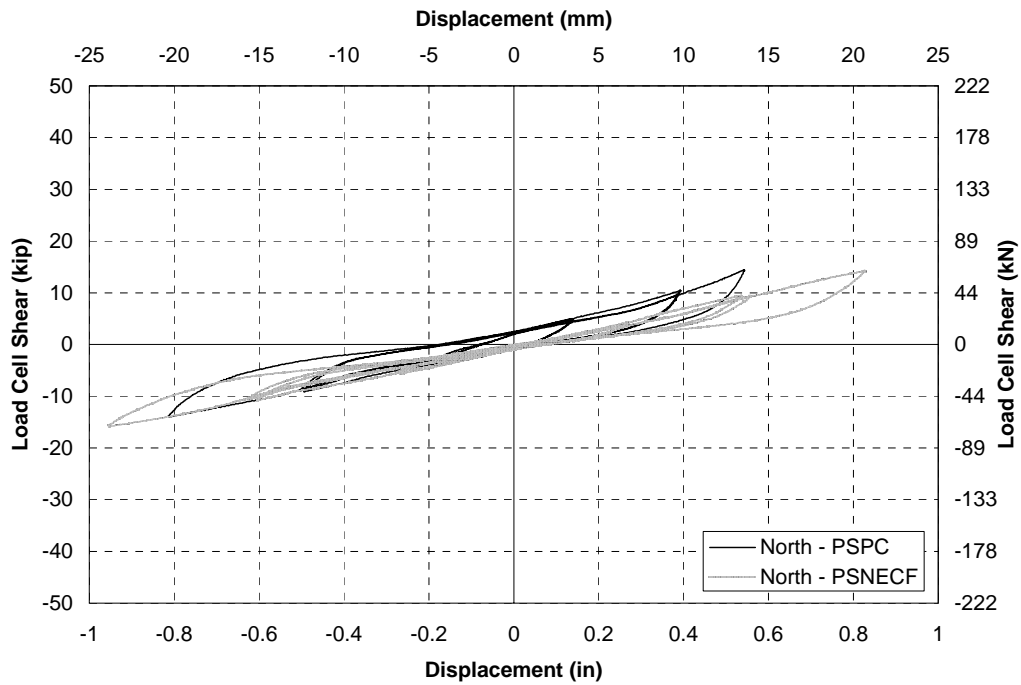


**FIGURE 5-9 RSPC, RSNECF - Comparative end hysteresis loops at north end**

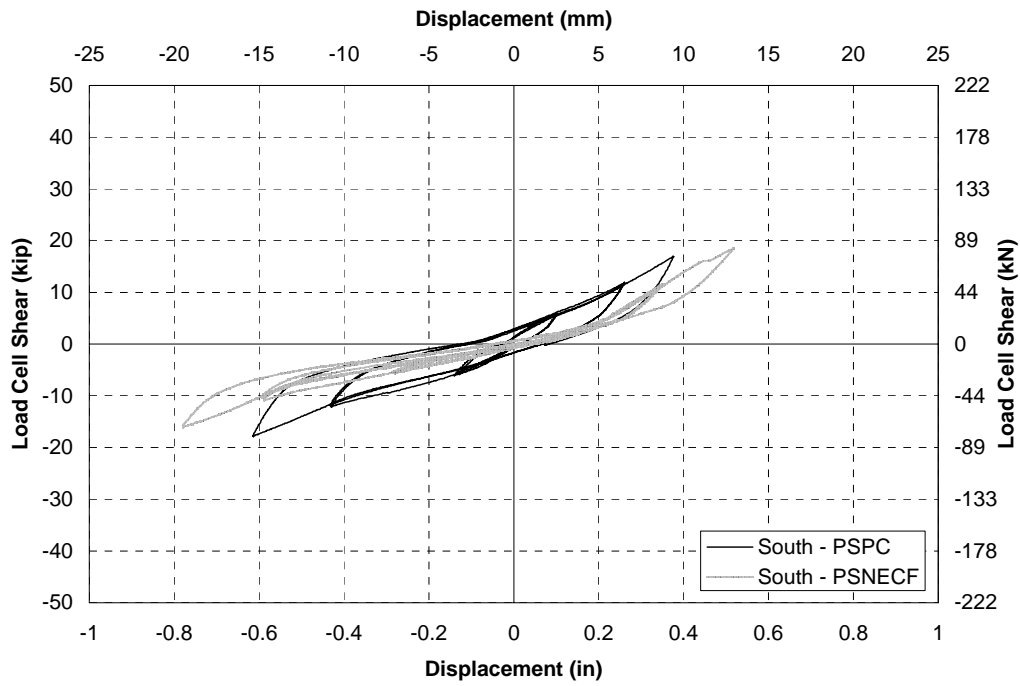


**FIGURE 5-10 RSPC, RSNECF - Comparative end hysteresis loops at south end**

**TABLE 5-2 Effective Elastic Contribution of Different Components to Transverse Stiffness for Heavy X-Brace Cross Frames**

Component	North End		South End	
	Stiffness (kN/mm)	Contribution (%)	Stiffness (kN/mm)	Contribution (%)
Diagonal Members	30	76%	34	75%
Top and Bottom Chords	7	17%	8	18%
Intermediate Cross Frames	1	1%	1	1%
Web Stiffeners, Bearings and Shear Studs	2	5%	3	6%
Total	39	100%	45	100%

**TABLE 5-3 Effective Elastic Contribution of Different Components to Transverse Stiffness for Light X-Brace Cross Frames**

Component	North End		South End	
	Stiffness (kN/mm)	Contribution (%)	Stiffness (kN/mm)	Contribution (%)
Diagonal Members	22	88%	33	88%
Top and Bottom Chords	0	1%	1	3%
Intermediate Cross Frames	1	2%	1	2%
Web Stiffeners, Bearings and Shear Studs	2	8%	3	7%
Total	24	100%	38	100%

welded connections. The stiffness of the pinned top and bottom chords was considerably less than the stiffness of the previous top and bottom chords. As a result the contribution of these dropped to between 1% and 3% for the two ends.



## SECTION 6

### IMPACT OF GIRDERS ON TRANSVERSE RESPONSE OF THE END CROSS FRAMES

#### 6.1 Introduction

In order for the end cross frames to deform when designed to be ductile, there needs to be some localized deformation at the ends of the girders. In the bridge model this deformation was effectively allowed by torsion in the girders between the end and first intermediate cross frames. The I-girders alone, being open sections, were torsionally flexible and therefore enabled this deformation relatively freely. However, the torsion was resisted by the shear studs and bearings depending on the rotational stiffness and strength that these components provided. Bending of the bearing stiffeners at the end cross frame location is an alternative method for allowing the transverse girder deformation. These factors were all considered in a model of the end of the girder, as described below.

#### 6.2 Transverse Stiffness of the End of the Girder

##### 6.2.1 Elements in the Model

The lateral deformation of a girder at the end is described by the model shown in Figure 6-1. A translational spring was used to model the torsional stiffness of the girder along a length between the end cross frame and the first intermediate cross frame. The web stiffeners were modeled using a beam element with stiffness,  $EI$ , representing the stiffness of the stiffened web. Rotational springs were used to model the bearings at the base of the girder and the shear studs on top of the girder.

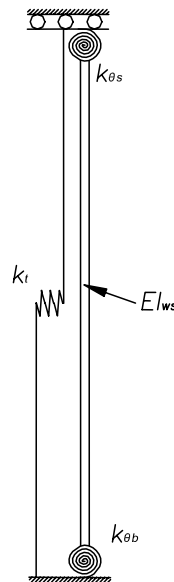


**FIGURE 6-1 Model of end of typical girder**

## 6.2.2 Torsional Properties of the Girder

In order to study the torsional deformation of the girders it was first assumed that the overall flexural stiffness of the superstructure was rigid for transverse loading. It was also assumed that at the first intermediate cross frame, the torsion of the girder about its longitudinal axis was negligible, due to restraint provided by the cross frame. Therefore along the span, between the first intermediate cross frames at each end, the superstructure was assumed to translate as a rigid body, although some localized girder rotations about their vertical axes were allowed.

The length of a girder between the end cross frame and first intermediate cross frame is shown in Figure 6-2a. It was assumed to be fixed to prevent torsional rotation and warping at the first intermediate cross frame. Consequently, the rotation of the girder about its longitudinal axis for pure torsion of the girder,  $\theta_g$ , at its free end is shown in Figure 6-2b. This shows that the translation at the end of the girder at the top flange was equal to  $\Delta_t$  and at the intermediate cross frame was equal to half of this value. The equation to describe the torsion of a cantilever I-section with a fixed end is (Brockenbrough, 1968):

$$\theta_g = \frac{T_g a}{J_g G} \left( \frac{L_1}{a} - \tanh\left(\frac{L_1}{a}\right) \right) \quad \dots 6.1$$

where:  $T_g$  is the torque applied to the end of the girder;  $G$  is the shear modulus of the steel;  $L_1$  is the length of the girder between the end cross frame and first intermediate cross frame;  $J_g$  is the torsional constant defined in Equation 6.2, and;  $a$  is defined in Equation 6.3, giving:

$$J_g = \sum \left( \frac{bt^3}{3} - 0.21t^4 \right) \quad \dots 6.2$$

where:  $b$  and  $t$  are the width and thickness of the plates in the built-up girder, and:

$$a = \frac{d_{gf}}{2} \sqrt{\frac{EI_{gy}}{J_g G}} \quad \dots 6.3$$

where:  $I_{gy}$  is the moment of inertia for the girder about its weak axis.

Equation 6.1 includes the effect of warping. Without consideration of warping the tanh term would be omitted and the equation would simplify to the more familiar form for the torsional rotation of a circular member. However warping was shown to dominate the response of the girder and therefore should be considered.

As an aside, the above comparison demonstrates the reason why the effective torsional moment of inertia for the entire superstructure was larger than calculated torsional moment of inertia for the section despite cracking and slippage between the deck slab and the girders. The simplified model of the superstructure uses elements which neglect warping in the section. The inclusion of

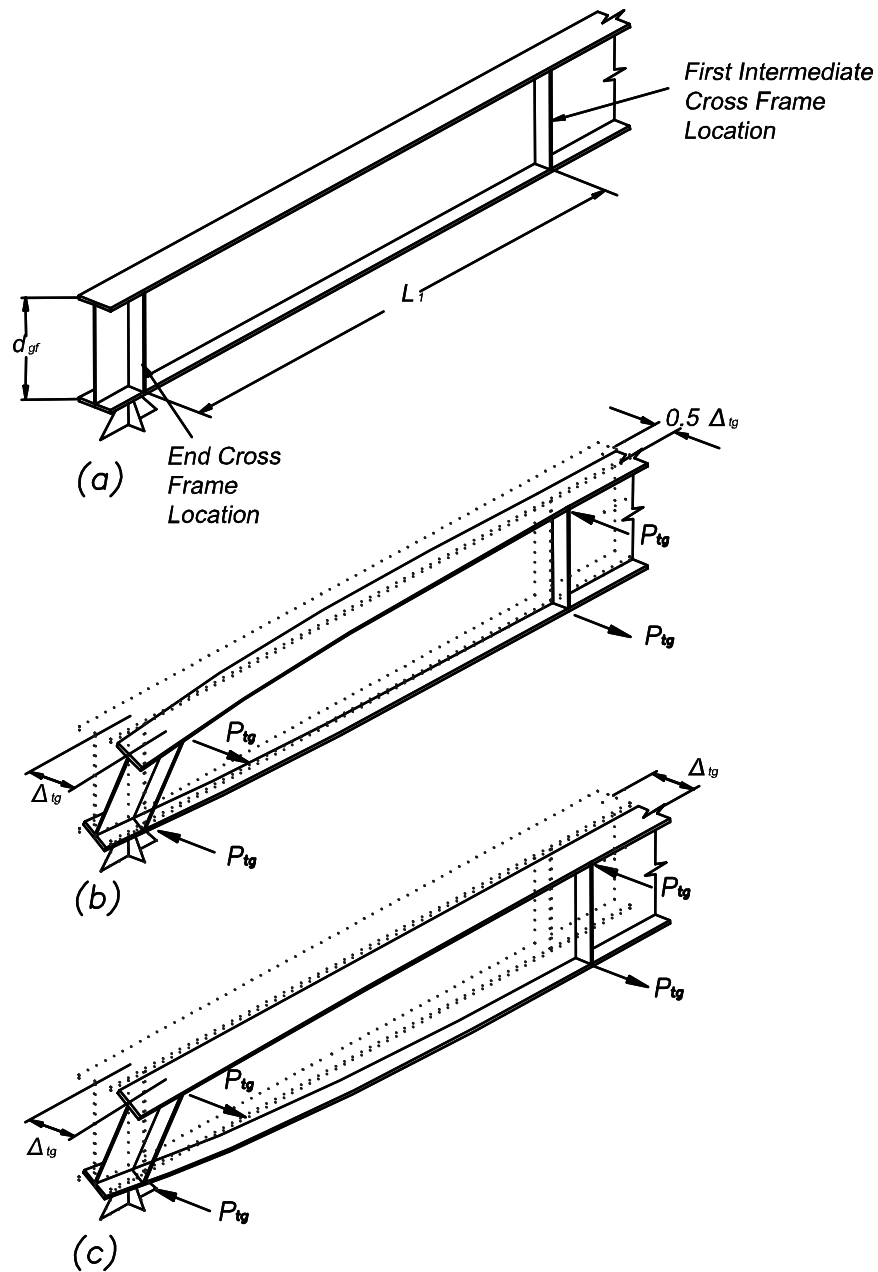


**FIGURE 6-2 Torsional girder deformations**

warping is shown to increase the torsional stiffness of a section. Therefore amplifying the torsional moment of inertia has the same overall effect as including warping in the analysis.

From Equation 6.1 the torsional stiffness of the girder over the length between the end and first intermediate cross frames,  $k_{0g}$ , is given by:

$$k_{\theta g} = \frac{J_g G}{a} \frac{1}{\left(\frac{L_1}{a} - \tanh\left(\frac{L_1}{a}\right)\right)} \quad \dots 6.4$$

The torsional stiffness can be expressed in terms of a transverse stiffness of a shear spring between the top and bottom flanges of the girder. The transverse relative displacements of the top and bottom flanges,  $\Delta_t$ , at the end of the girder due to torsion is defined as:

$$\Delta_g = \theta_g d_{gf} \quad \dots 6.5$$

and the force couple,  $F_{tg}$ , applied at the top and bottom flanges to create the torque,  $T_g$ , is:

$$F_{tg} = T_g d_{gf} \quad \dots 6.6$$

where:  $d_{gf}$  is the depth of the girder between the centre of the flanges (Fig. 6-2a). Therefore the stiffness of the equivalent horizontal spring to model the girder's torsional stiffness,  $k_t$ , as shown in Figure 6-1, is:

$$k_t = \frac{k_{\theta g}}{d_{gf}^2} \quad \dots 6.7$$

For pure torsional deformation, as shown in Figure 6-2b, there are equal and opposite deformations in the top and bottom flanges. In reality, assuming a rigid superstructure stiffness, the top flange had an equal translation as the cross section at the intermediate cross frame location, as illustrated in Figure 6-2c. This was allowed by some rotation of the girder about its vertical axis at the intermediate cross frame and some flexure in the flanges. Parametric studies to follow show that the flexure had minimal effect on the stiffness and Equation 6.7 can appropriately model the stiffness at the end of a girder. The transverse stiffness of the end of each of the girders in the bridge model, based on Equation 6.7 for a length of 2900 mm between the end and intermediate cross frames, was equal to 0.210 kN/mm.

In order to test the validity of the calculations presented above, a finite element model was constructed, shown in its deformed shape in Figure 6-3. The steel girder was modeled using a series of shell elements allowing for both membrane and plate action. The dimensions and thickness of the shell elements were specified as the actual values for the web and flanges respectively. The mesh was finer at the ends of the bridge where the maximum deformations were concentrated. Web and bearing stiffeners were modeled as shell elements at the appropriate locations.

The girder segment from the bridge model was modeled between the end and midspan of the girder, taking advantage of symmetry at the midspan. Web stiffeners were modeled on both sides of the web at cross frame locations and on one side of the web at intermediate locations, as in the bridge model. It was assumed that the top flange translated equally along its length but was allowed to rotate freely about its longitudinal axis. The bottom flange was fixed to translate at the



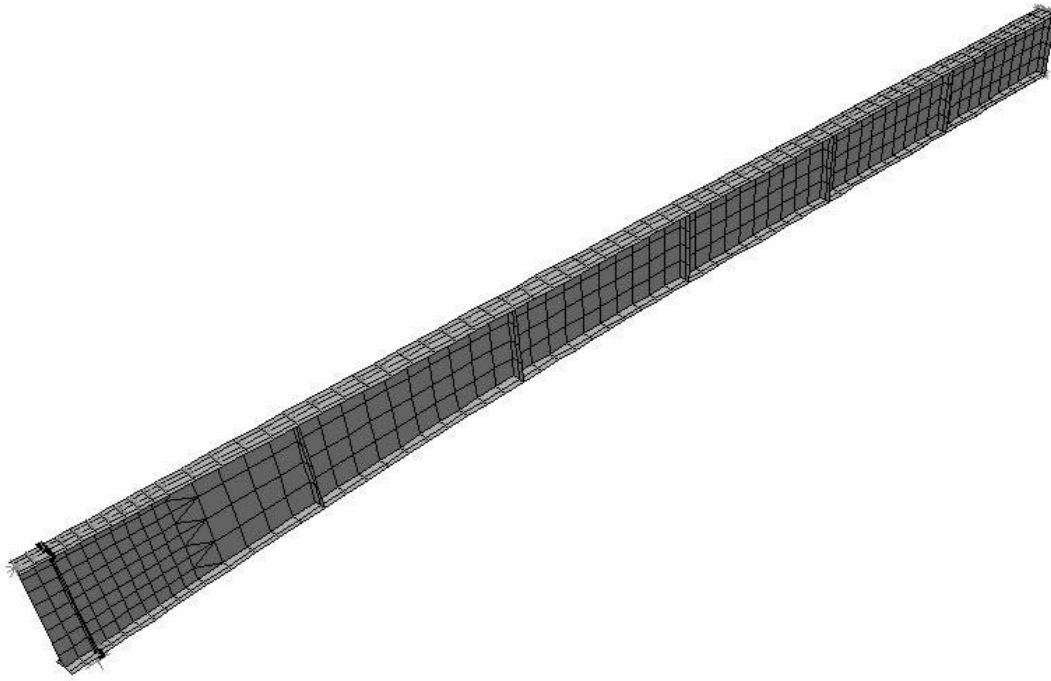


**FIGURE 6-3 Deformed finite element model of end girder segment for bridge model**

intermediate cross frame locations with a displacement equal to the top flange displacement. The bottom flange displacement was equal to zero at the end cross frame location and the resulting stiffness of the girder, comparing the base shear with the deflection of the top flange, was equal to 0.217 kN/mm. The difference between the stiffness calculated from the finite element model and that from Equation 6.7 was only 3%.

Parametric studies were performed in which the geometry of the girder was changed, spacing of the cross frames was varied and number of web stiffeners was varied. A summary of the different girder configurations and the resulting end stiffness, calculated using both Equation 6.7 and from the finite element model, is given in Table 6-1. The transverse girder stiffness for each of the different configurations using Equation 6.7, compares well to that calculated from the finite element model. With one exception the stiffness from the finite element model was marginally but consistently higher than that from the equation. The one factor which affected the stiffness of the girder that was not accounted for in Equation 6.7 was the stiffness of the web stiffeners. The web stiffeners partially restrained the free end from warping thereby increasing the torsional stiffness. With no web stiffeners the stiffness of the finite element model was slightly less than that calculated stiffness. Consistently higher stiffness in the finite element model can therefore be attributed to the web stiffeners. Stiffeners of practical dimensions as in the parametric study result no more than a 10% difference between the estimated stiffness using Equation 6.7 and that calculated from the finite element model.

**TABLE 6-1 Parametric Study on Transverse Stiffness of Simply Supported Girder**

Configuration	$L_s$ (mm)	$d_{gf}$ (mm)	$t_f$ (mm)	$b_f$ (mm)	$t_w$ (mm)	$t_{ws}$ (mm)	$L_1$ (mm)	$n_{cf}$	$n_{ws}$	$K_g$ (kN/mm)	$K_{gFE}$ (kN/mm)
Bridge Model As Built	18000	591	19	184	10	10	2900	7	13	0.210	0.217
Depth of Girders	18000	295	19	184	10	10	2900	7	13	0.435	0.448
	18000	1181	19	184	10	10	2900	7	13	0.148	0.155
Thickness of Flanges	18000	591	10	184	10	10	2900	7	13	0.086	0.091
	18000	591	38	184	10	10	2900	7	13	0.788	0.816
Width of Flanges	18000	591	19	92	10	10	2900	7	13	0.063	0.068
	18000	591	19	368	10	10	2900	7	13	1.145	1.180
Thickness of Web	18000	591	19	184	5	10	2900	7	13	0.196	0.202
	18000	591	19	184	19	10	2900	7	13	0.314	0.326
Thickness of Web Stiffeners	18000	591	19	184	10	0	2900	7	13	0.210	0.202
	18000	591	19	184	10	5	2900	7	13	0.210	0.214
	18000	591	19	184	10	19	2900	7	13	0.210	0.234
Number of Cross Frames	18000	591	19	184	10	10	1370	13	13	1.337	1.349
	18000	591	19	184	10	10	5940	4	13	0.031	0.033
Number of Web Stiffeners	18000	591	19	184	10	10	2900	7	7	0.210	0.216
	18000	591	19	184	10	10	2900	7	25	0.210	0.219

### 6.2.3 Rotational Bearing Stiffness

A further spring,  $k_{\theta b}$ , is used to model the rotational bearing stiffness (Fig. 6-1). This stiffness can be calculated for different types of bearings or may be provided by the manufacturer of the bearings. For the laminated rubber bearings used for reversed static experiments on the bridge model the rotational stiffness of the bearings was estimated to be 473 kNm about the longitudinal axis. For the lead rubber bearings the rotational stiffness was estimated to be 118 kNm. Further discussion associated with the properties and response of the bearings is presented in Chapter 7.

### 6.2.4 Bearing and Web Stiffeners

The flexural stiffness of the bearing stiffeners used to attach the end cross frames to the girders can have a considerable impact on the transverse stiffness of the girders. Their impact is particularly apparent when the shear studs provide a large rotational stiffness at the top of the girder or the bearings have a high rotational stiffness. Zahrai and Bruneau (1999) used stiffeners with a minimum possible width in order to decrease the contribution of the girder stiffness in the behavior of ductile end diaphragms. The equivalent moment of inertia,  $I_{ws}$ , for the model of the girder end region in Figure 6-1 is based on the dimensions of the stiffeners, and is defined as:

$$I_{ws} = \frac{b_{ws}^3 t_{ws}}{12} \quad \dots 6.8$$

where:  $b_{ws}$  is the combined width of the stiffeners on each side of the web including the web thickness, and;  $t_{ws}$  is the thickness of the stiffeners.

### 6.2.5 Shear Stud Stiffness

It is assumed that the top chord of the cross frames, when composite with the deck slab, causes the top flange of the girders to have an equal translation to the deck slab. Although there is no relative translation, the girder is able to rotate relative to the deck slab. The rotation of the girder is resisted by the shear studs connecting the top flange to the reinforced concrete deck slab. This effect was modeled using a rotational spring on top of the girder. The rotational spring, with stiffness,  $k_{\theta s}$ , as shown in Figure 6-1, was used to model the effect of those studs on top of the bearing stiffeners as well as the torsional stiffness of the top flange of the girder.

Assuming the failure mode of the shear studs is due to deformation in the steel cross section of the stud and not due to concrete cracking, the deformation mechanism for the studs can be assumed to be as shown in Figure 6-4. The deformation consists of a rotational component as well as an axial component. The resulting stiffness for the row of studs located directly above the bearing stiffener,  $k_{\theta s1}$ , can be described by:

$$k_{\theta s1} = \frac{EA_s}{L_s} \left( \sum_{i=1}^{n_{sd}} r_i^2 \right) + \frac{n_s 4EI_s}{L_s} \quad \dots 6.9$$

where:  $E$  is the elastic modulus of the shear studs;  $A_{sc}$  is the cross sectional area of each shear stud;  $L_{sc}$  is the clear length of the shear studs (Fig. 6-4);  $r_i$  is the distance from the centroid of the compression force (near the edge of the flange) to the location of each stud (comparable to  $d-a/2$  for a reinforced concrete beam (ACI, 2002));  $n_{sc}$  is the number of studs in each transverse row on a girder, and;  $I_{sc}$  is the moment of inertia for each stud. It is assumed in this model that the deck slab does not rotate about the longitudinal axis of the bridge, restrained by the top chord of the cross frame.

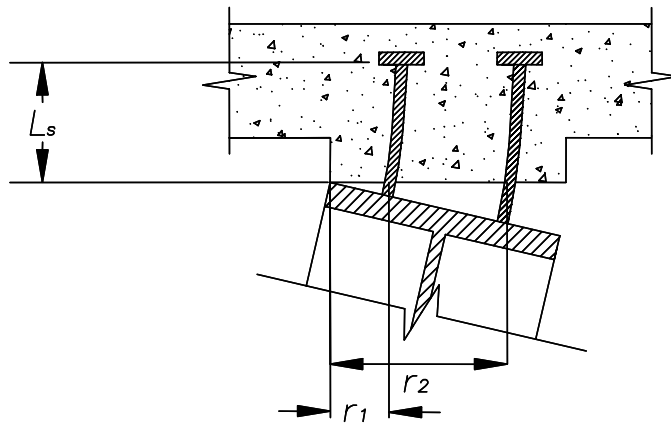


FIGURE 6-4 Shear stud deformations

As the top flange of the girder is relatively flexible for torsion, for the next row of studs placed at some distance from the bearing stiffener, the rotational stiffness at the top of the girder becomes dependent on the torsional stiffness of the top flange between the location of the bearing stiffener and location of the row of studs on top of the girder. Therefore  $k_{\theta s2}$  is given by:

$$k_{\theta s2} = \frac{GJ_f}{l_s} \quad \dots 6.10$$

where:  $G$  is the shear modulus of the top flange;  $J_f$  is the torsional moment of inertia for the top flange;  $l_s$  is the distance between the stiffener and the next row of shear studs along the girder. This formulation assumes that the rotational stiffness of a row of studs is notably larger than the torsional stiffness of top flange between the stiffener and the next row of studs. This should be satisfied for most configurations where studs have been removed from near the ends of the girders in order to accommodate torsional rotations of the girders and allow large displacements in the ductile end cross frames. The equivalent spring located at the girder support (at the bearing stiffener location),  $k_{\theta s}$ , (Fig. 6-1) is a combination of the two stiffnesses from Equations 6.9 and 6.10, although if studs are omitted from near the ends of the girders then only the latter will contribute. The length over which no shear studs are placed on the top flange can be determined by the allowable stresses in the top flange as will be discussed.

### 6.2.6 Influence of Different Components

The effect of the different components can be incorporated into a structural model with individual rotational strings to model the shear studs and bearings, transverse springs to model the transverse girder stiffness due to torsion and beam elements to model the bearing stiffeners. Each of these elements was incorporated into a finite element model described in Chapter 8. However, numerically the different components can also be combined using a matrix formulation to give an effective transverse girder stiffness. The matrix formulation for the model of the end region is shown the Figure 6-1, with appropriate boundary conditions, and is given by:

$$\begin{bmatrix} F_{bg} \\ F_{tg} \\ 0 \\ 0 \end{bmatrix} = \begin{bmatrix} \frac{12EI_{ws}}{d_{gf}^3} & \frac{-12EI_{ws}}{d_{gf}^3} & \frac{6EI_{ws}}{d_{gf}^2} & \frac{6EI_{ws}}{d_{gf}^2} \\ \frac{-12EI_{ws}}{d_{gf}^3} & \frac{12EI_{ws}}{d_{gf}^3} + k_t & \frac{-6EI_{ws}}{d_{gf}^2} & \frac{-6EI_{ws}}{d_{gf}^2} \\ \frac{6EI_{ws}}{d_{gf}^2} & \frac{-6EI_{ws}}{d_{gf}^2} & \frac{4EI_{ws}}{d_{gf}} + k_{\theta b} & \frac{2EI_{ws}}{d_{gf}} \\ \frac{6EI_{ws}}{d_{gf}^2} & \frac{-6EI_{ws}}{d_{gf}^2} & \frac{2EI_{ws}}{d_{gf}} & \frac{4EI_{ws}}{d_{gf}} + k_{\theta s} \end{bmatrix} \begin{bmatrix} 0 \\ \Delta_g \\ \theta_b \\ \theta_s \end{bmatrix} \quad \dots 6.11$$

where:  $F_{bg}$  is the shear at the base of the girder;  $F_{tg}$  is the known externally applied shear at the top of the girder;  $\Delta_g$  is the transverse displacement at the top of the girder;  $\theta_b$  is the rotation at the base of the girder, and;  $\theta_s$  is the rotation at the top of the girder. It is assumed that there are no externally applied bending moments, except those from the rotational springs which were incorporated into the stiffness matrix.

An equivalent girder stiffness incorporating all the components which contribute to the girder stiffness, including torsional girder stiffness, shear studs, and also bearings and web stiffeners can be found by static condensation of the stiffness matrix of Equation 6.11. The resulting equivalent girder stiffness,  $K_g$ , is given by:

$$K_g = k_t + \frac{12EI_{ws}}{d_{gf}^3}(1 - \rho) \quad \dots 6.12$$

where:  $k_t$  was defined in Equation 6.7, and  $\rho$  is equal to:

$$\rho = \frac{\frac{12EI_{ws}}{d_{gf}} + 3(k_{\theta b} + k_{\theta s})}{\left(\frac{4}{d_{gf}} + \frac{k_{\theta b}}{EI_{ws}}\right)\left(\frac{4}{d_{gf}} + \frac{k_{\theta s}}{EI_{ws}}\right)EI_{ws}d_{gf} - \frac{4EI_{ws}}{d_{gf}}} \quad \dots 6.13$$

where:  $k_{\theta b}$ ,  $k_{\theta s}$  and other variables were defined in previous equations. A few cases for  $\rho$  can be considered to demonstrate its validity. If the springs,  $k_{\theta s}$  and  $k_{\theta b}$  have a stiffness equal to zero then  $\rho$  is equal to 1 and the equivalent girder stiffness in Equation 6.12 is equal to only the torsional stiffness of the girder,  $k_t$ . If  $k_{\theta b}$  approaches a large value and  $k_{\theta s}$  is equal to zero, or vice versa, then  $\rho$  is equal to  $3/4$  and the equivalent girder stiffness is equal to  $k_t$  plus  $3EI_{ws}/d_{gf}^3$ . This is equivalent to web stiffeners pinned at one end and fixed at the other end. If both  $k_{\theta s}$  and  $k_{\theta b}$  approach a large value then  $\rho$  is equal to zero, for web stiffeners fixed at both ends. The condensed stiffness does not include shear deformations in the stiffeners, however these will be shown to have minimal effect.

In order to test the appropriateness of the above equations in modeling of the end of the girder a series of parametric studies were performed, as shown in Table 6-2. The parametric studies began with the finite element model of the girder in the bridge model described in Section 6.2.2. The accuracy of the shear stud modeling was investigated by considering different shear stud configurations and top flange thicknesses. Elements were added to the finite element model to model each shear stud connecting the girder to a rigidly assumed deck slab. Rigid elements were also added across the top and bottom flanges of the girder at the web stiffener locations to ensure that sections through the stiffeners remained plane. The web stiffeners were modeled using shell elements and a rotational spring to model the rotational bearing stiffness. The resulting equivalent transverse girder stiffness for the bridge model assuming no shear studs were damaged was

**TABLE 6-2 Parametric Study of Transverse Stiffness and Bending Moments at the End of a Girder**

Parameter	No.	$L_s$ (mm)	$L_1$ (mm)	$k_t$ (kN/mm)	$k_s$ (kN-m)	$k_b$ (kN-m)	$t_{ws}$ (mm)	$b_{ws}$ (mm)	$EI_{ws}$ (kN-m <sup>2</sup> )	$K_g^1$ (kN/mm)	$K_{gFE}^2$ (kN/mm)	$M_{fb}^1$ (kN-m)	$M_{fbFE}^2$ (kN-m)	$f_{uvft}^1$ (MPa)	$f_{uvftFE}^2$ (MPa)
Bridge Model As Built before Stud Damage	1	0	2900	0.210	3469	473	9.53	184	990	7.91	7.96	10.1	10.2	-	-
Girder Only	2	-	2900	0.210	0	0	9.53	184	990	0.21	0.22	10.1	10.8	-	-
Thickness of Flanges	3	0	2900	0.086	0	0	9.53	184	990	0.09	0.09	4.80	4.31	-	-
	4	0	2900	0.788	0	0	9.53	184	990	0.79	0.81	23.9	26.9	-	-
Removed	5	457	2900	0.210	67	473	9.53	184	990	1.66	1.79	10.1	10.1	2.90	3.19
Shear Studs, (Elastomeric Bearings)	6	914	2900	0.210	33	473	9.53	184	990	1.55	1.60	10.1	10.2	1.45	1.54
	7	1372	2900	0.210	22	473	9.53	184	990	1.52	1.52	10.1	10.8	0.97	0.96
Removed	8	1829	2900	0.210	17	473	9.53	184	990	1.50	1.48	10.1	10.8	0.72	0.71
	9	914	2900	0.210	33	118	9.53	184	990	0.64	0.69	10.1	10.6	1.45	1.50
Shear Studs, (LRBs)	10	1372	2900	0.210	22	118	9.53	184	990	0.60	0.61	10.1	10.8	0.97	0.93
	11	1829	2900	0.210	17	118	9.53	184	990	0.59	0.58	10.1	11.1	0.72	0.71
Intermediate Stiffener	12	914	2900	0.210	33	473	9.53	184	990	1.55	1.92	10.1	18.6	-	-
Intermediate Stiffener with Studs Above Removed	13	914	2900	0.210	33	473	9.53	184	990	1.55	1.65	10.1	9.4	-	-
Length to Intermediate Cross Frame	14	0	1370	1.337	3469	473	9.53	184	990	9.04	11.56	64.0	41.6	-	-
	15	0	5940	0.056	3469	473	9.53	184	990	7.76	7.91	2.67	3.96	-	-
Bearings	16	0	2900	0.210	3469	0	9.53	184	990	6.10	6.24	10.1	10.3	-	-
	17	0	2900	0.210	3469	1.E+07	9.53	184	990	29.37	26.86	10.1	9.3	-	-
Web Stiffener Thickness	18	0	2900	0.210	3469	473	4.76	184	496	6.34	6.26	10.1	10.2	-	-
	19	0	2900	0.210	3469	473	19.05	184	1982	9.26	9.47	10.1	10.5	-	-
Web Stiffener Width	20	0	2900	0.210	3469	473	9.53	106	188	4.24	4.20	10.1	10.2	-	-

Notes:

1. From analytical model
2. From finite element model

calculated to be 7.91 kN/mm using the above equations. From the finite element model the corresponding stiffness was equal to 7.96 kN/mm and compares well (Table 6-2 - No. 1).

The properties of the girder flanges, bearings, stiffeners and shears studs were varied to determine the impact of each. The calculated stiffness of the girder alone with no shear studs or bearings (No. 2) compared to within 3% of that from the finite element model. The analytical model was able to capture an increase and decrease in the flange thickness (No. 3 and 4 respectively) and compared to within 5% of the finite element model with these variations. The effect of removing of rows of shear studs from the bridge model (No. 5 to 11), was a considerable reduction in transverse stiffness. As the studs were removed the comparison between the analytical and finite element model remained within 8% where there were no intermediate web stiffeners. Upon addition of an intermediate stiffener between the end cross frame and first intermediate cross frame (No. 12) the stiffness was shown to increase by 20 percent. However, when the shear studs directly above the intermediate stiffener were removed (No. 13) the stiffness increased by only 3% indicating that the intermediate stiffener only appreciably affected the stiffness of the girder when it interacted with shear studs directly above it. An analytical procedure which captures the impact of the studs and intermediate stiffener was considered, however in most situations there is little need for this additional complication. When the length of the girder between the end cross frame and first intermediate cross frame was altered (No. 14 and 15) the models generally compared well, except for the shortest of lengths where the analytical model under-predicted the stiffness in the girder by 22 percent. The under prediction was as a result of the pin about the vertical axis and full warping restraint assumed for the girder at the intermediate cross frame in the analytical model, although the accuracy is considered acceptable for practical cases. The bearings and shears studs were varied between a zero and large stiffness with good comparisons observed between the analytical and finite element models (No. 16 and 17). The web stiffeners were assumed to have a thickness between two times and one half of the actual thickness, and a width of one half the actual width of the web stiffeners in the bridge model (No. 18 to 20). The change in stiffness from these modifications was captured accurately by the model.

Minimizing the transverse girder stiffness is considered beneficial in order to minimize the post-yield stiffness in ductile end cross frames making them effective ductile elements. Comparing the responses of girders in different configurations shows that the effective girder stiffness was lowest when shear studs were removed from the ends of the bridge. The stiffness was also reduced when the stiffeners were trimmed to half of their width, although the reduction was not as great. The stiffness was greatest when the bearings were assumed to be rigid and there was no reduction in stiffener or shear stud stiffness. Differences between the analytical and finite element model are relatively small when compared to the amount of fluctuation in stiffness (two orders of magnitude) between the different configurations.

### **6.2.7 Comparison with Measured Bridge Model Stiffness**

Some damage to the studs was observed in the bridge model during reversed static experiments with more damage observed at the north end. This was considered to make some of the studs near the ends ineffective. The stiffnesses of the different models in Table 6-2, multiplied by two for two girders, were considered. Based on the stiffnesses from the finite element models with one, two, three and four studs removed the stiffness of two girders would be 3.58, 3.20, 3.04 and 2.96 kN/mm. The finite element models were close to the observed stiffness in the bridge model with

two studs assumed to be ineffective at the south end and three studs at the north end (Table 5-1). This is consistent with observed distress to the deck slab around the studs.

Based on the shake table experiment (STNECF), with more rotationally flexible bearings, the stiffness of the north and south ends with no end cross frames was reduced. For this experiment two rows of studs had been removed by coring through the deck slab around the studs, at the north end damage from past experiments was observed in both the third and fourth rows, therefore, it was possible that these studs should also be considered ineffective. For removal of two, three and four rows of studs respectively from the finite element model the calculated stiffnesses were 1.38, 1.22 and 1.16 kN/mm for two girders. The calculated stiffnesses compare well with the measured stiffnesses assuming three to four rows of shear studs were ineffective at the north and south ends.

### 6.3 Strength Limits of Various Girder Components

#### 6.3.1 Overview

Calculation of the girder stiffness allows the effect of the girders on inelastic properties of a ductile end cross frames to be evaluated. Although, it is also important to understand the limit states of the various components. In the case of critical gravity supporting members such as the girders and bearings it is important that they are not damaged during an earthquake. For other components such as shear studs and web stiffeners some damage may be acceptable.

As ductile cross frames will be designed for a maximum displacement in response to a given level of earthquake, the capacity of each component needs to be evaluated in terms of the maximum displacement. For a given transverse displacement at the end of a girder, the capacity of the bearing stiffeners needs to be compared to maximum bending moment in the stiffeners. Similarly, the capacity of shear studs needs to be related to the rotation at the top of the web stiffeners and the rotational bearing capacity needs to be related to the rotation at the base of the web stiffeners. Each of the components is considered below.

#### 6.3.2 Girders

The maximum stresses in a cantilever I-beam subjected to torsion are found in the top and bottom flanges at the support location. Therefore at the end of a bridge girder between the end cross frame and first intermediate cross frame, the maximum stresses are found in the flanges at the first intermediate cross frame location. For pure torsion the maximum bending moment in each flange of a girder,  $M_f$ , is given by (Brockenbrough, 1968):

$$M_f = \frac{T_g a}{d_{gf}} \left( \tanh \frac{L_1}{a} \right) \quad \dots 6.14$$

In terms of the stiffness calculated earlier, this equation can be used to approximate the maximum bending moment in the bottom flange of the girder,  $M_{efb}$ , when the girder is deformed torsionally at an end cross frame location, giving:



$$M_{\text{efb}} = k_t a \left( \tanh \frac{L_1}{a} \right) \Delta_t \quad \dots 6.15$$

This is an approximation as the equation is based on the same assumptions used in calculating the girder stiffness with a pin about the vertical axis assumed at the first intermediate cross frame location along with full warping restraint. The bending moment in the top flange is negligible due to torsion of the girder as it is assumed to be restrained by the deck slab. The shear studs and bearings typically have minimal effect on the girder response except where there are intermediate web stiffeners that can interact with any shear studs located directly above the stiffeners.

The parametric study presented compared calculated girder bending moments for a nominal 25 mm end displacement with those estimated from finite element models (Table 6-2). Any intermediate stiffeners were omitted from the girders in the parametric studies except where specifically investigated. The bending moment from the finite element model was estimated using the average longitudinal stress at the two edges of the bottom flange at a position along the girder where the stresses were maximum. When the length of the girder between the end cross frames and first intermediate cross frames was 2900 mm, as in the actual bridge model, the bottom flange bending moment (calculated using Equation 6.15) compared well to that estimated from the finite element model (Table 6-2). The exception was in the configuration with an intermediate stiffener, where there were also shear studs directly above the stiffener which resulted in a significant increase in the maximum bending moment.

Bending moments in the bottom flange are more sensitive than girder stiffness to assumptions in the boundary conditions of the analytical model. This is demonstrated by the girders with longer and shorter lengths between the end cross frame and first intermediate cross frame. For a relatively short length (No. 14) the bending moment is overestimated by 54% compared to that in the finite element model because the assumed warping restraint at intermediate cross frame is in reality only a partial warping restraint. However, such a close spacing of cross frames leading to this inaccuracy is unlikely to be used in practice, and regardless the bending moment estimate in this case is conservative. When the length between the end and intermediate cross frame increased, the estimated bending moment became unconservative as the assumed warping restraint was more realistic meanwhile the assumed pin support that eliminated flexure in the bottom flange was less realistic. Thus flexural stresses in the flange added to torsional stresses resulting in an increased flange bending moment. While the longer length resulted in unconservative bending moment estimates the magnitude of these moments became trivial and consequently this error is inconsequential as other girder drift limitations will govern. As both the extremes described above that resulted in significant errors will not jeopardize the performance of the bridge, a more elaborate analysis to minimize the errors is not considered necessary.

In order to determine what levels of drift are acceptable, a combination of stresses due to transverse girder deformation and stresses due to gravity loading is considered. It was considered appropriate to combine the seismic actions with the effects of gravity loads using the same procedure as that described by the AASHTO specifications (AASHTO, 1998) to combine the effects of wind and gravity loads. The effective cross section of the girder required to carry gravity loads, for a level of loading associated with the earthquake load combination, can be calculated at any location along the girder. It is calculated from the maximum width of each flange required to carry the gravity loads, as illustrated in Figure 6-5. The remaining width at the

edge of each flange,  $b_{efb}$ , not required for gravity loads can be used to carry the stresses due to lateral girder deformations. The residual bending capacity of the bottom flange is given by:

$$M_{nfb} = b_{efb} t_{fb} F_y (b_{fb} - b_{efb}) \quad \dots 6.16$$

where:  $b_{fb}$  is the width of the bottom flange;  $t_{fb}$  is the thickness of the bottom flange, and;  $F_y$  is the yield strength of the bottom flange. The capacity of the flange can thus be compared to the demand from Equation 6.15 to determine the adequacy of the flange at the critical section.

The bridge model was excited in the transverse direction with no end cross frames resulting in maximum transverse displacement measured at the north end of the girders of 27 mm corresponding to a drift, calculated relative to the girder height of 4.6%. The bending moment in the bottom flange of the girder for this level of displacement is calculated at 10.9 kN-m using Equation 6.15. Based on an arbitrary effective flange width of 50% of the total flange width due to gravity load stresses the allowable bending moment, calculated using Equation 17, is 41.8 kN-m. Therefore the girder was easily adequate. Equating these bending moments, the girder could be subjected to much larger drifts of up to 17% illustrating that the girders have a theoretically large displacement capacity. Even if the elastic limits of the girder are reached, larger deformations will be possible with allowance of some localized plastic hinging. However, P-delta effects are likely to become significant for large drifts and will limit the allowable girder drifts.

### 6.3.3 Shear Studs and Top Flange

In order to facilitate rotation of the end of the girder shear studs can be omitted for some distance from the bearing stiffeners. The length of the girder over which there should be no studs can be calculated by comparing the torque in the top flange of the girder with the rotational capacity of the first row of shear studs, to ensure that no damage occurs in the studs and distress to the girder is avoided. The top flange girder stresses can then be checked to ensure that distress is also avoided in the top flange of the girder. The rotation at the top of the girder can be rigorously calculated from the matrix formulation of Equation 6.11, however this expression is long and cumbersome. Instead, the rotation can be conservatively approximated using the transverse top flange girder displacement divided by the height of girder when the stiffness of the bearing stiffeners is notably greater than the rotational stiffness of the studs and bearings. For a given rotation at the end of the girder the torque in the top flange of the girder,  $T_f$ , is given by:

$$T_f = \frac{GJ_{ft}\theta_s}{l_s} \quad \dots 6.17$$

where:  $J_{ft}$  is the torsional moment of inertia of the top flange and  $l_s$  is the distance between the bearing stiffener to which the ductile end cross frame is attached and the first row of shear studs on the girder. The torque is assumed to be resisted by the ultimate torsional resistance,  $T_{usr}$ , of a transverse row of shear studs which can be calculated by:

$$T_{usr} = P_u \sum r_i \quad \dots 6.18$$

where:  $P_u$  is the ultimate capacity of the studs calculated in accordance with AASHTO (1998), governed either by the strength of the steel section of the stud or the capacity around the studs. Equating the capacity of the studs with the torque in the flange, Equations 6.17 and 6.18 can be used to calculate a length over which to remove studs on the end of the girder, given by:

$$l_s = \frac{GJ_{ft}\theta_s}{P_u \sum r_i} \quad \dots 6.19$$

The girder stresses on the top flange of the girder should be checked to ensure that damage to the girder is prevented. If it is assumed that the top flange twists between the bearing stiffener location and the first row of shear studs the maximum shear stress in the flange,  $f_{uvft}$ , is given by (Brockenbrough, 1968):

$$f_{uvft} = \frac{Gt_{ft}\theta_s}{l_s} \quad \dots 6.20$$

where:  $t_{ft}$  is the thickness of the top flange. The parametric study investigated the calculated top flange shear stresses for those girder models where studs were omitted from different lengths near the end of the girder (Table 6-2). The calculated shear stresses in the top flange compared to within 9% of those calculated from the finite element model, taken at the midpoint of the length in which there were no studs.

The shear stress can be combined with the average normal stress due to flexure from gravity loads associated with the earthquake load case,  $f_{unft}$ , which can be calculated from the effective section for gravity loads (Fig. 6-5) by:

$$f_{unft} = \left(1 - \frac{2b_{eff}}{b_{ft}}\right) F_y \quad \dots 6.21$$

The combined stresses should be less than the strength of the flange such that:

$$\sqrt{f_{unft}^2 + 3f_{uvft}^2} \leq F_y \quad \dots 6.22$$

This is based on the Von Mises stress combination criteria and assumes a compact flange, although can be modified for a non-compact flange (AISC, 1997).

When studs are not placed near the ends of the girders or near intermediate supports of continuous girders, the top chord of the end cross frames should be connected to the deck slab with sufficient strength to carry the full transverse shear at the support, in order to allow adequate transverse load path between the deck slab and the girders. The deck slab will attempt to lift off the girder as the girder rotates which it should be allowed to do if there are no shear connectors near the ends of the girders. In order to allow this deformation the top chord of the cross frame needs to be able to accommodate the gap between the deck slab and the girders (Fig. 6-6). This can be achieved with

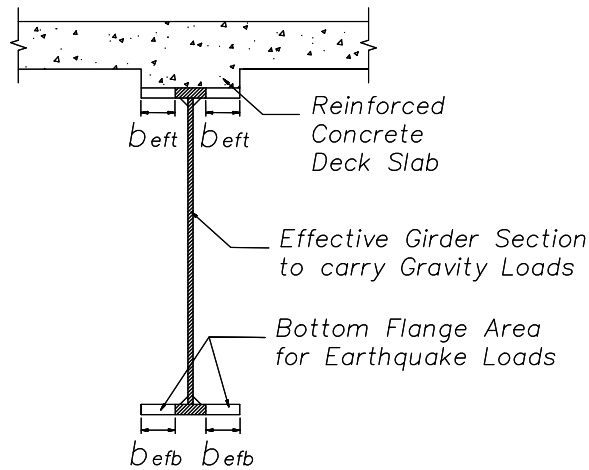


**FIGURE 6-5 Effective section required to carry gravity loads and remaining flange width for seismic forces**

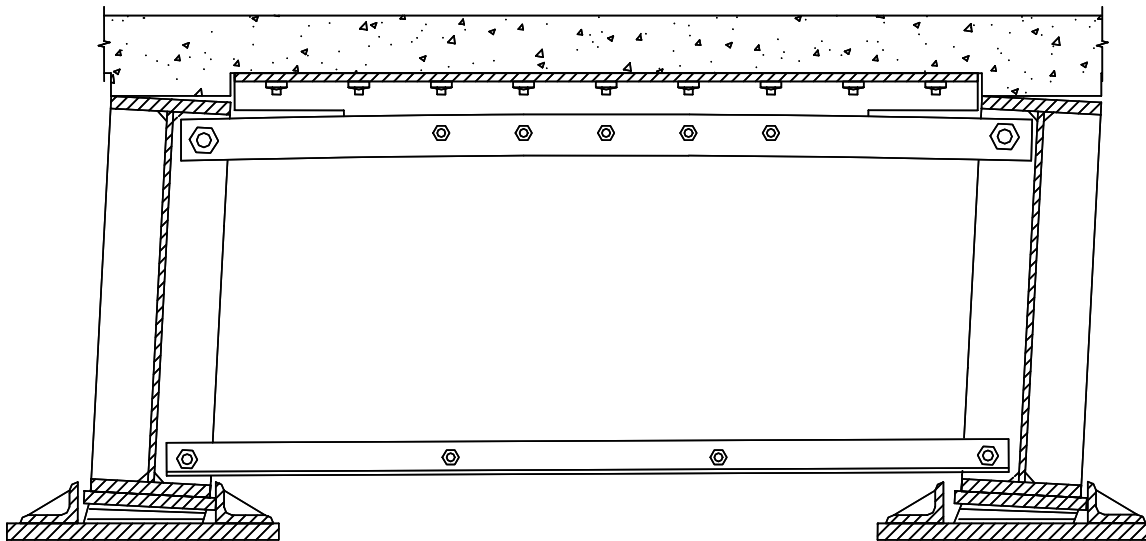


**FIGURE 6-6 Deformed end cross frame region of bridge model with gap opening between the deck slab and girders**

vertically slotted holes connecting the top chord to the bearing stiffener. Alternatively, the approach used in the bridge model was to select top chord members which were able to carry axial forces adequately without buckling, but have a relatively low flexural stiffness to allow the members to bend and accommodate the small vertical offset.

### 6.3.4 Rotational Capacity of the Bearings

The rotation at the top of the bearing can be calculated knowing the rotation at the base of the girder. The rotation at the base of the girder can be estimated in a similar manner to the rotation at the top of the girder. Comparing the resulting rotation to the rotational bearing capacity can ensure

that the bearings will not fail during an earthquake. The bearings are investigated in detail in Chapter 7.

### 6.3.5 Bearing Stiffeners

The maximum bending moments in the bearing stiffeners due to twisting of the girder can be estimated by  $k_{\theta s}\theta_s$  and  $k_{\theta b}\theta_b$  and the top and bottom of the bearing stiffeners respectively. The largest of these bending moments can be compared to the flexural capacity of the bearing stiffeners to determine whether or not these will be damaged with large displacements in the end region. For the bridge model, assuming the configuration at the north end in Experiment STNEXF with no effective studs 1830 mm from the end cross frames location along the girder, and a transverse girder displacement of 27 mm, the bending moment at the top of the girder was equal to 0.78 kNm based on the torsional stiffness of the top flange, and the bending moment at the base was equal to 5.39 kNm based on the bearing stiffness. The flexural capacity of the bearing stiffeners, equal to  $F_y Z_{ws}$  where  $Z_{ws}$  is the plastic section modulus of the stiffeners, was equal to 27.7 kNm. Therefore no damage was expected in the stiffeners at this displacement level.

Strain gages were placed at three heights on one of the bearing stiffeners at the north end of the bridge (Fig. 2-47). Using the strain gages, and converting the strains to stresses and bending moments, the resulting bending moments along the height of the stiffeners were plotted in Figure 6-7. While the uncertainty in such an analysis is recognized, as only two strain gages were used to calculate equivalent bending moments at each location, this figure shows a good correlation between the calculated and measured bending moments in the bridge model. Because the strain gages used to calculate the bending moments during STNECF were installed after completion of the reversed static experiments, no comparative bending moment was calculated for the reversed static experiments.

## 6.4 Continuous Girders

### 6.4.1 Girder Stiffness

The formulation for the transverse stiffness of a girder is described above for the end of a girder, however; in multi-span bridges a similar formulation can be developed for the intermediate supports of continuous girders. The length of a girder between two intermediate cross frames on adjacent spans is shown in Figure 6-8. If it is assumed that the support cross frame is located halfway between the intermediate cross frames and the girder is fixed to prevent warping at the intermediate cross frames, then the equation to describe the transverse stiffness of the girder at the intermediate support due to torsional deformation is given by (adapted from Brockenbrough, 1968):

$$k_{tt} = \frac{J_g G}{a d_{gf}^2} \frac{1}{\left(\frac{L_1}{2a} - \tanh\left(\frac{L_1}{2a}\right)\right)} \quad \dots 6.23$$

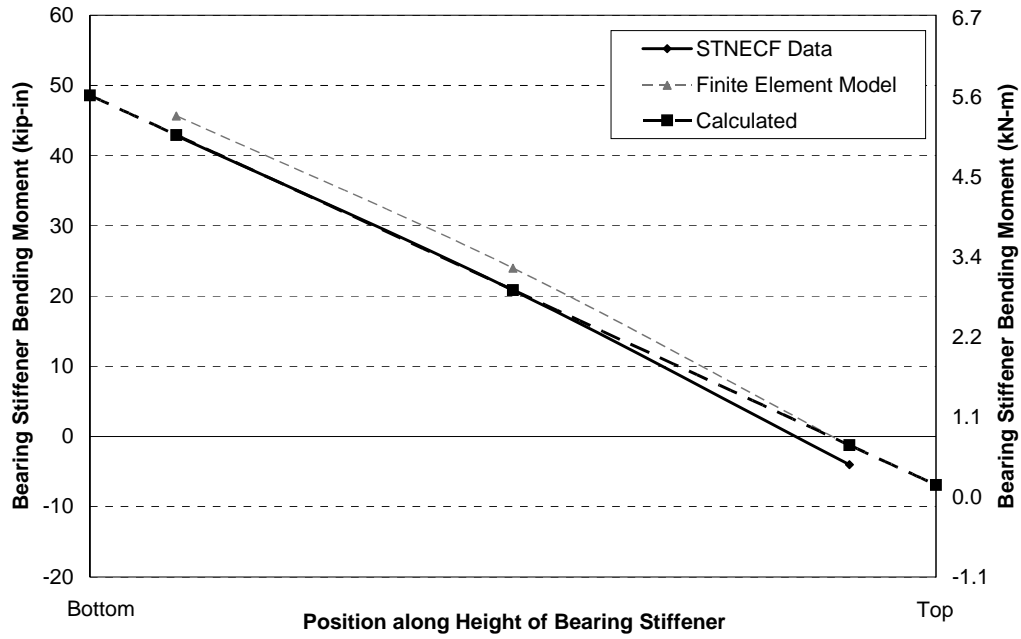


**FIGURE 6-7 Bearing stiffener bending moments**

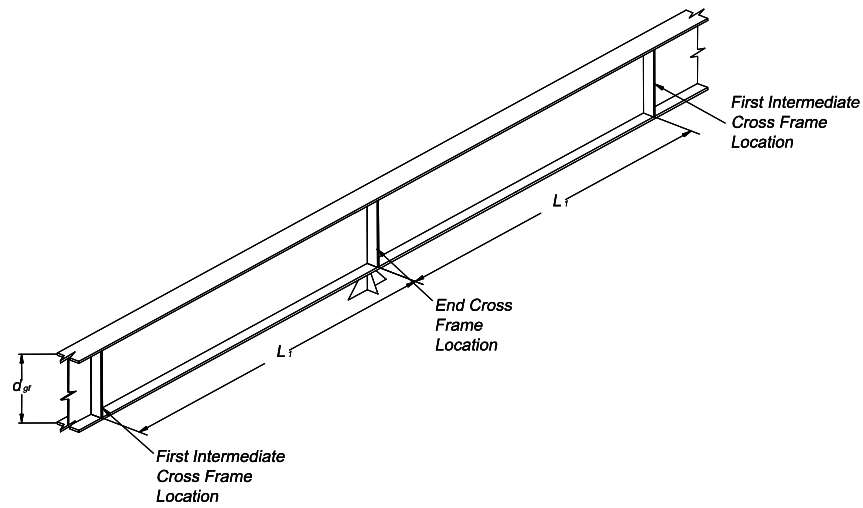


**FIGURE 6-8 Continuous bridge girder**

which is synonymous with Equation 6.7 for the end of a girder. However, due to the continuity of the girder flange, the effect of bending in the bottom flange cannot be neglected as it was for the end of the girder. The stiffness due to bending at the support of the girder is given by:

$$k_{tb} = \frac{3EI_{fb}}{L_1^2} \quad \dots 6.24$$

where:  $I_{fb}$  is the moment of inertia of the bottom flange. This equation is similar to that for the stiffness of a cantilever which is multiplied by 2 for the two adjacent spans and divided by 2 as flexure in the flange is associated with only half of the total transverse deformation due to the same reasoning as that illustrated for the end of the girder in Figure 6-2. The total transverse stiffness of the girder is given by the combination of Equations 6.23 and 6.24, giving:

$$k_t = \frac{J_g G}{a d_{gf}^2} \frac{1}{\left(\frac{L_1}{2a} - \tanh\left(\frac{L_1}{2a}\right)\right)} + \frac{3EI_{fb}}{L_1^2} \quad \dots 6.25$$

The stiffness including shear studs bearings and stiffeners is again given by Equations 6.12 and 6.13 with  $k_{\theta s}$  given by the summation of Equation 6.10, for studs located on top of the bearing stiffener, and for the next row of studs at some distance,  $l_{s1}$ , in one direction along the girder from the support cross frame location and,  $l_{s2}$ , in the other direction by:

$$k_{\theta s2} = GJ_f \left( \frac{1}{l_{s1}} + \frac{1}{l_{s2}} \right) \quad \dots 6.26$$

For the same girder as that in the bridge model, assuming 3.05 m between the end and intermediate stiffeners on each adjacent spans, the transverse stiffness was equal to 1.22 kN/mm. This is equivalent to a girder in the bridge model with a support at the mid-span of the bridge. Further parametric studies were performed with the continuous girder to calculate the overall effective transverse stiffness,  $K_g$ , including the effects of shear studs, bearings and web stiffeners. A girder with a length of 18.3 m was modeled assuming symmetric boundary conditions at each end and a support at mid-span. A parametric study for different girder configurations and the resulting transverse stiffness at the support calculated from analytical and finite element models, are given in Table 6-3. The analytical stiffness was within 10% of that calculated using the finite element models in all cases except where there were intermediate web stiffeners between the cross frames. The increase in stiffness due to the intermediate stiffeners was not captured by the analytical model, however; a parametric study shows that where there were no shear studs located directly above the intermediate stiffeners, the error was 16% or less.

#### 6.4.2 Girder Flange Bending Moments

For pure torsion the maximum bending moment in the flanges near an intermediate support of a continuous girder,  $M_f$ , which is found directly above the intermediate support is given by (Brockenbrough, 1968):

**TABLE 6-3 Parametric Study of Transverse Stiffness and Bending Moments at an Intermediate Support of a Continuous Girder**

Parameter	No.	L <sub>s</sub> (mm)	L <sub>1</sub> (mm)	k <sub>t</sub> (kN/mm)	k <sub>s</sub> (kN-m)	k <sub>b</sub> (kN-m)	t <sub>ws</sub> (mm)	b <sub>ws</sub> (mm)	EI <sub>ws</sub> (kN-m <sup>2</sup> )	K <sub>g</sub> <sup>1</sup> (kN/mm)	K <sub>gFE</sub> <sup>2</sup> (kN/mm)	M <sub>lib</sub> <sup>1</sup> (kN-m)	M <sub>libFE</sub> <sup>2</sup> (kN-m)	f <sub>uvft</sub> <sup>1</sup> (MPa)	f <sub>uvftFE</sub> <sup>2</sup> (MPa)
Bridge Model with Elastomeric Bearings	1	0	3050	1.22	3537	473	10	184	991	9.0	9.4	28.4	28.7	-	-
Girder Only	2	-	3050	1.22	0	0	10	184	991	1.22	1.18	28.4	25.2	-	-
Thickness of Flanges	3	0	3050	0.57	3537	473	10	184	991	8.35	8.58	14.2	15.0	-	-
	4	0	3050	3.15	3537	473	10	184	991	10.9	11.9	57.6	55.2	-	-
Removed Shear Studs,	5	457	3050	1.22	133	473	10	184	991	2.86	3.35	28.4	28.9	2.90	3.16
Elastomeric Bearings	6	914	3050	1.22	67	473	10	184	991	2.66	2.92	28.4	28.4	1.45	1.44
	7	1372	3050	1.22	44	473	10	184	991	2.59	2.71	28.4	27.6	0.97	0.91
	8	1829	3050	1.22	33	473	10	184	991	2.56	2.57	28.4	26.7	0.72	0.68
Removed Shear Studs, Lead Rubber Bearings	9	914	3050	1.22	67	118	10	184	991	1.74	2.01	28.4	28.3	1.45	1.40
	10	1372	3050	1.22	44	118	10	184	991	1.68	1.80	28.4	27.5	0.97	0.88
	11	1829	3050	1.22	33	118	10	184	991	1.64	1.66	28.4	26.6	0.72	0.66
Intermediate Stiffener	12	914	3050	1.22	67	473	10	184	991	2.66	5.29	28.4	51.5	-	-
Intermediate Stiffener with No Studs Above	13	914	3050	1.22	67	473	10	184	991	2.66	3.17	28.4	30.7	-	-
Length to Intermediate Cross Frame	14	0	1520	8.73	3537	473	10	184	991	16.5	16.1	89.3	93.8	-	-
Bearings	15	0	7100	0.21	3537	473	10	184	991	7.99	8.87	13.3	17.7	-	-
Web Stiffener Thickness	16	0	3050	1.22	3537	0	10	184	991	7.17	7.68	28.4	28.7	-	-
	17	0	3050	1.22	3537	1.E+07	10	184	991	30.6	29.5	28.4	30.4	-	-
Web Stiffener Width	18	0	3050	1.22	3537	473	5	184	495	7.38	7.72	28.4	28.9	-	-
	19	0	3050	1.22	3537	473	19	184	1982	10.4	11.0	28.4	29.0	-	-
	20	0	3050	1.22	3537	473	10	106	189	5.26	5.74	28.4	29.0	-	-

Notes:

1. From analytical model

2. From finite element model



$$M_f = \frac{T_g a}{2d_{gf}} \left( \tanh \frac{L_1}{2a} \right) \Delta_t \quad \dots 6.27$$

As bending in the bottom flanges adds to the torsional stresses at the support of a continuous girder, the bending moment from above equation is combined with the bending moment due to flexure and rearranged to give,  $M_{efb}$ , equal to:

$$M_{efb} = \left( \frac{T_g a}{2d_{gf}} \left( \tanh \frac{L_1}{2a} \right) + \frac{3EI_{fb}}{2L_1^2} \right) \Delta_t \quad \dots 6.28$$

The results from a parametric study in which the bottom flange bending moment was calculated for different girder configurations subjected to a 25 mm transverse displacement are given in Table 6-3. Bending moments calculated using the above equation are within 13% of those calculated from the finite element models, with two exceptions: the first being for No. 12 where there is an intermediate stiffener with shear studs directly above it which resulted in an increase in the flange bending moments. The second is for No. 15 when the length of the girder between the support cross frame and intermediate cross frame was a large proportion (two thirds) of the modeled length of the girder, thus there is significant rotational and torsional fixity at the intermediate cross frame resulting in bending moments with an error of around 25%. However, as with the end of the girder, when the length of the girder between the support and intermediate cross frames lengthened the magnitude of the bending moments decreased and became small for reasonable levels of drift in the girders, thus the error became inconsequential.

Comparing Table 6-2 to Table 6-3 shows that bending moments in the continuous girder are typically around 2.0 to 2.5 times the bending moments in the simply supported bridge. Therefore, bending moments in the bottom flange due to transverse girder drift are more critical for continuous girders.

A combination of seismic stress and stresses due to gravity loading was considered using Equation 6.16. For a continuous girder at the midspan of the bridge model with a midspan support, an assumed transverse top flange displacement equal to 25 mm, and 7 rows of shear studs assumed to be removed, the maximum bending moment calculated from the finite element analysis of the bridge model was equal to 27.8 kNm. Conservatively assuming that 50% of the bottom flange was available to carry the seismic loads, then the maximum bending moment the flange could carry due to seismic loading was 41.8 kNm. Therefore scaling the end displacement based on the ratio of the calculated to allowable bending moment would give a maximum allowable transverse drift of this girder during an earthquake of 38 mm. This corresponds to a girder drift of 6.5%, which is significantly reduced compared to the simply supported girder, but still likely to be greater than the allowable drift in the ductile end cross frames.

Finite element analysis showed that for the continuous girder the maximum stresses were located next to the cross frame located above the midspan support, and therefore they coincide with the maximum stresses from gravity loading. Consequently the potential for girder damage was expected to be higher for continuous girders than for a typical simply supported girder. The

importance of evaluating the girder bending moments due to seismic loading of a bridge with ductile end cross frames was increased for continuous girders.

## SECTION 7 DISTRIBUTION OF FORCES IN BEARINGS

### 7.1 Introduction

Bearings are necessary in bridges, particularly relatively long bridges, in conjunction with expansion joints to facilitate thermal deformations and live load rotations. Furthermore, as seismic isolation bearings, they can be used as a form of earthquake protection for a structure.

Steel reinforced elastomeric bearings (Fig. 2-9) were designed as typical bearings to be used at the bridge supports. They were fully vulcanized to masonry and sole plates to resist any uplift forces during seismic loading. The properties of these bearings are given in Appendix 1. The lead rubber bearings (Figs. 2-10 and 2-16) were designed to isolate the bridge model and modify its seismic response. The properties and design response of these bearings are given in Appendix 2. The response of the isolated bridge is focused on in a subsequent report (Carden, 2005). However, the isolation bearings were also transversely restrained to act as non-isolation bearings for shake table experiments on the bridge model with different end cross frame configurations.

### 7.2 Capacity of Elastomeric Bearings for Extreme Events

Elastomeric bearing limits are typically specified for service loading so that when axial compression loads are combined with other rotational and shear actions there will be no tensile strains in the bearings. This is to ensure longevity of the bearings, as their properties degrade more rapidly when subjected to tensile loads for long periods of time. However, a fully vulcanized elastomeric bearing is able to withstand significant tensile strains for occasional extreme loading conditions. The AASHTO Isolation Guidelines (1999) state that the combination of shear strains in lead rubber bearings due to axial shear and rotations should be less than the total strain limit which may result in tensile strains during extreme combinations of shear, axial and flexural actions. The same requirements can be used for fully vulcanized elastomeric bearings during an extreme seismic event. For the case when the bearing is subjected to earthquake loading the combination can be given by:

$$\gamma_c + \gamma_{s,eq} + 0.5\gamma_r + \gamma_{r,eq} \leq 5.5 \quad \dots 7.1$$

where:  $\gamma_c$  is the shear strain due to compression (or tension) axial loads;  $\gamma_{s,eq}$  is the shear strain due to shear deformations from seismic loads;  $\gamma_r$  is the shear strain due to rotation in the bearing from service loads, and;  $\gamma_{r,eq}$  is the shear strain due to rotation in the bearing from seismic loads. Equation 7.3 is modified from the AASHTO Isolation Guidelines to include a rotational component due to earthquake loading. The shear strain due to axial loads is defined by:

$$\gamma_c = \frac{3SP_b}{2A_r G(1 + 2\bar{k}S^2)} \quad \dots 7.2$$

where: S is the shape factor for the rubber layers (bonded area / divided by the area of the perimeter for a single rubber layer);  $P_b$  is the axial load;  $A_r$  is the overlap of the top and bottom

bonded rubber areas for a deformed bearing;  $G$  is the shear modulus of the rubber, and;  $\bar{k}$  is the rubber material constant (Malaysian, 1979). Slender bearings should also be checked for buckling due to axial compression loads as outlined in Appendix 2. The shear strain due to shear in the bearings is given by:

$$\gamma_{s, eq} = \frac{d_t}{T_r} \quad \dots 7.3$$

where:  $d_t$  is the total design shear displacement in the bearing, which will be minimal when transversely restrained, and  $T_r$  is the total rubber height. The shear strain due to rotation in the bearings is defined by:

$$\gamma_r = \frac{B_b^2 \theta_b}{2t_i T_r} \quad \dots 7.4$$

where:  $B_b$  is the bonded width or diameter of the bearing;  $\theta_b$  is the rotation of the bearing;  $t_i$  is the individual rubber layer thickness and  $T_r$  is the total rubber thickness.

The rotations, axial forces and shear forces on a bearing are each considered in the following sections.

### 7.3 Rotational Actions in the Bearings

As described in Chapter 6, the transversely restrained bearings were subjected to rotational deformations due to the rotation of the girders about their longitudinal axes. Because no instrumentation was provided to measure the direct rotation of the bearings in the bridge model, an approximation of the bearing rotation was necessary. As the bearings were relatively flexible and the top of the girders could also rotate due to the removal of shear studs, the rotation in each bearing could be estimated by the lateral displacement between the top and bottom flanges of the girders divided by the height of the girders. The maximum translation at the ends of the girders during reversed static experiments was equal to 29 mm. during experiment RSLXB. The corresponding rotation of the bearings for this displacement was equal to 0.0486 rad. During shake table experiments the maximum measured transverse end displacement was equal to 27 mm. recorded during experiment STNECF. This corresponds to a rotation in the bearing of 0.0464 rad.

The rotational stiffness of an elastomeric bearing is defined by:

$$k_{\theta b} = \frac{E_b I_b}{T_r} \quad \dots 7.5$$

where:  $E_b I_b$  defines the effective elastic properties of the bearing incorporating the shape factor, and;  $T_r$  is the total thickness of the rubber layers. For the elastomeric pads this equation resulted in a reasonable estimate of the stiffness in the bridge model according the response recorded at the

ends of the bridge. However, for the transversely restrained lead rubber isolation bearings, the equation appeared to underestimate the actual rotational stiffness in the bearings. It is possible that the lead core provided some rotational stiffness to the bearing. A stiffness calculated as three times that using Equation 7.5 resulted in a better rotational stiffness estimate for the bearings based on analysis of the bending moments in the bearing stiffeners, shown in Figure 6-7, which assumed this stiffness. To further illustrate this point, the bending moment in the bearing was assumed to be equal to the estimated bending moment measured using strain gages near the base of the web stiffener at different times. This bending moment was plotted against the estimated rotation in the bearings during increasing amplitude excitation applied to the bridge model with no end cross frames, as shown in Figure 7-1. The calculated theoretical stiffness using three times that calculated from Equation 7.5, matches the backbone response for the bearings reasonably well. This is contrary to past research into the rotational bearing stiffness for lead rubber bearings (Mori, 1999) which suggested a less than 10% difference in rotational stiffness between a lead rubber bearings and elastomeric bearing. Figure 7-1 shows that relationship between the bending moments at the base of the stiffener and the bearing rotation was highly non-linear. This non-linearity was attributed to hysteretic behavior due to deformations in the lead core. There was also the possibility of some friction between the bearing restraints and sole plate of the bearing, although analyses suggest that this was minimal.

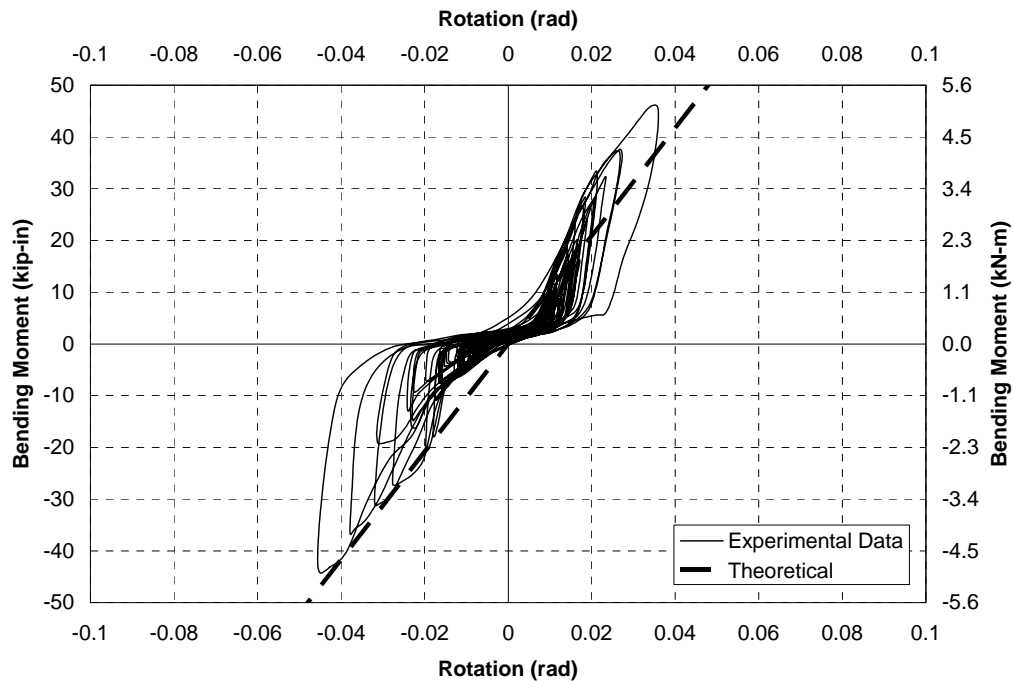


**FIGURE 7-1 STNECF - Measured bending moments in base of bearing stiffener at north end in response to 0.25 - 1.0 El Centro compared with theoretical bearing bending moment**



**FIGURE 7-2 Deformation of elastomeric bearing with rotation applied to bearing in bridge model**

#### **7.4 Axial Loads on the Bearings**

Both the elastomeric bearings and lead rubber bearings were subjected to axial loads due to both gravity loading and seismic loading. From Chapter 2, the axial load per bearing for the reversed static experiments on the bridge model from the weight of the bridge was equal to 33.4 kN. For the shake table experiments, with additional lead on the deck slab, the axial force per bearing was 85.4 kN.

Additional axial loads were applied to the bearings during the simulation of seismic loads due to overturning moments. The axial loads at the north end of the bridge model during laterally applied loading for the first five cycles of experiment RSLXB are shown in Figure 7-3. This figure illustrates that the forces in the west and east bearings were approximately equal and opposite at any given time with tension in the bearings being positive. Figure 7-4 shows the same result for the south end of the bridge model.

The axial forces were caused by an overturning moment at the end of the bridge as a result of the transverse loads being applied at the deck slab level then being resisted by the bearing restraints at the base on the girders. The overturning moment was primarily resisted by axial loads in the bearings, as illustrated in Figure 7-5. The expected axial load can be calculated based on the shear in the end of the bridge and the height of the transverse earthquake load. For a two girder bridge the axial load,  $P_b$ , is given by:

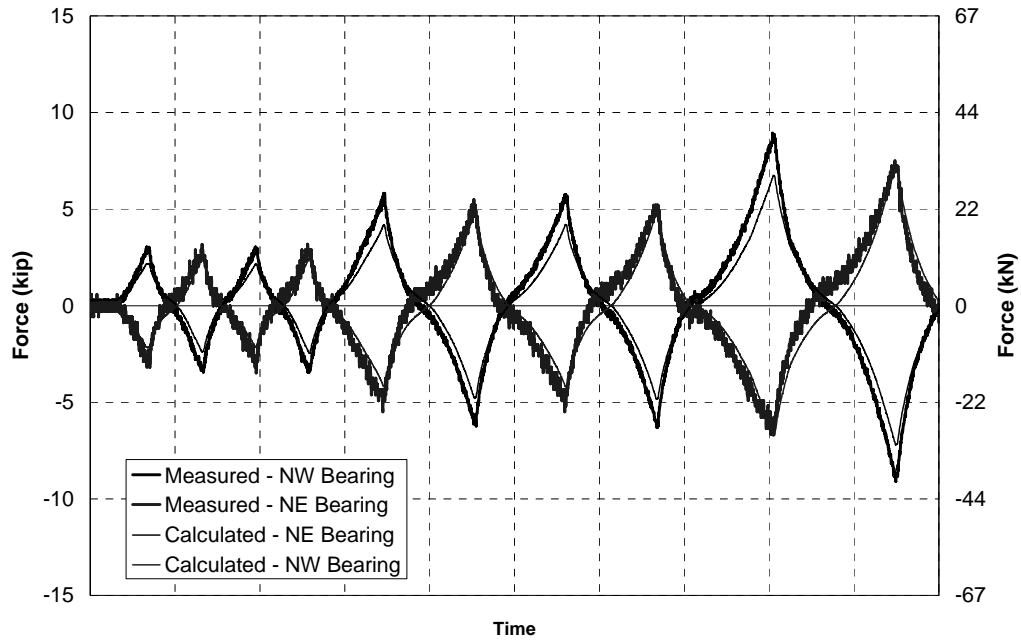


**FIGURE 7-3 RSLXB - Axial bearing forces at the north end for first five cycles**

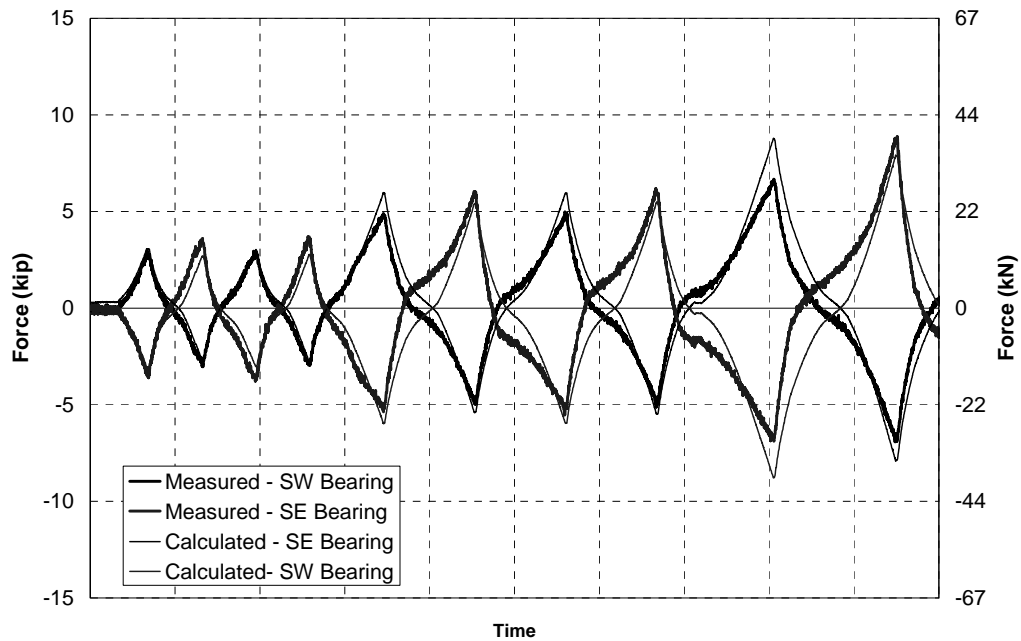


**FIGURE 7-4 RSLXB - Axial bearing forces at the south end for first five cycles**

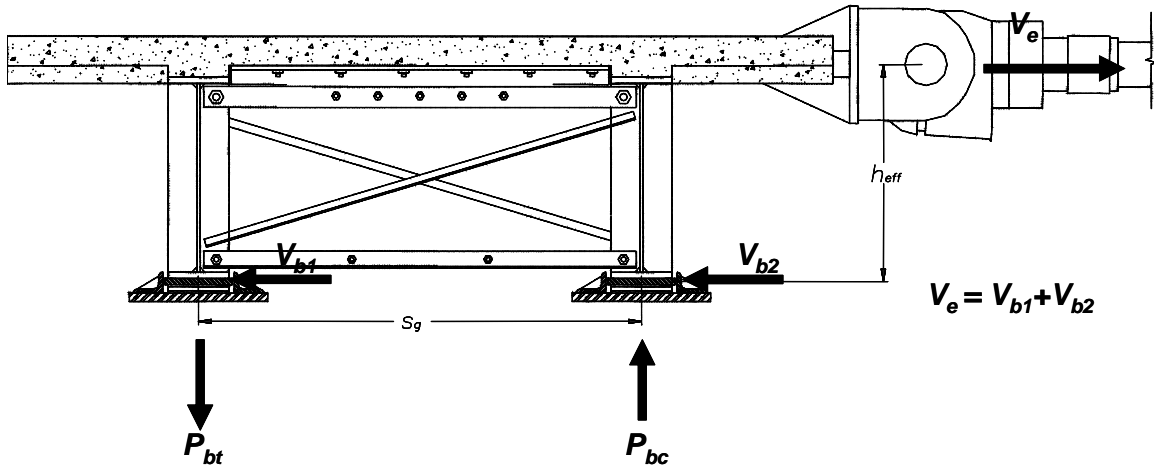


**FIGURE 7-5 Axial forces in bearings as a result of transverse force and overturning moment**

$$P_b = \frac{V_e h_{eff}}{s_g} \quad \dots 7.6$$

where:  $V_e$  is the shear at one support of the bridge;  $h_{eff}$  is the effective height between the applied load from the actuators (or center of mass for the bridge for dynamic loading) and the height of the reaction against the bearing restraint, and;  $s_g$  is the spacing between the girders.  $P_b$  is equal and opposite for the bearings beneath the two girders. While there is, theoretically, also a bending moment in the bearings which will help to resist the overturning moment, this bending moment was shown to have minimal effect and can be disregarded. This equation can be modified for multi-girder bridges with axial forces assumed to be proportional to the distance from the longitudinal centerline of the bridge. This implies that the forces in the bearings underneath the exterior girders will be larger than the forces on the interior bearings for bridges with more than two girders.

For early cycles of the reversed static experiment RSLXB the calculated axial bearing forces were plotted alongside the measured axial forces in each of the bearings as shown in Figures 7-3 and 7-4. Using Equation 7.6, and dimensions of  $h_{eff}$  equal 658 mm. and  $s_g$  equal to 1340 mm, the axial force in the bearings was expected to be equal to 0.49 times the end shear. These figures show that expected axial forces were generally within 20% of the measured forces. The error could be due some bending moments in the bearings and secondary axial forces from the actuators due to rotation of the bridge superstructure.

With no end cross frames for a given applied actuator force the deformations of the end region were much larger than with end cross frames, therefore the rotations in the bearings increased and the influence of bearing bending moment on the axial loads was expected to be larger. Despite this and continuing to disregard the bending moments in the bearings, Equation 7.6 was shown to result in a good estimate of the axial forces at the north end of the bridge model, as shown in Figure 7-6. Figure 7-7 shows that the comparison at the south end was not as good, indicating the



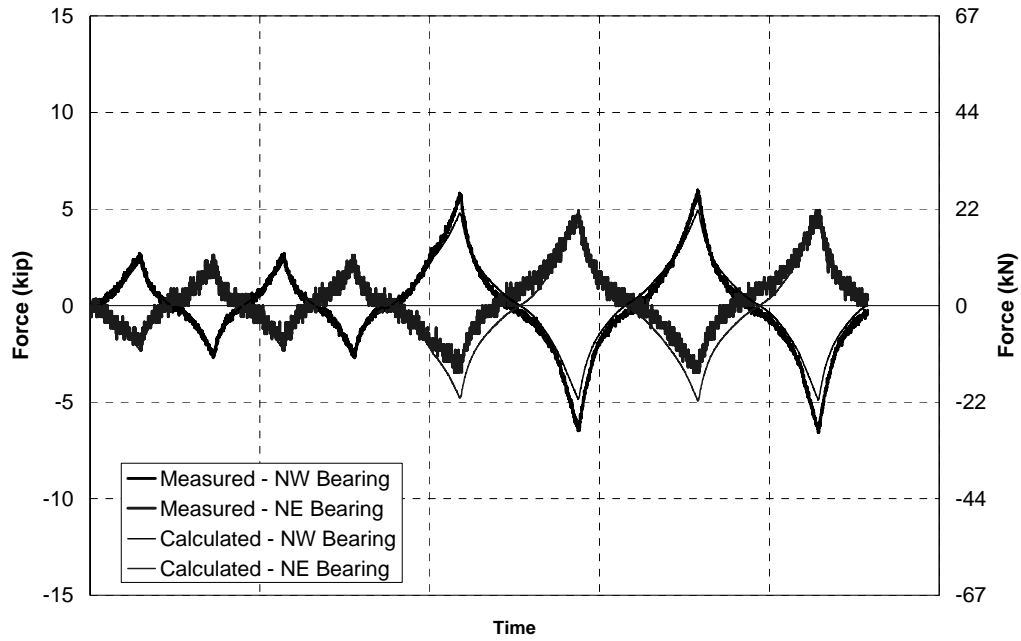


**FIGURE 7-6 RSNCF - Axial bearing forces at the north end**

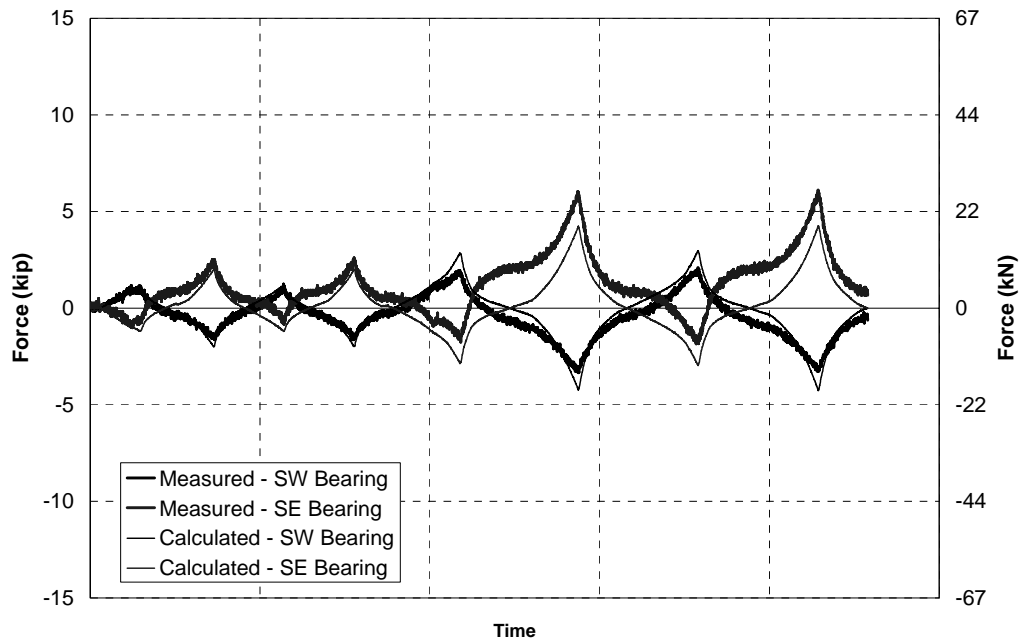


**FIGURE 7-7 RSNCF - Axial bearing forces at the south end**

bending moments had some effect. However, it was conservative to neglect the resistance of the bending moments in calculating the axial loads.

The axial loads in the bearings were also estimated for the shake table experiments. With the lead loaded on the deck slab of the bridge, the center of mass was calculated to be 11 mm. above the deck slab. With the transverse bearing restraints on the lead rubber bearings,  $h_{eff}$  was calculated to be 782 mm. for the shake table experiments, as illustrated in Figure 7-8. The relatively low bearing stiffness for the lead rubber bearings was calculated to have minimal impact on the axial loads in the bearings. The measured axial forces at the north and south ends of the bridge model, which had transversely restrained bearings during experiment STHXB, are shown in Figures 7-9 and 7-10 in the response to 2.0 x El Centro. These figures show that the calculated expected axial force based on the measured end shear was consistently lower than the measured axial force. Similar results for the bridge model with no end cross frames in response to 1.0 x El Centro, are shown in Figures 7-11 and 7-12. The calculated axial loads are again lower than the measured axial loads by as much as 50%. As the statically applied loads agreed better than the shake table experiments, it was apparent that there were additional axial loads due to a dynamic effect.

For the transversely unrestrained isolation bearings, the load path was slightly different than for the restrained bearings. Assuming there was no rotation at the top of the bearings due to rotational restraint of the girders provided by elastic end cross frames, the resulting bending moments in the bearings put the bearings in double curvature, as shown Figure 7-13. Consequently the bending moments at the mid height of the bearings were equal to zero. Equation 7.6 can be used to calculate the axial forces in the bearings with zero bending moments by summing moments about the mid height of the bearings, resulting in an effective height of 851 mm. The calculated and measured axial loads for the unrestrained isolator bearings in response to 2.0 x El Centro are shown in Figures 7-14 and 7-15. Figures 7-14 and 7-15 show that like with the restrained

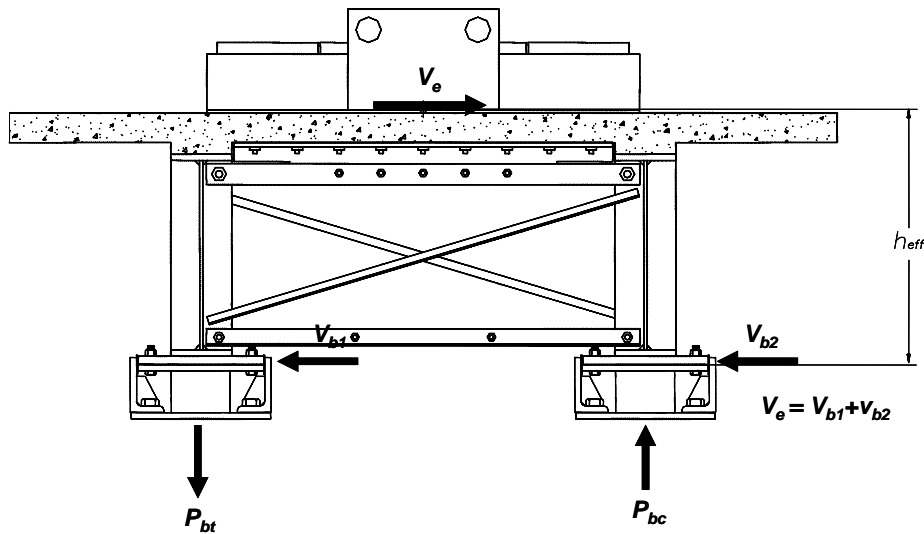


**FIGURE 7-8 Axial forces in restrained bearings as a result of transverse force and overturning moment from shake table experiments**

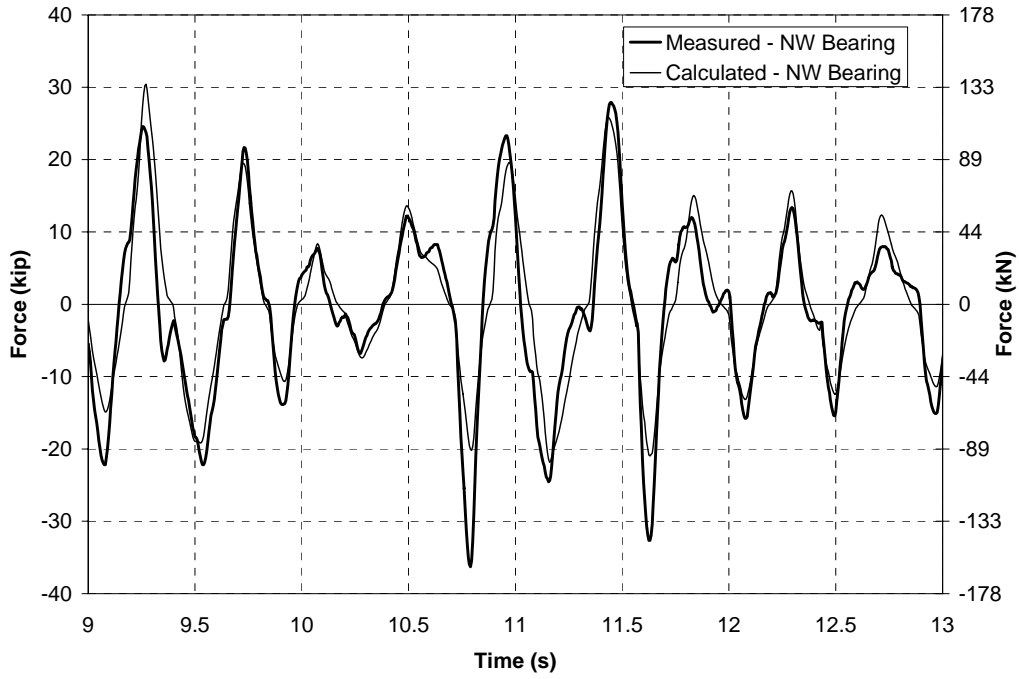


**FIGURE 7-9 STHXB - Axial bearing forces at the north end for 2.0 El Centro (NE load cell faulty)**

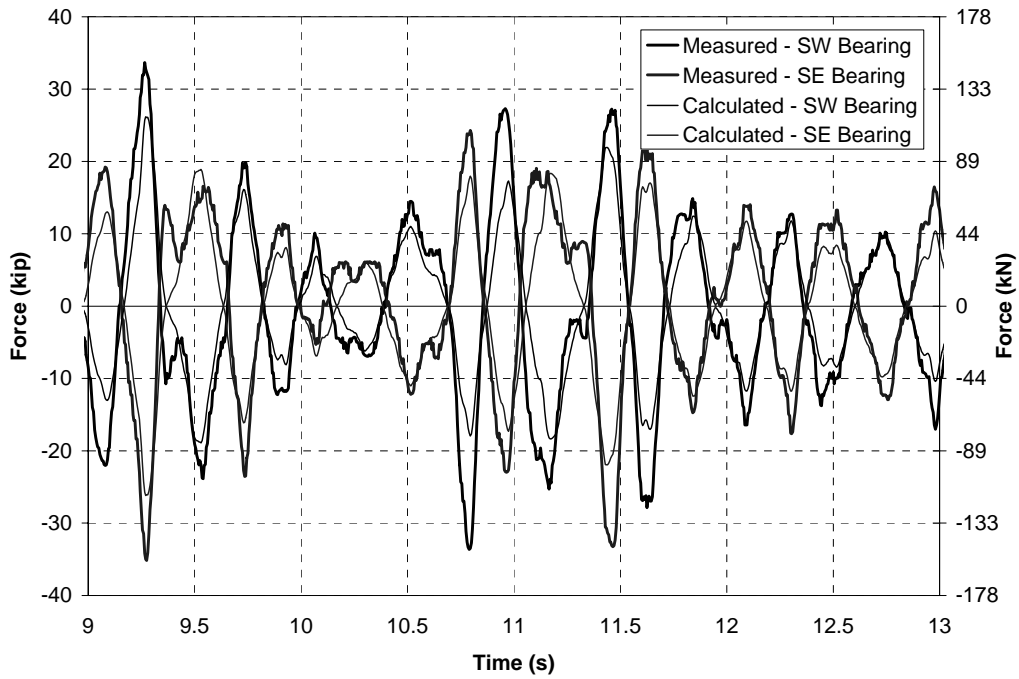


**FIGURE 7-10 STHXB - Axial bearing forces at the south end for 2.0 El Centro**

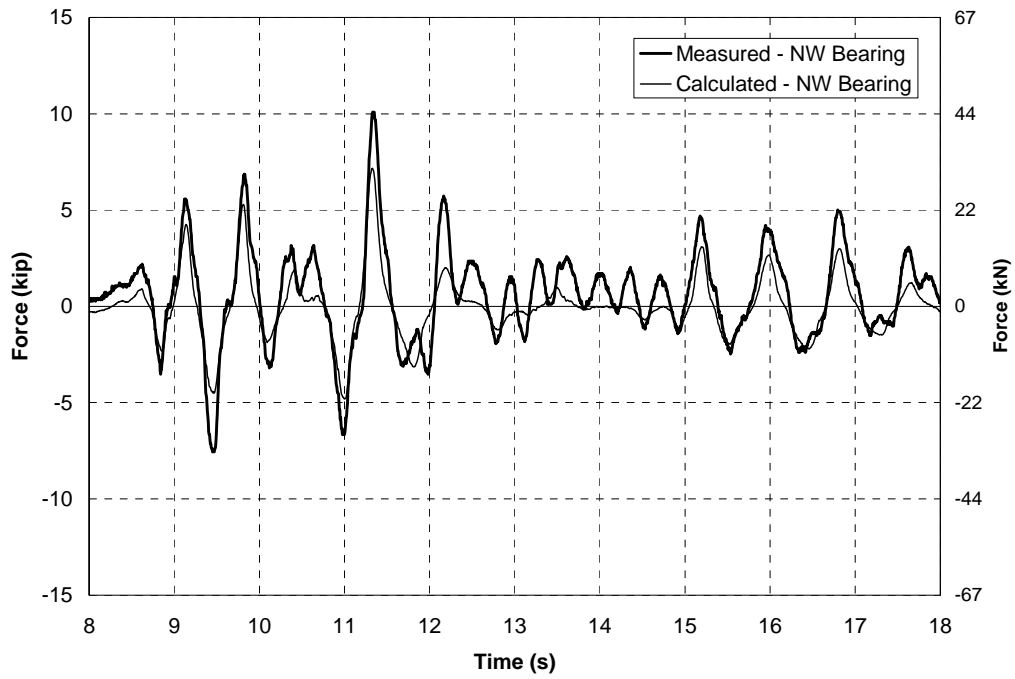


**FIGURE 7-11 STNECF - Axial bearing forces at the north end for 1.0 El Centro (NE load cell faulty)**

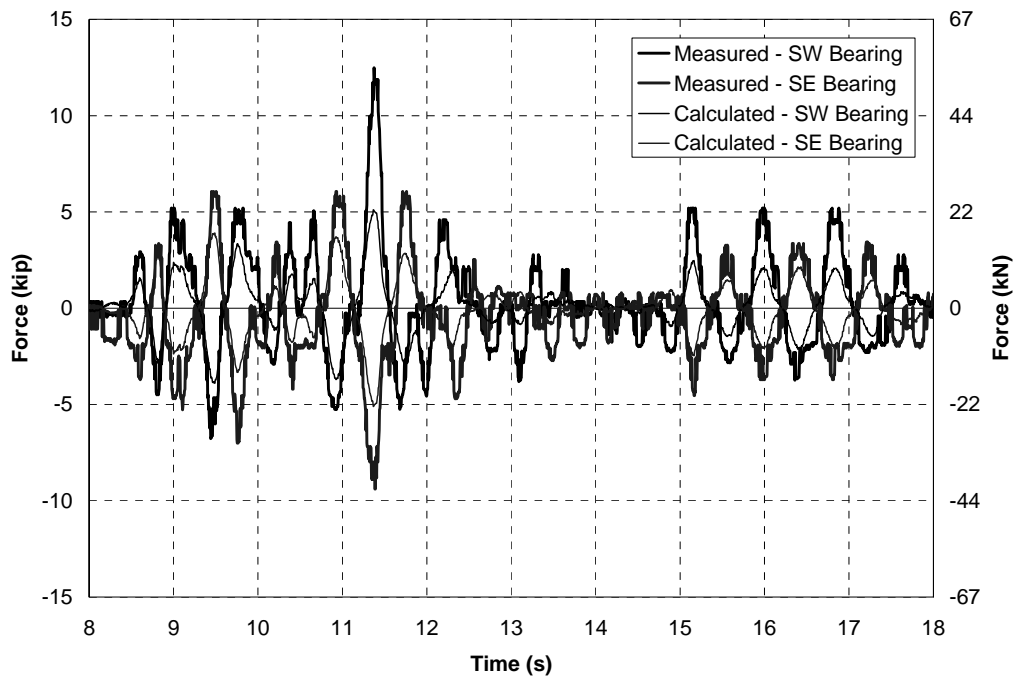


**FIGURE 7-12 STNECF - Axial bearing forces at the south end for 1.0 El Centro**

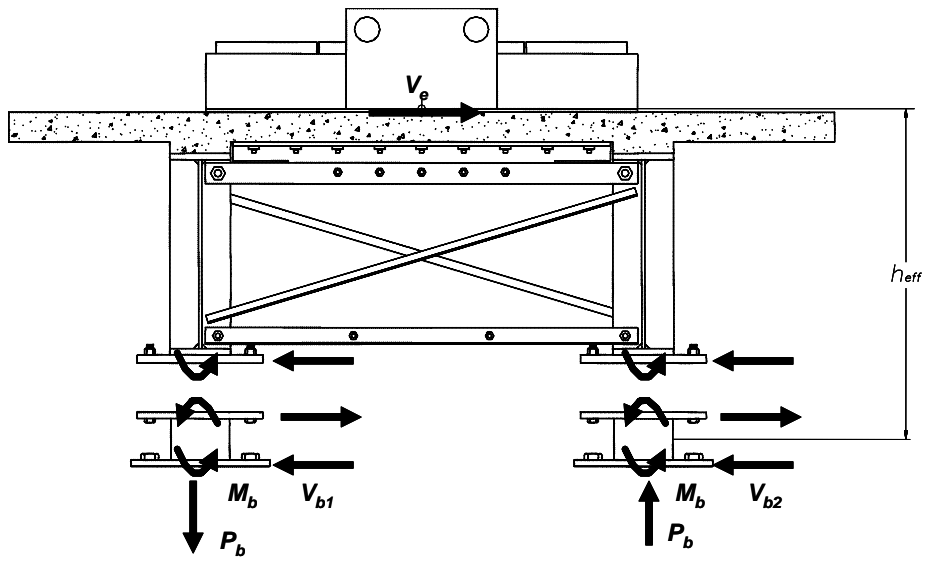


**FIGURE 7-13 Axial forces in isolator bearings as a result of transverse force and overturning moment from shake table experiments**

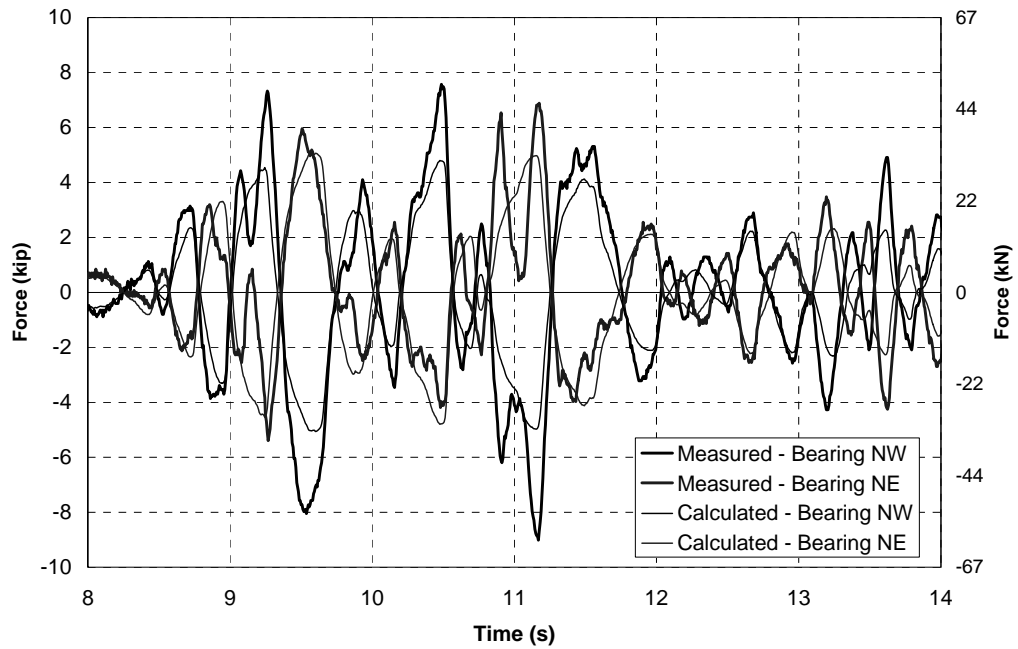


**FIGURE 7-14 STLRB - Axial bearing forces at the north end for 2.0 El Centro**

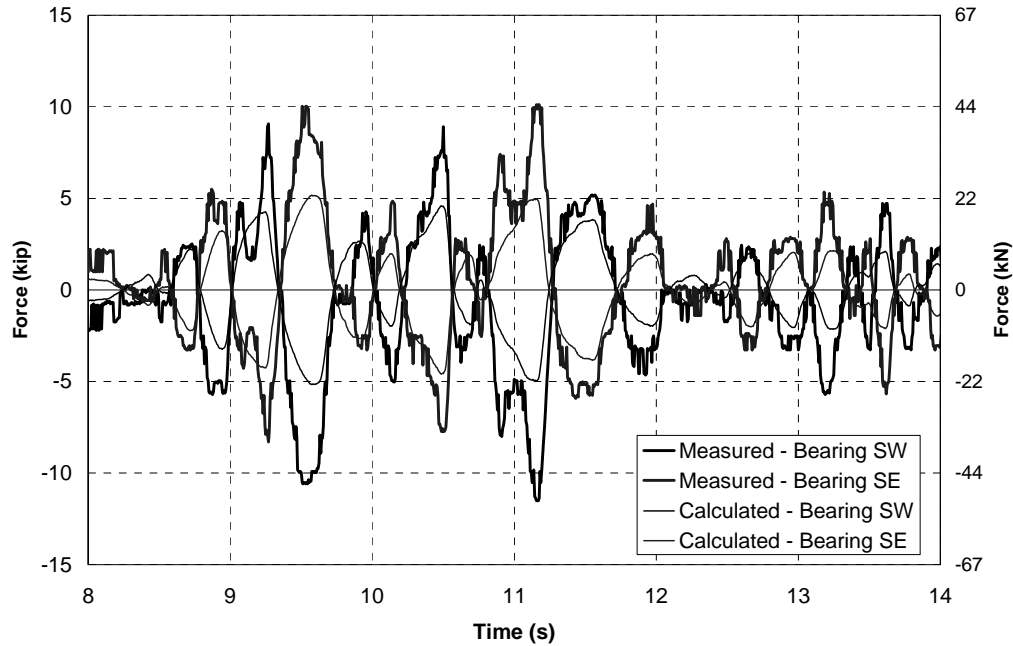


**FIGURE 7-15 STLRB - Axial bearing forces at the south end for 2.0 El Centro**

bearings, the calculated axial loads typically underestimate the loads measured in the load cells by as much as two times.

It was observed that the axial forces in isolation bearings in response to 2.0 x El Centro were much smaller than the forces in the restrained bridge model in response to the same earthquake. This is expected because the transverse shear was much larger in the restrained model. However, for the isolated model the maximum axial forces and axial strains in the bearings were in phase with the maximum shear strains in the bearings. Combined strains in the bearings were larger than strains from the individual shear and axial components. The impact of the combined strains can be calculated using Equation 7.1.

The largest axial forces in the bearings due to transverse loading measured in the bridge model during reversed static experiments were 116 kN in tension and 151 kN in compression. These forces occurred during experiment RSHXB2. During shake table experiments the maximum axial forces measured were 165 kN in tension and 209 kN in compression in response to 0.75 x Kobe for the restrained bearings during experiment STHXB. The axial compression force in each bearing due to gravity loads were much less than these levels, therefore, the axial loads resulting from the transverse loading subjected the bearings to tensile forces or significant amplification of the compression forces in the opposing bearings.

The previous analyses focused on a the response of the bridge in the transverse direction, as this is the direction in which overturning moments and subsequent axial loads were expected. In the longitudinal direction no axial bearing forces were expected due to seismic loading, because there was negligible overturning in this direction. Similarly no additional forces were expected from

vertical loads as the shake tables were not excited vertically. Investigation of the axial forces in the load cells show that there were small axial loads in the bearings when the bridge was excited in the longitudinal direction, as shown in Figures 7-16 and 7-17. These forces were relatively minor when compared to the those from transverse excitation and those from gravity loads. However, they do show that there was some excitation of the bridge model in the vertical direction due to longitudinal loading.

In order to account for the larger than calculated dynamic axial forces in the bearings due to transverse excitation, a dynamic amplification factor is proposed for these axial forces. The maximum calculated axial force is compared to the measured axial force for selected transverse earthquake excitations in Table 7-1.

**TABLE 7-1 Ratio of measured maximum axial load to calculated maximum axial load in bearings for selected experiments**

Expt.	Excitation	Bearing	Maximum Axial Loads (kN)		Ratio Meas. / Calc.
			Calculated	Measured	
STHXB	2.0 El Centro	NW	134.55	161.37	1.20
		NE	134.55	1	
		SW	116.29	149.83	1.29
		SE	116.29	156.32	1.34
STNECF	1.0 El Centro	NW	31.86	44.83	1.41
		NE	31.86	1	
		SW	22.71	55.51	2.44
		SE	22.71	41.78	1.84
STLRB	2.0 El Centro	NW	22.52	40.11	1.78
		NE	22.52	30.62	1.36
		SW	23.04	51.17	2.22
		SE	23.04	44.99	1.95

Notes: 1. Axial circuit of load cell faulty

This table shows a wide range of differences between the measured and calculated axial loads with an average ratios of: 1.28 for the “heavy” cross frames, 1.90 for the bridge with no end cross frames and 1.83 for the isolated bridge model. Further research is necessary to determine the cause for such a large variation, however at this stage a dynamic amplification factor of 2.0 is recommended to account for this discrepancy. This is conservative for all but the largest loaded bearings, and was exceeded by 22% in the worse case.

### 7.5 Shear Forces in Transversely Restrained Bearings

The transverse forces in the bridge model were resisted by bearing restraints except in the isolated configuration. Transverse restraints on a bridge model are typically designed with a small gap between the bearing and the restraint. However in an attempt to simplify the response of the bridge model, the gap was minimized with shims so that the forces were transferred into the bearing restraints immediately on application of transverse loading.

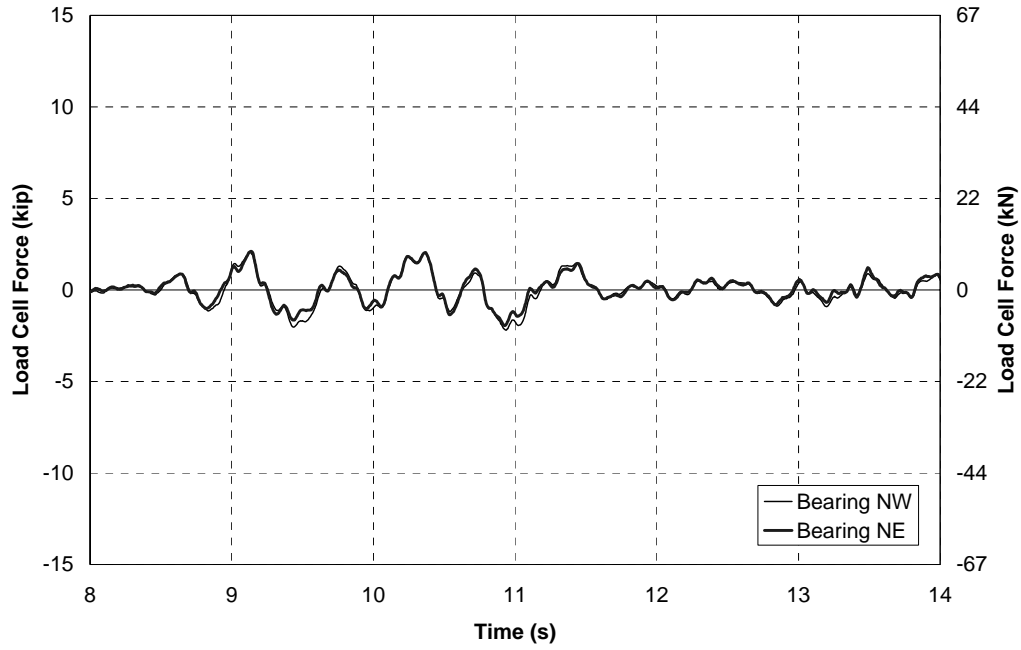


**FIGURE 7-16 STLRB - Axial bearing forces at the north end for 2.0 El Centro in the longitudinal direction**

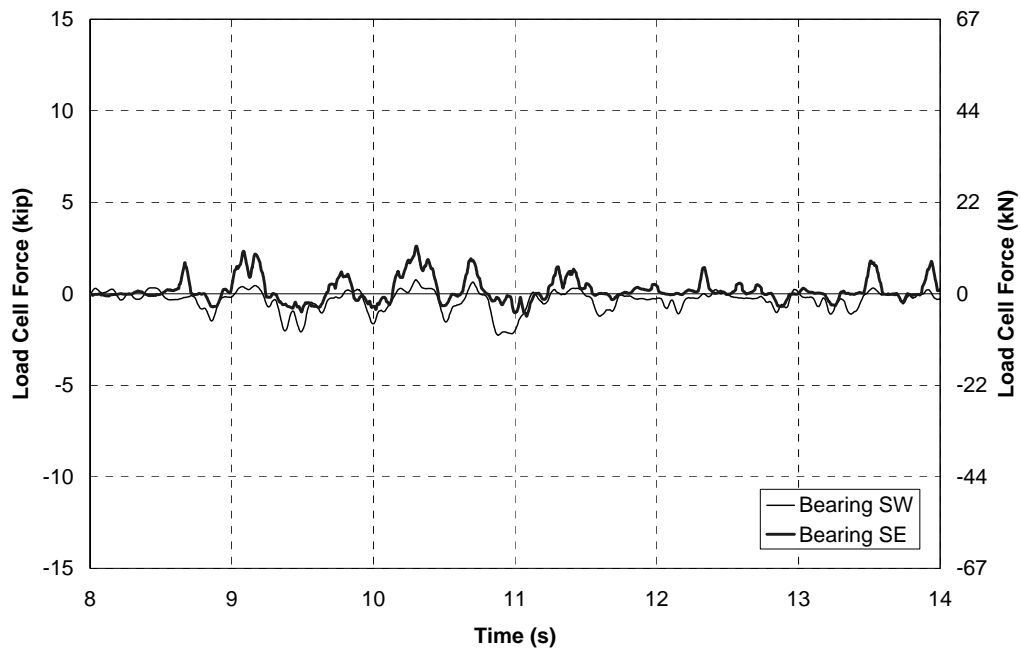


**FIGURE 7-17 STLRB - Axial bearing forces at the south end for 2.0 El Centro in the longitudinal direction**



With the shims it was expected that the total end shear would be equally distributed between the bearings, but the experiments demonstrated that this was not always the case. Figure 7-18 shows the transverse shear forces in each of the different bearings during the first reversed static experiment with load cells under the bearings. For early cycles of this experiment the forces were relatively evenly distributed between the different bearings. However the last cycle shows that the force in the east bearing at the north end of the bridge model was almost two times the force in the west bearing. At the south end the forces in the two bearings were similar. The difference in forces between the two bearings at the north end was attributed to differential slippage of the restraints which resulted in gaps opening between the bearing and their restraints. For the final reversed static experiment, Figure 7-19 shows that the forces in each of the bearings were quite different. The largest difference occurred at the south end for negative reversal of loading, where it was seen that the east bearing was carrying a large proportion of the total end shear. The distribution of forces for positive and negative reversals was quite different as the restraints on either side of each bearing deformed differently during the experiments.

The transverse bearing forces during shake table experiments were also variable between the different bearings. Figures 7-20 and 7-21 show examples of forces in the bearings for experiments with the “heavy” and “light” cross frames respectively. The maximum difference between the bearings is approximately a factor of two, therefore the bearing on one side was carrying two times the force than the bearing on the other side.

These results show that bearings need to be designed for a greater proportion of force than equally assumed forces in the bearings. For the two girder bridge model forces in one bearing equal to two times the forces in the other bearing were typical at a given support. It is difficult to extrapolate these results to a bridge with more girders, and a finite element analysis is not helpful for estimating bearing force distributions. Therefore, more experimental studies would be beneficial. Based on these preliminary findings, in order to prevent progressive failure of bearings, restraints could be designed with at least limited ductility, as such if one restraint is overloaded and deformed beyond its elastic limit, the forces can be distributed to the other bearings. If a single bearing restraint was overloaded resulting in failure, it is possible that subsequent bearings will be overloaded and also fail resulting in progressive failure of the bearings. Alternatively, each bearing restraint could be designed for the full shear at a support. The elastic limit of the bearing restraints was not exceeded during experiments on the bridge model therefore failure was not observed, however, it has been observed in past earthquakes (Fig. 1-6).

For the end cross frames used in the bridge model, a bottom chord was provided to ensure that forces could be distributed from the base of one girder to the other girders. Without a bottom chord unbalanced forces, which occur when the X-braces buckle or due to asymmetry in the buckling restrained cross frames, would result in concentrations of shears in certain bearings. Furthermore if one bearing is overstressed, the bottom chord is able to provide a direct load path for redistribution of shears to the other bearings. Therefore use of this type of bottom chord is recommended.

## **7.6 Combined Actions in the Bearings**

For the elastomeric bearings in the bridge model some separation between the masonry plate and elastomer was observed at the edges of the bearing with a large combined tensile and rotational strains (Fig. 7-2). Despite this, no delamination was observed in the remainder of each bearing,

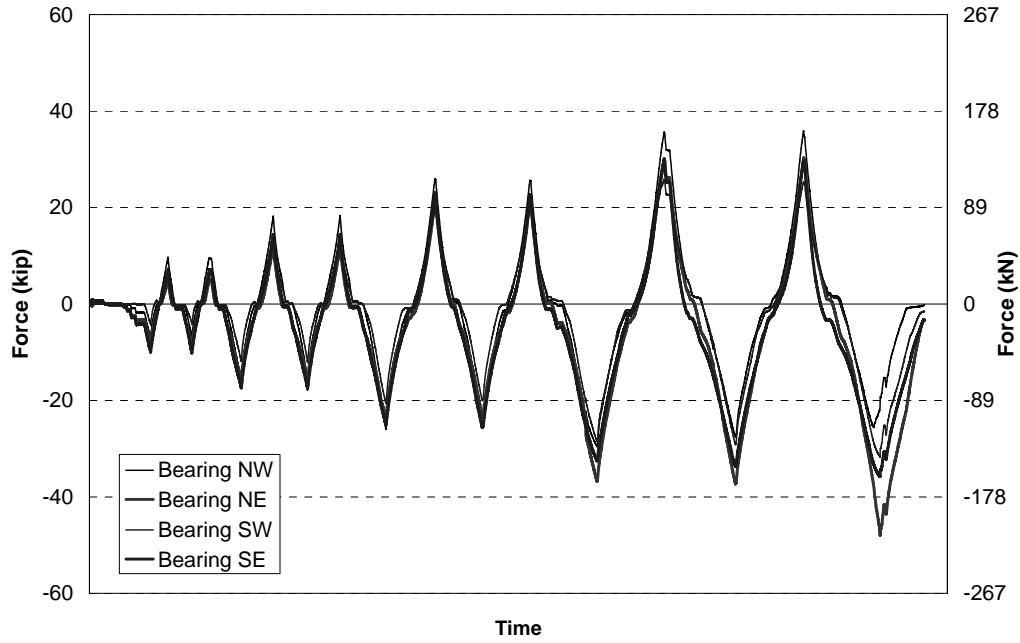


**FIGURE 7-18 RSHXB2 - Transverse shear forces in bearings**

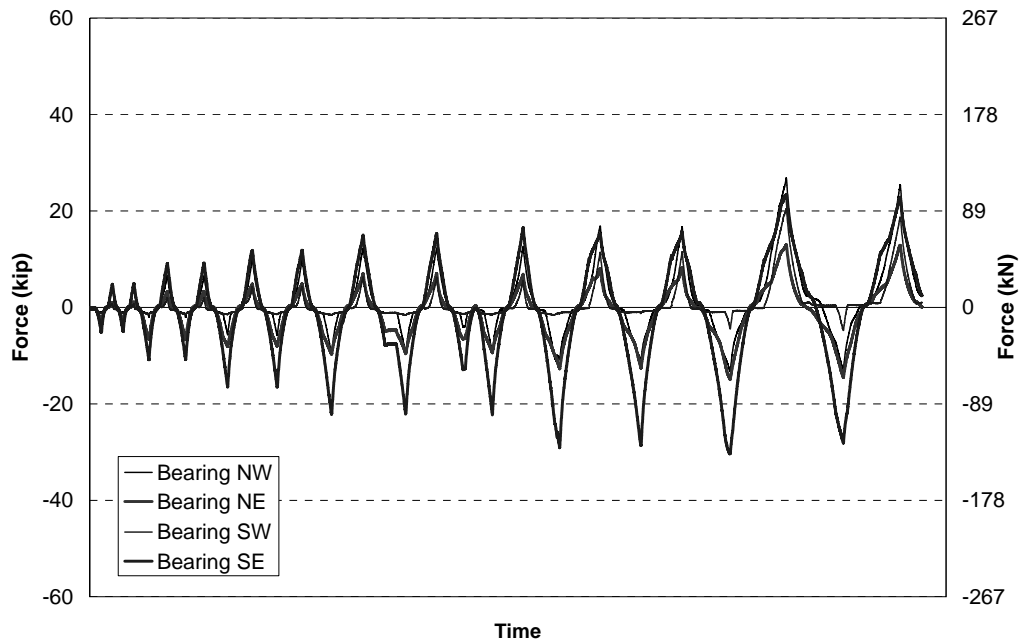


**FIGURE 7-19 RSLXB - Transverse shear forces in bearings**

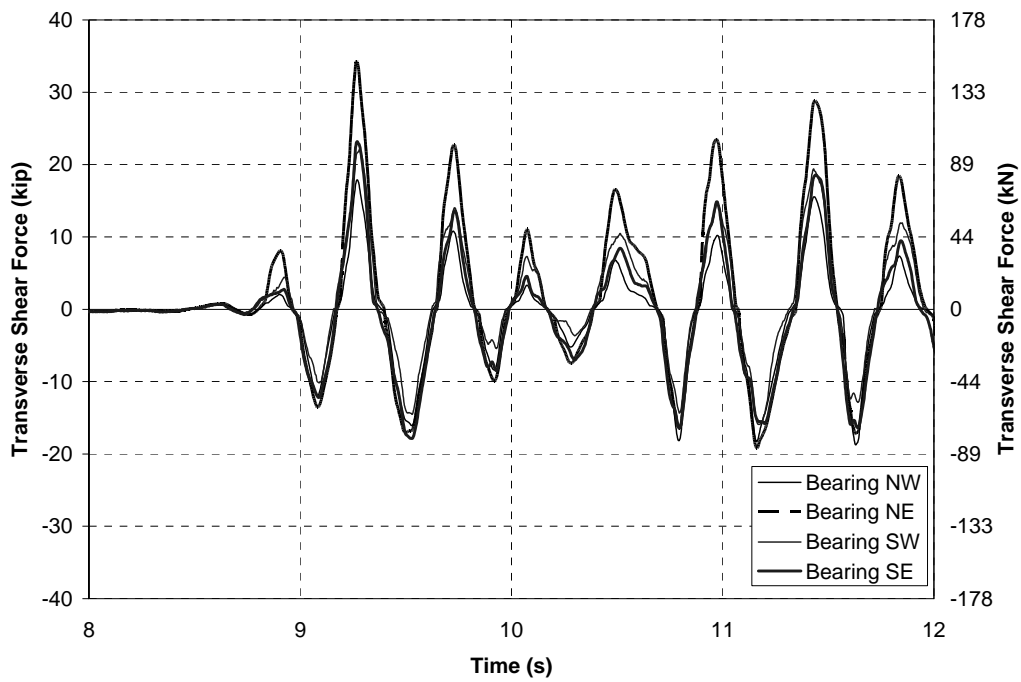


**FIGURE 7-20 STHXB - Transverse shear forces in bearings in response to 2.0 El Centro**

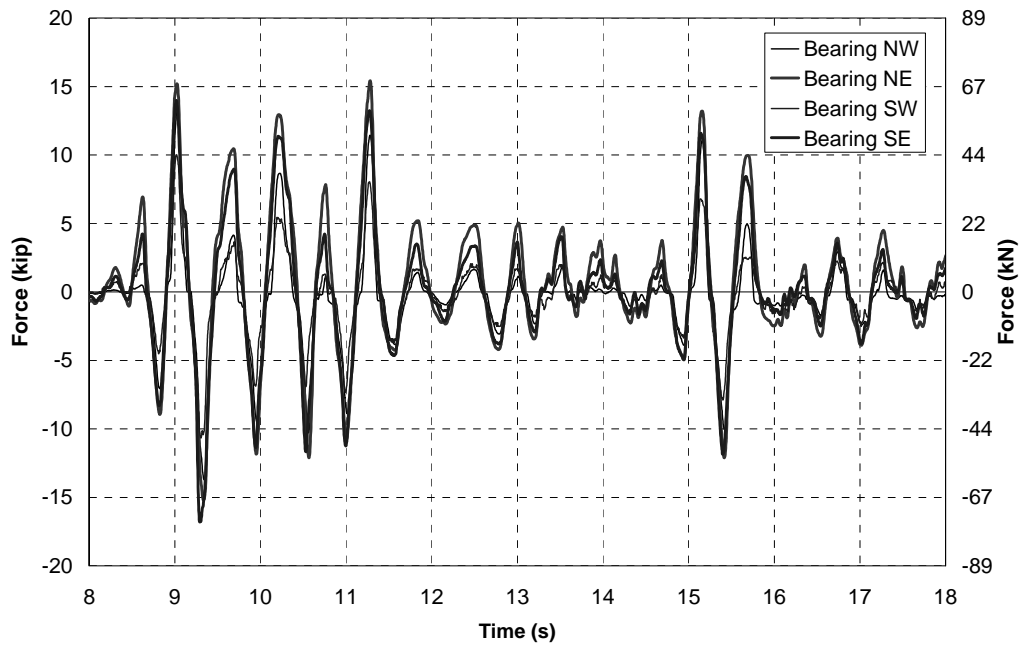


**FIGURE 7-21 STLXB - Transverse shear forces in bearings in response to 2.0 El Centro**

likewise, no damage was observed in the lead rubber bearings at large combined strains from axial, shear and rotational actions.

For the bridge model with elastomeric bearings, the axial load on each bearing (without lead as in the reversed static experiments) was 151 kN. The resulting maximum shear strain in the bearing due to compression was 0.87, easily below the allowable design shear strain for axial load alone of 2.5 (AASHTO, 1999). For the transversely restrained bearings the shear strain was close to zero and the rotation due to service loads was assumed to be equal to zero. Using Equation 7.1 the resulting allowable maximum shear strain due to rotation was 4.63, giving an allowable rotation in the 13 mm thick layer of the bearings of 0.044 (Eq. 7.4). Assuming the rotation was distributed into the different rubber layers according to their stiffnesses, 66% of the rotation will be concentrated in the 13 mm thick layer. Therefore the total rotation in the bearing would be 0.066 which corresponds to a girder drift of approximately 6.6%. Accordingly these reinforced elastomeric bearings were expected to accommodate large rotations necessary for ductile end cross frames. Due to their height, the lead rubber bearings were able to accommodate rotations much greater than in the elastomeric bearings.

### **7.7 Distribution of Forces between Supports**

For the simply supported bridge model it was expected that the reactions at the two ends of the bridge, and consequently the forces in the end cross frames, would be equal in response to transverse loading because the bridge was statically determinate. The reversed static experiments, with the exception of the first experiment, were controlled so that there were equal forces in each actuator. Therefore by equilibrium, due to symmetric loading, it was expected that the forces at the ends of the bridge model would also be equal, despite the potential for one end to be more flexible than the other. The shears at each end of the bridge for experiment RSHXB2 are shown in Figure 7-22. This figure shows that all of the forces are equal to within 15%. The differences could be due to instrumentation error and some partial rotational restraint in the certain bearings resulting in an unbalance of forces between the ends. A similar result is shown for the shake table experiments as shown for example in Figure 7-23.

The bridge model with a support at midspan was not statically determinate therefore the distribution of forces was not only dependent on the distribution of loading but also on the relative stiffness throughout the bridge model. For a uniform loading and stiffness throughout the two span bridge model it was expected that the reactions should be proportioned with 62% of the load at midspan and 19% at each of the end supports. However unlike the statically determinate simply supported model relative stiffnesses could result in a different distribution of forces. The two span bridge model was studied with unbonded braces at each support. When the bridge model was subjected to low amplitude excitations, as shown in Figure 7-24, the relative forces were shown to be approximately equal to the above proportions. For experiment STUB2S in response to 0.5 x El Centro at the maximum measured base shear the forces were proportioned with 23% at the north end, 63% at midspan and 18% at the south end. Note that the combined shears at the three supports summed to 104%, resulting because the maximum end shears occurred at different times. This indicates the presence of a second transverse mode which can explain the difference in shears at the two ends. The effect of the second mode can be considered minimal as the combined ends shears were only 4% greater than the total shear expected for a single mode.

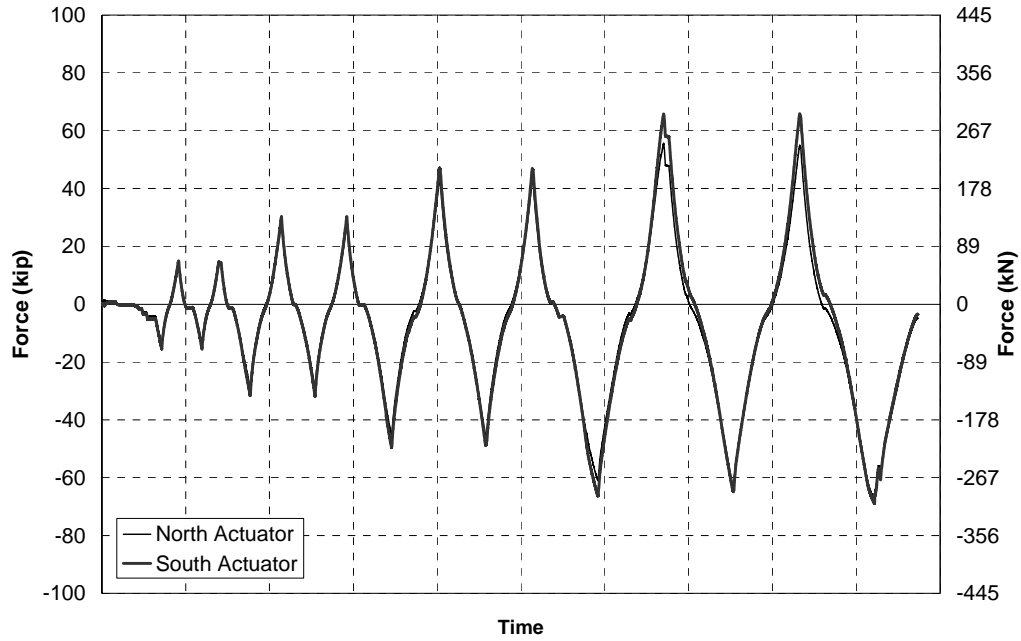


**FIGURE 7-22 RSHXB2 - End shear forces measured in the load cells**

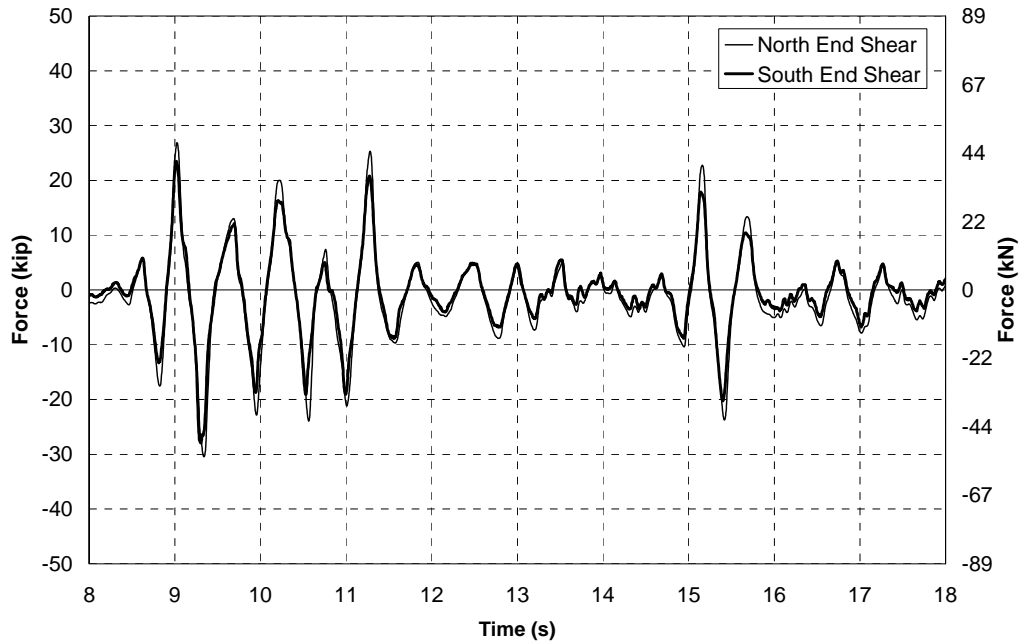


**FIGURE 7-23 STLXB - End shear forces measured by the load cells in response to 2.0 El Centro**

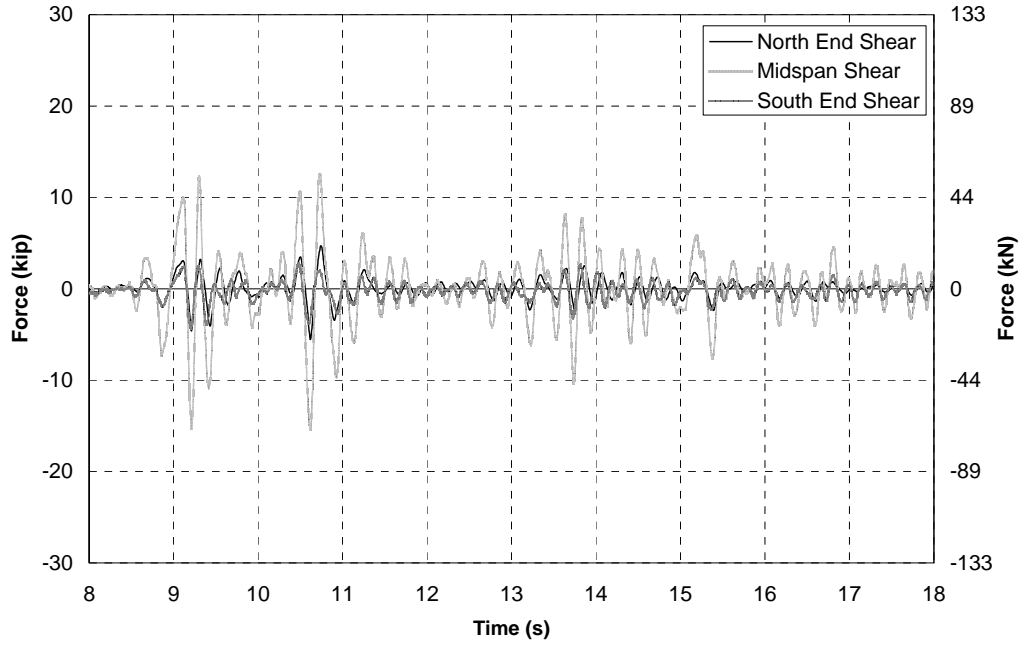


**FIGURE 7-24 STUB2S - End shear forces measured by the load cells in response to 0.5 El Centro**

## SECTION 8

### ANALYTICAL MODEL TO REPRESENT THE STEEL GIRDER BRIDGE SUPERSTRUCTURE

#### 8.1 Introduction

Based on the identification and discussion of all the critical components in the transverse seismic load path a simplified analytical model was developed which was intended for use in non-linear modeling of the bridge model and also to provide a methodology for analysis and design of steel plate girder bridges.

#### 8.2 Description of the Model

Itani and Sedarat (2000) showed that analytical models with the superstructure modeled using a series of frame elements with lumped masses at discrete locations along the superstructure could capture the dynamic properties of a steel plate girder bridge. This concept was used to develop analytical models for different configurations of the bridge model. The development of a simplified model in this chapter deals with only those properties modeled as equivalent linear elastic properties. The insertion of non-linear X-braces, unbonded braces and bearings is discussed in a subsequent report (Carden, 2005). The model was generated in SAP2000 v8.30 (Computer and Structures, 2003).

The analytical model developed is illustrated in Figure 8-1 (without end cross frames). The superstructure was modeled using frame elements spanning between the two ends of the model, with the properties reflecting those equivalent section properties that were necessary in the capturing the overall transverse response. The important properties were the moment of inertia about the vertical axis and torsional stiffness about the longitudinal axis of the bridge. The cross sectional area and moment of inertia about the horizontal axis were assumed to be infinitely large values as these properties had no affect on the transverse seismic response. The shear areas were also assumed to be rigid as shear deformations can be shown to be small.

In order to model the translational stiffness of the bridge the height of the superstructure is inconsequential. However, in order to model the axial forces in the bearings it is necessary to model the mass of the bridge at the center of mass in order to generate the correct overturning moment that is resisted by the bearings. Furthermore, in order to appropriately model torsion in the bridge the eccentricity between the center of mass and shear center should be correctly modeled. Thus, the frame elements used to model the superstructure were located at the height of the shear center, as illustrated in Figure 8-1, in order to allow the loading to be applied at the same level as the actual loading, and result in the same translation and rotation as in the bridge model. The weight of the bridge in the analytical model was assumed to be lumped at the ends and five intermediate locations along the bridge. It was located at the height of the calculated center of mass, connected to the superstructure elements through rigid links.

In order to test the validity of this analytical model a two girder bridge superstructure was analyzed, similar to the bridge model, but with a couple of modifications to eliminate the effects of deck slab cracking and partial composite action. Both detailed finite element model and simplified analytical model were generated for this assumed bridge. The deck slab was assumed to be constructed from steel with a thickness of 12 mm, the same as that for the gross transformed deck

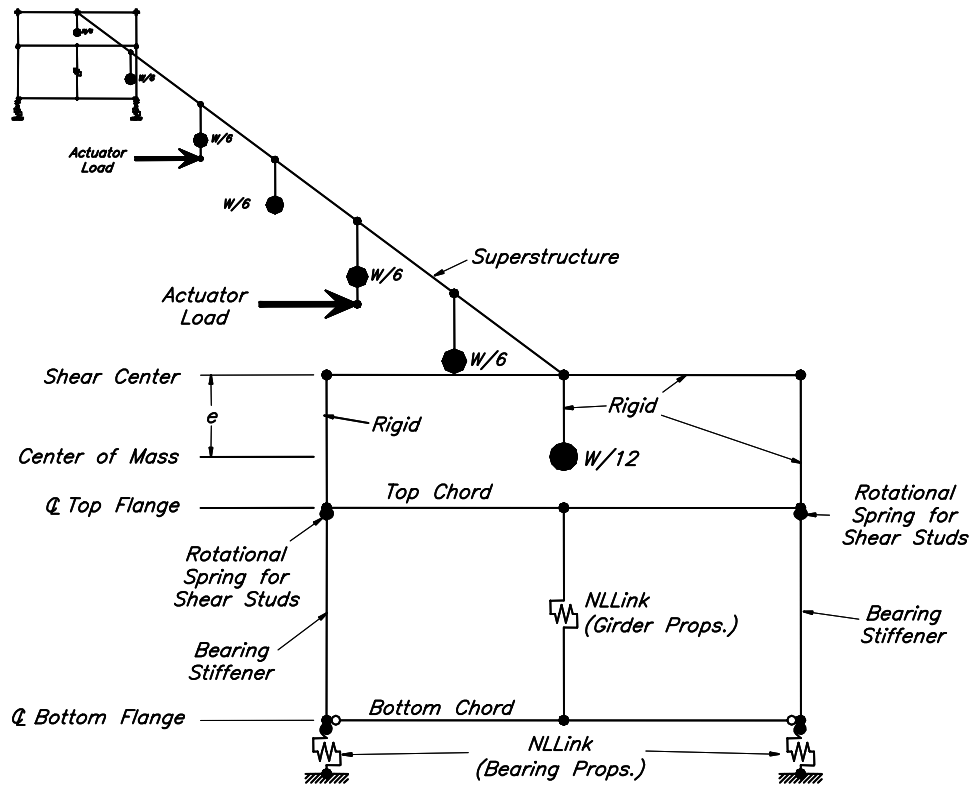


**FIGURE 8-1 Illustration of simplified non-linear analytical model of bridge**

slab section. The connection between the deck slab and the girders was assumed to be with a rigid steel plate rather than the shear studs. The cross section was braced with axially rigid cross frames at each of the cross frame locations in the bridge model to minimize section distortions. As for the actual bridge model the clear length of the bridge was assumed to be 18.0 m. The end restraints allowed rotation about the vertical axis but the rigid braces restrained any deformation or distortion at the ends. Bearings were also used to prevent lateral and vertical translations and end rotations about the longitudinal axis. The detailed finite element model was similar to that shown in Figure 3-38, while the simplified model was like that in Figure 8-1. The moment of inertia about the vertical axis was calculated as  $68600 \text{ in}^4$  (Eq. 4.1). The torsional moment of inertia, assuming it can be calculated from the sum of torsional stiffnesses of the plates, was calculated as  $80.0 \times 10^6 \text{ mm}^4$  (Eq. 4.2). The shear area was assumed to be equal to the area of the deck slab ( $29100 \text{ mm}^2$ ).

The center of mass of the above section was calculated at a height of 168 mm. below the centroid of the deck slab. The shear center was calculated at a height of 156 mm. above the centroid of the deck slab (Eq. 4.7), resulting in an eccentricity between the shear center and center of mass of 324 mm. Analysis of the detailed finite element model showed that zero rotation was calculated in the bridge model when a lateral load was applied at a height of 314 mm above the center of mass of the bridge, therefore compared to within 6% of the calculated shear center eccentricity. A unit transverse force and unit torque about the shear center were each applied to the simplified and detailed finite element models. The resulting displacements due to shear deformation and flexural



deformation were 0.095 and 0.009 mm, respectively, calculated by assuming infinitely large flexural and shear stiffnesses respectively in the analytical model. The shear displacement was shown to be around 10% of the flexural displacement in this model. The total transverse displacement from the analytical model (0.103 mm) was within 6% of the total transverse deformation in the detailed finite element model (0.109 mm). However, the torsional deformations as a result of the torque applied to the bridge, did not agree nearly so well. The detailed finite element model was found to have rotations of around 40% of those in the simplified model. This was attributed to warping not being included in the elements used to model the superstructure of the simplified bridge model. In order to correct for the effect of warping the torsional moment of inertia for the simplified bridge model needed to be amplified by 250%.

For the actual bridge model slippage in the connection between the deck slab and the girders and cracking in the deck slab complicated the properties of the superstructure. Therefore equivalent properties were found by calibrating stiffnesses with the experimental data. Assuming no deck slab cracking and slippage between the deck slab and the girders, the moment of inertia about the vertical axis for the equivalent transformed section was  $26.6 \times 10^9 \text{ mm}^4$ , and a torsional moment of inertia using Equation 4.2 was  $79.1 \times 10^6 \text{ mm}^4$ . The moment of inertia for the bridge model was found to be considerably less than that calculated using the gross area properties. As with the modified model assumed above, the torsional moment of inertia calibrated for the bridge model was greater than that calculated.

### **8.3 Calibration of the Simplified Finite Element Model to the Experimental Model**

As described in Chapter 4, the stiffness of the superstructure decreased considerably during the first experiment on the bridge model. Therefore different effective stiffnesses were assumed for the different cycles of loading in order to generate a backbone curve for the midspan translation and rotation which matched those from the simplified and detailed models. The resulting backbone curves are illustrated in Figures 8-2 and 8-3, and are shown to match the measured response well. The resulting effective moment of inertia and torsional moment of inertia for the bridge model, as loading was increased, are plotted in Figure 8-4. At the beginning of the experiment the deck slab was modeled with 40% of the gross section moment of inertia. This allows for initial shrinkage cracking and slippage in the connection between the deck slab and the girders. The moment of inertia degraded to a value of around 20% of the gross value after large lateral loads were applied which resulted in a deterioration of the bridge deck slab. The effective torsional moment of inertia started at 2.5 times the calculated values and degraded by a similar amount as the effective moment of inertia to 1.3 times the calculated torsional moment of inertia. The initial values were considered to be most likely to represent the properties of a typical bridge during an earthquake as large transverse loads caused the deck slab to be deformed repeatedly, at amplitudes in excess of those likely in a normal bridge during an earthquake.

For the second experiment a constant moment of inertia equal to 20% of the gross section moment of inertia and a torsional moment of inertia equal to the value 130% of the calculated value was assumed. For subsequent experiments, as the properties stabilized, the moment inertia was assumed to be 12% of the gross moment of inertia and a torsional moment of inertia of 130% of that calculated was used. All transverse deformation was assumed to be flexural with transverse shear deformations not considered. The torsional flexibility was shown to affect the effective period for the first mode of the bridge model by only 5% therefore a large nominal value could

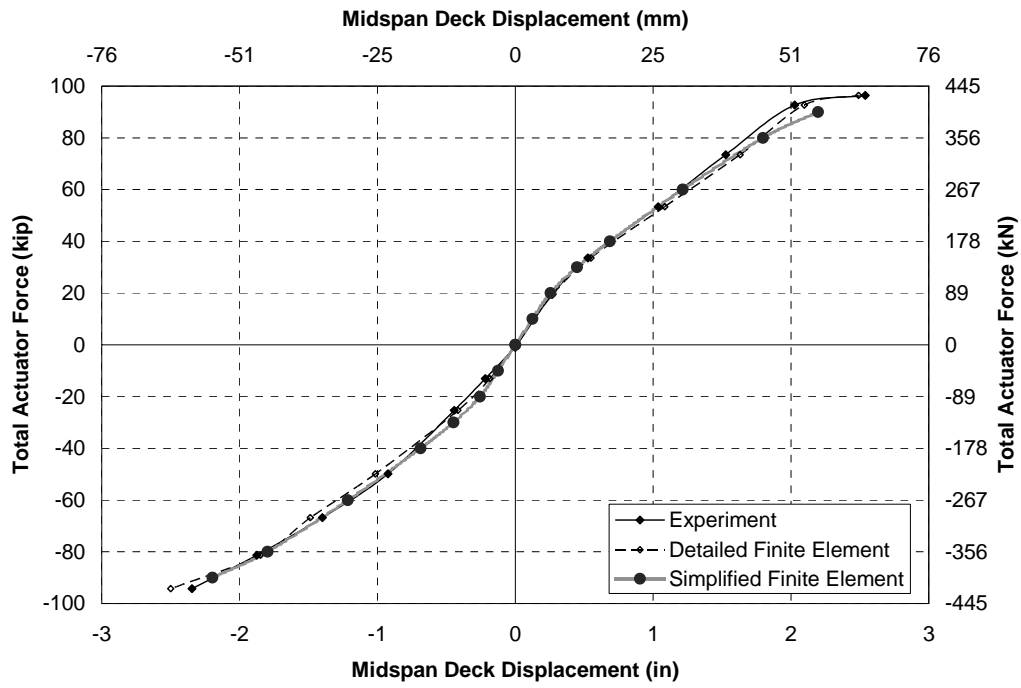


FIGURE 8-2 RSHXB1 - Backbone curve for displacement of deck slab at midspan

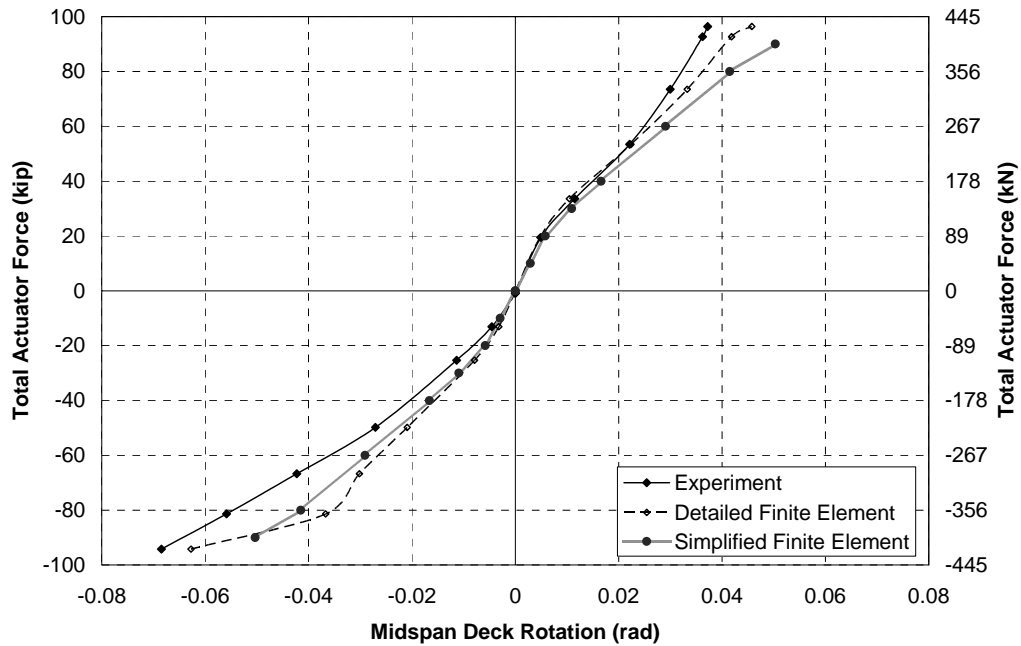
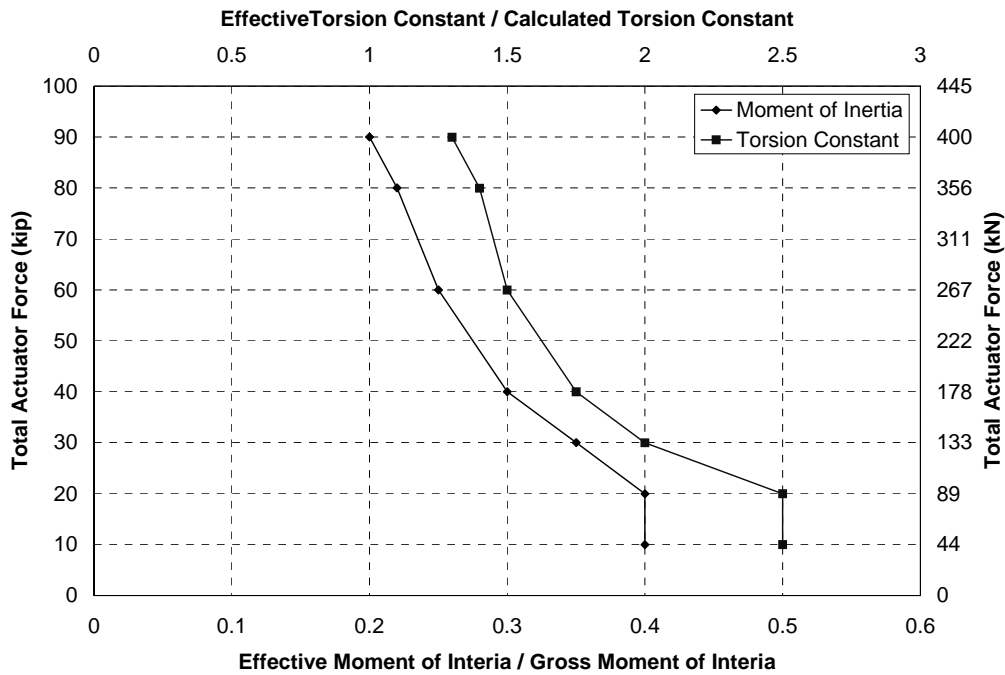


FIGURE 8-3 RSHXB1 - Backbone curve for rotation of superstructure at midspan



**FIGURE 8-4 RSHXB1 - Degradation in the effective moment of inertia and torsion constant for the bridge model during the first experiment**

have been assumed for the torsional moment of inertia with little change in dynamic behavior. The response of the bridge model during the different experiments is further compared to the analytical model in a subsequent report during parametric studies.

The properties of the end regions were modeled using the properties of the girders, shear studs and bearings developed in this chapter. Rigid links were used to distribute forces from the shear center and superstructure elements to the top flange of girders. A top chord was modeled as rigid in order to distribute forces between the top flanges of the girders and attach an element to model the transverse stiffness of the girder. A bottom chord was also modeled as axially rigid but with pin ended connections to compare with those in the bridge model. It was assumed that damage to the shear studs made one and two rows of studs ineffective at the south and north ends respectively during reversed static experiments. Three and four rows of studs were assumed to be ineffective at the south and north ends respectively during shake table experiments. Appropriate springs were modeled at the top of the girders to allow for the shear studs as calculated using the appropriate model from Table 6-2. The girder stiffness was modeled as a non-linear link element placed between the top and bottom chords able to deform in shear with a prescribed stiffness as based on the corresponding model in Table 6-2. The bearing stiffeners were assumed to have purely flexural behavior with deformations confined to the plane of the cross frames. The moment of inertia was calculated using Equation 4.1, as also given in Table 6-2 multiplied by the elastic modulus. The properties of the bearings were based on the design properties given in Appendices 1 and 2 for the elastomeric pads and lead rubber bearings respectively. For the transversely restrained bearings only the rotational stiffness was quantified with the transverse and axial stiffnesses assumed to be nominally high values. Assuming the design axial stiffness was shown

to result in minimal change in response, and consequently the added complexity of including it in the model was not warranted.

Damping was defined in the bridge model as Rayleigh damping with mass and stiffness proportional coefficients defined by 5% viscous damping at periods of 0.1 and 1.0s respectively. This resulted in equivalent viscous damping ranging between 3% and 7% for structural periods in the range of interest for the bridge model between 0.1 and 1.5 s. The Rayleigh damping was in addition to the hysteretic damping provided by the non-linear components in the end regions where appropriate.

The shear center for the bridge model was calculated to be 242 mm. above the deck slab of the bridge, for all models after the properties were assumed to have stabilized, and was shown to be close to the measured location from the detailed finite element model. Therefore the eccentricities in height between, the shear center and the load point for reversed static experiments, or the center of mass for shake table experiments, were determined (335 mm and 231 mm respectively).

The weight of the finite element model was assumed to be equal to the measured weight of the bridge model (341 kN) including added lead, as described in Chapter 2, lumped at the ends and five intermediate locations along the bridge model. It was located at a height 231 mm below the shear center of the bridge at the estimated height of the center of mass.

#### **8.4 Comparisons of Analytical Model with Detailed Finite Element Model**

Dynamic properties including the natural periods for the first three transverse modes and the value of  $\alpha$  to describe the mode shape of the first transverse mode of different configurations of the bridge model, based on the detailed finite element model, were given in Table 3-7. The mass modal participation factors for each of the corresponding modes were given in Table 3-8. Comparable dynamic properties for the analytical model are given in Tables 8-1 and 8-2. The natural period for the first and third modes are shown to compare well between the detailed and analytical models. However the second mode, that is the mode for which the bridge model “rocks” on the bearings as illustrated in Figures 3-41 and 3-42, is not present in the simplified finite model. This has little consequence in most of the models, particularly those which have relatively flexible end conditions, as the second mode has little associated modal mass as indicated in Table 3-8. For the models with relatively rigid end cross frames, the participation of the second mode is not trivial, however, for the systems used in this study in which the ends were designed to yield, the effective contribution of the second mode was expected to be small. Therefore, with the appropriate non-linear elements, the simplified model was expected to capture the non-linear response of the bridge model with reasonable accuracy.

This simplified model was used to simulate both reversed static and shake table experiments, with the properties of the model varied as necessary for the different configurations of the bridge model, as described in the subsequent report (Carden, 2005).

**TABLE 8-1 Natural Periods for Three Transverse Modes of Simplified Analytical Model**

Experiment Series	Natural Period (s)			Modeshape Alpha <sup>1</sup>
	Mode 1	Mode 2	Mode 3	
LRBs	0.58	-	0.15	0.48
LRBs (2 Span)	0.41	-	-	-
"Light" X-Braces	0.41	-	0.08	0.90
Unbonded Braces	0.40	-	0.07	0.95
Unbonded Braces (2 Span)	0.14	-	0.06	-
No End Cross Frames	0.74	-	0.17	0.29
"Heavy" X-Braces	0.40	-	0.07	0.96

Notes: 1. Alpha given for mode 1

2. The second mode was not captured by the analytical model.

**TABLE 8-2 Modal Mass Participation Factors for Three Transverse Modes of Simplified Analytical Model**

Experiment Series	Mass Participation Factor (%)			
	Mode 1	Mode 2	Mode 3	Sum
LRBs	100	-	0	100
LRBs (2 Span)	98	-	-	98
"Light" X-Braces	82	-	15	97
Unbonded Braces	79	-	13	92
Unbonded Braces (2 Span)	88	-	2	90
No End Cross Frames	98	-	1	99
"Heavy" X-Braces	79	-	12	91

Notes: 1. The second mode was not captured by the analytical model.



## SECTION 9 SUMMARY, CONCLUSIONS AND RECOMMENDATIONS

### 9.1 Summary

Past earthquakes showed that critical components in the transverse load path of a steel girder bridge superstructure need to be explicitly designed for seismic loads to ensure the desired performance is achieved. The experimental and analytical study described in this report identifies the critical components and quantifies the seismic actions to which they are subjected.

Section 2 describes prototype four and two girder bridges used to derive properties for a  $2/5$ th scale model of a two girder 18 m long bridge used in experiments. The properties of the bridge model are described as well as instrumentation and simulation of earthquake loading.

The transverse response of the bridge model was investigated during reversed static and shake table experiments in Chapter 3. While the end cross frames remained elastic, the deformation in the bridge model was largely due to flexural-torsional deformation along the span, with the shear center located above the deck slab of the bridge. When the end cross frames were removed the deformation was concentrated in the ends of the bridge. The response of the bridge model with no end cross frames was comparable to that of the isolated bridge model, highlighting the potential for using flexible ductile end cross frames to help protect a bridge from transverse earthquake excitation. Two span configurations resulted in a much higher superstructure stiffness with deformations concentrated more in the end cross frames or isolation system. Fourier analysis compared the measured bridge response with the finite element response and correlated well. Modal participation factors from the calibrated finite element analysis showed that for the isolated bridge model and bridge model with no end cross frames over 90% of the mass was concentrated in the first mode. For the bridge model with end cross frames, the second mode also made a large contribution. This is due to the axially flexible lead rubber bearings resulting in a “rocking” mode. With more flexible cross frames the first mode contribution increased, and as such, a design procedure based on the first mode deformation was expected to accurately capture the bridge response with ductile end cross frames. A sine sweep showed that the experimental properties of the isolated bridge model were close to the calculated properties although equivalent viscous damping was overestimated by the initial calculations.

Each component in the transverse seismic load path of the bridge model, except special ductile components, is investigated in Chapters 4 to 7. The flexural properties of the deck slab were critical in calculating the transverse stiffness of the bridge model. Effective stiffnesses for the deck slab as low as 15% of the gross slab stiffness were calculated for the bridge model based on a calibrated finite element analysis. The low stiffness can be explained as the bridge model was also subjected to much higher deck slab stresses than likely in most bridges during a seismic event, thereby causing extensive cracking and yielding of some of the deck slab reinforcement. However, even at low levels of transverse loading the deck slab stiffness was less than 50% of the gross deck stiffness. The level of composite action also played an important role in the response of the bridge. The simplified model was calibrated to the experimental data with an effective moment of inertia for the superstructure starting 40% of the calculated gross moment of inertia. This reduced to a level of 12% after several experiments. While the effective transverse moment of inertia was much lower than the gross value, the effective torsional moment of inertia was found to

be greater than that calculated using an assuming torsional moment of inertia for an open cross section. This was attributed to the effects of warping in the section.

Observed damage to the shear connectors at the ends of the bridge were explained by large concentrations of forces in the studs located above the supports, with transverse longitudinal and vertical forces observed in the studs. The composite top chord which connected the cross frames to the deck slab was seen to be effective in providing a transverse load path for forces from the deck slab into the end cross frames, which are shown in Chapter 5 to carry almost all of the transverse loading, with minimal forces in the intermediate cross frames.

In Chapter 6 equations are developed to quantify the lateral stiffness of the girders incorporating the effect of shear studs, bearings, stiffeners and girder properties. The deformation capacity of the girders was also calculated for consideration in designing ductile end cross frames. The level of estimated bending moments in the girders of the bridge model showed that the simply supported girder could withstand very large drifts of up to 18%. For the continuous girder configuration the drift level was reduced to around 6%, which is still likely to be greater than the allowable drift in a ductile end cross frame system. Removing the shear studs allowed the top of the girder to rotate relatively freely enabling these large drifts in the girders.

Chapter 7 shows that the bearings were subjected to axial loads, flexural and transverse shear actions. The elastomeric bearings were capable of accomodating the combined strain requirements from these actions. Rotations in the bearings during experiments with large girder drifts were within the allowable limits when the shear strains due to rotation were combined with the axial shear strains based on the AASHTO isolation guidelines. Axial forces in the bearings were found to be an important consideration because tensile forces were observed in the bearings under the most severe loading. The axial forces were higher than calculated based on equilibrium of the end region during dynamic loading and consequently, based on the data from this series of bridge experiments, an amplification factor of 2.0 is recommended in calculating the overturning moments. The calculated allowable forces based on maximum shear strains were shown to be conservative for bearings in the bridge model compared to measured forces.

Combining the properties of each of the critical components into an analytical model, described in Chapter 8, shows that the response of the bridge could be reasonably captured. As such, this model is used to simulate the response of the bridge with non-linear components (Carden, 2005).

## **9.2 Conclusions**

The conclusions from the study described in this report are:

- The transverse deformation of a steel girder bridge superstructure is described by a flexural and torsional mode, with the shear center located above the bridge deck.
- The deck slab stiffness is lower than the gross stiffness even at low levels of earthquake loading with the bridge model having a stiffness equal 40% of the gross stiffness reducing to 15% after a number of increasing amplitude loads.
- The number shear connectors between the deck slab and the girders affects the transverse stiffness of the superstructure.



- The shear studs at the ends are critical in transferring the transverse seismic forces from the deck slab into the steel superstructure. A top chord connecting the deck slab to the end cross frames was found to be effective in transferring these forces in the absence of sufficient studs on top of the girders. The shear studs near the ends of the girders also resist rotation at the top of the girders.
- The end cross frames at each support carry the majority of transverse loads with intermediate cross frames having minimal contribution.
- The region of the girders near the supports provide a significant contribution to the transverse stiffness to the end cross frames. The stiffness can be calculated by a simplified model that considers the connection between the deck slab and top flange, bearing stiffeners, rotational bearing stiffness and torsional girder stiffness. The girder stiffness is not critical in the elastic response of the cross frames but is critical in evaluating the performance of ductile end cross frames.
- With appropriate details at the support regions of the girders, including elimination of shear studs in localized regions, the girders can be designed for very large drifts in excess of 6% of the girder height.
- The bearings are also critical in the transverse load path, with axial, rotational and shear actions in the bearings.
  - Axial loads were attributed to overturning of the superstructure due to transverse loading, although, the measured axial loads were larger than calculated.
  - Rotational actions were due to deformation of the girders where large translations were allowed in the cross frames.
  - Shear forces were not evenly distributed between the bearings due to variation in the properties of the shear restraints.

### 9.3 Recommendations

As a result of studying the transverse load path of steel plate girder bridges, constructed from straight unskewed I-girders, the following is recommended:

- The stiffness of the superstructure is notably lower than the stiffness calculated from gross section properties. A transformed section using concrete properties of no more than 0.4 times the gross cross sectional properties should be considered in modelling the superstructure of a steel girder bridge.
- The shear connectors at the supports of a girder, within a length tentatively equal to the depth of the girder, should be designed to transfer the full end shear into the end cross frames. Alternatively, a top chord in end cross frames connected to the deck through shear connectors can be designed to transfer the shear into the end cross frames.
- The end cross frames should be designed to carry the full transverse end shear. The contribution of the intermediate cross frames can be neglected.

- The region of the girders near the supports should be considered in a ductile design of the end cross frames. This is discussed further in the second report (Carden, 2005).
- The bearings should be design for combined actions. As the dynamic axial loads on the bearings were larger than calculated, probably due to higher mode effects such as vertical or coupled torsional modes. Until further study can provide further insight into the dynamic effect of these forces, an amplification factor of 2.0 for the calculated axial loads is recommended. The rotational actions can be designed for based on the girder drift. The bearings or transverse restraints should also be designed to accomodate non-uniform transverse shear forces. This can be achieved through details with limited ductility and cross frames designed to redistribute the forces between bearings if necessary. Alternatively, the bearings could each be designed to carry the full end shear.

Further investigation of ductile components to reduce the elastic seismic demand in a steel girder bridge superstructure and further analysis and design provisions are investigated in a subsequent report (Carden, 2005).

## **SECTION 10 REFERENCES**

American Association of State Highway and Transportation Officials (AASHTO), (1996). *Standard Specifications for Highway Bridges*. AASHTO, Washington, DC.

American Association of State Highway and Transportation Officials (AASHTO), (1998). *AASHTO LRFD Bridge Design Specifications (Customary U.S. Units Second Ed.)*. AASHTO, Washington, DC.

American Association of State Highway and Transportation Officials (AASHTO), (1999). *Guide Specifications for Seismic Isolation Design, (Second Edition including 2000 Interim Revisions)*. AASHTO, Washington, DC.

American Concrete Institute (ACI), (2002). *Building Code Requirements for Structural Concrete (ACI 318-02) and Commentary (ACI318R-02)*. ACI, Farmington Hills, MN.

American Iron and Steel Institute (AISI), (1996). *Steel Bridge Bearing Selection and Design Guide - Highway Structures Design Handbook - Vol. II, Chap. 4*. AISI, Washington, DC.

American Institute of Steel Construction (AISC), (1997). *Manual of Steel Construction - Load Factor and Resistance Design, 2nd Edition*. AISC, Chicago, IL.

American Institute of Steel Construction (AISC), (2002). *Seismic Provisions for Structural Steel Buildings*. AISC, Chicago, IL.

Applied Technology Council (ATC), (1996). *ATC 32 - Improved Seismic Design Criteria for California Bridges: Provisional Recommendations*. ATC, Redwood City, CA.

Applied Technology Council (ATC), (1996). *ATC 32-1 - Improved Seismic Design Criteria for California Bridges: Resource Document*. ATC, Redwood City, CA.

Applied Technology Council (ATC), (1992). *ATC 24 - Guidelines for Cyclic Seismic Testing of Components of Steel Structures*. ATC, Redwood City, CA.

Applied Technology Council (ATC) / Multidisciplinary Center for Earthquake Engineering Research (MCEER), (2003). *Recommended LRFD Guidelines for Seismic Design of Highway Bridges (2 Volumes)*. Report ATC/MCEER 49 (joint venture), Redwood City, CA.

Astaneh-Asl, A., (1996). *Notes on the Cyclic Behavior and Design of Steel Bridges - Volume I - Response Modification Factor Based Design*. Report, American Iron and Steel Institute, Washington DC, November.

Astaneh-Asl, A., Bolt, B., McMullin, K.M., Donikian, R.R., Modjtahedi, D., and Cho, S., (1994). *Seismic Performance of Steel Bridges During the 1994 Northridge Earthquake*. Report UCB/CE-STEEL-94/01. Department of Civil and Environmental Engineering, University of California, Berkeley, CA.

Black, C., Makris, N., and Aiken, I., (2002). *Component Testing, Stability Analysis and Characterization of Buckling Restrained Unbonded Braces*<sup>TM</sup>. PEER Report 2002/08, Berkeley, CA, September.

Brockenbrough, R.L., and Johnston, B.G., (1968). *Steel Design Manual*. United States Steel Corporation, Pittsburgh, PA.

Bruneau, M., Wilson, J.W., and Tremblay, R., (1996). Performance of Steel Bridges during the 1995 Hyogoken-Nanbu (Kobe, Japan) Earthquake, *Canadian J. of Civil Engrg*, 23(3), 678-713.

California Department of Transportation (CALTRANS), (1992). *PEQIT Report - Highway Bridge Damage - Petrolia Earthquakes No. 1, No. 2, No. 3. of April 25-26, 1992*, California Department of Transportation, Sacramento, CA.

California Department of Transportation (CALTRANS), (1993). *Bridge Design Specifications*. California Department of Transportation, Sacramento, CA.

California Department of Transportation (CALTRANS), (2001). *Seismic Design Criteria (Version 1.2)*. CALTRANS, Sacramento, CA.

Carden, L.P., Itani, A.M., and Buckle, I.G., (2005). *Seismic Performance of Steel Girder Bridge Superstructures with Ductile End Cross Frames and Seismic Isolators*. Report CCEER 04-04, Center for Civil Engineering Earthquake Research, University of Nevada - Reno, Reno, NV.

Carden, L.P., Itani, A.M., and Buckle, I.G., (2002). Composite Action in Steel Girder Bridge Superstructures Subjected to Transverse Earthquake Loading. *Transportation Research Record*, 1814, (02-2455), 245-252.

Chopra, A.K., (1996). *Dynamics of Structures - Theory and Applications to Earthquake Engineering (2nd Edition)*. Prentice Hill, Upper Saddle River, NJ.

Chung, R. (Editor), (1996). *The January 17, 1995 Hyogoken-Nanbu (Kobe) Earthquake – Performance of Structures, Lifelines, and Fire Protection Systems*. NIST Special Publication 901. Building and Fire Research Laboratory, National Institute of Standards and Technology. Gaithersburg, MD.

Clark, P.W., Aiken, I.D., Tajirian, F.F., Kasai, K., Ko, E., Kimura, I., (1999). Design Procedures for Buildings Incorporating Hysteretic Damping Devices. *International Post-SMiRT Conference Seminar on Seismic Isolation, Passive Energy Dissipation and Active Control of Vibrations of Structures*, Cheju, Korea, August 23-25.

Computers and Structures, Inc., (2003). *SAP2000 Nonlinear (Version 8.3.0): Structural Analysis Program*. Computers and Structures, Inc. Berkeley, CA.

Earthquake Engineering Research Institute (EERI), (2001). *The Nisqually, Washington, Earthquake February 28, Preliminary Reconnaissance Report*. Report EERI 2001-01. Earthquake Engineering Research Institute, Oakland, CA.

EduPro Civil Systems, (1999). *EduShake (Version 1.10)*. EduPro Civil Systems, Inc., Redmond, WA. <http://www.proshake.com>.

Garcia-Alvarez, F., (2001). *Cyclic Behavior of Cross-Frames in Steel Plate Girder Bridges*. M.S. Thesis. University of Nevada, Reno, Reno, NV.

Gattesco, N., and Giuriani, E., (1996). Experimental Study on Stud Shear Connectors Subjected to Cyclic Loading. *J. of Construct. Steel Res.*, 38(1), 1-21.

Hawkins, N.M. and Mitchell, D., (1984). Seismic Response of Composite Shear Connections. *J. of Struct. Engrg.*, 110(1984), 2120-2136.

Itani, A.M., and Rimal, P.P., (1996). Seismic Analysis and Design of Modern Steel Highway Connectors. *Earthquake Spectra*, 12(2) 275-296.

Itani, A.M. and Sedarat, H., (2000). Seismic Analysis and Design of the AISI LRFD Design Examples for Steel Highway Bridges. CCEER Report 00-8, University of Nevada, Reno, November.

Johnson, R.P., and May, I.M., (1975). Partial-interaction Design of Composite Beams. *Struct. Engineer*, 53(8), 305-311.

McMullin, K.M. and Astaneh-Asl, A., (1994). Cyclic Behavior of Welded Shear Studs. *Proc. of Structures Congress XII*, Atlanta, GA. April 24-28.

Malaysian Rubber Producers' Research Association, (1979). *Natural Rubber Engineering Data Sheet (EDS 23)*. Malaysian Rubber Research and Development Board Organization, England.

Mori, A., Moss, P.J., Cooke, N., and Carr, A.J., (1999). The Behavior of Bearings used for Seismic Isolation under Rotation and Axial Load. *Earthquake Spectra*, 15(2), 225-244.

Mertz, D. P., (2001). *Designer's Guide to Cross-Frame Diaphragms*. American Iron and Steel Institute, Washington, DC. [www.steel.org/infrastructure/bridges](http://www.steel.org/infrastructure/bridges).

Oehlers, D.J. and Coughlan, C.G., (1986). The Shear Stiffness of Stud Shear Connections in Composite Beams. *J. of Construct. Steel Research*, 6, 273-284.

Pacific Center for Earthquake Engineering Research (PEER) Strong Motion Database, (2002). Website: <http://peer.berkeley.edu/smcat/>

Priestley, M. J. N., F. Seible, and G. M. Calvi, (1996). *Seismic Design and Retrofit of Highway Bridges*, John Wiley and Sons, Inc., New York.

Public Works Research Institute (PWRI)/Civil Engineering Research Laboratory (CRL), (2002). *Japan Road Association Specifications for Highway Bridges - Part V Seismic Design (Preliminary English Version)*. PWRI, Ibaraki-Ken/CRL Tokyo, Japan, November.

Reinhorn, A.M., Bracci, J. and Pekhan, G., (2001). *Design of Six Axes Load Cell*. Personal Communication.

Seracino, R., Oehlers, D.J. and Yeo, M.F., (2001). Partial-interaction Flexural Stresses in Composite Steel and Concrete Bridge Beams. *Engrg. Structures*, 23(2001), 1186-1193.

Shinozuka, M.(ed), Ballantyne, D., Borchardt, R., Buckle, I., O'Rourke, T., and Schiff, A., (1995). *The Hanshin-Awaji Earthquake of January 17, 1995 Performance of Lifelines*. Technical Report NCEER-95-0015, National Center for Earthquake Engineering Research, Buffalo, New York.

TRW Nelson Division, (1977). *Embedment Properties of Headed Studs*. TRW Nelson Division, Elyria, Ohio.

TRW Nelson Division, (1988). *Nelson – Standard In-Shock Studs Brochure*. TRW Nelson Division, Elyria, Ohio.

Wang, Y.C., (1998). Deflection of Steel-Concrete Composite Beams with Partial Shear Interaction. *J. of Struct. Engrg.*, 124(10), 1159-1165.

Washington State Department of Transportation (WSDOT), (2001). Photos of Damage During the 2001 Nisqually Earthquake. *Personal communication*.

Wright, H.D., (1990). The Deformation of Composite Beams with Discrete Flexible Connection. *J. of Construct. Steel Research*, 15, 49-64.

Yamaguchi, T., Nakata, Y., Takeuchi, T., Ikebe, T., Nagao, T., Minami, A., Suzuki, T., (1998). *Seismic Control Devices using Low-Yield Point Steel*. Nippon Steel Technical Report, No. 77, July. Tokyo, Japan.

Zahrai, S. M., and Bruneau, M., (1998). Impact of Diaphragms on Seismic Response of Straight Slab-on-Girder Steel Bridges, *J. of Struct. Engrg.*, 124(8), 938-947.

Zahrai, S. M., and Bruneau, M., (1999). Cyclic Testing of Ductile End-Diaphragms for Slab-on-Girder Steel Bridges, *J. of Struct. Engrg.*, 125(9), 987-996.

**APPENDIX A. PROPERTIES OF ELASTOMERIC BEARINGS IN BRIDGE  
MODEL**

## Bearing Properties

A summary of the bearing properties are described below.

Rubber properties:

$$\begin{array}{lll} G = 860 & \text{kPa} & \\ E = 4 \cdot G & E = 3440 & \text{kPa} \quad \text{Typical (AASHTO 1999)} \\ & k_{\text{bar}} = 0.65 & \text{From Natural Rubber Bulletin} \\ & & \text{(Malaysian 1979)} \end{array}$$

Rubber layers, there are two different rubber layer thicknesses:

$$\begin{array}{ll} t_{i1} = 6 & \text{mm} \\ n_{r1} = 2 & \\ t_{i2} = 13 & \text{mm} \\ n_{r2} = 1 & \\ T_{r1} = t_{i1} \cdot n_{r1} & T_{r1} = 12 \quad \text{in} \\ T_{r2} = t_{i2} \cdot n_{r2} & T_{r2} = 13 \quad \text{in} \end{array}$$

Shims and top and bottom embedded plates:

$$\begin{array}{ll} t_s = 1.5 & \text{mm} \\ T_s = 2 \cdot t_s & T_s = 3 \quad \text{mm} \end{array}$$

Total height:

$$H = T_{r1} + T_{r2} + T_s \quad H = 28 \quad \text{mm}$$

Length and width:

$$B_{b1} = 279 \quad \text{mm}$$

$$B_{b2} = 184 \quad \text{mm}$$

Area of bearing:

$$A_b = B_{b1} \cdot B_{b2} \quad A_b = 51336 \quad \text{mm}^2$$

The bonded area is approximately equal to the total area of the bearing.

$$A_t = A_b \quad A_t = 51336 \quad \text{mm}^2$$

$$B_{t1} = B_{b1} \quad B_{t1} = 279 \quad \text{mm}$$

$$B_{t2} = B_{b2} \quad B_{t2} = 184 \quad \text{mm}$$



## Stiffness Properties

Axial

$$S_1 = \frac{A_b}{2 \cdot (B_{b1} + B_{b2}) \cdot t_{i1}} \quad S_1 = 9.24$$

$$S_2 = \frac{A_b}{2 \cdot (B_{b1} + B_{b2}) \cdot t_{i2}} \quad S_2 = 4.264$$

$$E_1 = E \cdot (1 + 2 \cdot k_{\text{bar}} \cdot S_1^2) \quad E_1 = 385227 \quad \text{kPa}$$

$$E_2 = E \cdot (1 + 2 \cdot k_{\text{bar}} \cdot S_2^2) \quad E_2 = 84767 \quad \text{kPa}$$

$$k_a = \frac{10^{-6}}{\frac{T_{r1}}{E_1 \cdot A_t} + \frac{T_{r2}}{E_2 \cdot A_t}} \quad k_a = 278 \quad \text{kN/mm}$$

Shear

$$k_s = \frac{G \cdot A_t \cdot 10^{-6}}{T_{r1} + T_{r2}} \quad k_s = 1.77 \quad \text{kN/mm}$$

Rotation

$$f_{b1} = 1 + 0.74 \cdot S_1^2 \quad f_{b1} = 64.2$$

$$f_{b2} = 1 + 0.74 \cdot S_2^2 \quad f_{b2} = 14.5$$

$$E_{b1} = E \cdot f_{b1} \quad E_{b1} = 220765 \quad \text{kPa}$$

$$E_{b2} = E \cdot f_{b2} \quad E_{b2} = 49734 \quad \text{kPa}$$

$$I_{by} = \frac{B_{t1} \cdot B_{t2}^3}{12} \quad I_{by} = 1.45 \times 10^8 \quad \text{mm}^4 \quad \text{Used total bearing width to calculate I}$$

$$k_{\theta by} = \frac{10^{-9}}{\frac{T_{r1}}{E_{b1} \cdot I_{by}} + \frac{T_{r2}}{E_{b2} \cdot I_{by}}} \quad k_{\theta by} = 459 \quad \text{kNm}$$

### Axial Strain due to Dead Load

Check the bearing strains for axial loads:

$$P_b = 33.4 \quad \text{kN}$$

$$A_r = A_b$$

$$A_r = 51336 \quad \text{mm}^2$$

$$\gamma_{c1} = \frac{3 \cdot S_1 \cdot P_b \cdot 10^6}{2 \cdot A_r \cdot G \cdot (1 + 2 \cdot k_{\text{bar}} \cdot S_1^2)}$$

$$\gamma_{c1} = 0.094$$

$$\gamma_{c2} = \frac{3 \cdot S_2 \cdot P_b \cdot 10^6}{2 \cdot A_r \cdot G \cdot (1 + 2 \cdot k_{\text{bar}} \cdot S_2^2)}$$

$$\gamma_{c2} = 0.196$$

Strain limit:

$$\gamma_c < 2.5$$

OK for dead load

**APPENDIX B. PROPERTIES OF LEAD RUBBER BEARINGS FOR BRIDGE  
MODEL**

## Bearing Properties

A summary of the bearing properties are described below.

Rubber properties:

$$G = 430 \quad \text{kPa}$$

$$E = 4 \cdot G$$

$$E = 1720 \quad \text{kPa}$$

Typical (AASHTO 1999)

$$k_{\text{bar}} = 0.86$$

From Natural Rubber Bulletin  
(Malaysian 1979)

Rubber layers:

$$t_i = 6.0 \quad \text{mm}$$

$$n_r = 10$$

$$T_r = t_i \cdot n_r$$

$$T_r = 60 \quad \text{mm}$$

Shims and top and bottom embedded plates:

$$t_s = 3.0 \quad \text{mm}$$

$$T_s = (n_r - 1) \cdot t_s$$

$$T_s = 27 \quad \text{mm}$$

$$t_p = 13 \quad \text{mm}$$

Total height:

$$H = T_r + (n_r - 1) \cdot t_s + 2 \cdot t_p$$

$$H = 113 \quad \text{mm}$$

Total rubber diameter including cover:

$$B_t = 178 \quad \text{mm}$$

Thickness of cover:

$$t_c = 13 \quad \text{mm}$$

Bonded width:

$$B_b = B_t - 2 \cdot t_c$$

$$B_b = 152 \quad \text{mm}$$

Total and bonded areas:

$$A_t = \frac{\pi \cdot B_t^2}{4}$$

$$A_t = 24885 \quad \text{mm}^2$$

$$A_b = \frac{\pi \cdot B_b^2}{4}$$

$$A_b = 18146 \quad \text{mm}^2$$

Lead core diameter:

$$B_c = 38 \quad \text{mm}$$

Check limits on diameter:

$$B_c > \frac{B_t}{6} \quad B_c < \frac{B_t}{3} \quad \text{Limits OK}$$

Core area:

$$A_c = \frac{\pi \cdot B_c^2}{4} \quad A_c = 1134 \quad \text{mm}^2$$

Total bearing area excluding the core:

$$A_i = A_t - A_c \quad A_i = 23750 \quad \text{mm}^2$$

Shear modulus of lead:

$$G_l = 130 \cdot 10^3 \quad \text{kPa}$$

Yield strength of lead:

$$\tau_y = 9.7 \cdot 10^3 \quad \text{kPa (Buckle 1978)}$$

### Seismic Response

The seismic response of the bearings is calculated for the following seismic demand.

Acceleration and site coefficients:

$$S = 1.5 \quad (\text{AASHTO 1999})$$

$$A = 0.4$$

Average axial load on bearing:

$$W_i = 89 \quad \text{kN/bearing}$$

Calculated bi-linear properties:

$$k_s = \frac{G \cdot A_i}{T_r} \cdot 10^{-6} \quad k_s = 0.170 \quad \text{kN/mm}$$

$$k_l = \frac{G_l \cdot A_c}{(T_r + T_s)} \cdot 10^{-6} \quad k_l = 1.695 \quad \text{kN/mm}$$

$$k_{di} = k_s \quad k_{di} = 0.17 \quad \text{kN/mm}$$

$$k_u = k_l + k_s \quad k_u = 1.86 \quad \text{kN/mm}$$

$$F_y = \tau_y \cdot A_c \cdot 10^{-6} \quad F_y = 11.0 \quad \text{kN}$$

$$Q_{di} = F_y \cdot \left( 1 - \frac{k_{di}}{k_u} \right) \quad Q_{di} = 10.0 \quad \text{kN}$$

Response of isolation system:

$$\text{Estimate} \quad d_i = 53 \quad \text{mm}$$

$$F_d = Q_{di} + k_{di} \cdot d_i \quad F_d = 19.0 \quad \text{kN}$$

$$k_{effi} = \frac{F_d}{d_i} \quad k_{effi} = 0.359 \quad \text{kN/mm}$$

$$g = 9.81 \quad \text{m/s}^2$$

$$T_{eff} = 2 \cdot \pi \cdot \sqrt{\frac{W_i}{g \cdot k_{effi} \cdot 10^3}} \quad T_{eff} = 1.00 \quad \text{s}$$

$$\beta_i = \frac{2 \cdot Q_{di}}{\pi \cdot F_d} \quad \beta_i = 0.335$$

$$B = 1.77$$

$$d_i = \frac{157 \cdot A \cdot S \cdot T_{eff}}{B} \quad d_i = 53 \quad \text{mm}$$

Final calculated displacement matches the initial displacement estimate for final iteration. The effect of torsion in the bridge is not considered.

### Buckling and Rollover

The calculated critical buckling load, following procedure by Buckle (2002), is:

$$S = \frac{A_b}{\pi \cdot B_b \cdot t_i} \quad S = 6.33$$

$$R = k_s \cdot H \quad R = 19.2 \quad \text{kN}$$

$$f_b = 1 + 0.67 \cdot S^2 \quad f_b = 27.87$$

$$E_b = E \cdot f_b \quad E_b = 4.79 \times 10^4 \quad \text{kPa}$$

$$I_b = \frac{\pi \cdot B_t^4}{64} \quad I_b = 4.9 \times 10^7 \quad \text{mm}^4$$

assuming the total bearing width.

$$k_{\theta b} = \frac{E_b \cdot I_b}{T_r} \cdot 10^{-9} \quad k_{\theta b} = 39.4 \quad \text{kNm} \quad 3 \cdot k_{\theta b} = 118 \quad \text{kNm}$$

$$T = k_{\theta b} \cdot H \cdot 10^{-3} \quad T = 4.45 \quad \text{kN/m}^2$$

$$P_e = \frac{\pi^2 \cdot T}{H^2} \cdot 10^6 \quad P_e = 3439 \quad \text{kN}$$

$$P_{cro} = \sqrt{R \cdot P_e} \quad P_{cro} = 257 \quad \text{kN}$$

This is the critical buckling load for an undisplaced bearing.

Check critical buckling load at 1.5 x design displacement:

$$d_{i,max} = 1.5d_i \quad d_{i,max} = 80 \quad \text{mm}$$

$$\delta = 2 \cdot \arccos\left(\frac{d_{i,max}}{B_b}\right) \quad \delta = 2.037$$

$$A_r = \frac{B_b^2}{4} \cdot (\delta - \sin(\delta)) \quad A_r = 6605 \quad \text{mm}^2$$

$$\frac{A_r}{A_b} = 0.364$$

$$P_{cr} = \frac{A_r}{A_b} \cdot P_{cro} \quad P_{cr} = 93.6 \quad \text{kN}$$

This is the critical buckling load for at 1.5 times the design displacement. The average axial load applied to the bearings is:

$$P_{b,ave} = W_i \quad P_{b,ave} = 89 \quad \text{kip}$$

Therefore applied axial load is just less than calculated buckling load and bearing is OK for buckling.

Bearing should be OK for rollover as the plates are fully vulcanised to the rubber.

### Bearing Rubber Strains

Shear strain due to shear deformation at design displacement (AASHTO 1999):

$$\gamma_{s.eq} = \frac{d_i}{T_r} \quad \gamma_{s.eq} = 0.886$$

Shear strain due to axial load at zero displacement:

$$A_r = A_b \quad A_r = 18146 \quad \text{mm}^2$$

$$\gamma_{c1} = \frac{3 \cdot S \cdot P_{b.ave} \cdot 10^6}{2 \cdot A_r \cdot G \cdot (1 + 2 \cdot k_{bar} \cdot S^2)} \quad \gamma_{c1} = 1.55$$

Axial strain at design displacement:

$$h_{eff} = 33.5 \quad h_{eff} = 33.5 \quad \text{mm}$$

$$s_g = 52.83 \quad s_g = 52.8 \quad \text{mm}$$

$$P_{b.max} = W_i + 2 \cdot F_d \cdot \frac{h_{eff}}{s_g} \quad P_{b.max} = 113 \quad \text{kN}$$

$$\delta = 2 \cdot \arccos\left(\frac{d_i}{B_b}\right) \quad \delta = 2.43$$

$$A_r = \frac{B_b^2}{4} \cdot (\delta - \sin(\delta)) \quad A_r = 10232 \quad \text{mm}^2$$

$$\gamma_{c2} = \frac{3 \cdot S \cdot P_{b.max} \cdot 10^6}{2 \cdot A_r \cdot G \cdot (1 + 2 \cdot k_{bar} \cdot S^2)} \quad \gamma_{c2} = 3.49$$

Rotational strain:

$$\gamma_r = 0$$

Strain limits:

$$\gamma_c < 2.5 \quad \gamma_{c1} = 1.55 \quad \text{OK for zero displacement}$$

$$\gamma_{c2} = 3.49 \quad \text{Violated}$$

Note that this limit is violated by the axial strain at the design transverse displacement. This suggests that instability is possible. However, the previous buckling analysis shows that the bearing was stable for buckling in excess of 1.5 times the design displacement, therefore the strain limit appears conservative when a lateral displacement is considered.

$$\gamma_c + \gamma_{s.eq} + 0.5\gamma_r < 5.5 \quad \gamma_{c2} + \gamma_{s.eq} + 0.5\gamma_r = 4.376 \quad \text{OK}$$



**APPENDIX C. LIST OF SHAKE TABLE SIMULATIONS**

Test Record - Shake Table Expts. on Bridge Model with LRBs									
No.	Time	Level	Earthquake	Comp.	Excitation - Long/Trans			Notes	
					Table1	Table2	Table3		
<b>Lead Rubber Bearings - Single Span - 12/03/02</b>									
1	11:45	1.0	White Noise	long	x		x	Not Recorded	
2	11:52	1.0	White Noise	trans	x		x		
3	11:56	1.0	White Noise	bi	x		x		
4	2:02	0.25	EI Centro	long	NS		NS		
5	2:04	0.25	EI Centro	long	NS		NS		
6	2:11	0.25	EI Centro	trans	NS		NS		
7	2:14	0.5	EI Centro	long	NS		NS		
8	2:16	0.5	EI Centro	trans	NS		NS		
9	2:22	0.75	EI Centro	long	NS		NS		
10	2:24	0.75	EI Centro	trans	NS		NS		
11	2:27	1.0	EI Centro	long	NS		NS		
12	2:30	1.0	EI Centro	trans	NS		NS		
13	2:49	1.0	EI Centro	long	Soil		Soil		
14	2:52	1.0	EI Centro	trans	Soil		Soil		
15	2:59	1.0	EI Centro	bi	NS/EW		NS/EW		
16	3:01	1.0	EI Centro	bi	EW/NS		EW/NS		
17	3:04	1.0	EI Centro	long	NS		Soil		
18	3:07	1.0	EI Centro	trans	NS		Soil		
19	3:14	1.0	EI Centro	long	Soil		NS		
20	3:17	1.0	EI Centro	trans	Soil		NS		
21	3:22	1.0	White Noise	long	x		x		
22	3:31	1.0	White Noise	trans	x		x		
23	3:34	1.0	White Noise	bi	x		x		
24	3:38	2.0	White Noise	trans	x		x		
25	4:15	4.0	White Noise	bi	x		x		Pump shutdown - disregard data
26	4:20	4.0	White Noise	bi	x		x		0.33-30 Hz - Magnitude in g
27	4:44	0.025	Sinesweep	trans	x		x		
28	4:46	0.05	Sinesweep	trans	x		x		
29	4:48	0.075	Sinesweep	trans	x		x		
30	4:50	0.1	Sinesweep	trans	x		x		
31	4:54	0.1	Sinesweep	trans	x		x		
32	4:57	0.15	Sinesweep	trans	x		x		
<b>Lead Rubber Bearings - Single Span - 12/04/02</b>									
33	10:19	1.25	EI Centro	long	NS		NS	Pump Shutdown - disregard data	
34	10:21	1.25	EI Centro	trans	NS		NS		
35	10:32	1.5	EI Centro	long	NS		NS		
36	10:35		EI Centro	trans	NS		NS		
37	10:40	1.75	EI Centro	long	NS		NS		
38	10:42	1.75	EI Centro	trans	NS		NS		
39	10:44	2.0	EI Centro	long	NS		NS		
40	10:46	2.0	EI Centro	trans	NS		NS		
41	11:04	1.5	EI Centro	long	Soil		Soil		
42	11:09	1.5	EI Centro	trans	Soil		Soil		
43	11:11	2.0	EI Centro	bi	NS/EW		NS/EW		
44	11:25	2.0	EI Centro	bi	NS/EW		NS/EW		

Test Record - Shake Table Expts. on Bridge Model with LRBs								
No.	Time	Level	Earthquake	Comp.	Excitation - Long/Trans			Notes
					Table1	Table2	Table3	
45	11:28	2.0	El Centro	bi	EW/NS		EW/NS	Buckling of bearing observed
46	11:31	2.0	El Centro	long	NS		Soil	
47	12:18	1.0	White Noise	long	x		x	
48	12:20	1.0	White Noise	trans	x		x	Buckling again observed
49	2:35	1.5	El Centro	long	NS		Soil	
50	3:39	0.25	Sylmar	long	NS		NS	
51	3:42	0.25	Sylmar	trans	NS		NS	
52	3:45	0.25	Sylmar	bi	NS/EW		NS/EW	
53	3:48	0.5	Sylmar	long	NS		NS	
54	3:50	0.5	Sylmar	trans	NS		NS	
55	3:52	0.25	Kobe	long	NS		NS	
56	3:56	0.25	Kobe	trans	NS		NS	
57	3:58	0.5	Kobe	long	NS		NS	
58	4:00	0.5	Kobe	trans	NS		NS	

Test Record - Shake Table Expts. on 2 Span Bridge Model with LRBs								
No.	Time	Level	Earthquake	Comp.	Excitation - Long/Trans			Notes
					Table1	Table2	Table3	
<b>Lead Rubber Bearings - 2 Span - 12/05/02</b>								
1	10:55	1.0	White Noise	long	x	x	x	
2	10:57	1.0	White Noise	trans	x	x	x	
3	11:00	1.0	White Noise	bi	x	x	x	
4	11:02	0.5	EI Centro	long	NS	NS	NS	
5	11:12	0.5	EI Centro	trans	NS	NS	NS	
6	11:15	1.0	EI Centro	long	NS	NS	NS	
7	11:18	1.0	EI Centro	trans	NS	NS	NS	
8	11:33	1.0	EI Centro	long	Soil	Soil	Soil	
9	11:40	1.0	EI Centro	trans	Soil	Soil	Soil	
10	11:48	1.0	EI Centro	bi	NS/EW	NS/EW	NS/EW	
11	11:51	1.0	EI Centro	bi	EW/NS	EW/NS	EW/NS	
12	11:53	1.0	EI Centro	long	NS	NS	Soil	
13	11:57	0.5	EI Centro	long	NS	Soil	NS	
14	12:02	0.5	EI Centro	trans	NS	NS	Soil	
15	12:05	0.5	EI Centro	trans	NS	Soil	NS	
16	12:09	0.5	EI Centro	long	NS	NS	Soil	
17	12:11	1.0	White Noise	long	x	x	x	
18	12:13	1.0	White Noise	trans	x	x	x	
19	12:15	1.0	White Noise	bi	x	x	x	
20	12:20	1.5	EI Centro	long	NS	NS	NS	
21	12:22	1.5	EI Centro	trans	NS	NS	NS	
22	12:24	2.0	EI Centro	long	NS	NS	NS	
23	12:26	2.0	EI Centro	trans	NS	NS	NS	
24	12:28	2.0	EI Centro	bi	NS/EW	NS/EW	NS/EW	
25	12:32	1.5	EI Centro	long	Soil	Soil	Soil	
26	12:36	0.5	Kobe	long	NS	NS	NS	
27	12:38	0.5	Kobe	trans	NS	NS	NS	
28	12:41	0.5	Sylmar	long	NS	NS	NS	
29	12:43	0.5	Sylmar	trans	NS	NS	NS	
30	12:46	0.5	Kobe	bi	NS/EW	NS/EW	NS/EW	
31	12:50	0.5	Sylmar	bi	NS/EW	NS/EW	NS/EW	
32	12:53	0.75	Kobe	long	NS	NS	NS	
33	12:55	0.75	Kobe	trans	NS	NS	NS	
34	12:57	0.75	Sylmar	long	NS	NS	NS	
35	12:59	0.75	Sylmar	trans	NS	NS	NS	
36	1:01	0.75	Kobe	bi	NS/EW	NS/EW	NS/EW	
37	1:03	0.75	Sylmar	bi	NS/EW	NS/EW	NS/EW	
38	2:27	0.75	Kobe	bi	NS/EW	NS/EW	NS/EW	
39	5:01	1.0	Kobe	long	NS	NS	NS	
40	5:07	1.0	Kobe	trans	NS	NS	NS	
41	5:11	1.0	Kobe	long	EW	EW	EW	
42	5:14	1.0	Kobe	trans	EW	EW	EW	
43	5:16	1.0	Kobe	bi	NS/EW	NS/EW	NS/EW	
44	5:19	1.0	Sylmar	long	NS	NS	NS	
45	5:21	1.0	Sylmar	trans	NS	NS	NS	
46	5:23	1.0	Sylmar	long	EW	EW	EW	
47	5:25	1.0	Sylmar	trans	EW	EW	EW	
48	5:27	1.0	Sylmar	bi	NS/EW	NS/EW	NS/EW	

Test Record - Shake Table Expts. on Bridge Model with Single Angle XFs								
No.	Time	Level	Earthquake	Comp.	Excitation - Long/Trans			Notes
					Table1	Table2	Table3	
<b>Single Angle Cross Frames - 12/13/02</b>								
1	1:58	0.25	El Centro	trans	NS		NS	Repeated  Buckling observed in X-braces
2	2:03	0.5	El Centro	trans	NS		NS	
3	2:05	0.75	El Centro	trans	NS		NS	
4	2:35	0.75	El Centro	trans	NS		NS	
5	2:45	1.0	El Centro	trans	NS		NS	
6	3:19	1.25	El Centro	trans	NS		NS	
7	3:32	1.5	El Centro	trans	NS		NS	
8	3:47	1.0	White Noise	trans	x		x	
9	3:50	1.8	El Centro	trans	NS		NS	
10	3:55	2.0	El Centro	trans	NS		NS	
11	4:00	1.0	White Noise	trans	x		x	

Test Record - Shake Table Expts. on Bridge Model with Unbonded Brace								
No.	Time	Level	Earthquake	Comp.	Excitation - Long/Trans			Notes
					Table1	Table2	Table3	
<b>Single Span Unbonded Braces Composite Action - 12/20/02</b>								
1	10:20	1.0	White Noise	trans	x		x	Load Cells and Displacements rezerod
2	10:23	0.25	El Centro	trans	NS		NS	Incorrect label in Labview
3	10:26	0.5	El Centro	trans	NS		NS	
<b>Single Span Unbonded Braces Composite Action Removed - 12/23/02</b>								
4	10:10	1.0	White Noise	trans	x		x	Video times not correct for following
5	10:19	0.25	El Centro	trans	NS		NS	
6	10:22	0.5	El Centro	trans	NS		NS	
7	10:24	0.75	El Centro	trans	NS		NS	
8	10:27	1.0	El Centro	trans	NS		NS	
9	10:29	1.0	White Noise	trans	x		x	
10	10:33	1.25	El Centro	trans	NS		NS	Wrong header in Labview
11	11:29	1.5	El Centro	trans	NS		NS	
12	10:31	1.0	White Noise	trans	x		x	
13	11:34	1.75	El Centro	trans	NS		NS	
14	11:59	2.0	El Centro	trans	NS		NS	
15	12:23	1.0	White Noise	trans	x		x	
16	12:27	2.25	El Centro	trans	NS		NS	
17	3:35	2.25	El Centro	trans	NS		NS	Shims welded, bolts checked and tightened
<b>Single Span Unbonded Braces Composite Action Removed Connections Welded- 12/24/02</b>								
18	9:30	2.25	El Centro	trans	NS		NS	Inadequate weld quality - Welds fractured at South end
<b>Single Span Unbonded Braces Composite Action Removed Connections Welded- 12/27/02</b>								
19	11:26	1.0	White Noise	trans	x		x	No weld fracture observed
20	11:29	2.0	El Centro	trans	NS		NS	
21	11:39	2.25	El Centro	trans	NS		NS	
22	11:42	2.5	El Centro	trans	NS		NS	
23	11:49	1	Kobe	trans	NS		NS	
24	11:53	1	Sylmar	trans	NS		NS	
25	11:57	1	White Noise	trans	x		x	

Test Record - Shake Table Expts. On 2 Span Bridge Model with UB								
No.	Time	Level	Earthquake	Comp.	Excitation - Long/Trans			Notes
					Table1	Table2	Table3	
<b>2 Span Unbonded Braces Composite Action Removed- 12/27/02</b>								
1	3:03	1.0	White Noise	trans	x	x	x	Incorrect header in Labview
2	3:05	0.25	El Centro	trans	NS	NS	NS	
3	3:07	0.5	El Centro	trans	NS	NS	NS	
4	3:09	0.75	El Centro	trans	NS	NS	NS	
5	3:12	1.0	El Centro	trans	NS	NS	NS	
6	3:13	1.0	White Noise	trans	x	x	x	
7	3:16	1.25	El Centro	trans	NS	NS	NS	
8	3:18	1.5	El Centro	trans	NS	NS	NS	
9	3:22	1.75	El Centro	trans	NS	NS	NS	
10	3:25	2.0	El Centro	trans	NS	NS	NS	
11	3:33	1.0	White Noise	trans	x	x	x	
12	3:36	2.25	El Centro	trans	NS	NS	NS	
13	3:39	2.5	El Centro	trans	NS	NS	NS	
14	3:55	1.0	Kobe	trans	NS	NS	NS	
15	4:00	1.0	Sylmar	trans	NS	NS	NS	
16	4:03	1.0	White Noise	trans	x	x	x	
17	4:07	1.25	Kobe	trans	NS	NS	NS	
18	4:10	1.5	Kobe	trans	NS	NS	NS	

Test Record - Shake Table Expts. on Bridge Model with No End X Frames									
No.	Time	Level	Earthquake	Comp.	Excitation - Long/Trans			Video	Notes
					Table1	Table2	Table3		
<b>No Cross Frames - Single Span - 08/05/02</b>									
1	4:13	1.0	White Noise	trans	x		x	Not Complete	
2	4:32	0.25	El Centro	trans	NS		NS		
3	4:33	0.25	El Centro	trans	NS		NS		
4	4:35	0.50	El Centro	trans	NS		NS		
5	4:37	0.75	El Centro	trans	NS		NS		
6	4:42	1.00	El Centro	trans	NS		NS		
7	4:49	1.00	White Noise	trans	x		x		

<b>Test Record - Shake Table Expts. on Bridge Model with Heavy X-Braces</b>									
No.	Time	Level	Earthquake	Comp.	Excitation - Long/Trans			Video	Notes
					Table1	Table2	Table3		
<b>Heavy X-Braces - Single Span - 08/07/03</b>									
1	2:43	1.0	White Noise	trans	x		x	-	
2	2:45	0.25	El Centro	trans	NS		NS	-	
3	2:46	0.50	El Centro	trans	NS		NS	-	
4	2:48	0.75	El Centro	trans	NS		NS	-	
5	2:56	1.00	El Centro	trans	NS		NS	20	
6	2:58	1.00	White Noise	trans	x		x	21	
7	3:01	1.25	El Centro	trans	NS		NS	22	
8	3:04	1.50	El Centro	trans	NS		NS	23	
9	3:17	1.75	El Centro	trans	NS		NS	24	
10	3:22	2.00	El Centro	trans	NS		NS	25	
11	3:25	1.00	White Noise	trans	x		x	-	
12	3:36	0.50	Sylmar	trans	NS		NS	26	
13	3:40	0.50	Kobe	trans	NS		NS	27	
14	3:50	0.75	Sylmar	trans	NS		NS	28	
15	4:15	0.75	Kobe	trans	NS		NS	29	
16	4:21	1.00	Sylmar	trans	NS		NS	30	

<b>Test Record - Shake Table Expts. on Bridge Model with LRBs (Series 2)</b>									
No.	Time	Level	Earthquake	Comp.	Excitation - Long/Trans			Video	Notes
					Table1	Table2	Table3		
<b>Lead Rubber Bearings - Single Span - 08/08/03</b>									
1	10:01	1.0	White Noise	long	x		x	-	
2	10:04	1.0	White Noise	trans	x		x	-	
3	10:06	1.0	White Noise	bi	x		x	-	
4	10:19	1.00	El Centro	long	NS		NS	-	
5	10:21	1.00	El Centro	trans	NS		NS	31	
6	10:24	1.00	El Centro	bi	NS/EW		NS/EW	32	
7	10:28	2.00	El Centro	long	NS		NS	33	
8	10:30	2.00	El Centro	trans	NS		NS	34	
9	10:32	2.00	El Centro	bi	NS/EW		NS/EW	35	
10	10:34	0.50	Sylmar	long	NS		NS	36	
11	10:36	0.50	Sylmar	trans	NS		NS	37	
12	10:38	0.50	Sylmar	bi	NS/EW		NS/EW	38	
13	10:39	0.50	Kobe	long	NS		NS	39	
14	10:41	0.50	Kobe	trans	NS		NS	40	
15	10:44	0.50	Kobe	bi	NS/EW		NS/EW	41	



## **APPENDIX D. LOAD CELL CALIBRATIONS**

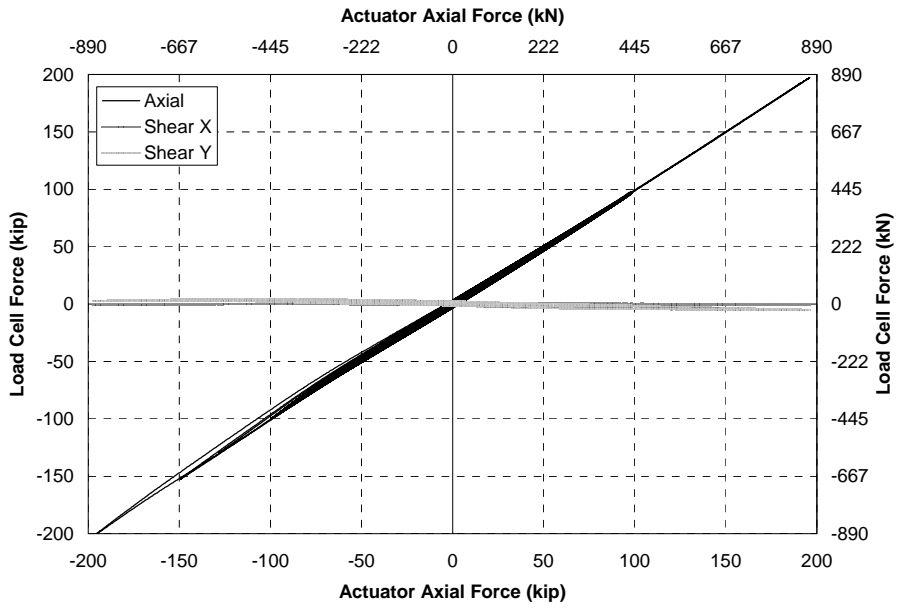


**FIGURE A4.1 Load Cell 1 Axial**

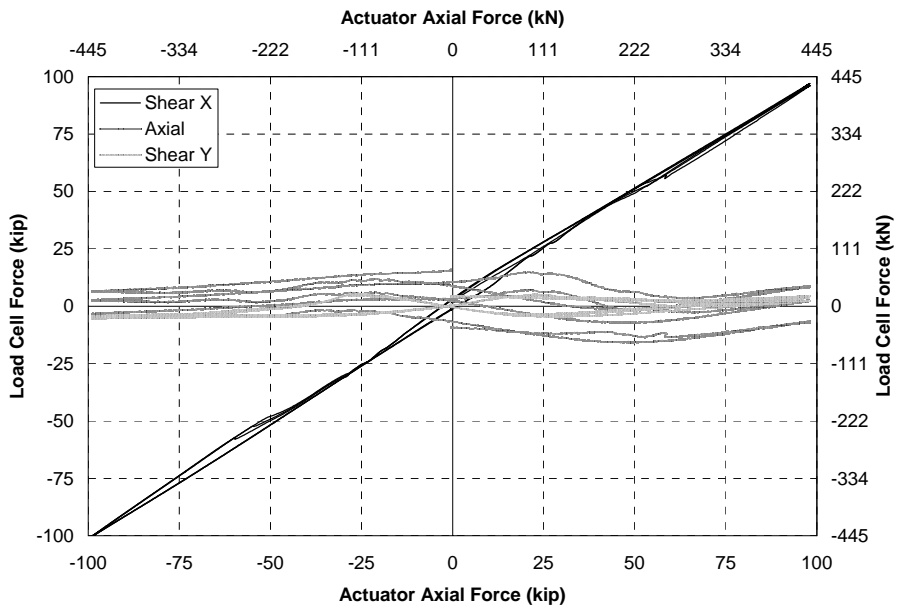


**FIGURE A4.2 Load Cell 1 Shear X**

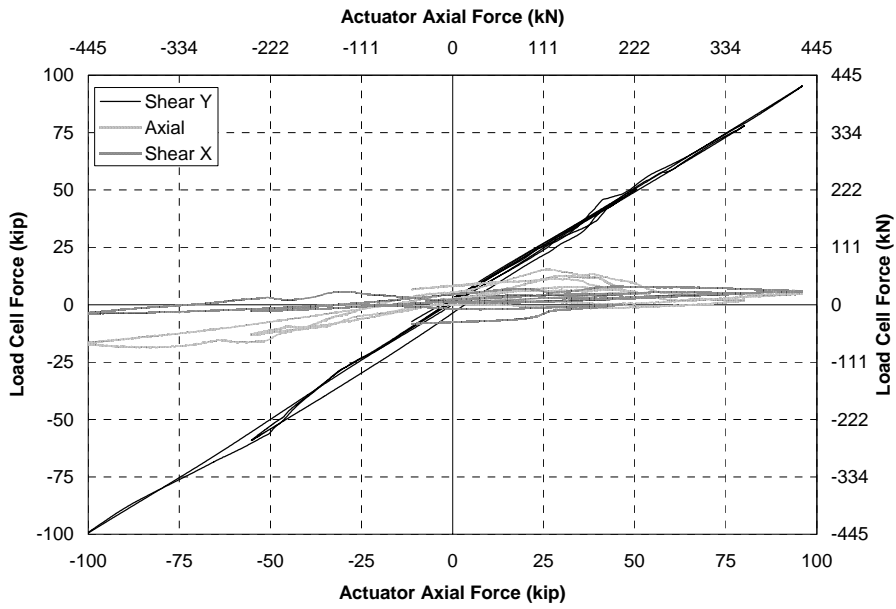


**FIGURE A4.3 Load Cell 1 Shear Y**

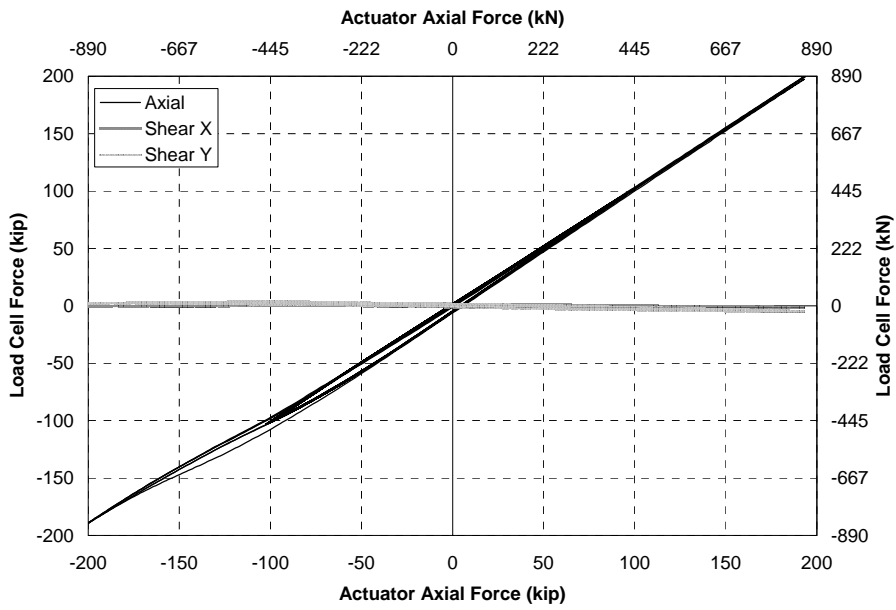


**FIGURE A4.4 Load Cell 2 Axial**

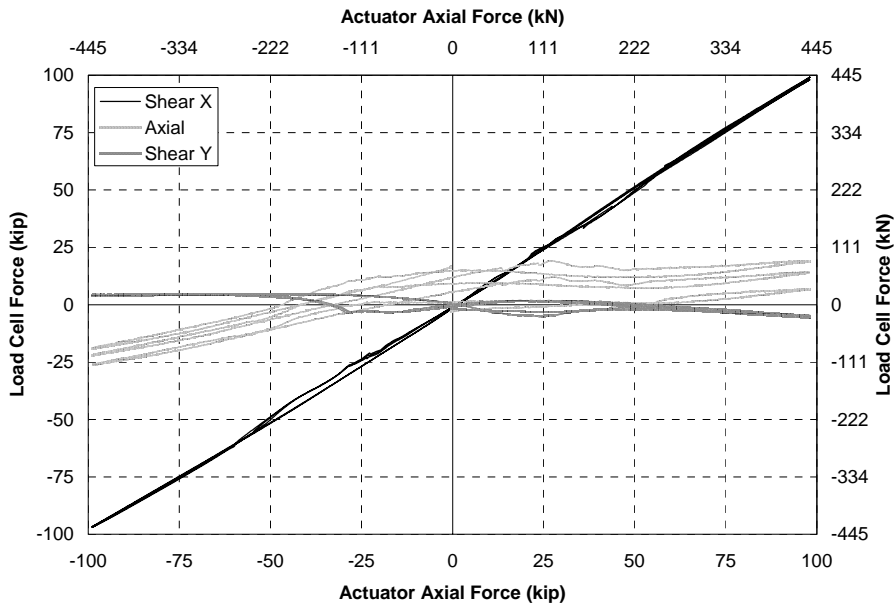


**FIGURE A4.5 Load Cell 2 Shear X**

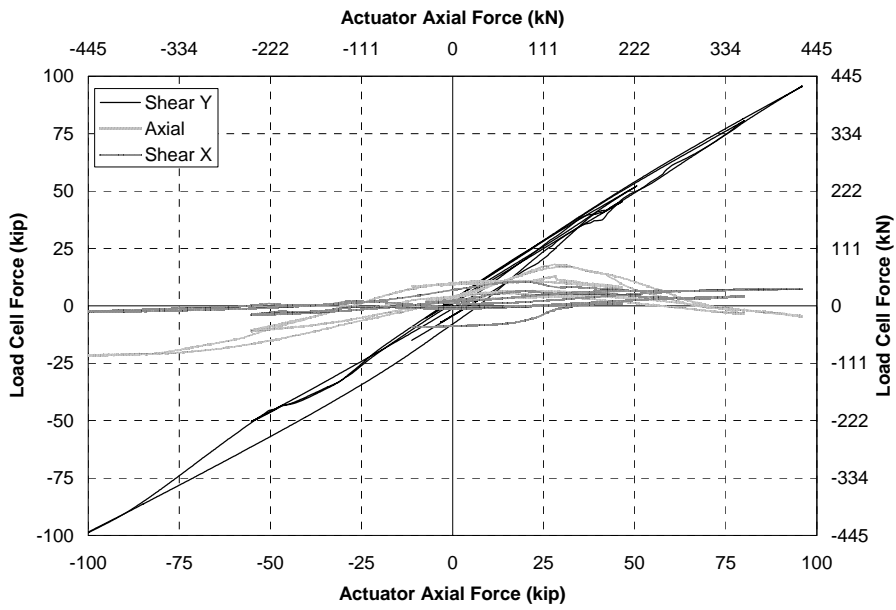


**FIGURE A4.6 Load Cell 2 Shear Y**

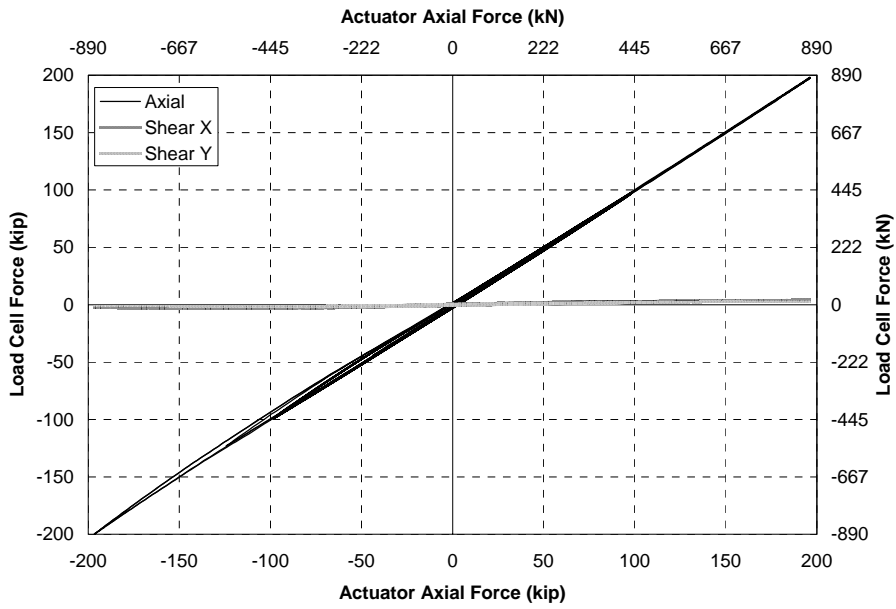


**FIGURE A4.7 Load Cell 3 Axial**

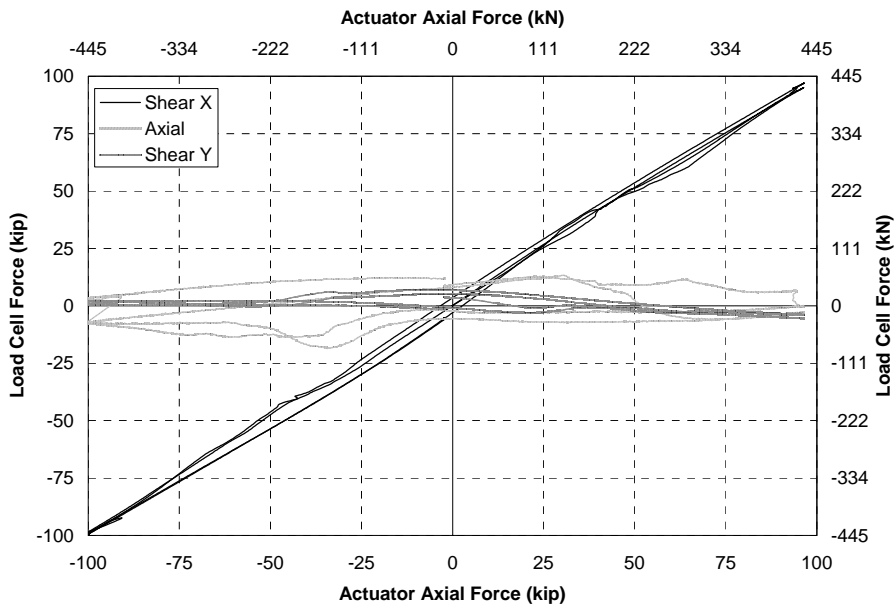


**FIGURE A4.8 Load Cell 3 Shear X**

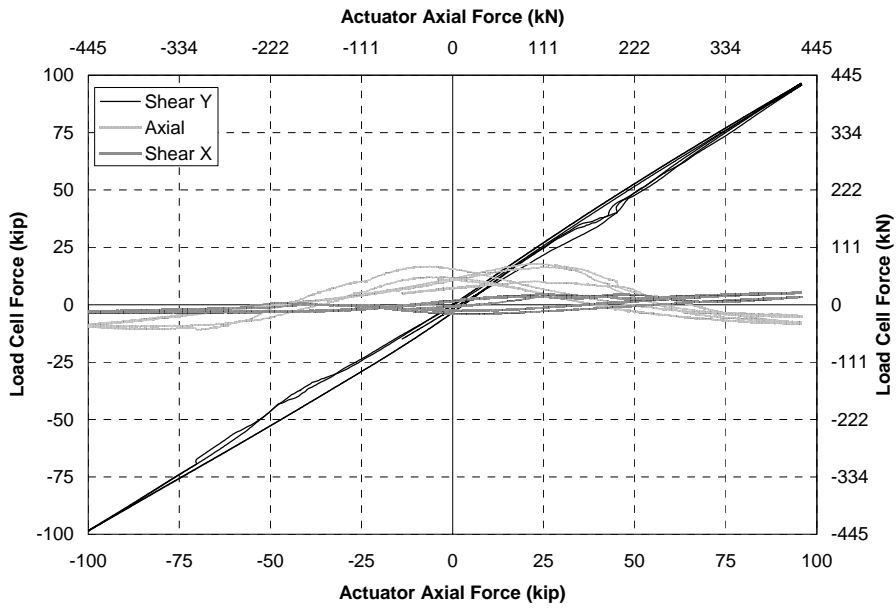


**FIGURE A4.9 Load Cell 3 Shear Y**

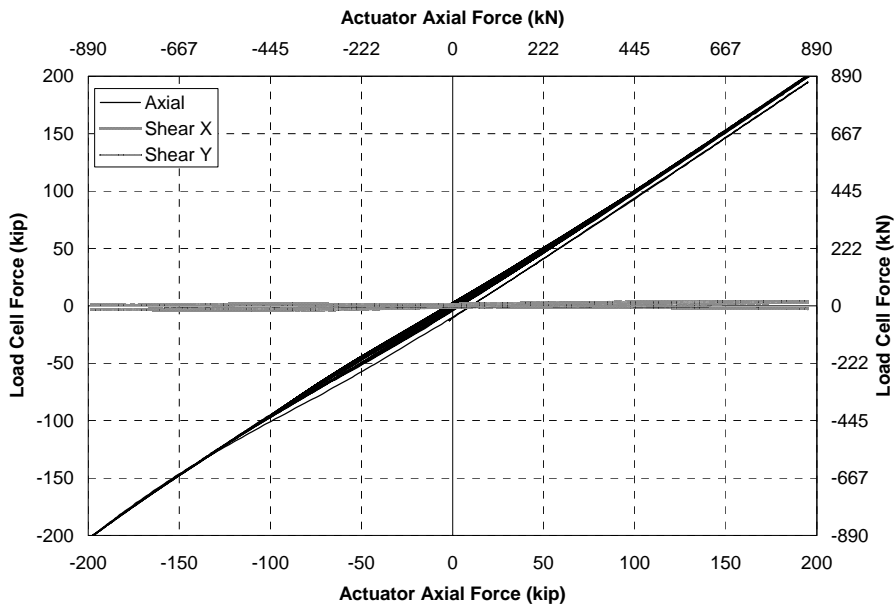


**FIGURE A4.10 Load Cell 4 Axial**

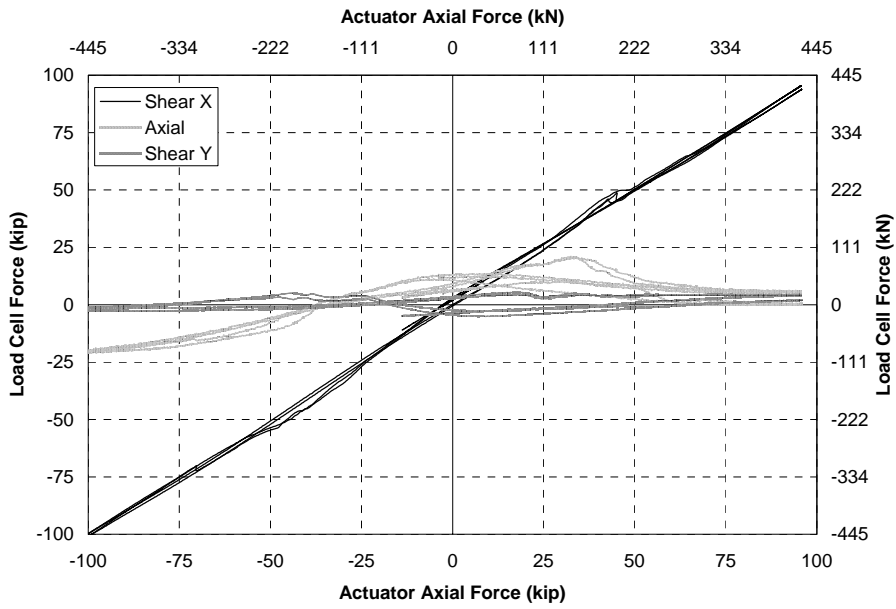


**FIGURE A4.11 Load Cell 4 Shear X**

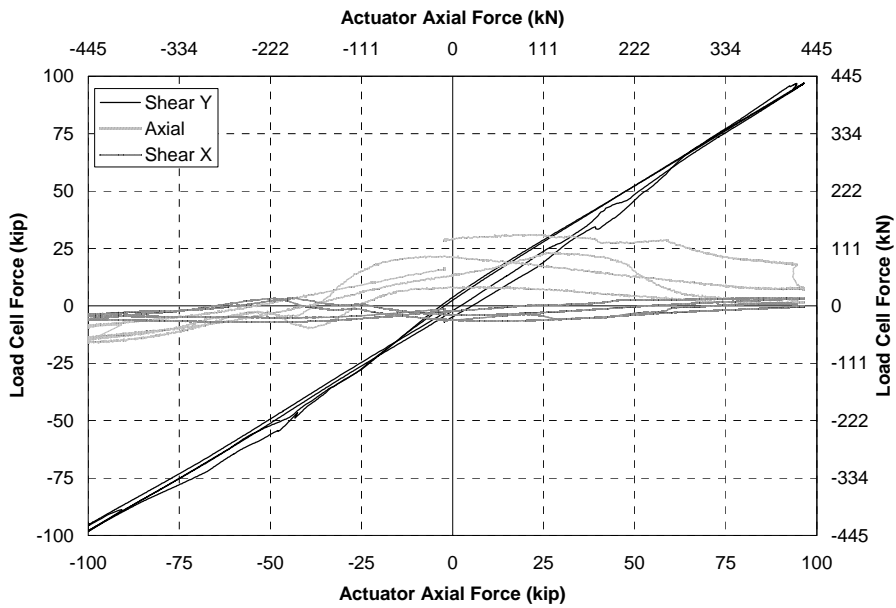


**FIGURE A4.12 Load Cell 4 Shear Y**

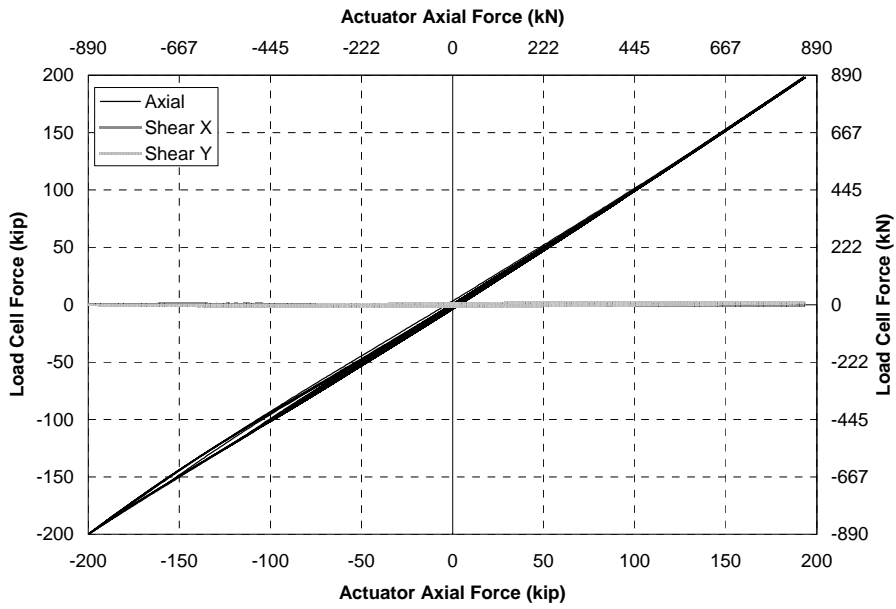


**FIGURE A4.13 Load Cell 5 Axial**

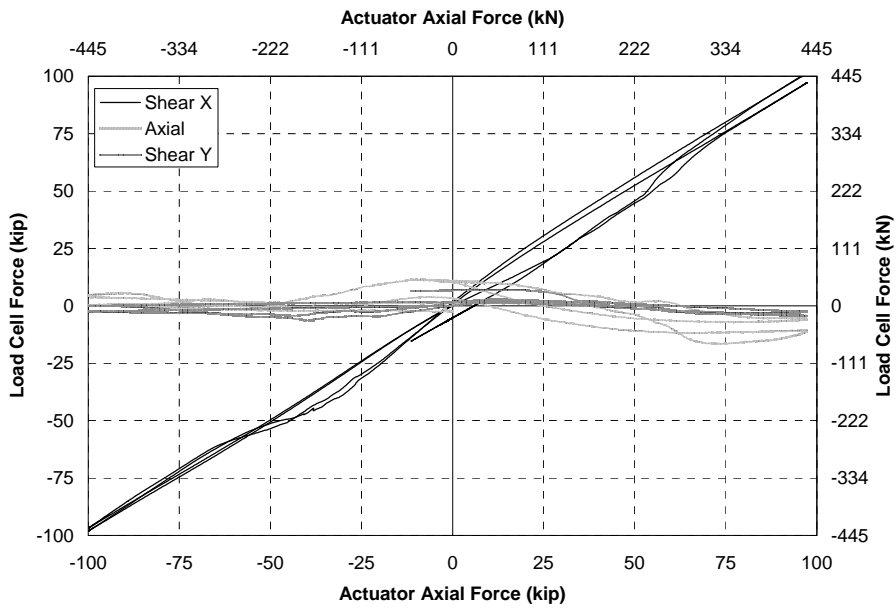


**FIGURE A4.14 Load Cell 5 Shear X**



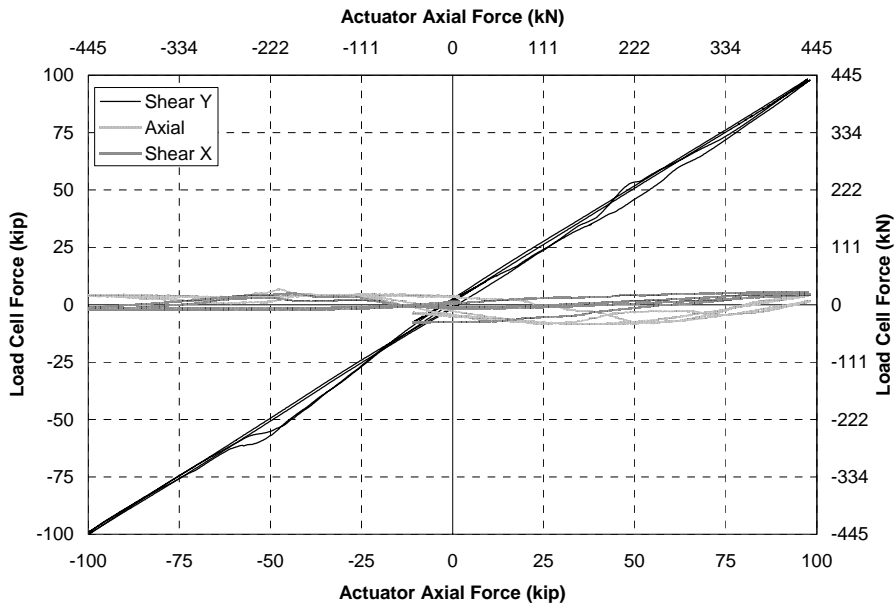


**FIGURE A4.15 Load Cell 5 Shear Y**

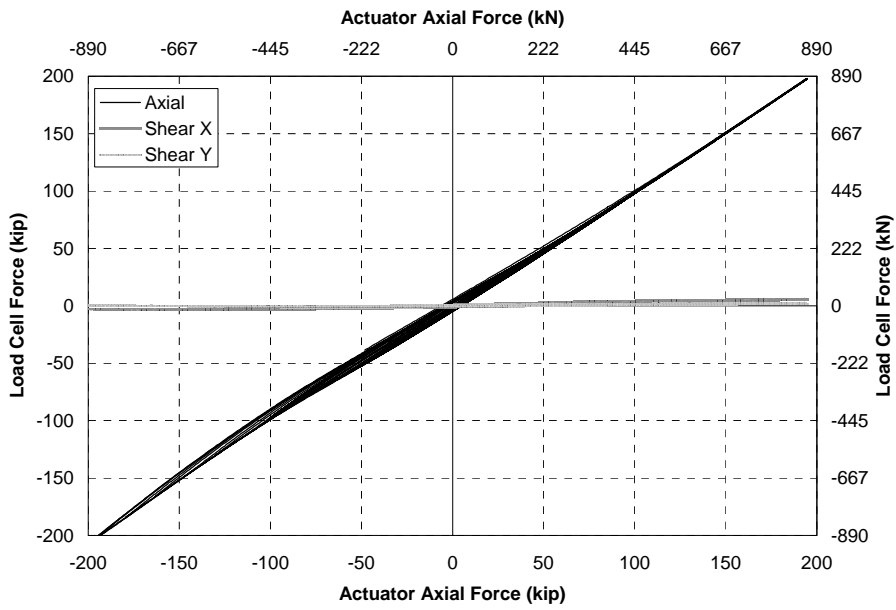


**FIGURE A4.16 Load Cell 6 Axial**

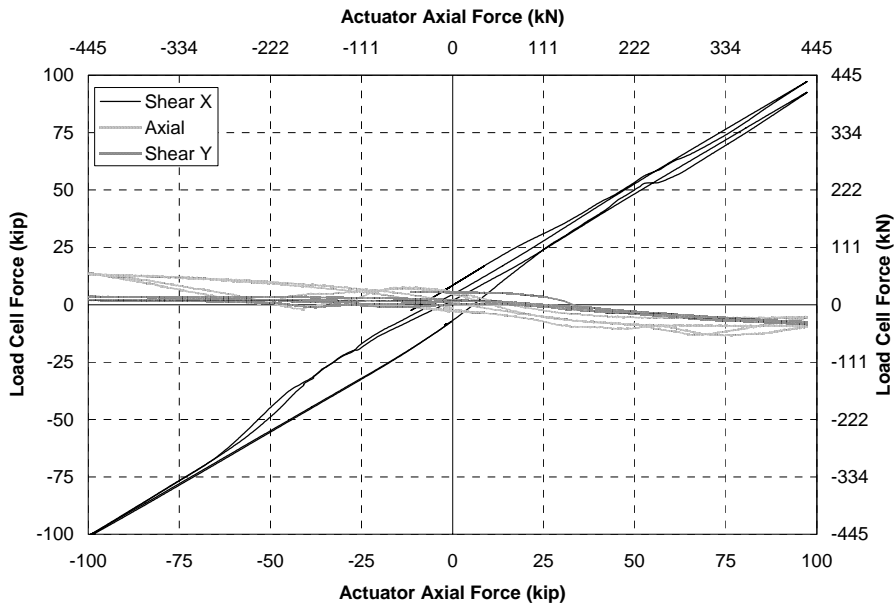


**FIGURE A4.17 Load Cell 6 Shear X**

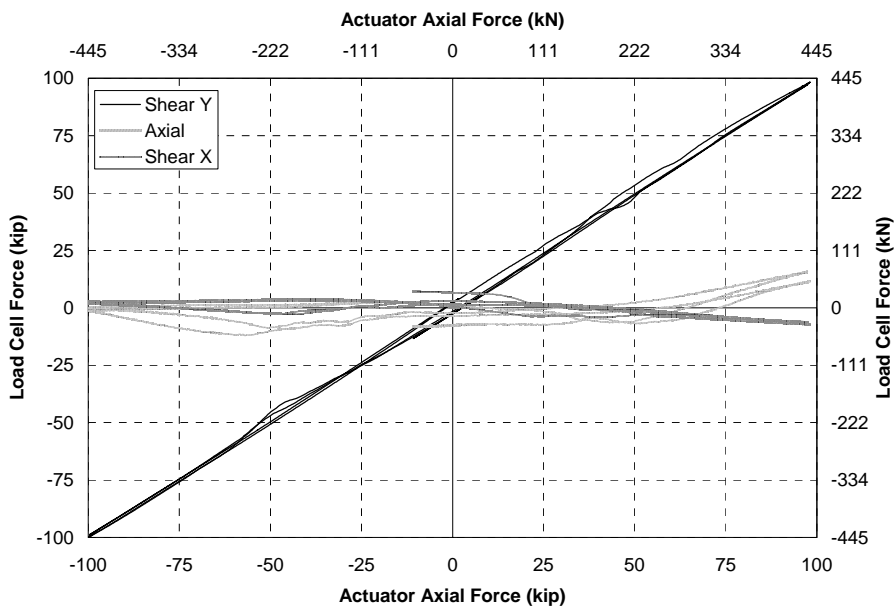


**FIGURE A4.18 Load Cell 6 Shear Y**

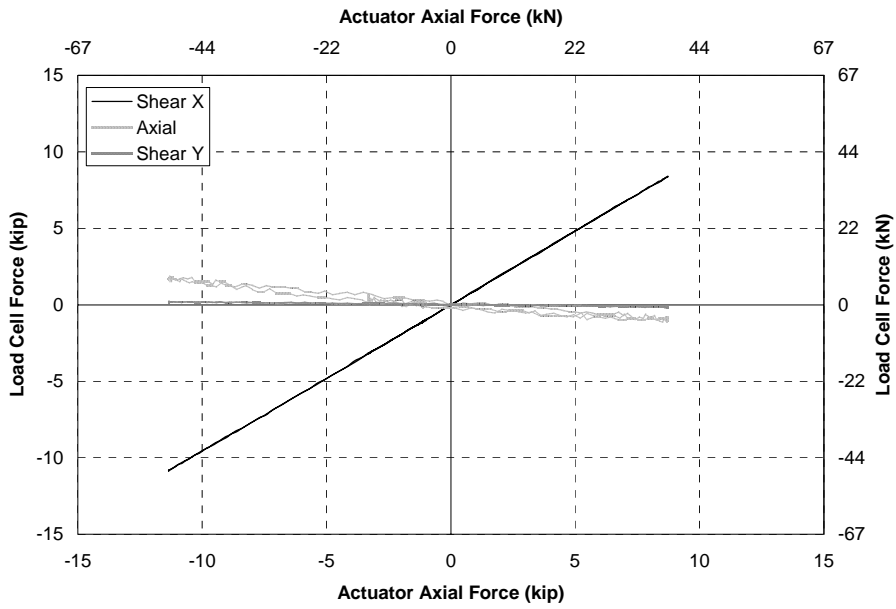


**FIGURE A4.19 Load Cell 6 Shear X for small amplitude cycles**

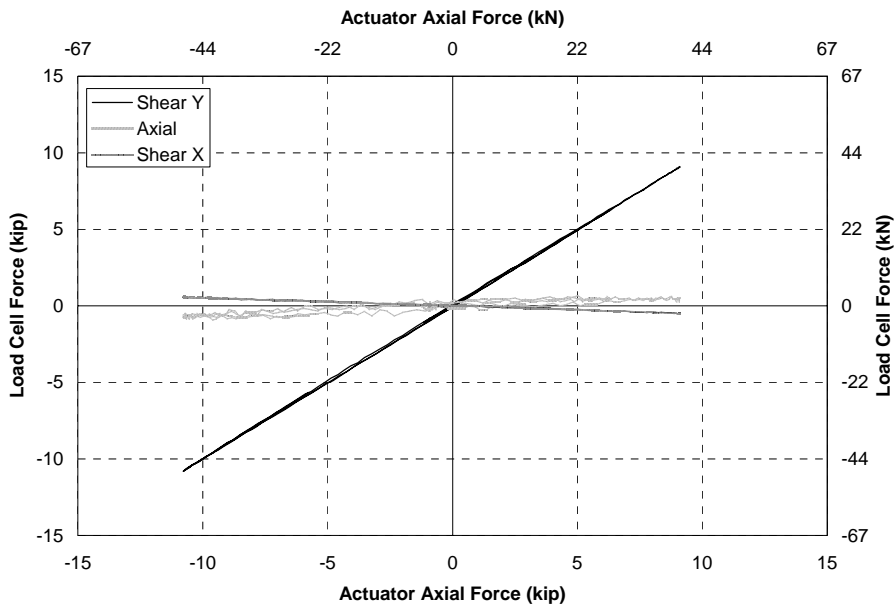


**FIGURE A4.20 Load Cell 6 Shear Y for small amplitude cycles**



**APPENDIX E. VALIDATION OF SINE SWEEP FOR CALCULATING  
DYNAMIC PROPERTIES OF THE BRIDGE MODEL**

In order to test the accuracy of the sine sweep in calculating the dynamic properties of the bridge model, the same sine sweep as that measured from the shake tables was used in a time history analysis of a simple single degree of freedom system with three different natural periods. The amplification of the relative displacement of the oscillator compared to the displacement of the ground motion was plotted against the period of the oscillator. The oscillator was assigned a modal damping of 5%. From dynamic theory the steady state dynamic amplification of the oscillator displacement at resonance with 5% damping is 10.0 (Chopra 1995). Figures A3-1 through A3-3 show that for oscillators with natural periods of 1 s, 0.5 s and 0.25 s respectively the dynamic amplification at resonance is 8.9, 10.1 and 10.4. Therefore the maximum error is 11%. The peaks are within 10% of the natural periods of the systems.

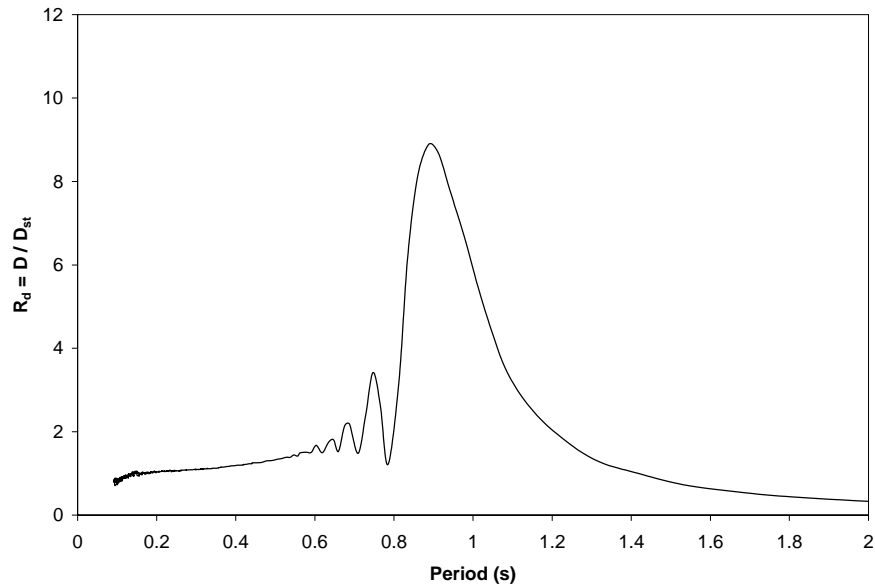


**FIGURE A3-1 Dynamic amplification of response for SDOF oscillator with period of 1.0 s**

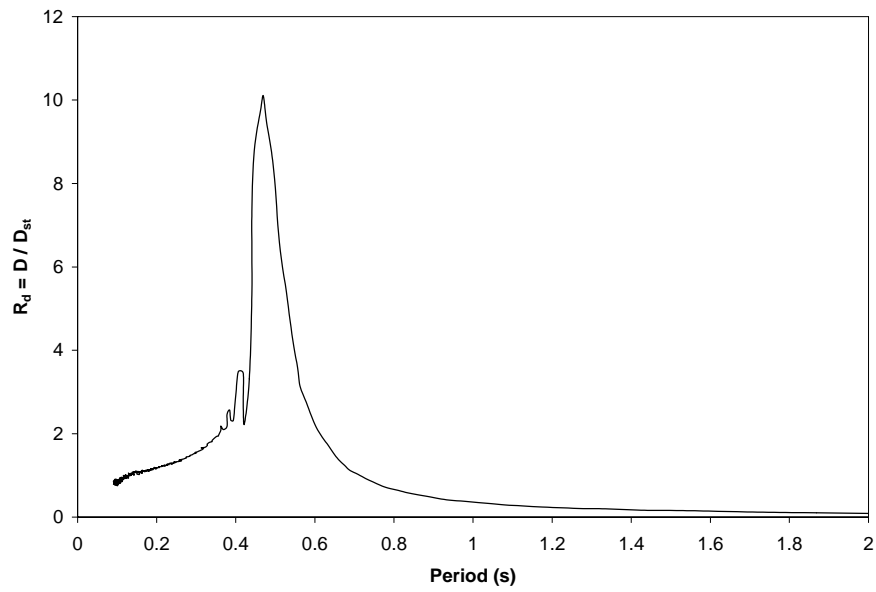


**Figure A3-2. Dynamic amplification of response for SDOF oscillator with period of 0.5 s.**

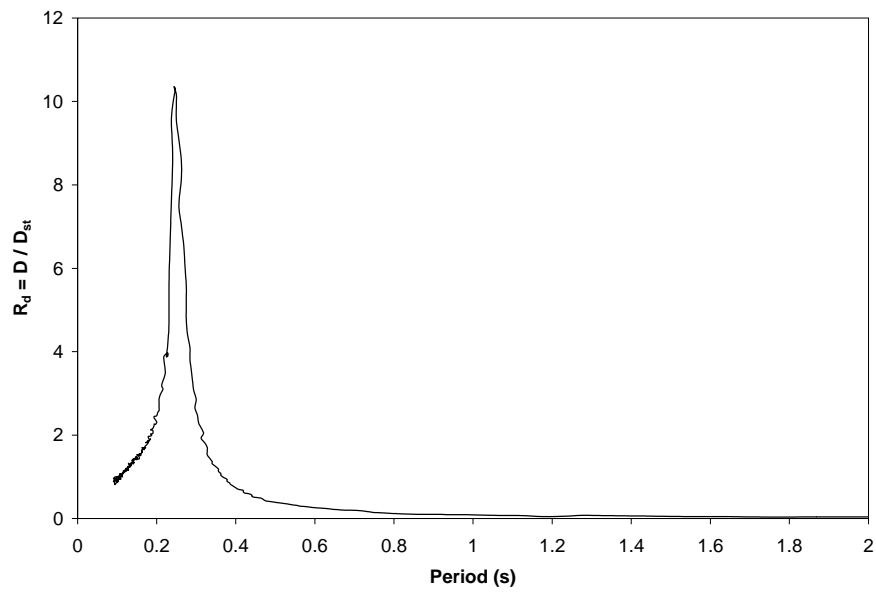


**Figure A3-3. Dynamic amplification of response for SDOF oscillator with period of 0.25 s.**





## MCEER Technical Reports

MCEER publishes technical reports on a variety of subjects written by authors funded through MCEER. These reports are available from both MCEER Publications and the National Technical Information Service (NTIS). Requests for reports should be directed to MCEER Publications, MCEER, University at Buffalo, State University of New York, Red Jacket Quadrangle, Buffalo, New York 14261. Reports can also be requested through NTIS, 5285 Port Royal Road, Springfield, Virginia 22161. NTIS accession numbers are shown in parenthesis, if available.

- NCEER-87-0001 "First-Year Program in Research, Education and Technology Transfer," 3/5/87, (PB88-134275, A04, MF-A01).
- NCEER-87-0002 "Experimental Evaluation of Instantaneous Optimal Algorithms for Structural Control," by R.C. Lin, T.T. Soong and A.M. Reinhorn, 4/20/87, (PB88-134341, A04, MF-A01).
- NCEER-87-0003 "Experimentation Using the Earthquake Simulation Facilities at University at Buffalo," by A.M. Reinhorn and R.L. Ketter, to be published.
- NCEER-87-0004 "The System Characteristics and Performance of a Shaking Table," by J.S. Hwang, K.C. Chang and G.C. Lee, 6/1/87, (PB88-134259, A03, MF-A01). This report is available only through NTIS (see address given above).
- NCEER-87-0005 "A Finite Element Formulation for Nonlinear Viscoplastic Material Using a Q Model," by O. Gyebi and G. Dasgupta, 11/2/87, (PB88-213764, A08, MF-A01).
- NCEER-87-0006 "Symbolic Manipulation Program (SMP) - Algebraic Codes for Two and Three Dimensional Finite Element Formulations," by X. Lee and G. Dasgupta, 11/9/87, (PB88-218522, A05, MF-A01).
- NCEER-87-0007 "Instantaneous Optimal Control Laws for Tall Buildings Under Seismic Excitations," by J.N. Yang, A. Akbarpour and P. Ghaemmaghami, 6/10/87, (PB88-134333, A06, MF-A01). This report is only available through NTIS (see address given above).
- NCEER-87-0008 "IDARC: Inelastic Damage Analysis of Reinforced Concrete Frame - Shear-Wall Structures," by Y.J. Park, A.M. Reinhorn and S.K. Kunnath, 7/20/87, (PB88-134325, A09, MF-A01). This report is only available through NTIS (see address given above).
- NCEER-87-0009 "Liquefaction Potential for New York State: A Preliminary Report on Sites in Manhattan and Buffalo," by M. Budhu, V. Vijayakumar, R.F. Giese and L. Baumgras, 8/31/87, (PB88-163704, A03, MF-A01). This report is available only through NTIS (see address given above).
- NCEER-87-0010 "Vertical and Torsional Vibration of Foundations in Inhomogeneous Media," by A.S. Veletsos and K.W. Dotson, 6/1/87, (PB88-134291, A03, MF-A01). This report is only available through NTIS (see address given above).
- NCEER-87-0011 "Seismic Probabilistic Risk Assessment and Seismic Margins Studies for Nuclear Power Plants," by Howard H.M. Hwang, 6/15/87, (PB88-134267, A03, MF-A01). This report is only available through NTIS (see address given above).
- NCEER-87-0012 "Parametric Studies of Frequency Response of Secondary Systems Under Ground-Acceleration Excitations," by Y. Yong and Y.K. Lin, 6/10/87, (PB88-134309, A03, MF-A01). This report is only available through NTIS (see address given above).
- NCEER-87-0013 "Frequency Response of Secondary Systems Under Seismic Excitation," by J.A. HoLung, J. Cai and Y.K. Lin, 7/31/87, (PB88-134317, A05, MF-A01). This report is only available through NTIS (see address given above).
- NCEER-87-0014 "Modelling Earthquake Ground Motions in Seismically Active Regions Using Parametric Time Series Methods," by G.W. Ellis and A.S. Cakmak, 8/25/87, (PB88-134283, A08, MF-A01). This report is only available through NTIS (see address given above).
- NCEER-87-0015 "Detection and Assessment of Seismic Structural Damage," by E. DiPasquale and A.S. Cakmak, 8/25/87, (PB88-163712, A05, MF-A01). This report is only available through NTIS (see address given above).

- NCEER-87-0016 "Pipeline Experiment at Parkfield, California," by J. Isenberg and E. Richardson, 9/15/87, (PB88-163720, A03, MF-A01). This report is available only through NTIS (see address given above).
- NCEER-87-0017 "Digital Simulation of Seismic Ground Motion," by M. Shinozuka, G. Deodatis and T. Harada, 8/31/87, (PB88-155197, A04, MF-A01). This report is available only through NTIS (see address given above).
- NCEER-87-0018 "Practical Considerations for Structural Control: System Uncertainty, System Time Delay and Truncation of Small Control Forces," J.N. Yang and A. Akbarpour, 8/10/87, (PB88-163738, A08, MF-A01). This report is only available through NTIS (see address given above).
- NCEER-87-0019 "Modal Analysis of Nonclassically Damped Structural Systems Using Canonical Transformation," by J.N. Yang, S. Sarkani and F.X. Long, 9/27/87, (PB88-187851, A04, MF-A01).
- NCEER-87-0020 "A Nonstationary Solution in Random Vibration Theory," by J.R. Red-Horse and P.D. Spanos, 11/3/87, (PB88-163746, A03, MF-A01).
- NCEER-87-0021 "Horizontal Impedances for Radially Inhomogeneous Viscoelastic Soil Layers," by A.S. Veletsos and K.W. Dotson, 10/15/87, (PB88-150859, A04, MF-A01).
- NCEER-87-0022 "Seismic Damage Assessment of Reinforced Concrete Members," by Y.S. Chung, C. Meyer and M. Shinozuka, 10/9/87, (PB88-150867, A05, MF-A01). This report is available only through NTIS (see address given above).
- NCEER-87-0023 "Active Structural Control in Civil Engineering," by T.T. Soong, 11/11/87, (PB88-187778, A03, MF-A01).
- NCEER-87-0024 "Vertical and Torsional Impedances for Radially Inhomogeneous Viscoelastic Soil Layers," by K.W. Dotson and A.S. Veletsos, 12/87, (PB88-187786, A03, MF-A01).
- NCEER-87-0025 "Proceedings from the Symposium on Seismic Hazards, Ground Motions, Soil-Liquefaction and Engineering Practice in Eastern North America," October 20-22, 1987, edited by K.H. Jacob, 12/87, (PB88-188115, A23, MF-A01). This report is available only through NTIS (see address given above).
- NCEER-87-0026 "Report on the Whittier-Narrows, California, Earthquake of October 1, 1987," by J. Pantelic and A. Reinhorn, 11/87, (PB88-187752, A03, MF-A01). This report is available only through NTIS (see address given above).
- NCEER-87-0027 "Design of a Modular Program for Transient Nonlinear Analysis of Large 3-D Building Structures," by S. Srivastav and J.F. Abel, 12/30/87, (PB88-187950, A05, MF-A01). This report is only available through NTIS (see address given above).
- NCEER-87-0028 "Second-Year Program in Research, Education and Technology Transfer," 3/8/88, (PB88-219480, A04, MF-A01).
- NCEER-88-0001 "Workshop on Seismic Computer Analysis and Design of Buildings With Interactive Graphics," by W. McGuire, J.F. Abel and C.H. Conley, 1/18/88, (PB88-187760, A03, MF-A01). This report is only available through NTIS (see address given above).
- NCEER-88-0002 "Optimal Control of Nonlinear Flexible Structures," by J.N. Yang, F.X. Long and D. Wong, 1/22/88, (PB88-213772, A06, MF-A01).
- NCEER-88-0003 "Substructuring Techniques in the Time Domain for Primary-Secondary Structural Systems," by G.D. Manolis and G. Juhn, 2/10/88, (PB88-213780, A04, MF-A01).
- NCEER-88-0004 "Iterative Seismic Analysis of Primary-Secondary Systems," by A. Singhal, L.D. Lutes and P.D. Spanos, 2/23/88, (PB88-213798, A04, MF-A01).
- NCEER-88-0005 "Stochastic Finite Element Expansion for Random Media," by P.D. Spanos and R. Ghanem, 3/14/88, (PB88-213806, A03, MF-A01).

- NCEER-88-0006 "Combining Structural Optimization and Structural Control," by F.Y. Cheng and C.P. Pantelides, 1/10/88, (PB88-213814, A05, MF-A01).
- NCEER-88-0007 "Seismic Performance Assessment of Code-Designed Structures," by H.H-M. Hwang, J-W. Jaw and H-J. Shau, 3/20/88, (PB88-219423, A04, MF-A01). This report is only available through NTIS (see address given above).
- NCEER-88-0008 "Reliability Analysis of Code-Designed Structures Under Natural Hazards," by H.H-M. Hwang, H. Ushiba and M. Shinozuka, 2/29/88, (PB88-229471, A07, MF-A01). This report is only available through NTIS (see address given above).
- NCEER-88-0009 "Seismic Fragility Analysis of Shear Wall Structures," by J-W Jaw and H.H-M. Hwang, 4/30/88, (PB89-102867, A04, MF-A01).
- NCEER-88-0010 "Base Isolation of a Multi-Story Building Under a Harmonic Ground Motion - A Comparison of Performances of Various Systems," by F-G Fan, G. Ahmadi and I.G. Tadjbakhsh, 5/18/88, (PB89-122238, A06, MF-A01). This report is only available through NTIS (see address given above).
- NCEER-88-0011 "Seismic Floor Response Spectra for a Combined System by Green's Functions," by F.M. Lavelle, L.A. Bergman and P.D. Spanos, 5/1/88, (PB89-102875, A03, MF-A01).
- NCEER-88-0012 "A New Solution Technique for Randomly Excited Hysteretic Structures," by G.Q. Cai and Y.K. Lin, 5/16/88, (PB89-102883, A03, MF-A01).
- NCEER-88-0013 "A Study of Radiation Damping and Soil-Structure Interaction Effects in the Centrifuge," by K. Weissman, supervised by J.H. Prevost, 5/24/88, (PB89-144703, A06, MF-A01).
- NCEER-88-0014 "Parameter Identification and Implementation of a Kinematic Plasticity Model for Frictional Soils," by J.H. Prevost and D.V. Griffiths, to be published.
- NCEER-88-0015 "Two- and Three- Dimensional Dynamic Finite Element Analyses of the Long Valley Dam," by D.V. Griffiths and J.H. Prevost, 6/17/88, (PB89-144711, A04, MF-A01).
- NCEER-88-0016 "Damage Assessment of Reinforced Concrete Structures in Eastern United States," by A.M. Reinhorn, M.J. Seidel, S.K. Kunnath and Y.J. Park, 6/15/88, (PB89-122220, A04, MF-A01). This report is only available through NTIS (see address given above).
- NCEER-88-0017 "Dynamic Compliance of Vertically Loaded Strip Foundations in Multilayered Viscoelastic Soils," by S. Ahmad and A.S.M. Israil, 6/17/88, (PB89-102891, A04, MF-A01).
- NCEER-88-0018 "An Experimental Study of Seismic Structural Response With Added Viscoelastic Dampers," by R.C. Lin, Z. Liang, T.T. Soong and R.H. Zhang, 6/30/88, (PB89-122212, A05, MF-A01). This report is available only through NTIS (see address given above).
- NCEER-88-0019 "Experimental Investigation of Primary - Secondary System Interaction," by G.D. Manolis, G. Juhn and A.M. Reinhorn, 5/27/88, (PB89-122204, A04, MF-A01).
- NCEER-88-0020 "A Response Spectrum Approach For Analysis of Nonclassically Damped Structures," by J.N. Yang, S. Sarkani and F.X. Long, 4/22/88, (PB89-102909, A04, MF-A01).
- NCEER-88-0021 "Seismic Interaction of Structures and Soils: Stochastic Approach," by A.S. Veletsos and A.M. Prasad, 7/21/88, (PB89-122196, A04, MF-A01). This report is only available through NTIS (see address given above).
- NCEER-88-0022 "Identification of the Serviceability Limit State and Detection of Seismic Structural Damage," by E. DiPasquale and A.S. Cakmak, 6/15/88, (PB89-122188, A05, MF-A01). This report is available only through NTIS (see address given above).
- NCEER-88-0023 "Multi-Hazard Risk Analysis: Case of a Simple Offshore Structure," by B.K. Bhartia and E.H. Vanmarcke, 7/21/88, (PB89-145213, A05, MF-A01).

- NCEER-88-0024 "Automated Seismic Design of Reinforced Concrete Buildings," by Y.S. Chung, C. Meyer and M. Shinozuka, 7/5/88, (PB89-122170, A06, MF-A01). This report is available only through NTIS (see address given above).
- NCEER-88-0025 "Experimental Study of Active Control of MDOF Structures Under Seismic Excitations," by L.L. Chung, R.C. Lin, T.T. Soong and A.M. Reinhorn, 7/10/88, (PB89-122600, A04, MF-A01).
- NCEER-88-0026 "Earthquake Simulation Tests of a Low-Rise Metal Structure," by J.S. Hwang, K.C. Chang, G.C. Lee and R.L. Ketter, 8/1/88, (PB89-102917, A04, MF-A01).
- NCEER-88-0027 "Systems Study of Urban Response and Reconstruction Due to Catastrophic Earthquakes," by F. Kozin and H.K. Zhou, 9/22/88, (PB90-162348, A04, MF-A01).
- NCEER-88-0028 "Seismic Fragility Analysis of Plane Frame Structures," by H.H-M. Hwang and Y.K. Low, 7/31/88, (PB89-131445, A06, MF-A01).
- NCEER-88-0029 "Response Analysis of Stochastic Structures," by A. Kardara, C. Bucher and M. Shinozuka, 9/22/88, (PB89-174429, A04, MF-A01).
- NCEER-88-0030 "Nonnormal Accelerations Due to Yielding in a Primary Structure," by D.C.K. Chen and L.D. Lutes, 9/19/88, (PB89-131437, A04, MF-A01).
- NCEER-88-0031 "Design Approaches for Soil-Structure Interaction," by A.S. Veletsos, A.M. Prasad and Y. Tang, 12/30/88, (PB89-174437, A03, MF-A01). This report is available only through NTIS (see address given above).
- NCEER-88-0032 "A Re-evaluation of Design Spectra for Seismic Damage Control," by C.J. Turkstra and A.G. Tallin, 11/7/88, (PB89-145221, A05, MF-A01).
- NCEER-88-0033 "The Behavior and Design of Noncontact Lap Splices Subjected to Repeated Inelastic Tensile Loading," by V.E. Sagan, P. Gergely and R.N. White, 12/8/88, (PB89-163737, A08, MF-A01).
- NCEER-88-0034 "Seismic Response of Pile Foundations," by S.M. Mamoon, P.K. Banerjee and S. Ahmad, 11/1/88, (PB89-145239, A04, MF-A01).
- NCEER-88-0035 "Modeling of R/C Building Structures With Flexible Floor Diaphragms (IDARC2)," by A.M. Reinhorn, S.K. Kunnath and N. Panahshahi, 9/7/88, (PB89-207153, A07, MF-A01).
- NCEER-88-0036 "Solution of the Dam-Reservoir Interaction Problem Using a Combination of FEM, BEM with Particular Integrals, Modal Analysis, and Substructuring," by C-S. Tsai, G.C. Lee and R.L. Ketter, 12/31/88, (PB89-207146, A04, MF-A01).
- NCEER-88-0037 "Optimal Placement of Actuators for Structural Control," by F.Y. Cheng and C.P. Pantelides, 8/15/88, (PB89-162846, A05, MF-A01).
- NCEER-88-0038 "Teflon Bearings in Aseismic Base Isolation: Experimental Studies and Mathematical Modeling," by A. Mokha, M.C. Constantinou and A.M. Reinhorn, 12/5/88, (PB89-218457, A10, MF-A01). This report is available only through NTIS (see address given above).
- NCEER-88-0039 "Seismic Behavior of Flat Slab High-Rise Buildings in the New York City Area," by P. Weidlinger and M. Ettouney, 10/15/88, (PB90-145681, A04, MF-A01).
- NCEER-88-0040 "Evaluation of the Earthquake Resistance of Existing Buildings in New York City," by P. Weidlinger and M. Ettouney, 10/15/88, to be published.
- NCEER-88-0041 "Small-Scale Modeling Techniques for Reinforced Concrete Structures Subjected to Seismic Loads," by W. Kim, A. El-Attar and R.N. White, 11/22/88, (PB89-189625, A05, MF-A01).
- NCEER-88-0042 "Modeling Strong Ground Motion from Multiple Event Earthquakes," by G.W. Ellis and A.S. Cakmak, 10/15/88, (PB89-174445, A03, MF-A01).

- NCEER-88-0043 "Nonstationary Models of Seismic Ground Acceleration," by M. Grigoriu, S.E. Ruiz and E. Rosenblueth, 7/15/88, (PB89-189617, A04, MF-A01).
- NCEER-88-0044 "SARCF User's Guide: Seismic Analysis of Reinforced Concrete Frames," by Y.S. Chung, C. Meyer and M. Shinozuka, 11/9/88, (PB89-174452, A08, MF-A01).
- NCEER-88-0045 "First Expert Panel Meeting on Disaster Research and Planning," edited by J. Pantelic and J. Stoyke, 9/15/88, (PB89-174460, A05, MF-A01).
- NCEER-88-0046 "Preliminary Studies of the Effect of Degrading Infill Walls on the Nonlinear Seismic Response of Steel Frames," by C.Z. Chrysostomou, P. Gergely and J.F. Abel, 12/19/88, (PB89-208383, A05, MF-A01).
- NCEER-88-0047 "Reinforced Concrete Frame Component Testing Facility - Design, Construction, Instrumentation and Operation," by S.P. Pessiki, C. Conley, T. Bond, P. Gergely and R.N. White, 12/16/88, (PB89-174478, A04, MF-A01).
- NCEER-89-0001 "Effects of Protective Cushion and Soil Compliancy on the Response of Equipment Within a Seismically Excited Building," by J.A. HoLung, 2/16/89, (PB89-207179, A04, MF-A01).
- NCEER-89-0002 "Statistical Evaluation of Response Modification Factors for Reinforced Concrete Structures," by H.H-M. Hwang and J-W. Jaw, 2/17/89, (PB89-207187, A05, MF-A01).
- NCEER-89-0003 "Hysteretic Columns Under Random Excitation," by G-Q. Cai and Y.K. Lin, 1/9/89, (PB89-196513, A03, MF-A01).
- NCEER-89-0004 "Experimental Study of 'Elephant Foot Bulge' Instability of Thin-Walled Metal Tanks," by Z-H. Jia and R.L. Ketter, 2/22/89, (PB89-207195, A03, MF-A01).
- NCEER-89-0005 "Experiment on Performance of Buried Pipelines Across San Andreas Fault," by J. Isenberg, E. Richardson and T.D. O'Rourke, 3/10/89, (PB89-218440, A04, MF-A01). This report is available only through NTIS (see address given above).
- NCEER-89-0006 "A Knowledge-Based Approach to Structural Design of Earthquake-Resistant Buildings," by M. Subramani, P. Gergely, C.H. Conley, J.F. Abel and A.H. Zaghaw, 1/15/89, (PB89-218465, A06, MF-A01).
- NCEER-89-0007 "Liquefaction Hazards and Their Effects on Buried Pipelines," by T.D. O'Rourke and P.A. Lane, 2/1/89, (PB89-218481, A09, MF-A01).
- NCEER-89-0008 "Fundamentals of System Identification in Structural Dynamics," by H. Imai, C-B. Yun, O. Maruyama and M. Shinozuka, 1/26/89, (PB89-207211, A04, MF-A01).
- NCEER-89-0009 "Effects of the 1985 Michoacan Earthquake on Water Systems and Other Buried Lifelines in Mexico," by A.G. Ayala and M.J. O'Rourke, 3/8/89, (PB89-207229, A06, MF-A01).
- NCEER-89-R010 "NCEER Bibliography of Earthquake Education Materials," by K.E.K. Ross, Second Revision, 9/1/89, (PB90-125352, A05, MF-A01). This report is replaced by NCEER-92-0018.
- NCEER-89-0011 "Inelastic Three-Dimensional Response Analysis of Reinforced Concrete Building Structures (IDARC-3D), Part I - Modeling," by S.K. Kunnath and A.M. Reinhorn, 4/17/89, (PB90-114612, A07, MF-A01). This report is available only through NTIS (see address given above).
- NCEER-89-0012 "Recommended Modifications to ATC-14," by C.D. Poland and J.O. Malley, 4/12/89, (PB90-108648, A15, MF-A01).
- NCEER-89-0013 "Repair and Strengthening of Beam-to-Column Connections Subjected to Earthquake Loading," by M. Corazao and A.J. Durrani, 2/28/89, (PB90-109885, A06, MF-A01).
- NCEER-89-0014 "Program EXKAL2 for Identification of Structural Dynamic Systems," by O. Maruyama, C-B. Yun, M. Hoshiya and M. Shinozuka, 5/19/89, (PB90-109877, A09, MF-A01).

- NCEER-89-0015 "Response of Frames With Bolted Semi-Rigid Connections, Part I - Experimental Study and Analytical Predictions," by P.J. DiCorso, A.M. Reinhorn, J.R. Dickerson, J.B. Radzinski and W.L. Harper, 6/1/89, to be published.
- NCEER-89-0016 "ARMA Monte Carlo Simulation in Probabilistic Structural Analysis," by P.D. Spanos and M.P. Mignolet, 7/10/89, (PB90-109893, A03, MF-A01).
- NCEER-89-P017 "Preliminary Proceedings from the Conference on Disaster Preparedness - The Place of Earthquake Education in Our Schools," Edited by K.E.K. Ross, 6/23/89, (PB90-108606, A03, MF-A01).
- NCEER-89-0017 "Proceedings from the Conference on Disaster Preparedness - The Place of Earthquake Education in Our Schools," Edited by K.E.K. Ross, 12/31/89, (PB90-207895, A012, MF-A02). This report is available only through NTIS (see address given above).
- NCEER-89-0018 "Multidimensional Models of Hysteretic Material Behavior for Vibration Analysis of Shape Memory Energy Absorbing Devices, by E.J. Graesser and F.A. Cozzarelli, 6/7/89, (PB90-164146, A04, MF-A01).
- NCEER-89-0019 "Nonlinear Dynamic Analysis of Three-Dimensional Base Isolated Structures (3D-BASIS)," by S. Nagarajaiah, A.M. Reinhorn and M.C. Constantinou, 8/3/89, (PB90-161936, A06, MF-A01). This report has been replaced by NCEER-93-0011.
- NCEER-89-0020 "Structural Control Considering Time-Rate of Control Forces and Control Rate Constraints," by F.Y. Cheng and C.P. Pantelides, 8/3/89, (PB90-120445, A04, MF-A01).
- NCEER-89-0021 "Subsurface Conditions of Memphis and Shelby County," by K.W. Ng, T-S. Chang and H-H.M. Hwang, 7/26/89, (PB90-120437, A03, MF-A01).
- NCEER-89-0022 "Seismic Wave Propagation Effects on Straight Jointed Buried Pipelines," by K. Elhadi and M.J. O'Rourke, 8/24/89, (PB90-162322, A10, MF-A02).
- NCEER-89-0023 "Workshop on Serviceability Analysis of Water Delivery Systems," edited by M. Grigoriu, 3/6/89, (PB90-127424, A03, MF-A01).
- NCEER-89-0024 "Shaking Table Study of a 1/5 Scale Steel Frame Composed of Tapered Members," by K.C. Chang, J.S. Hwang and G.C. Lee, 9/18/89, (PB90-160169, A04, MF-A01).
- NCEER-89-0025 "DYNA1D: A Computer Program for Nonlinear Seismic Site Response Analysis - Technical Documentation," by Jean H. Prevost, 9/14/89, (PB90-161944, A07, MF-A01). This report is available only through NTIS (see address given above).
- NCEER-89-0026 "1:4 Scale Model Studies of Active Tendon Systems and Active Mass Dampers for Aseismic Protection," by A.M. Reinhorn, T.T. Soong, R.C. Lin, Y.P. Yang, Y. Fukao, H. Abe and M. Nakai, 9/15/89, (PB90-173246, A10, MF-A02). This report is available only through NTIS (see address given above).
- NCEER-89-0027 "Scattering of Waves by Inclusions in a Nonhomogeneous Elastic Half Space Solved by Boundary Element Methods," by P.K. Hadley, A. Askar and A.S. Cakmak, 6/15/89, (PB90-145699, A07, MF-A01).
- NCEER-89-0028 "Statistical Evaluation of Deflection Amplification Factors for Reinforced Concrete Structures," by H.H.M. Hwang, J-W. Jaw and A.L. Ch'ng, 8/31/89, (PB90-164633, A05, MF-A01).
- NCEER-89-0029 "Bedrock Accelerations in Memphis Area Due to Large New Madrid Earthquakes," by H.H.M. Hwang, C.H.S. Chen and G. Yu, 11/7/89, (PB90-162330, A04, MF-A01).
- NCEER-89-0030 "Seismic Behavior and Response Sensitivity of Secondary Structural Systems," by Y.Q. Chen and T.T. Soong, 10/23/89, (PB90-164658, A08, MF-A01).
- NCEER-89-0031 "Random Vibration and Reliability Analysis of Primary-Secondary Structural Systems," by Y. Ibrahim, M. Grigoriu and T.T. Soong, 11/10/89, (PB90-161951, A04, MF-A01).

- NCEER-89-0032 "Proceedings from the Second U.S. - Japan Workshop on Liquefaction, Large Ground Deformation and Their Effects on Lifelines, September 26-29, 1989," Edited by T.D. O'Rourke and M. Hamada, 12/1/89, (PB90-209388, A22, MF-A03).
- NCEER-89-0033 "Deterministic Model for Seismic Damage Evaluation of Reinforced Concrete Structures," by J.M. Bracci, A.M. Reinhorn, J.B. Mander and S.K. Kunnath, 9/27/89, (PB91-108803, A06, MF-A01).
- NCEER-89-0034 "On the Relation Between Local and Global Damage Indices," by E. DiPasquale and A.S. Cakmak, 8/15/89, (PB90-173865, A05, MF-A01).
- NCEER-89-0035 "Cyclic Undrained Behavior of Nonplastic and Low Plasticity Silts," by A.J. Walker and H.E. Stewart, 7/26/89, (PB90-183518, A10, MF-A01).
- NCEER-89-0036 "Liquefaction Potential of Surficial Deposits in the City of Buffalo, New York," by M. Budhu, R. Giese and L. Baumgrass, 1/17/89, (PB90-208455, A04, MF-A01).
- NCEER-89-0037 "A Deterministic Assessment of Effects of Ground Motion Incoherence," by A.S. Veletsos and Y. Tang, 7/15/89, (PB90-164294, A03, MF-A01).
- NCEER-89-0038 "Workshop on Ground Motion Parameters for Seismic Hazard Mapping," July 17-18, 1989, edited by R.V. Whitman, 12/1/89, (PB90-173923, A04, MF-A01).
- NCEER-89-0039 "Seismic Effects on Elevated Transit Lines of the New York City Transit Authority," by C.J. Costantino, C.A. Miller and E. Heymsfield, 12/26/89, (PB90-207887, A06, MF-A01).
- NCEER-89-0040 "Centrifugal Modeling of Dynamic Soil-Structure Interaction," by K. Weissman, Supervised by J.H. Prevost, 5/10/89, (PB90-207879, A07, MF-A01).
- NCEER-89-0041 "Linearized Identification of Buildings With Cores for Seismic Vulnerability Assessment," by I-K. Ho and A.E. Aktan, 11/1/89, (PB90-251943, A07, MF-A01).
- NCEER-90-0001 "Geotechnical and Lifeline Aspects of the October 17, 1989 Loma Prieta Earthquake in San Francisco," by T.D. O'Rourke, H.E. Stewart, F.T. Blackburn and T.S. Dickerman, 1/90, (PB90-208596, A05, MF-A01).
- NCEER-90-0002 "Nonnormal Secondary Response Due to Yielding in a Primary Structure," by D.C.K. Chen and L.D. Lutes, 2/28/90, (PB90-251976, A07, MF-A01).
- NCEER-90-0003 "Earthquake Education Materials for Grades K-12," by K.E.K. Ross, 4/16/90, (PB91-251984, A05, MF-A05). This report has been replaced by NCEER-92-0018.
- NCEER-90-0004 "Catalog of Strong Motion Stations in Eastern North America," by R.W. Busby, 4/3/90, (PB90-251984, A05, MF-A01).
- NCEER-90-0005 "NCEER Strong-Motion Data Base: A User Manual for the GeoBase Release (Version 1.0 for the Sun3)," by P. Friberg and K. Jacob, 3/31/90 (PB90-258062, A04, MF-A01).
- NCEER-90-0006 "Seismic Hazard Along a Crude Oil Pipeline in the Event of an 1811-1812 Type New Madrid Earthquake," by H.H.M. Hwang and C-H.S. Chen, 4/16/90, (PB90-258054, A04, MF-A01).
- NCEER-90-0007 "Site-Specific Response Spectra for Memphis Sheahan Pumping Station," by H.H.M. Hwang and C.S. Lee, 5/15/90, (PB91-108811, A05, MF-A01).
- NCEER-90-0008 "Pilot Study on Seismic Vulnerability of Crude Oil Transmission Systems," by T. Ariman, R. Dobry, M. Grigoriu, F. Kozin, M. O'Rourke, T. O'Rourke and M. Shinozuka, 5/25/90, (PB91-108837, A06, MF-A01).
- NCEER-90-0009 "A Program to Generate Site Dependent Time Histories: EQGEN," by G.W. Ellis, M. Srinivasan and A.S. Cakmak, 1/30/90, (PB91-108829, A04, MF-A01).
- NCEER-90-0010 "Active Isolation for Seismic Protection of Operating Rooms," by M.E. Talbott, Supervised by M. Shinozuka, 6/8/9, (PB91-110205, A05, MF-A01).

- NCEER-90-0011 "Program LINEARID for Identification of Linear Structural Dynamic Systems," by C-B. Yun and M. Shinozuka, 6/25/90, (PB91-110312, A08, MF-A01).
- NCEER-90-0012 "Two-Dimensional Two-Phase Elasto-Plastic Seismic Response of Earth Dams," by A.N. Yiagos, Supervised by J.H. Prevost, 6/20/90, (PB91-110197, A13, MF-A02).
- NCEER-90-0013 "Secondary Systems in Base-Isolated Structures: Experimental Investigation, Stochastic Response and Stochastic Sensitivity," by G.D. Manolis, G. Juhn, M.C. Constantinou and A.M. Reinhorn, 7/1/90, (PB91-110320, A08, MF-A01).
- NCEER-90-0014 "Seismic Behavior of Lightly-Reinforced Concrete Column and Beam-Column Joint Details," by S.P. Pessiki, C.H. Conley, P. Gergely and R.N. White, 8/22/90, (PB91-108795, A11, MF-A02).
- NCEER-90-0015 "Two Hybrid Control Systems for Building Structures Under Strong Earthquakes," by J.N. Yang and A. Daniellians, 6/29/90, (PB91-125393, A04, MF-A01).
- NCEER-90-0016 "Instantaneous Optimal Control with Acceleration and Velocity Feedback," by J.N. Yang and Z. Li, 6/29/90, (PB91-125401, A03, MF-A01).
- NCEER-90-0017 "Reconnaissance Report on the Northern Iran Earthquake of June 21, 1990," by M. Mehrain, 10/4/90, (PB91-125377, A03, MF-A01).
- NCEER-90-0018 "Evaluation of Liquefaction Potential in Memphis and Shelby County," by T.S. Chang, P.S. Tang, C.S. Lee and H. Hwang, 8/10/90, (PB91-125427, A09, MF-A01).
- NCEER-90-0019 "Experimental and Analytical Study of a Combined Sliding Disc Bearing and Helical Steel Spring Isolation System," by M.C. Constantinou, A.S. Mokha and A.M. Reinhorn, 10/4/90, (PB91-125385, A06, MF-A01). This report is available only through NTIS (see address given above).
- NCEER-90-0020 "Experimental Study and Analytical Prediction of Earthquake Response of a Sliding Isolation System with a Spherical Surface," by A.S. Mokha, M.C. Constantinou and A.M. Reinhorn, 10/11/90, (PB91-125419, A05, MF-A01).
- NCEER-90-0021 "Dynamic Interaction Factors for Floating Pile Groups," by G. Gazetas, K. Fan, A. Kaynia and E. Kausel, 9/10/90, (PB91-170381, A05, MF-A01).
- NCEER-90-0022 "Evaluation of Seismic Damage Indices for Reinforced Concrete Structures," by S. Rodriguez-Gomez and A.S. Cakmak, 9/30/90, PB91-171322, A06, MF-A01).
- NCEER-90-0023 "Study of Site Response at a Selected Memphis Site," by H. Desai, S. Ahmad, E.S. Gazetas and M.R. Oh, 10/11/90, (PB91-196857, A03, MF-A01).
- NCEER-90-0024 "A User's Guide to Strongmo: Version 1.0 of NCEER's Strong-Motion Data Access Tool for PCs and Terminals," by P.A. Friberg and C.A.T. Susch, 11/15/90, (PB91-171272, A03, MF-A01).
- NCEER-90-0025 "A Three-Dimensional Analytical Study of Spatial Variability of Seismic Ground Motions," by L-L. Hong and A.H.-S. Ang, 10/30/90, (PB91-170399, A09, MF-A01).
- NCEER-90-0026 "MUMOID User's Guide - A Program for the Identification of Modal Parameters," by S. Rodriguez-Gomez and E. DiPasquale, 9/30/90, (PB91-171298, A04, MF-A01).
- NCEER-90-0027 "SARCF-II User's Guide - Seismic Analysis of Reinforced Concrete Frames," by S. Rodriguez-Gomez, Y.S. Chung and C. Meyer, 9/30/90, (PB91-171280, A05, MF-A01).
- NCEER-90-0028 "Viscous Dampers: Testing, Modeling and Application in Vibration and Seismic Isolation," by N. Makris and M.C. Constantinou, 12/20/90 (PB91-190561, A06, MF-A01).
- NCEER-90-0029 "Soil Effects on Earthquake Ground Motions in the Memphis Area," by H. Hwang, C.S. Lee, K.W. Ng and T.S. Chang, 8/2/90, (PB91-190751, A05, MF-A01).



- NCEER-91-0001 "Proceedings from the Third Japan-U.S. Workshop on Earthquake Resistant Design of Lifeline Facilities and Countermeasures for Soil Liquefaction, December 17-19, 1990," edited by T.D. O'Rourke and M. Hamada, 2/1/91, (PB91-179259, A99, MF-A04).
- NCEER-91-0002 "Physical Space Solutions of Non-Proportionally Damped Systems," by M. Tong, Z. Liang and G.C. Lee, 1/15/91, (PB91-179242, A04, MF-A01).
- NCEER-91-0003 "Seismic Response of Single Piles and Pile Groups," by K. Fan and G. Gazetas, 1/10/91, (PB92-174994, A04, MF-A01).
- NCEER-91-0004 "Damping of Structures: Part 1 - Theory of Complex Damping," by Z. Liang and G. Lee, 10/10/91, (PB92-197235, A12, MF-A03).
- NCEER-91-0005 "3D-BASIS - Nonlinear Dynamic Analysis of Three Dimensional Base Isolated Structures: Part II," by S. Nagarajaiah, A.M. Reinhorn and M.C. Constantinou, 2/28/91, (PB91-190553, A07, MF-A01). This report has been replaced by NCEER-93-0011.
- NCEER-91-0006 "A Multidimensional Hysteretic Model for Plasticity Deforming Metals in Energy Absorbing Devices," by E.J. Graesser and F.A. Cozzarelli, 4/9/91, (PB92-108364, A04, MF-A01).
- NCEER-91-0007 "A Framework for Customizable Knowledge-Based Expert Systems with an Application to a KBES for Evaluating the Seismic Resistance of Existing Buildings," by E.G. Ibarra-Anaya and S.J. Fennes, 4/9/91, (PB91-210930, A08, MF-A01).
- NCEER-91-0008 "Nonlinear Analysis of Steel Frames with Semi-Rigid Connections Using the Capacity Spectrum Method," by G.G. Deierlein, S-H. Hsieh, Y-J. Shen and J.F. Abel, 7/2/91, (PB92-113828, A05, MF-A01).
- NCEER-91-0009 "Earthquake Education Materials for Grades K-12," by K.E.K. Ross, 4/30/91, (PB91-212142, A06, MF-A01). This report has been replaced by NCEER-92-0018.
- NCEER-91-0010 "Phase Wave Velocities and Displacement Phase Differences in a Harmonically Oscillating Pile," by N. Makris and G. Gazetas, 7/8/91, (PB92-108356, A04, MF-A01).
- NCEER-91-0011 "Dynamic Characteristics of a Full-Size Five-Story Steel Structure and a 2/5 Scale Model," by K.C. Chang, G.C. Yao, G.C. Lee, D.S. Hao and Y.C. Yeh, 7/2/91, (PB93-116648, A06, MF-A02).
- NCEER-91-0012 "Seismic Response of a 2/5 Scale Steel Structure with Added Viscoelastic Dampers," by K.C. Chang, T.T. Soong, S-T. Oh and M.L. Lai, 5/17/91, (PB92-110816, A05, MF-A01).
- NCEER-91-0013 "Earthquake Response of Retaining Walls; Full-Scale Testing and Computational Modeling," by S. Alampalli and A-W.M. Elgamal, 6/20/91, to be published.
- NCEER-91-0014 "3D-BASIS-M: Nonlinear Dynamic Analysis of Multiple Building Base Isolated Structures," by P.C. Tsopelas, S. Nagarajaiah, M.C. Constantinou and A.M. Reinhorn, 5/28/91, (PB92-113885, A09, MF-A02).
- NCEER-91-0015 "Evaluation of SEAOC Design Requirements for Sliding Isolated Structures," by D. Theodossiou and M.C. Constantinou, 6/10/91, (PB92-114602, A11, MF-A03).
- NCEER-91-0016 "Closed-Loop Modal Testing of a 27-Story Reinforced Concrete Flat Plate-Core Building," by H.R. Somaprasad, T. Toksoy, H. Yoshiyuki and A.E. Aktan, 7/15/91, (PB92-129980, A07, MF-A02).
- NCEER-91-0017 "Shake Table Test of a 1/6 Scale Two-Story Lightly Reinforced Concrete Building," by A.G. El-Attar, R.N. White and P. Gergely, 2/28/91, (PB92-222447, A06, MF-A02).
- NCEER-91-0018 "Shake Table Test of a 1/8 Scale Three-Story Lightly Reinforced Concrete Building," by A.G. El-Attar, R.N. White and P. Gergely, 2/28/91, (PB93-116630, A08, MF-A02).
- NCEER-91-0019 "Transfer Functions for Rigid Rectangular Foundations," by A.S. Veletsos, A.M. Prasad and W.H. Wu, 7/31/91, to be published.

- NCEER-91-0020 "Hybrid Control of Seismic-Excited Nonlinear and Inelastic Structural Systems," by J.N. Yang, Z. Li and A. Daniellians, 8/1/91, (PB92-143171, A06, MF-A02).
- NCEER-91-0021 "The NCEER-91 Earthquake Catalog: Improved Intensity-Based Magnitudes and Recurrence Relations for U.S. Earthquakes East of New Madrid," by L. Seeber and J.G. Armbruster, 8/28/91, (PB92-176742, A06, MF-A02).
- NCEER-91-0022 "Proceedings from the Implementation of Earthquake Planning and Education in Schools: The Need for Change - The Roles of the Changemakers," by K.E.K. Ross and F. Winslow, 7/23/91, (PB92-129998, A12, MF-A03).
- NCEER-91-0023 "A Study of Reliability-Based Criteria for Seismic Design of Reinforced Concrete Frame Buildings," by H.H.M. Hwang and H-M. Hsu, 8/10/91, (PB92-140235, A09, MF-A02).
- NCEER-91-0024 "Experimental Verification of a Number of Structural System Identification Algorithms," by R.G. Ghanem, H. Gavin and M. Shinozuka, 9/18/91, (PB92-176577, A18, MF-A04).
- NCEER-91-0025 "Probabilistic Evaluation of Liquefaction Potential," by H.H.M. Hwang and C.S. Lee," 11/25/91, (PB92-143429, A05, MF-A01).
- NCEER-91-0026 "Instantaneous Optimal Control for Linear, Nonlinear and Hysteretic Structures - Stable Controllers," by J.N. Yang and Z. Li, 11/15/91, (PB92-163807, A04, MF-A01).
- NCEER-91-0027 "Experimental and Theoretical Study of a Sliding Isolation System for Bridges," by M.C. Constantinou, A. Kartoum, A.M. Reinhorn and P. Bradford, 11/15/91, (PB92-176973, A10, MF-A03).
- NCEER-92-0001 "Case Studies of Liquefaction and Lifeline Performance During Past Earthquakes, Volume 1: Japanese Case Studies," Edited by M. Hamada and T. O'Rourke, 2/17/92, (PB92-197243, A18, MF-A04).
- NCEER-92-0002 "Case Studies of Liquefaction and Lifeline Performance During Past Earthquakes, Volume 2: United States Case Studies," Edited by T. O'Rourke and M. Hamada, 2/17/92, (PB92-197250, A20, MF-A04).
- NCEER-92-0003 "Issues in Earthquake Education," Edited by K. Ross, 2/3/92, (PB92-222389, A07, MF-A02).
- NCEER-92-0004 "Proceedings from the First U.S. - Japan Workshop on Earthquake Protective Systems for Bridges," Edited by I.G. Buckle, 2/4/92, (PB94-142239, A99, MF-A06).
- NCEER-92-0005 "Seismic Ground Motion from a Haskell-Type Source in a Multiple-Layered Half-Space," A.P. Theoharis, G. Deodatis and M. Shinozuka, 1/2/92, to be published.
- NCEER-92-0006 "Proceedings from the Site Effects Workshop," Edited by R. Whitman, 2/29/92, (PB92-197201, A04, MF-A01).
- NCEER-92-0007 "Engineering Evaluation of Permanent Ground Deformations Due to Seismically-Induced Liquefaction," by M.H. Baziar, R. Dobry and A-W.M. Elgamal, 3/24/92, (PB92-222421, A13, MF-A03).
- NCEER-92-0008 "A Procedure for the Seismic Evaluation of Buildings in the Central and Eastern United States," by C.D. Poland and J.O. Malley, 4/2/92, (PB92-222439, A20, MF-A04).
- NCEER-92-0009 "Experimental and Analytical Study of a Hybrid Isolation System Using Friction Controllable Sliding Bearings," by M.Q. Feng, S. Fujii and M. Shinozuka, 5/15/92, (PB93-150282, A06, MF-A02).
- NCEER-92-0010 "Seismic Resistance of Slab-Column Connections in Existing Non-Ductile Flat-Plate Buildings," by A.J. Durrani and Y. Du, 5/18/92, (PB93-116812, A06, MF-A02).
- NCEER-92-0011 "The Hysteretic and Dynamic Behavior of Brick Masonry Walls Upgraded by Ferrocement Coatings Under Cyclic Loading and Strong Simulated Ground Motion," by H. Lee and S.P. Prawl, 5/11/92, to be published.
- NCEER-92-0012 "Study of Wire Rope Systems for Seismic Protection of Equipment in Buildings," by G.F. Demetriades, M.C. Constantinou and A.M. Reinhorn, 5/20/92, (PB93-116655, A08, MF-A02).

- NCEER-92-0013 "Shape Memory Structural Dampers: Material Properties, Design and Seismic Testing," by P.R. Witting and F.A. Cozzarelli, 5/26/92, (PB93-116663, A05, MF-A01).
- NCEER-92-0014 "Longitudinal Permanent Ground Deformation Effects on Buried Continuous Pipelines," by M.J. O'Rourke, and C. Nordberg, 6/15/92, (PB93-116671, A08, MF-A02).
- NCEER-92-0015 "A Simulation Method for Stationary Gaussian Random Functions Based on the Sampling Theorem," by M. Grigoriu and S. Balopoulou, 6/11/92, (PB93-127496, A05, MF-A01).
- NCEER-92-0016 "Gravity-Load-Designed Reinforced Concrete Buildings: Seismic Evaluation of Existing Construction and Detailing Strategies for Improved Seismic Resistance," by G.W. Hoffmann, S.K. Kunnath, A.M. Reinhorn and J.B. Mander, 7/15/92, (PB94-142007, A08, MF-A02).
- NCEER-92-0017 "Observations on Water System and Pipeline Performance in the Limón Area of Costa Rica Due to the April 22, 1991 Earthquake," by M. O'Rourke and D. Ballantyne, 6/30/92, (PB93-126811, A06, MF-A02).
- NCEER-92-0018 "Fourth Edition of Earthquake Education Materials for Grades K-12," Edited by K.E.K. Ross, 8/10/92, (PB93-114023, A07, MF-A02).
- NCEER-92-0019 "Proceedings from the Fourth Japan-U.S. Workshop on Earthquake Resistant Design of Lifeline Facilities and Countermeasures for Soil Liquefaction," Edited by M. Hamada and T.D. O'Rourke, 8/12/92, (PB93-163939, A99, MF-E11).
- NCEER-92-0020 "Active Bracing System: A Full Scale Implementation of Active Control," by A.M. Reinhorn, T.T. Soong, R.C. Lin, M.A. Riley, Y.P. Wang, S. Aizawa and M. Higashino, 8/14/92, (PB93-127512, A06, MF-A02).
- NCEER-92-0021 "Empirical Analysis of Horizontal Ground Displacement Generated by Liquefaction-Induced Lateral Spreads," by S.F. Bartlett and T.L. Youd, 8/17/92, (PB93-188241, A06, MF-A02).
- NCEER-92-0022 "IDARC Version 3.0: Inelastic Damage Analysis of Reinforced Concrete Structures," by S.K. Kunnath, A.M. Reinhorn and R.F. Lobo, 8/31/92, (PB93-227502, A07, MF-A02).
- NCEER-92-0023 "A Semi-Empirical Analysis of Strong-Motion Peaks in Terms of Seismic Source, Propagation Path and Local Site Conditions, by M. Kamiyama, M.J. O'Rourke and R. Flores-Berrones, 9/9/92, (PB93-150266, A08, MF-A02).
- NCEER-92-0024 "Seismic Behavior of Reinforced Concrete Frame Structures with Nonductile Details, Part I: Summary of Experimental Findings of Full Scale Beam-Column Joint Tests," by A. Beres, R.N. White and P. Gergely, 9/30/92, (PB93-227783, A05, MF-A01).
- NCEER-92-0025 "Experimental Results of Repaired and Retrofitted Beam-Column Joint Tests in Lightly Reinforced Concrete Frame Buildings," by A. Beres, S. El-Borgi, R.N. White and P. Gergely, 10/29/92, (PB93-227791, A05, MF-A01).
- NCEER-92-0026 "A Generalization of Optimal Control Theory: Linear and Nonlinear Structures," by J.N. Yang, Z. Li and S. Vongchavalitkul, 11/2/92, (PB93-188621, A05, MF-A01).
- NCEER-92-0027 "Seismic Resistance of Reinforced Concrete Frame Structures Designed Only for Gravity Loads: Part I - Design and Properties of a One-Third Scale Model Structure," by J.M. Bracci, A.M. Reinhorn and J.B. Mander, 12/1/92, (PB94-104502, A08, MF-A02).
- NCEER-92-0028 "Seismic Resistance of Reinforced Concrete Frame Structures Designed Only for Gravity Loads: Part II - Experimental Performance of Subassemblages," by L.E. Aycaardi, J.B. Mander and A.M. Reinhorn, 12/1/92, (PB94-104510, A08, MF-A02).
- NCEER-92-0029 "Seismic Resistance of Reinforced Concrete Frame Structures Designed Only for Gravity Loads: Part III - Experimental Performance and Analytical Study of a Structural Model," by J.M. Bracci, A.M. Reinhorn and J.B. Mander, 12/1/92, (PB93-227528, A09, MF-A01).

- NCEER-92-0030 "Evaluation of Seismic Retrofit of Reinforced Concrete Frame Structures: Part I - Experimental Performance of Retrofitted Subassemblages," by D. Choudhuri, J.B. Mander and A.M. Reinhorn, 12/8/92, (PB93-198307, A07, MF-A02).
- NCEER-92-0031 "Evaluation of Seismic Retrofit of Reinforced Concrete Frame Structures: Part II - Experimental Performance and Analytical Study of a Retrofitted Structural Model," by J.M. Bracci, A.M. Reinhorn and J.B. Mander, 12/8/92, (PB93-198315, A09, MF-A03).
- NCEER-92-0032 "Experimental and Analytical Investigation of Seismic Response of Structures with Supplemental Fluid Viscous Dampers," by M.C. Constantinou and M.D. Symans, 12/21/92, (PB93-191435, A10, MF-A03). This report is available only through NTIS (see address given above).
- NCEER-92-0033 "Reconnaissance Report on the Cairo, Egypt Earthquake of October 12, 1992," by M. Khater, 12/23/92, (PB93-188621, A03, MF-A01).
- NCEER-92-0034 "Low-Level Dynamic Characteristics of Four Tall Flat-Plate Buildings in New York City," by H. Gavin, S. Yuan, J. Grossman, E. Pekelis and K. Jacob, 12/28/92, (PB93-188217, A07, MF-A02).
- NCEER-93-0001 "An Experimental Study on the Seismic Performance of Brick-Infilled Steel Frames With and Without Retrofit," by J.B. Mander, B. Nair, K. Wojtkowski and J. Ma, 1/29/93, (PB93-227510, A07, MF-A02).
- NCEER-93-0002 "Social Accounting for Disaster Preparedness and Recovery Planning," by S. Cole, E. Pantoja and V. Razak, 2/22/93, (PB94-142114, A12, MF-A03).
- NCEER-93-0003 "Assessment of 1991 NEHRP Provisions for Nonstructural Components and Recommended Revisions," by T.T. Soong, G. Chen, Z. Wu, R-H. Zhang and M. Grigoriu, 3/1/93, (PB93-188639, A06, MF-A02).
- NCEER-93-0004 "Evaluation of Static and Response Spectrum Analysis Procedures of SEAOC/UBC for Seismic Isolated Structures," by C.W. Winters and M.C. Constantinou, 3/23/93, (PB93-198299, A10, MF-A03).
- NCEER-93-0005 "Earthquakes in the Northeast - Are We Ignoring the Hazard? A Workshop on Earthquake Science and Safety for Educators," edited by K.E.K. Ross, 4/2/93, (PB94-103066, A09, MF-A02).
- NCEER-93-0006 "Inelastic Response of Reinforced Concrete Structures with Viscoelastic Braces," by R.F. Lobo, J.M. Bracci, K.L. Shen, A.M. Reinhorn and T.T. Soong, 4/5/93, (PB93-227486, A05, MF-A02).
- NCEER-93-0007 "Seismic Testing of Installation Methods for Computers and Data Processing Equipment," by K. Kosar, T.T. Soong, K.L. Shen, J.A. HoLung and Y.K. Lin, 4/12/93, (PB93-198299, A07, MF-A02).
- NCEER-93-0008 "Retrofit of Reinforced Concrete Frames Using Added Dampers," by A. Reinhorn, M. Constantinou and C. Li, to be published.
- NCEER-93-0009 "Seismic Behavior and Design Guidelines for Steel Frame Structures with Added Viscoelastic Dampers," by K.C. Chang, M.L. Lai, T.T. Soong, D.S. Hao and Y.C. Yeh, 5/1/93, (PB94-141959, A07, MF-A02).
- NCEER-93-0010 "Seismic Performance of Shear-Critical Reinforced Concrete Bridge Piers," by J.B. Mander, S.M. Waheed, M.T.A. Chaudhary and S.S. Chen, 5/12/93, (PB93-227494, A08, MF-A02).
- NCEER-93-0011 "3D-BASIS-TABS: Computer Program for Nonlinear Dynamic Analysis of Three Dimensional Base Isolated Structures," by S. Nagarajaiah, C. Li, A.M. Reinhorn and M.C. Constantinou, 8/2/93, (PB94-141819, A09, MF-A02).
- NCEER-93-0012 "Effects of Hydrocarbon Spills from an Oil Pipeline Break on Ground Water," by O.J. Helweg and H.H.M. Hwang, 8/3/93, (PB94-141942, A06, MF-A02).
- NCEER-93-0013 "Simplified Procedures for Seismic Design of Nonstructural Components and Assessment of Current Code Provisions," by M.P. Singh, L.E. Suarez, E.E. Matheu and G.O. Maldonado, 8/4/93, (PB94-141827, A09, MF-A02).
- NCEER-93-0014 "An Energy Approach to Seismic Analysis and Design of Secondary Systems," by G. Chen and T.T. Soong, 8/6/93, (PB94-142767, A11, MF-A03).

- NCEER-93-0015 "Proceedings from School Sites: Becoming Prepared for Earthquakes - Commemorating the Third Anniversary of the Loma Prieta Earthquake," Edited by F.E. Winslow and K.E.K. Ross, 8/16/93, (PB94-154275, A16, MF-A02).
- NCEER-93-0016 "Reconnaissance Report of Damage to Historic Monuments in Cairo, Egypt Following the October 12, 1992 Dahshur Earthquake," by D. Sykora, D. Look, G. Croci, E. Karaesmen and E. Karaesmen, 8/19/93, (PB94-142221, A08, MF-A02).
- NCEER-93-0017 "The Island of Guam Earthquake of August 8, 1993," by S.W. Swan and S.K. Harris, 9/30/93, (PB94-141843, A04, MF-A01).
- NCEER-93-0018 "Engineering Aspects of the October 12, 1992 Egyptian Earthquake," by A.W. Elgamal, M. Amer, K. Adalier and A. Abul-Fadl, 10/7/93, (PB94-141983, A05, MF-A01).
- NCEER-93-0019 "Development of an Earthquake Motion Simulator and its Application in Dynamic Centrifuge Testing," by I. Krstelj, Supervised by J.H. Prevost, 10/23/93, (PB94-181773, A-10, MF-A03).
- NCEER-93-0020 "NCEER-Taisei Corporation Research Program on Sliding Seismic Isolation Systems for Bridges: Experimental and Analytical Study of a Friction Pendulum System (FPS)," by M.C. Constantinou, P. Tsopelas, Y-S. Kim and S. Okamoto, 11/1/93, (PB94-142775, A08, MF-A02).
- NCEER-93-0021 "Finite Element Modeling of Elastomeric Seismic Isolation Bearings," by L.J. Billings, Supervised by R. Shepherd, 11/8/93, to be published.
- NCEER-93-0022 "Seismic Vulnerability of Equipment in Critical Facilities: Life-Safety and Operational Consequences," by K. Porter, G.S. Johnson, M.M. Zadeh, C. Scawthorn and S. Eder, 11/24/93, (PB94-181765, A16, MF-A03).
- NCEER-93-0023 "Hokkaido Nansei-oki, Japan Earthquake of July 12, 1993, by P.I. Yanev and C.R. Scawthorn, 12/23/93, (PB94-181500, A07, MF-A01).
- NCEER-94-0001 "An Evaluation of Seismic Serviceability of Water Supply Networks with Application to the San Francisco Auxiliary Water Supply System," by I. Markov, Supervised by M. Grigoriu and T. O'Rourke, 1/21/94, (PB94-204013, A07, MF-A02).
- NCEER-94-0002 "NCEER-Taisei Corporation Research Program on Sliding Seismic Isolation Systems for Bridges: Experimental and Analytical Study of Systems Consisting of Sliding Bearings, Rubber Restoring Force Devices and Fluid Dampers," Volumes I and II, by P. Tsopelas, S. Okamoto, M.C. Constantinou, D. Ozaki and S. Fujii, 2/4/94, (PB94-181740, A09, MF-A02 and PB94-181757, A12, MF-A03).
- NCEER-94-0003 "A Markov Model for Local and Global Damage Indices in Seismic Analysis," by S. Rahman and M. Grigoriu, 2/18/94, (PB94-206000, A12, MF-A03).
- NCEER-94-0004 "Proceedings from the NCEER Workshop on Seismic Response of Masonry Infills," edited by D.P. Abrams, 3/1/94, (PB94-180783, A07, MF-A02).
- NCEER-94-0005 "The Northridge, California Earthquake of January 17, 1994: General Reconnaissance Report," edited by J.D. Goltz, 3/11/94, (PB94-193943, A10, MF-A03).
- NCEER-94-0006 "Seismic Energy Based Fatigue Damage Analysis of Bridge Columns: Part I - Evaluation of Seismic Capacity," by G.A. Chang and J.B. Mander, 3/14/94, (PB94-219185, A11, MF-A03).
- NCEER-94-0007 "Seismic Isolation of Multi-Story Frame Structures Using Spherical Sliding Isolation Systems," by T.M. Al-Hussaini, V.A. Zayas and M.C. Constantinou, 3/17/94, (PB94-193745, A09, MF-A02).
- NCEER-94-0008 "The Northridge, California Earthquake of January 17, 1994: Performance of Highway Bridges," edited by I.G. Buckle, 3/24/94, (PB94-193851, A06, MF-A02).
- NCEER-94-0009 "Proceedings of the Third U.S.-Japan Workshop on Earthquake Protective Systems for Bridges," edited by I.G. Buckle and I. Friedland, 3/31/94, (PB94-195815, A99, MF-A06).

- NCEER-94-0010 "3D-BASIS-ME: Computer Program for Nonlinear Dynamic Analysis of Seismically Isolated Single and Multiple Structures and Liquid Storage Tanks," by P.C. Tsopelas, M.C. Constantinou and A.M. Reinhorn, 4/12/94, (PB94-204922, A09, MF-A02).
- NCEER-94-0011 "The Northridge, California Earthquake of January 17, 1994: Performance of Gas Transmission Pipelines," by T.D. O'Rourke and M.C. Palmer, 5/16/94, (PB94-204989, A05, MF-A01).
- NCEER-94-0012 "Feasibility Study of Replacement Procedures and Earthquake Performance Related to Gas Transmission Pipelines," by T.D. O'Rourke and M.C. Palmer, 5/25/94, (PB94-206638, A09, MF-A02).
- NCEER-94-0013 "Seismic Energy Based Fatigue Damage Analysis of Bridge Columns: Part II - Evaluation of Seismic Demand," by G.A. Chang and J.B. Mander, 6/1/94, (PB95-18106, A08, MF-A02).
- NCEER-94-0014 "NCEER-Taisei Corporation Research Program on Sliding Seismic Isolation Systems for Bridges: Experimental and Analytical Study of a System Consisting of Sliding Bearings and Fluid Restoring Force/Damping Devices," by P. Tsopelas and M.C. Constantinou, 6/13/94, (PB94-219144, A10, MF-A03).
- NCEER-94-0015 "Generation of Hazard-Consistent Fragility Curves for Seismic Loss Estimation Studies," by H. Hwang and J-R. Huo, 6/14/94, (PB95-181996, A09, MF-A02).
- NCEER-94-0016 "Seismic Study of Building Frames with Added Energy-Absorbing Devices," by W.S. Pong, C.S. Tsai and G.C. Lee, 6/20/94, (PB94-219136, A10, A03).
- NCEER-94-0017 "Sliding Mode Control for Seismic-Excited Linear and Nonlinear Civil Engineering Structures," by J. Yang, J. Wu, A. Agrawal and Z. Li, 6/21/94, (PB95-138483, A06, MF-A02).
- NCEER-94-0018 "3D-BASIS-TABS Version 2.0: Computer Program for Nonlinear Dynamic Analysis of Three Dimensional Base Isolated Structures," by A.M. Reinhorn, S. Nagarajaiah, M.C. Constantinou, P. Tsopelas and R. Li, 6/22/94, (PB95-182176, A08, MF-A02).
- NCEER-94-0019 "Proceedings of the International Workshop on Civil Infrastructure Systems: Application of Intelligent Systems and Advanced Materials on Bridge Systems," Edited by G.C. Lee and K.C. Chang, 7/18/94, (PB95-252474, A20, MF-A04).
- NCEER-94-0020 "Study of Seismic Isolation Systems for Computer Floors," by V. Lambrou and M.C. Constantinou, 7/19/94, (PB95-138533, A10, MF-A03).
- NCEER-94-0021 "Proceedings of the U.S.-Italian Workshop on Guidelines for Seismic Evaluation and Rehabilitation of Unreinforced Masonry Buildings," Edited by D.P. Abrams and G.M. Calvi, 7/20/94, (PB95-138749, A13, MF-A03).
- NCEER-94-0022 "NCEER-Taisei Corporation Research Program on Sliding Seismic Isolation Systems for Bridges: Experimental and Analytical Study of a System Consisting of Lubricated PTFE Sliding Bearings and Mild Steel Dampers," by P. Tsopelas and M.C. Constantinou, 7/22/94, (PB95-182184, A08, MF-A02).
- NCEER-94-0023 "Development of Reliability-Based Design Criteria for Buildings Under Seismic Load," by Y.K. Wen, H. Hwang and M. Shinozuka, 8/1/94, (PB95-211934, A08, MF-A02).
- NCEER-94-0024 "Experimental Verification of Acceleration Feedback Control Strategies for an Active Tendon System," by S.J. Dyke, B.F. Spencer, Jr., P. Quast, M.K. Sain, D.C. Kaspari, Jr. and T.T. Soong, 8/29/94, (PB95-212320, A05, MF-A01).
- NCEER-94-0025 "Seismic Retrofitting Manual for Highway Bridges," Edited by I.G. Buckle and I.F. Friedland, published by the Federal Highway Administration (PB95-212676, A15, MF-A03).
- NCEER-94-0026 "Proceedings from the Fifth U.S.-Japan Workshop on Earthquake Resistant Design of Lifeline Facilities and Countermeasures Against Soil Liquefaction," Edited by T.D. O'Rourke and M. Hamada, 11/7/94, (PB95-220802, A99, MF-E08).

- NCEER-95-0001 “Experimental and Analytical Investigation of Seismic Retrofit of Structures with Supplemental Damping: Part 1 - Fluid Viscous Damping Devices,” by A.M. Reinhorn, C. Li and M.C. Constantinou, 1/3/95, (PB95-266599, A09, MF-A02).
- NCEER-95-0002 “Experimental and Analytical Study of Low-Cycle Fatigue Behavior of Semi-Rigid Top-And-Seat Angle Connections,” by G. Pekcan, J.B. Mander and S.S. Chen, 1/5/95, (PB95-220042, A07, MF-A02).
- NCEER-95-0003 “NCEER-ATC Joint Study on Fragility of Buildings,” by T. Anagnos, C. Rojahn and A.S. Kiremidjian, 1/20/95, (PB95-220026, A06, MF-A02).
- NCEER-95-0004 “Nonlinear Control Algorithms for Peak Response Reduction,” by Z. Wu, T.T. Soong, V. Gattulli and R.C. Lin, 2/16/95, (PB95-220349, A05, MF-A01).
- NCEER-95-0005 “Pipeline Replacement Feasibility Study: A Methodology for Minimizing Seismic and Corrosion Risks to Underground Natural Gas Pipelines,” by R.T. Eguchi, H.A. Seligson and D.G. Honegger, 3/2/95, (PB95-252326, A06, MF-A02).
- NCEER-95-0006 “Evaluation of Seismic Performance of an 11-Story Frame Building During the 1994 Northridge Earthquake,” by F. Naeim, R. DiSulio, K. Benuska, A. Reinhorn and C. Li, to be published.
- NCEER-95-0007 “Prioritization of Bridges for Seismic Retrofitting,” by N. Basöz and A.S. Kiremidjian, 4/24/95, (PB95-252300, A08, MF-A02).
- NCEER-95-0008 “Method for Developing Motion Damage Relationships for Reinforced Concrete Frames,” by A. Singhal and A.S. Kiremidjian, 5/11/95, (PB95-266607, A06, MF-A02).
- NCEER-95-0009 “Experimental and Analytical Investigation of Seismic Retrofit of Structures with Supplemental Damping: Part II - Friction Devices,” by C. Li and A.M. Reinhorn, 7/6/95, (PB96-128087, A11, MF-A03).
- NCEER-95-0010 “Experimental Performance and Analytical Study of a Non-Ductile Reinforced Concrete Frame Structure Retrofitted with Elastomeric Spring Dampers,” by G. Pekcan, J.B. Mander and S.S. Chen, 7/14/95, (PB96-137161, A08, MF-A02).
- NCEER-95-0011 “Development and Experimental Study of Semi-Active Fluid Damping Devices for Seismic Protection of Structures,” by M.D. Symans and M.C. Constantinou, 8/3/95, (PB96-136940, A23, MF-A04).
- NCEER-95-0012 “Real-Time Structural Parameter Modification (RSPM): Development of Innervated Structures,” by Z. Liang, M. Tong and G.C. Lee, 4/11/95, (PB96-137153, A06, MF-A01).
- NCEER-95-0013 “Experimental and Analytical Investigation of Seismic Retrofit of Structures with Supplemental Damping: Part III - Viscous Damping Walls,” by A.M. Reinhorn and C. Li, 10/1/95, (PB96-176409, A11, MF-A03).
- NCEER-95-0014 “Seismic Fragility Analysis of Equipment and Structures in a Memphis Electric Substation,” by J-R. Huo and H.H.M. Hwang, 8/10/95, (PB96-128087, A09, MF-A02).
- NCEER-95-0015 “The Hanshin-Awaji Earthquake of January 17, 1995: Performance of Lifelines,” Edited by M. Shinozuka, 11/3/95, (PB96-176383, A15, MF-A03).
- NCEER-95-0016 “Highway Culvert Performance During Earthquakes,” by T.L. Youd and C.J. Beckman, available as NCEER-96-0015.
- NCEER-95-0017 “The Hanshin-Awaji Earthquake of January 17, 1995: Performance of Highway Bridges,” Edited by I.G. Buckle, 12/1/95, to be published.
- NCEER-95-0018 “Modeling of Masonry Infill Panels for Structural Analysis,” by A.M. Reinhorn, A. Madan, R.E. Valles, Y. Reichmann and J.B. Mander, 12/8/95, (PB97-110886, MF-A01, A06).
- NCEER-95-0019 “Optimal Polynomial Control for Linear and Nonlinear Structures,” by A.K. Agrawal and J.N. Yang, 12/11/95, (PB96-168737, A07, MF-A02).

- NCEER-95-0020 “Retrofit of Non-Ductile Reinforced Concrete Frames Using Friction Dampers,” by R.S. Rao, P. Gergely and R.N. White, 12/22/95, (PB97-133508, A10, MF-A02).
- NCEER-95-0021 “Parametric Results for Seismic Response of Pile-Supported Bridge Bents,” by G. Mylonakis, A. Nikolaou and G. Gazetas, 12/22/95, (PB97-100242, A12, MF-A03).
- NCEER-95-0022 “Kinematic Bending Moments in Seismically Stressed Piles,” by A. Nikolaou, G. Mylonakis and G. Gazetas, 12/23/95, (PB97-113914, MF-A03, A13).
- NCEER-96-0001 “Dynamic Response of Unreinforced Masonry Buildings with Flexible Diaphragms,” by A.C. Costley and D.P. Abrams, 10/10/96, (PB97-133573, MF-A03, A15).
- NCEER-96-0002 “State of the Art Review: Foundations and Retaining Structures,” by I. Po Lam, to be published.
- NCEER-96-0003 “Ductility of Rectangular Reinforced Concrete Bridge Columns with Moderate Confinement,” by N. Wehbe, M. Saiidi, D. Sanders and B. Douglas, 11/7/96, (PB97-133557, A06, MF-A02).
- NCEER-96-0004 “Proceedings of the Long-Span Bridge Seismic Research Workshop,” edited by I.G. Buckle and I.M. Friedland, to be published.
- NCEER-96-0005 “Establish Representative Pier Types for Comprehensive Study: Eastern United States,” by J. Kulicki and Z. Prucz, 5/28/96, (PB98-119217, A07, MF-A02).
- NCEER-96-0006 “Establish Representative Pier Types for Comprehensive Study: Western United States,” by R. Imbsen, R.A. Schamber and T.A. Osterkamp, 5/28/96, (PB98-118607, A07, MF-A02).
- NCEER-96-0007 “Nonlinear Control Techniques for Dynamical Systems with Uncertain Parameters,” by R.G. Ghanem and M.I. Bujakov, 5/27/96, (PB97-100259, A17, MF-A03).
- NCEER-96-0008 “Seismic Evaluation of a 30-Year Old Non-Ductile Highway Bridge Pier and Its Retrofit,” by J.B. Mander, B. Mahmoodzadegan, S. Bhadra and S.S. Chen, 5/31/96, (PB97-110902, MF-A03, A10).
- NCEER-96-0009 “Seismic Performance of a Model Reinforced Concrete Bridge Pier Before and After Retrofit,” by J.B. Mander, J.H. Kim and C.A. Ligozio, 5/31/96, (PB97-110910, MF-A02, A10).
- NCEER-96-0010 “IDARC2D Version 4.0: A Computer Program for the Inelastic Damage Analysis of Buildings,” by R.E. Valles, A.M. Reinhorn, S.K. Kunnath, C. Li and A. Madan, 6/3/96, (PB97-100234, A17, MF-A03).
- NCEER-96-0011 “Estimation of the Economic Impact of Multiple Lifeline Disruption: Memphis Light, Gas and Water Division Case Study,” by S.E. Chang, H.A. Seligson and R.T. Eguchi, 8/16/96, (PB97-133490, A11, MF-A03).
- NCEER-96-0012 “Proceedings from the Sixth Japan-U.S. Workshop on Earthquake Resistant Design of Lifeline Facilities and Countermeasures Against Soil Liquefaction, Edited by M. Hamada and T. O’Rourke, 9/11/96, (PB97-133581, A99, MF-A06).
- NCEER-96-0013 “Chemical Hazards, Mitigation and Preparedness in Areas of High Seismic Risk: A Methodology for Estimating the Risk of Post-Earthquake Hazardous Materials Release,” by H.A. Seligson, R.T. Eguchi, K.J. Tierney and K. Richmond, 11/7/96, (PB97-133565, MF-A02, A08).
- NCEER-96-0014 “Response of Steel Bridge Bearings to Reversed Cyclic Loading,” by J.B. Mander, D-K. Kim, S.S. Chen and G.J. Premus, 11/13/96, (PB97-140735, A12, MF-A03).
- NCEER-96-0015 “Highway Culvert Performance During Past Earthquakes,” by T.L. Youd and C.J. Beckman, 11/25/96, (PB97-133532, A06, MF-A01).
- NCEER-97-0001 “Evaluation, Prevention and Mitigation of Pounding Effects in Building Structures,” by R.E. Valles and A.M. Reinhorn, 2/20/97, (PB97-159552, A14, MF-A03).
- NCEER-97-0002 “Seismic Design Criteria for Bridges and Other Highway Structures,” by C. Rojahn, R. Mayes, D.G. Anderson, J. Clark, J.H. Hom, R.V. Nutt and M.J. O’Rourke, 4/30/97, (PB97-194658, A06, MF-A03).



- NCEER-97-0003 "Proceedings of the U.S.-Italian Workshop on Seismic Evaluation and Retrofit," Edited by D.P. Abrams and G.M. Calvi, 3/19/97, (PB97-194666, A13, MF-A03).
- NCEER-97-0004 "Investigation of Seismic Response of Buildings with Linear and Nonlinear Fluid Viscous Dampers," by A.A. Seleemah and M.C. Constantinou, 5/21/97, (PB98-109002, A15, MF-A03).
- NCEER-97-0005 "Proceedings of the Workshop on Earthquake Engineering Frontiers in Transportation Facilities," edited by G.C. Lee and I.M. Friedland, 8/29/97, (PB98-128911, A25, MR-A04).
- NCEER-97-0006 "Cumulative Seismic Damage of Reinforced Concrete Bridge Piers," by S.K. Kunnath, A. El-Bahy, A. Taylor and W. Stone, 9/2/97, (PB98-108814, A11, MF-A03).
- NCEER-97-0007 "Structural Details to Accommodate Seismic Movements of Highway Bridges and Retaining Walls," by R.A. Imbsen, R.A. Schamber, E. Thorkildsen, A. Kartoum, B.T. Martin, T.N. Rosser and J.M. Kulicki, 9/3/97, (PB98-108996, A09, MF-A02).
- NCEER-97-0008 "A Method for Earthquake Motion-Damage Relationships with Application to Reinforced Concrete Frames," by A. Singhal and A.S. Kiremidjian, 9/10/97, (PB98-108988, A13, MF-A03).
- NCEER-97-0009 "Seismic Analysis and Design of Bridge Abutments Considering Sliding and Rotation," by K. Fishman and R. Richards, Jr., 9/15/97, (PB98-108897, A06, MF-A02).
- NCEER-97-0010 "Proceedings of the FHWA/NCEER Workshop on the National Representation of Seismic Ground Motion for New and Existing Highway Facilities," edited by I.M. Friedland, M.S. Power and R.L. Mayes, 9/22/97, (PB98-128903, A21, MF-A04).
- NCEER-97-0011 "Seismic Analysis for Design or Retrofit of Gravity Bridge Abutments," by K.L. Fishman, R. Richards, Jr. and R.C. Divito, 10/2/97, (PB98-128937, A08, MF-A02).
- NCEER-97-0012 "Evaluation of Simplified Methods of Analysis for Yielding Structures," by P. Tsopelas, M.C. Constantinou, C.A. Kircher and A.S. Whittaker, 10/31/97, (PB98-128929, A10, MF-A03).
- NCEER-97-0013 "Seismic Design of Bridge Columns Based on Control and Repairability of Damage," by C-T. Cheng and J.B. Mander, 12/8/97, (PB98-144249, A11, MF-A03).
- NCEER-97-0014 "Seismic Resistance of Bridge Piers Based on Damage Avoidance Design," by J.B. Mander and C-T. Cheng, 12/10/97, (PB98-144223, A09, MF-A02).
- NCEER-97-0015 "Seismic Response of Nominally Symmetric Systems with Strength Uncertainty," by S. Balopoulou and M. Grigoriu, 12/23/97, (PB98-153422, A11, MF-A03).
- NCEER-97-0016 "Evaluation of Seismic Retrofit Methods for Reinforced Concrete Bridge Columns," by T.J. Wipf, F.W. Klaiber and F.M. Russo, 12/28/97, (PB98-144215, A12, MF-A03).
- NCEER-97-0017 "Seismic Fragility of Existing Conventional Reinforced Concrete Highway Bridges," by C.L. Mullen and A.S. Cakmak, 12/30/97, (PB98-153406, A08, MF-A02).
- NCEER-97-0018 "Loss Assessment of Memphis Buildings," edited by D.P. Abrams and M. Shinozuka, 12/31/97, (PB98-144231, A13, MF-A03).
- NCEER-97-0019 "Seismic Evaluation of Frames with Infill Walls Using Quasi-static Experiments," by K.M. Mosalam, R.N. White and P. Gergely, 12/31/97, (PB98-153455, A07, MF-A02).
- NCEER-97-0020 "Seismic Evaluation of Frames with Infill Walls Using Pseudo-dynamic Experiments," by K.M. Mosalam, R.N. White and P. Gergely, 12/31/97, (PB98-153430, A07, MF-A02).
- NCEER-97-0021 "Computational Strategies for Frames with Infill Walls: Discrete and Smeared Crack Analyses and Seismic Fragility," by K.M. Mosalam, R.N. White and P. Gergely, 12/31/97, (PB98-153414, A10, MF-A02).

- NCEER-97-0022 "Proceedings of the NCEER Workshop on Evaluation of Liquefaction Resistance of Soils," edited by T.L. Youd and I.M. Idriss, 12/31/97, (PB98-155617, A15, MF-A03).
- MCEER-98-0001 "Extraction of Nonlinear Hysteretic Properties of Seismically Isolated Bridges from Quick-Release Field Tests," by Q. Chen, B.M. Douglas, E.M. Maragakis and I.G. Buckle, 5/26/98, (PB99-118838, A06, MF-A01).
- MCEER-98-0002 "Methodologies for Evaluating the Importance of Highway Bridges," by A. Thomas, S. Eshenaur and J. Kulicki, 5/29/98, (PB99-118846, A10, MF-A02).
- MCEER-98-0003 "Capacity Design of Bridge Piers and the Analysis of Overstrength," by J.B. Mander, A. Dutta and P. Goel, 6/1/98, (PB99-118853, A09, MF-A02).
- MCEER-98-0004 "Evaluation of Bridge Damage Data from the Loma Prieta and Northridge, California Earthquakes," by N. Basoz and A. Kiremidjian, 6/2/98, (PB99-118861, A15, MF-A03).
- MCEER-98-0005 "Screening Guide for Rapid Assessment of Liquefaction Hazard at Highway Bridge Sites," by T. L. Youd, 6/16/98, (PB99-118879, A06, not available on microfiche).
- MCEER-98-0006 "Structural Steel and Steel/Concrete Interface Details for Bridges," by P. Ritchie, N. Kaulh and J. Kulicki, 7/13/98, (PB99-118945, A06, MF-A01).
- MCEER-98-0007 "Capacity Design and Fatigue Analysis of Confined Concrete Columns," by A. Dutta and J.B. Mander, 7/14/98, (PB99-118960, A14, MF-A03).
- MCEER-98-0008 "Proceedings of the Workshop on Performance Criteria for Telecommunication Services Under Earthquake Conditions," edited by A.J. Schiff, 7/15/98, (PB99-118952, A08, MF-A02).
- MCEER-98-0009 "Fatigue Analysis of Unconfined Concrete Columns," by J.B. Mander, A. Dutta and J.H. Kim, 9/12/98, (PB99-123655, A10, MF-A02).
- MCEER-98-0010 "Centrifuge Modeling of Cyclic Lateral Response of Pile-Cap Systems and Seat-Type Abutments in Dry Sands," by A.D. Gadre and R. Dobry, 10/2/98, (PB99-123606, A13, MF-A03).
- MCEER-98-0011 "IDARC-BRIDGE: A Computational Platform for Seismic Damage Assessment of Bridge Structures," by A.M. Reinhorn, V. Simeonov, G. Mylonakis and Y. Reichman, 10/2/98, (PB99-162919, A15, MF-A03).
- MCEER-98-0012 "Experimental Investigation of the Dynamic Response of Two Bridges Before and After Retrofitting with Elastomeric Bearings," by D.A. Wendichansky, S.S. Chen and J.B. Mander, 10/2/98, (PB99-162927, A15, MF-A03).
- MCEER-98-0013 "Design Procedures for Hinge Restrainers and Hinge Sear Width for Multiple-Frame Bridges," by R. Des Roches and G.L. Fenves, 11/3/98, (PB99-140477, A13, MF-A03).
- MCEER-98-0014 "Response Modification Factors for Seismically Isolated Bridges," by M.C. Constantinou and J.K. Quarshie, 11/3/98, (PB99-140485, A14, MF-A03).
- MCEER-98-0015 "Proceedings of the U.S.-Italy Workshop on Seismic Protective Systems for Bridges," edited by I.M. Friedland and M.C. Constantinou, 11/3/98, (PB2000-101711, A22, MF-A04).
- MCEER-98-0016 "Appropriate Seismic Reliability for Critical Equipment Systems: Recommendations Based on Regional Analysis of Financial and Life Loss," by K. Porter, C. Scawthorn, C. Taylor and N. Blais, 11/10/98, (PB99-157265, A08, MF-A02).
- MCEER-98-0017 "Proceedings of the U.S. Japan Joint Seminar on Civil Infrastructure Systems Research," edited by M. Shinozuka and A. Rose, 11/12/98, (PB99-156713, A16, MF-A03).
- MCEER-98-0018 "Modeling of Pile Footings and Drilled Shafts for Seismic Design," by I. PoLam, M. Kapuskar and D. Chaudhuri, 12/21/98, (PB99-157257, A09, MF-A02).

- MCEER-99-0001 "Seismic Evaluation of a Masonry Infilled Reinforced Concrete Frame by Pseudodynamic Testing," by S.G. Buonopane and R.N. White, 2/16/99, (PB99-162851, A09, MF-A02).
- MCEER-99-0002 "Response History Analysis of Structures with Seismic Isolation and Energy Dissipation Systems: Verification Examples for Program SAP2000," by J. Scheller and M.C. Constantinou, 2/22/99, (PB99-162869, A08, MF-A02).
- MCEER-99-0003 "Experimental Study on the Seismic Design and Retrofit of Bridge Columns Including Axial Load Effects," by A. Dutta, T. Kokorina and J.B. Mander, 2/22/99, (PB99-162877, A09, MF-A02).
- MCEER-99-0004 "Experimental Study of Bridge Elastomeric and Other Isolation and Energy Dissipation Systems with Emphasis on Uplift Prevention and High Velocity Near-source Seismic Excitation," by A. Kasalanati and M. C. Constantinou, 2/26/99, (PB99-162885, A12, MF-A03).
- MCEER-99-0005 "Truss Modeling of Reinforced Concrete Shear-flexure Behavior," by J.H. Kim and J.B. Mander, 3/8/99, (PB99-163693, A12, MF-A03).
- MCEER-99-0006 "Experimental Investigation and Computational Modeling of Seismic Response of a 1:4 Scale Model Steel Structure with a Load Balancing Supplemental Damping System," by G. Pekcan, J.B. Mander and S.S. Chen, 4/2/99, (PB99-162893, A11, MF-A03).
- MCEER-99-0007 "Effect of Vertical Ground Motions on the Structural Response of Highway Bridges," by M.R. Button, C.J. Cronin and R.L. Mayes, 4/10/99, (PB2000-101411, A10, MF-A03).
- MCEER-99-0008 "Seismic Reliability Assessment of Critical Facilities: A Handbook, Supporting Documentation, and Model Code Provisions," by G.S. Johnson, R.E. Sheppard, M.D. Quilici, S.J. Eder and C.R. Scawthorn, 4/12/99, (PB2000-101701, A18, MF-A04).
- MCEER-99-0009 "Impact Assessment of Selected MCEER Highway Project Research on the Seismic Design of Highway Structures," by C. Rojahn, R. Mayes, D.G. Anderson, J.H. Clark, D'Appolonia Engineering, S. Gloyd and R.V. Nutt, 4/14/99, (PB99-162901, A10, MF-A02).
- MCEER-99-0010 "Site Factors and Site Categories in Seismic Codes," by R. Dobry, R. Ramos and M.S. Power, 7/19/99, (PB2000-101705, A08, MF-A02).
- MCEER-99-0011 "Restrainer Design Procedures for Multi-Span Simply-Supported Bridges," by M.J. Randall, M. Saiidi, E. Maragakis and T. Isakovic, 7/20/99, (PB2000-101702, A10, MF-A02).
- MCEER-99-0012 "Property Modification Factors for Seismic Isolation Bearings," by M.C. Constantinou, P. Tsopelas, A. Kasalanati and E. Wolff, 7/20/99, (PB2000-103387, A11, MF-A03).
- MCEER-99-0013 "Critical Seismic Issues for Existing Steel Bridges," by P. Ritchie, N. Kauh and J. Kulicki, 7/20/99, (PB2000-101697, A09, MF-A02).
- MCEER-99-0014 "Nonstructural Damage Database," by A. Kao, T.T. Soong and A. Vender, 7/24/99, (PB2000-101407, A06, MF-A01).
- MCEER-99-0015 "Guide to Remedial Measures for Liquefaction Mitigation at Existing Highway Bridge Sites," by H.G. Cooke and J. K. Mitchell, 7/26/99, (PB2000-101703, A11, MF-A03).
- MCEER-99-0016 "Proceedings of the MCEER Workshop on Ground Motion Methodologies for the Eastern United States," edited by N. Abrahamson and A. Becker, 8/11/99, (PB2000-103385, A07, MF-A02).
- MCEER-99-0017 "Quindío, Colombia Earthquake of January 25, 1999: Reconnaissance Report," by A.P. Asfura and P.J. Flores, 10/4/99, (PB2000-106893, A06, MF-A01).
- MCEER-99-0018 "Hysteretic Models for Cyclic Behavior of Deteriorating Inelastic Structures," by M.V. Sivaselvan and A.M. Reinhorn, 11/5/99, (PB2000-103386, A08, MF-A02).

- MCEER-99-0019 "Proceedings of the 7<sup>th</sup> U.S.- Japan Workshop on Earthquake Resistant Design of Lifeline Facilities and Countermeasures Against Soil Liquefaction," edited by T.D. O'Rourke, J.P. Bardet and M. Hamada, 11/19/99, (PB2000-103354, A99, MF-A06).
- MCEER-99-0020 "Development of Measurement Capability for Micro-Vibration Evaluations with Application to Chip Fabrication Facilities," by G.C. Lee, Z. Liang, J.W. Song, J.D. Shen and W.C. Liu, 12/1/99, (PB2000-105993, A08, MF-A02).
- MCEER-99-0021 "Design and Retrofit Methodology for Building Structures with Supplemental Energy Dissipating Systems," by G. Pekcan, J.B. Mander and S.S. Chen, 12/31/99, (PB2000-105994, A11, MF-A03).
- MCEER-00-0001 "The Marmara, Turkey Earthquake of August 17, 1999: Reconnaissance Report," edited by C. Scawthorn; with major contributions by M. Bruneau, R. Eguchi, T. Holzer, G. Johnson, J. Mander, J. Mitchell, W. Mitchell, A. Papageorgiou, C. Scaethorn, and G. Webb, 3/23/00, (PB2000-106200, A11, MF-A03).
- MCEER-00-0002 "Proceedings of the MCEER Workshop for Seismic Hazard Mitigation of Health Care Facilities," edited by G.C. Lee, M. Ettouney, M. Grigoriu, J. Hauer and J. Nigg, 3/29/00, (PB2000-106892, A08, MF-A02).
- MCEER-00-0003 "The Chi-Chi, Taiwan Earthquake of September 21, 1999: Reconnaissance Report," edited by G.C. Lee and C.H. Loh, with major contributions by G.C. Lee, M. Bruneau, I.G. Buckle, S.E. Chang, P.J. Flores, T.D. O'Rourke, M. Shinozuka, T.T. Soong, C-H. Loh, K-C. Chang, Z-J. Chen, J-S. Hwang, M-L. Lin, G-Y. Liu, K-C. Tsai, G.C. Yao and C-L. Yen, 4/30/00, (PB2001-100980, A10, MF-A02).
- MCEER-00-0004 "Seismic Retrofit of End-Sway Frames of Steel Deck-Truss Bridges with a Supplemental Tendon System: Experimental and Analytical Investigation," by G. Pekcan, J.B. Mander and S.S. Chen, 7/1/00, (PB2001-100982, A10, MF-A02).
- MCEER-00-0005 "Sliding Fragility of Unrestrained Equipment in Critical Facilities," by W.H. Chong and T.T. Soong, 7/5/00, (PB2001-100983, A08, MF-A02).
- MCEER-00-0006 "Seismic Response of Reinforced Concrete Bridge Pier Walls in the Weak Direction," by N. Abo-Shadi, M. Saiidi and D. Sanders, 7/17/00, (PB2001-100981, A17, MF-A03).
- MCEER-00-0007 "Low-Cycle Fatigue Behavior of Longitudinal Reinforcement in Reinforced Concrete Bridge Columns," by J. Brown and S.K. Kunnath, 7/23/00, (PB2001-104392, A08, MF-A02).
- MCEER-00-0008 "Soil Structure Interaction of Bridges for Seismic Analysis," I. PoLam and H. Law, 9/25/00, (PB2001-105397, A08, MF-A02).
- MCEER-00-0009 "Proceedings of the First MCEER Workshop on Mitigation of Earthquake Disaster by Advanced Technologies (MEDAT-1), edited by M. Shinozuka, D.J. Inman and T.D. O'Rourke, 11/10/00, (PB2001-105399, A14, MF-A03).
- MCEER-00-0010 "Development and Evaluation of Simplified Procedures for Analysis and Design of Buildings with Passive Energy Dissipation Systems, Revision 01," by O.M. Ramirez, M.C. Constantinou, C.A. Kircher, A.S. Whittaker, M.W. Johnson, J.D. Gomez and C. Chrysostomou, 11/16/01, (PB2001-105523, A23, MF-A04).
- MCEER-00-0011 "Dynamic Soil-Foundation-Structure Interaction Analyses of Large Caissons," by C-Y. Chang, C-M. Mok, Z-L. Wang, R. Settgast, F. Waggoner, M.A. Ketchum, H.M. Gonnermann and C-C. Chin, 12/30/00, (PB2001-104373, A07, MF-A02).
- MCEER-00-0012 "Experimental Evaluation of Seismic Performance of Bridge Restrainers," by A.G. Vlassis, E.M. Maragakis and M. Saiid Saiidi, 12/30/00, (PB2001-104354, A09, MF-A02).
- MCEER-00-0013 "Effect of Spatial Variation of Ground Motion on Highway Structures," by M. Shinozuka, V. Saxena and G. Deodatis, 12/31/00, (PB2001-108755, A13, MF-A03).
- MCEER-00-0014 "A Risk-Based Methodology for Assessing the Seismic Performance of Highway Systems," by S.D. Werner, C.E. Taylor, J.E. Moore, II, J.S. Walton and S. Cho, 12/31/00, (PB2001-108756, A14, MF-A03).

- MCEER-01-0001 “Experimental Investigation of P-Delta Effects to Collapse During Earthquakes,” by D. Vian and M. Bruneau, 6/25/01, (PB2002-100534, A17, MF-A03).
- MCEER-01-0002 “Proceedings of the Second MCEER Workshop on Mitigation of Earthquake Disaster by Advanced Technologies (MEDAT-2),” edited by M. Bruneau and D.J. Inman, 7/23/01, (PB2002-100434, A16, MF-A03).
- MCEER-01-0003 “Sensitivity Analysis of Dynamic Systems Subjected to Seismic Loads,” by C. Roth and M. Grigoriu, 9/18/01, (PB2003-100884, A12, MF-A03).
- MCEER-01-0004 “Overcoming Obstacles to Implementing Earthquake Hazard Mitigation Policies: Stage 1 Report,” by D.J. Alesch and W.J. Petak, 12/17/01, (PB2002-107949, A07, MF-A02).
- MCEER-01-0005 “Updating Real-Time Earthquake Loss Estimates: Methods, Problems and Insights,” by C.E. Taylor, S.E. Chang and R.T. Eguchi, 12/17/01, (PB2002-107948, A05, MF-A01).
- MCEER-01-0006 “Experimental Investigation and Retrofit of Steel Pile Foundations and Pile Bents Under Cyclic Lateral Loadings,” by A. Shama, J. Mander, B. Blabac and S. Chen, 12/31/01, (PB2002-107950, A13, MF-A03).
- MCEER-02-0001 “Assessment of Performance of Bolu Viaduct in the 1999 Duzce Earthquake in Turkey” by P.C. Roussis, M.C. Constantinou, M. Erdik, E. Durukal and M. Dicleli, 5/8/02, (PB2003-100883, A08, MF-A02).
- MCEER-02-0002 “Seismic Behavior of Rail Counterweight Systems of Elevators in Buildings,” by M.P. Singh, Rildova and L.E. Suarez, 5/27/02. (PB2003-100882, A11, MF-A03).
- MCEER-02-0003 “Development of Analysis and Design Procedures for Spread Footings,” by G. Mylonakis, G. Gazetas, S. Nikolaou and A. Chauncey, 10/02/02, (PB2004-101636, A13, MF-A03, CD-A13).
- MCEER-02-0004 “Bare-Earth Algorithms for Use with SAR and LIDAR Digital Elevation Models,” by C.K. Huyck, R.T. Eguchi and B. Houshmand, 10/16/02, (PB2004-101637, A07, CD-A07).
- MCEER-02-0005 “Review of Energy Dissipation of Compression Members in Concentrically Braced Frames,” by K.Lee and M. Bruneau, 10/18/02, (PB2004-101638, A10, CD-A10).
- MCEER-03-0001 “Experimental Investigation of Light-Gauge Steel Plate Shear Walls for the Seismic Retrofit of Buildings” by J. Berman and M. Bruneau, 5/2/03, (PB2004-101622, A10, MF-A03, CD-A10).
- MCEER-03-0002 “Statistical Analysis of Fragility Curves,” by M. Shinozuka, M.Q. Feng, H. Kim, T. Uzawa and T. Ueda, 6/16/03, (PB2004-101849, A09, CD-A09).
- MCEER-03-0003 “Proceedings of the Eighth U.S.-Japan Workshop on Earthquake Resistant Design of Lifeline Facilities and Countermeasures Against Liquefaction,” edited by M. Hamada, J.P. Bardet and T.D. O’Rourke, 6/30/03, (PB2004-104386, A99, CD-A99).
- MCEER-03-0004 “Proceedings of the PRC-US Workshop on Seismic Analysis and Design of Special Bridges,” edited by L.C. Fan and G.C. Lee, 7/15/03, (PB2004-104387, A14, CD-A14).
- MCEER-03-0005 “Urban Disaster Recovery: A Framework and Simulation Model,” by S.B. Miles and S.E. Chang, 7/25/03, (PB2004-104388, A07, CD-A07).
- MCEER-03-0006 “Behavior of Underground Piping Joints Due to Static and Dynamic Loading,” by R.D. Meis, M. Maragakis and R. Siddharthan, 11/17/03, (PB2005-102194, A13, MF-A03, CD-A00).
- MCEER-03-0007 “Seismic Vulnerability of Timber Bridges and Timber Substructures,” by A.A. Shama, J.B. Mander, I.M. Friedland and D.R. Allicock, 12/15/03.
- MCEER-04-0001 “Experimental Study of Seismic Isolation Systems with Emphasis on Secondary System Response and Verification of Accuracy of Dynamic Response History Analysis Methods,” by E. Wolff and M. Constantinou, 1/16/04 (PB2005-102195, A99, MF-E08, CD-A00).

- MCEER-04-0002 “Tension, Compression and Cyclic Testing of Engineered Cementitious Composite Materials,” by K. Kesner and S.L. Billington, 3/1/04, (PB2005-102196, A08, CD-A08).
- MCEER-04-0003 “Cyclic Testing of Braces Laterally Restrained by Steel Studs to Enhance Performance During Earthquakes,” by O.C. Celik, J.W. Berman and M. Bruneau, 3/16/04, (PB2005-102197, A13, MF-A03, CD-A00).
- MCEER-04-0004 “Methodologies for Post Earthquake Building Damage Detection Using SAR and Optical Remote Sensing: Application to the August 17, 1999 Marmara, Turkey Earthquake,” by C.K. Huyck, B.J. Adams, S. Cho, R.T. Eguchi, B. Mansouri and B. Houshmand, 6/15/04, (PB2005-104888, A10, CD-A00).
- MCEER-04-0005 “Nonlinear Structural Analysis Towards Collapse Simulation: A Dynamical Systems Approach,” by M.V. Sivaselvan and A.M. Reinhorn, 6/16/04, (PB2005-104889, A11, MF-A03, CD-A00).
- MCEER-04-0006 “Proceedings of the Second PRC-US Workshop on Seismic Analysis and Design of Special Bridges,” edited by G.C. Lee and L.C. Fan, 6/25/04, (PB2005-104890, A16, CD-A00).
- MCEER-04-0007 “Seismic Vulnerability Evaluation of Axially Loaded Steel Built-up Laced Members,” by K. Lee and M. Bruneau, 6/30/04, (PB2005-104891, A16, CD-A00).
- MCEER-04-0008 “Evaluation of Accuracy of Simplified Methods of Analysis and Design of Buildings with Damping Systems for Near-Fault and for Soft-Soil Seismic Motions,” by E.A. Pavlou and M.C. Constantinou, 8/16/04, (PB2005-104892, A08, MF-A02, CD-A00).
- MCEER-04-0009 “Assessment of Geotechnical Issues in Acute Care Facilities in California,” by M. Lew, T.D. O’Rourke, R. Dobry and M. Koch, 9/15/04, (PB2005-104893, A08, CD-A00).
- MCEER-04-0010 “Scissor-Jack-Damper Energy Dissipation System,” by A.N. Sigaher-Boyle and M.C. Constantinou, 12/1/04 (PB2005-108221).
- MCEER-04-0011 “Seismic Retrofit of Bridge Steel Truss Piers Using a Controlled Rocking Approach,” by M. Pollino and M. Bruneau, 12/20/04 (PB2006-105795).
- MCEER-05-0001 “Experimental and Analytical Studies of Structures Seismically Isolated with an Uplift-Restraint Isolation System,” by P.C. Roussis and M.C. Constantinou, 1/10/05 (PB2005-108222).
- MCEER-05-0002 “A Versatile Experimentation Model for Study of Structures Near Collapse Applied to Seismic Evaluation of Irregular Structures,” by D. Kusumastuti, A.M. Reinhorn and A. Rutenberg, 3/31/05 (PB2006-101523).
- MCEER-05-0003 “Proceedings of the Third PRC-US Workshop on Seismic Analysis and Design of Special Bridges,” edited by L.C. Fan and G.C. Lee, 4/20/05, (PB2006-105796).
- MCEER-05-0004 “Approaches for the Seismic Retrofit of Braced Steel Bridge Piers and Proof-of-Concept Testing of an Eccentrically Braced Frame with Tubular Link,” by J.W. Berman and M. Bruneau, 4/21/05 (PB2006-101524).
- MCEER-05-0005 “Simulation of Strong Ground Motions for Seismic Fragility Evaluation of Nonstructural Components in Hospitals,” by A. Wanitkorkul and A. Filiatrault, 5/26/05 (PB2006-500027).
- MCEER-05-0006 “Seismic Safety in California Hospitals: Assessing an Attempt to Accelerate the Replacement or Seismic Retrofit of Older Hospital Facilities,” by D.J. Alesch, L.A. Arendt and W.J. Petak, 6/6/05 (PB2006-105794).
- MCEER-05-0007 “Development of Seismic Strengthening and Retrofit Strategies for Critical Facilities Using Engineered Cementitious Composite Materials,” by K. Kesner and S.L. Billington, 8/29/05 (PB2006-111701).
- MCEER-05-0008 “Experimental and Analytical Studies of Base Isolation Systems for Seismic Protection of Power Transformers,” by N. Murota, M.Q. Feng and G-Y. Liu, 9/30/05 (PB2006-111702).
- MCEER-05-0009 “3D-BASIS-ME-MB: Computer Program for Nonlinear Dynamic Analysis of Seismically Isolated Structures,” by P.C. Tsopelas, P.C. Roussis, M.C. Constantinou, R. Buchanan and A.M. Reinhorn, 10/3/05 (PB2006-111703).


- MCEER-05-0010 “Steel Plate Shear Walls for Seismic Design and Retrofit of Building Structures,” by D. Vian and M. Bruneau, 12/15/05 (PB2006-111704).
- MCEER-05-0011 “The Performance-Based Design Paradigm,” by M.J. Astrella and A. Whittaker, 12/15/05 (PB2006-111705).
- MCEER-06-0001 “Seismic Fragility of Suspended Ceiling Systems,” H. Badillo-Almaraz, A.S. Whittaker, A.M. Reinhorn and G.P. Cimellaro, 2/4/06 (PB2006-111706).
- MCEER-06-0002 “Multi-Dimensional Fragility of Structures,” by G.P. Cimellaro, A.M. Reinhorn and M. Bruneau, 3/1/06 (PB2007-106974, A09, MF-A02, CD A00).
- MCEER-06-0003 “Built-Up Shear Links as Energy Dissipators for Seismic Protection of Bridges,” by P. Dusicka, A.M. Itani and I.G. Buckle, 3/15/06 (PB2006-111708).
- MCEER-06-0004 “Analytical Investigation of the Structural Fuse Concept,” by R.E. Vargas and M. Bruneau, 3/16/06 (PB2006-111709).
- MCEER-06-0005 “Experimental Investigation of the Structural Fuse Concept,” by R.E. Vargas and M. Bruneau, 3/17/06 (PB2006-111710).
- MCEER-06-0006 “Further Development of Tubular Eccentrically Braced Frame Links for the Seismic Retrofit of Braced Steel Truss Bridge Piers,” by J.W. Berman and M. Bruneau, 3/27/06 (PB2007-105147).
- MCEER-06-0007 “REDARS Validation Report,” by S. Cho, C.K. Huyck, S. Ghosh and R.T. Eguchi, 8/8/06 (PB2007-106983).
- MCEER-06-0008 “Review of Current NDE Technologies for Post-Earthquake Assessment of Retrofitted Bridge Columns,” by J.W. Song, Z. Liang and G.C. Lee, 8/21/06 06 (PB2007-106984).
- MCEER-06-0009 “Liquefaction Remediation in Silty Soils Using Dynamic Compaction and Stone Columns,” by S. Thevanayagam, G.R. Martin, R. Nashed, T. Shenthan, T. Kanagalingam and N. Ecemis, 8/28/06 06 (PB2007-106985).
- MCEER-06-0010 “Conceptual Design and Experimental Investigation of Polymer Matrix Composite Infill Panels for Seismic Retrofitting,” by W. Jung, M. Chiewanichakorn and A.J. Aref, 9/21/06 (PB2007-106986).
- MCEER-06-0011 “A Study of the Coupled Horizontal-Vertical Behavior of Elastomeric and Lead-Rubber Seismic Isolation Bearings,” by G.P. Warn and A.S. Whittaker, 9/22/06 (PB2007-108679).
- MCEER-06-0012 “Proceedings of the Fourth PRC-US Workshop on Seismic Analysis and Design of Special Bridges: Advancing Bridge Technologies in Research, Design, Construction and Preservation,” Edited by L.C. Fan, G.C. Lee and L. Ziang, 10/12/06 (PB2007-109042).
- MCEER-06-0013 “Cyclic Response and Low Cycle Fatigue Characteristics of Plate Steels,” by P. Dusicka, A.M. Itani and I.G. Buckle, 11/1/06 06 (PB2007-106987).
- MCEER-06-0014 “Proceedings of the Second US-Taiwan Bridge Engineering Workshop,” edited by W.P. Yen, J. Shen, J-Y. Chen and M. Wang, 11/15/06.
- MCEER-06-0015 “User Manual and Technical Documentation for the REDARS™ Import Wizard,” by S. Cho, S. Ghosh, C.K. Huyck and S.D. Werner, 11/30/06 (PB2007-114766).
- MCEER-06-0016 “Hazard Mitigation Strategy and Monitoring Technologies for Urban and Infrastructure Public Buildings: Proceedings of the China-US Workshops,” edited by X.Y. Zhou, A.L. Zhang, G.C. Lee and M. Tong, 12/12/06 (PB2008-500018).
- MCEER-07-0001 “Static and Kinetic Coefficients of Friction for Rigid Blocks,” by C. Kafali, S. Fathali, M. Grigoriu and A.S. Whittaker, 3/20/07 (PB2007-114767).
- MCEER-07-0002 “Hazard Mitigation Investment Decision Making: Organizational Response to Legislative Mandate,” by L.A. Arendt, D.J. Alesch and W.J. Petak, 4/9/07 (PB2007-114768).

- MCEER-07-0003 “Seismic Behavior of Bidirectional-Resistant Ductile End Diaphragms with Unbonded Braces in Straight or Skewed Steel Bridges,” by O. Celik and M. Bruneau, 4/11/07 (PB2008-105141).
- MCEER-07-0004 “Modeling Pile Behavior in Large Pile Groups Under Lateral Loading,” by A.M. Dodds and G.R. Martin, 4/16/07(PB2008-105142).
- MCEER-07-0005 “Experimental Investigation of Blast Performance of Seismically Resistant Concrete-Filled Steel Tube Bridge Piers,” by S. Fujikura, M. Bruneau and D. Lopez-Garcia, 4/20/07 (PB2008-105143).
- MCEER-07-0006 “Seismic Analysis of Conventional and Isolated Liquefied Natural Gas Tanks Using Mechanical Analogs,” by I.P. Christovasilis and A.S. Whittaker, 5/1/07.
- MCEER-07-0007 “Experimental Seismic Performance Evaluation of Isolation/Restraint Systems for Mechanical Equipment – Part 1: Heavy Equipment Study,” by S. Fathali and A. Filiatrault, 6/6/07 (PB2008-105144).
- MCEER-07-0008 “Seismic Vulnerability of Timber Bridges and Timber Substructures,” by A.A. Sharma, J.B. Mander, I.M. Friedland and D.R. Allicock, 6/7/07 (PB2008-105145).
- MCEER-07-0009 “Experimental and Analytical Study of the XY-Friction Pendulum (XY-FP) Bearing for Bridge Applications,” by C.C. Marin-Artieda, A.S. Whittaker and M.C. Constantinou, 6/7/07.
- MCEER-07-0010 “Proceedings of the PRC-US Earthquake Engineering Forum for Young Researchers,” Edited by G.C. Lee and X.Z. Qi, 6/8/07.
- MCEER-07-0011 “Design Recommendations for Perforated Steel Plate Shear Walls,” by R. Purba and M. Bruneau, 6/18/07.
- MCEER-07-0012 “Performance of Seismic Isolation Hardware Under Service and Seismic Loading,” by M.C. Constantinou, A.S. Whittaker, Y. Kalpakidis, D.M. Fenz and G.P. Warn, 8/27/07.
- MCEER-07-0013 “Experimental Evaluation of the Seismic Performance of Hospital Piping Subassemblies,” by E.R. Goodwin, E. Maragakis and A.M. Itani, 9/4/07.
- MCEER-07-0014 “A Simulation Model of Urban Disaster Recovery and Resilience: Implementation for the 1994 Northridge Earthquake,” by S. Miles and S.E. Chang, 9/7/07.
- MCEER-07-0015 “Statistical and Mechanistic Fragility Analysis of Concrete Bridges,” by M. Shinozuka, S. Banerjee and S-H. Kim, 9/10/07.
- MCEER-07-0016 “Three-Dimensional Modeling of Inelastic Buckling in Frame Structures,” by M. Schachter and AM. Reinhorn, 9/13/07.
- MCEER-07-0017 “Modeling of Seismic Wave Scattering on Pile Groups and Caissons,” by I. Po Lam, H. Law and C.T. Yang, 9/17/07.
- MCEER-07-0018 “Bridge Foundations: Modeling Large Pile Groups and Caissons for Seismic Design,” by I. Po Lam, H. Law and G.R. Martin (Coordinating Author), 12/1/07.
- MCEER-07-0019 “Principles and Performance of Roller Seismic Isolation Bearings for Highway Bridges,” by G.C. Lee, Y.C. Ou, Z. Liang, T.C. Niu and J. Song, 12/10/07.
- MCEER-07-0020 “Centrifuge Modeling of Permeability and Pinning Reinforcement Effects on Pile Response to Lateral Spreading,” by L.L. Gonzalez-Lagos, T. Abdoun and R. Dobry, 12/10/07.
- MCEER-07-0021 “Damage to the Highway System from the Pisco, Perú Earthquake of August 15, 2007,” by J.S. O’Connor, L. Mesa and M. Nykamp, 12/10/07.
- MCEER-07-0022 “Experimental Seismic Performance Evaluation of Isolation/Restraint Systems for Mechanical Equipment – Part 2: Light Equipment Study,” by S. Fathali and A. Filiatrault, 12/13/07.
- MCEER-07-0023 “Fragility Considerations in Highway Bridge Design,” by M. Shinozuka, S. Banerjee and S.H. Kim, 12/14/07.




MCEER-07-0024 "Performance Estimates for Seismically Isolated Bridges," by G.P. Warn and A.S. Whittaker, 12/30/07.

MCEER-08-0001 "Seismic Performance of Steel Girder Bridge Superstructures with Conventional Cross Frames," by L.P. Carden, A.M. Itani and I.G. Buckle, 1/7/08.



**EARTHQUAKE ENGINEERING TO EXTREME EVENTS**

University at Buffalo, The State University of New York  
Red Jacket Quadrangle ■ Buffalo, New York 14261  
Phone: (716) 645-3391 ■ Fax: (716) 645-3399  
E-mail: [mceer@buffalo.edu](mailto:mceer@buffalo.edu) ■ WWW Site <http://mceer.buffalo.edu>



University at Buffalo *The State University of New York*

ISSN 1520-295X